Dynamic habitat models for estuary-dependent Chinook salmon: informing management in the face of climate impacts

Melanie Jeanne Davis

A dissertation

submitted in partial fulfillment of the

requirements for the degree of

Doctor of Philosophy

University of Washington

2019

Reading Committee:

Julian D. Olden, Co-Chair

David A. Beauchamp, Co-Chair

Charles A. Simenstad

Program Authorized to Offer Degree:

School of Aquatic and Fishery Sciences

University of Washington

Abstract

Dynamic habitat models for estuary-dependent Chinook salmon: informing management in the face of climate impacts

Melanie Jeanne Davis

Co-chairs of the Supervisory Committee:
Dr. Julian D. Olden
Dr. David A. Beauchamp

A complex mosaic of estuarine habitats is postulated to bolster the growth and survival of juvenile Chinook salmon by diversifying the availability and configuration of prey and refugia. Consequently, efforts are underway along the North American Pacific Coast to return modified coastal ecosystems to historical or near-historical conditions, but *restoring* habitats are often more sensitive to anthropogenic or climate-mediated disturbance than *relict* (unaltered) habitats. Estuaries are expected to experience longer inundation durations as sea-levels rise, leading to reductions in intertidal emergent marshes, mudflats, and eelgrass beds. Furthermore, rising ocean temperatures may have metabolic consequences for fall-run populations of Chinook salmon, which tend to out-migrate during the spring and summer. Extensive monitoring programs have allowed managers to assess the initial benefits of management efforts (including restoration) for juvenile salmon at local and regional scales, but at present they have limited options for predicting and responding to the concurrent effects of climate change in restoring and relict coastal ecosystems.

For my dissertation I addressed this gap in knowledge using a comprehensive monitoring dataset from the restoring Nisqually River Delta in southern Puget Sound, Washington. I focused on the following questions: 1) How do juvenile Chinook salmon prey consumption and dietary energy density vary throughout a mosaic of estuarine habitats, and is this variation related to differences in physiological condition? 2) How do among-habitat differences in thermal regime and prey consumption affect the bioenergetic growth potential of juvenile Chinook salmon? 3) How will shifts in the estuarine habitat mosaic vary under different sea-level rise and

management scenarios? and 4) How will these climate- and management-mediated shifts in the estuarine habitat mosaic impact habitat quality for juvenile Chinook salmon? To address the first question, I used stomach content and stable isotope analyses to analyze the diets of wild and hatchery Chinook salmon captured in different estuarine habitats during the out-migration season (March–July of 2014 and 2015). I also linked measures of stomach fullness and dietary energy density to body condition. To address the second question, I used a bioenergetics model to determine how among-habitat differences in water temperature and diet might affect juvenile Chinook salmon growth. To address the third question, I designed and calibrated a marsh accretion model and decision support tool using post-restoration monitoring data sets and spatial coverages. Finally, to address the fourth question, I combined output from the marsh accretion model, a hydrological model, and measurements of prey availability into a spatially explicit version of the bioenergetics model to assess the habitat quality and growth rate potential of the entire estuarine habitat mosaic under different sea-level rise and management scenarios.

When considered in tandem, these chapters represent a novel approach to habitat management. Assessments of juvenile salmon diet and physiology, marsh accretion models, and bioenergetics models have been independently implemented along the Pacific Coast, but the amalgamation of all three approaches into a single, spatially explicit analysis represents a novel and significant contribution to the scientific literature. In conducting these analyses for the Nisqually River Delta, some major themes emerged regarding the importance and vulnerability of specific habitats. An integrative diet analysis using stomach contents and stable isotopes found distinct dietary niches between wild and hatchery Chinook salmon. Wild fish were more likely to utilize the freshwater tidal forested and transitional brackish marsh habitats along the main stem river, where energy-rich insect drift made up most of their dietary biomass. The availability and consumption of insect prey resulted in distinct benefits to body condition and growth, as determined by direct physiological measurements and output from the habitat-specific bioenergetics model. These findings highlight the importance of freshwater and brackish emergent marsh habitats with overhanging vegetation, which can regulate water temperatures and supply insect drift. Unfortunately, freshwater tidal forests, brackish marshes, and low and high elevation emergent salt marshes are highly vulnerable to sea-level rise, especially when geological and anthropogenic features limit sediment accretion or lateral expansion. When spatial layers from the marsh accretion model were incorporated into the spatially explicit

version of the bioenergetics model, output indicated that loss of low and high salt marsh reduced the amount of prey available for juvenile salmon, thus decreasing modeled growth rate potential. In all, these findings highlight the importance of preserving the estuarine habitat mosaic for out-migrating juvenile salmon, especially as tidal regimes and ocean temperatures continue to shift through time.

TABLE OF CONTENTS

LIST OF FIGURES

Chapter 5. Climate-mediated reduction in the extent of tidal wetland habitat limits prey availability and reduces estuarine nursery quality for juvenile salmon

LIST OF TABLES

Chapter 5. Climate-mediated reduction in the extent of tidal wetland habitat limits prey availability and reduces estuarine nursery quality for juvenile salmon

ACKNOWLEDGMENTS

First and foremost, I would like to thank my supervisory committee, Dave Beauchamp, Julian Olden, Charles “Si” Simenstad, and Christian Torgersen for their support and guidance throughout this entire process. I don’t think I could’ve picked a better “bunch of dudes” to help me navigate the intellectual rigors of graduate school. Thank you for challenging me to seek new perspectives, to learn new quantitative techniques, and to use data in novel and creative ways. To my bosses at USGS, Isa Woo and Susan De La Cruz, thank you for believing in me (and constantly scraping together funding for me). You are amazing women, awesome co-workers, and admirable role models. I would also like to acknowledge my parents, my grandparents, my siblings, and my aunts. Dad, thank you for fostering my intellect and curiosity, and teaching me to seek the truth in all things. Mom, thank you for encouraging me to be creative, independent, and passionate. To my partner Quinn, I cannot thank you enough for putting up with me throughout this entire process (and for writing sappy letters in colored marker to cheer me on during my qualifying exams). You are the light of my life. Cheers to my girlfriends from my time at Colorado State, my buddies from Bozeman and Jackson, my friends and ex-technicians throughout the Pacific Northwest, and my amazing friends/peers in the School of Aquatic and Fishery Sciences. I could not have done this without such a solid support system. Finally, my sincerest thanks go out to my colleagues at the Nisqually Indian Tribe, Billy Frank Jr. Nisqually National Wildlife Refuge, and USGS Western Ecological Research Center for believing in my work as both a collaborator and a student. To all these people and the ones I’m sure I’ve forgotten to list, I cannot express my gratitude enough. This dissertation would never have come to fruition without your love and support.

DEDICATION

To Martin and Lisa. You are the very best.

Chapter 1

Coastal habitat loss and its effect on salmon in the Pacific Northwest

Introduction

Many anadromous Pacific salmon (*Oncorhynchus* spp.) species are in rapid decline, especially in the Pacific Northwest USA, where populations have been extirpated from nearly 40% of their historic range (Nehlsen et al. 1991; Levin and Schiewe 2001; Gustafson et al. 2007). Coastal habitat loss, including a 50% reduction in the extent of tidal wetlands, has been pinpointed as one of the primary drivers of salmon decline (Gregory and Bisson 1997; Simenstad and Cordell 2000; Magnusson and Hilborn 2003; Maier and Simenstad 2009). Not only are coastal habitats such as estuaries and their associated tidal wetlands highly productive, but they may contribute to the growth and survival of out-migrating juvenile salmon by providing a diverse portfolio of habitat types (a *delta* or *estuarine habitat mosaic*), thus bolstering population persistence (Schindler et al. 2015). For instance, transitional brackish marshes allow for gradual physiological adaptation between freshwater and saltwater conditions; fractal channel networks in emergent marshes offer refuge from predators and enhance the connectivity between land and sea; and productive seagrass beds provide abundant prey resources (Simenstad et al. 1982; Simenstad et al. 2000; Semmens 2008). For juvenile salmon that are not large enough to exhibit piscivory, insect drift can be twice as energy-rich as plankton (Gray 2005), further exemplifying the importance of the "terrestrial-aquatic interface" that can only be found in vulnerable coastal ecosystems (Simenstad and Cordell 2000; McLusky and Elliott 2004; Beaumont et al. 2007; Beauchamp 2009).

Restoration and enhancement programs are a widely-touted option for mitigating coastal habitat loss and bolstering Pacific salmon populations (Nehlsen et al. 1991; NRC 1996; Simenstad and Cordell 2000); however, management actions are often confounded by the complexity of the salmon life cycle and consequent variation in habitat needs at multiple spatiotemporal scales (Simenstad et al. 2000). ESA-listed Chinook salmon (*O. tshawytscha*), which spend more time using estuarine habitats during their out-migration than other Pacific salmon species, have several life history strategies that vary widely within and among populations (Healey 1991). After hatching, fry and parr migrants travel downstream, using freshwater, transitional, nearshore, and offshore habitat types for different periods of time (Simenstad et al. 1982; Bottom et al. 2005; Volk et al. 2010). This strategy takes advantage of the estuarine habitat mosaic to promote population resilience by buffering against yearly and seasonal variation in environmental conditions (Healey 1991; Thorpe 1994; Healey 2009). Given this species' life history diversity, managers should strive to make informed decisions concerning the functional role and energetic contribution of each habitat type within the estuarine habitat mosaic (Simenstad et al. 2000; Roni et al. 2002). Data on how its composition and configuration may affect juvenile salmon growth potential would benefit future and ongoing management actions, especially given strong evidence for foraging advantages in estuaries and floodplains (Thorpe 1994; Jeffres et al. 2008).

In addition to the difficulties associated with managing habitat for an anadromous species with complex life history strategies, restoring or highly-managed coastal ecosystems are often subject to subsidence and degradation, making them especially sensitive to anthropogenic and climate-mediated disturbance (Vandenbruwaene 2011; Ellings et al. 2016). With the risk of global climate change, coastal ecosystems are expected to experience greater inundation

frequencies and durations, leading to a decline in intertidal emergent marshes, mudflats, and eelgrass beds (Morris et al. 2002; Kirwan et al. 2010; Geselbracht et al. 2011). Thorne et al. (2015) predict that given worst-case-scenario sea-level rise estimates, over 75% of Pacific Coast's tidal marshes will be converted to mudflat or subtidal zones by 2100. Such a scenario could result in substantial decreases in habitat suitability for key species, including Chinook salmon (Simenstad et al. 1982; Nehlsen et al. 1991; Galbraith et al. 2002). Furthermore, rising ocean temperatures may have metabolic consequences for fall-run populations, which tend to out-migrate during the spring and summer (Beauchamp 2009). Detailed monitoring programs have allowed managers to thoroughly assess the initial benefits of management efforts for juvenile salmon at local and regional scales, but they currently have limited options for predicting and responding to the potential consequences of climate change. In short, managers need to know how resilient a specific system will be to climate change *and* whether salmon will be able to access and benefit from a persistently changing mosaic of coastal habitats.

To address these gaps in knowledge, I have integrated an empirically-derived climate change model with a spatially explicit bioenergetics model for juvenile Chinook salmon. My research uses a comprehensive monitoring data set from the restoring Nisqually River Delta in southern Puget Sound, Washington to evaluate juvenile Chinook growth potential under various sea-level rise and management scenarios. In the following four chapters I address the research questions: 1) How do juvenile Chinook salmon prey consumption and dietary energy density vary throughout the delta habitat mosaic, and is this variation related to differences in physiological condition? 2) How do among-habitat differences in thermal regime and prey consumption affect the bioenergetic growth potential of juvenile Chinook salmon? 3) How will shifts in the delta habitat mosaic vary under different sea-level rise and management scenarios?

and 4) How will these climate- and management-mediated shifts in the delta habitat mosaic impact habitat quality for juvenile Chinook salmon? Each of these questions is explored in detail in Chapters 2 through 5 (respectively) using a range of appropriate empirical and quantitative techniques.

In Chapter 2 (*Integrated diet analyses reveal contrasting trophic niches for wild and hatchery juvenile Chinook salmon in a large river delta;* Davis et al. 2018) I use stomach content and stable isotope analyses to analyze the diets of wild and hatchery Chinook salmon captured in different delta habitats during the out-migration season (March–July). I then link these dietary assessments, including measures of stomach fullness and dietary energy density, to the body condition of juvenile salmon. In Chapter 3 (*Freshwater tidal forests and estuarine wetlands may confer early-life growth advantages for delta-rearing Chinook Salmon*; Davis et al. 2019), I use a habitat-specific bioenergetics model to determine how present day, seasonal differences in water temperature and diet might affect juvenile Chinook salmon growth. In Chapter 4 (*Development and implementation of an empirical habitat change model and decision support tool for estuarine ecosystems*) I design and calibrate a marsh accretion model and decision support tool using post-restoration monitoring data sets and spatial coverages. Finally, in Chapter 5 (*Climate-mediated reduction in the extent of tidal wetland habitat limits prey availability and reduces nursery habitat quality for juvenile salmon*), I combine output from the marsh accretion model, a hydrological model, and measurements of prey availability into a spatially explicit version of the bioenergetics model to assess the habitat quality and growth rate potential of the entire delta habitat mosaic under different sea-level rise and management scenarios.

When considered together, these chapters represent a novel approach to habitat management. Assessments of juvenile salmon diet and physiology, marsh accretion models, and

bioenergetics models have been independently implemented in the Pacific Northwest, but the amalgamation of all three approaches into a single, spatially explicit analysis represents a novel and significant contribution to the scientific literature. The integrative methods described in detail below were used to assess the functional capacity of the Nisqually River Delta for juvenile Chinook salmon, but the techniques outlined in this dissertation are broadly applicable to other coastal systems and can be modified for other delta-dependent fish and wildlife species (e.g., waterbirds; Dybala et al. 2017). Furthermore, I expect my findings will be used to guide future management actions, including habitat enhancement programs for the Nisqually River Delta and throughout the Pacific Northwest.

References

Beauchamp, D.A. 2009. Bioenergetic ontogeny: linking climate and mass-specific feeding to life-cycle growth and survival of salmon. American Fisheries Society Symposium 70:1–19.

Beaumont, N.J., M.C. Austen, J.P. Atkins, D. Burdon, S. Degraer, T.P. Dentinho, S. Derous, P. Holm, T. Horton, E. van Ierland, A.H. Marboe, D.J. Starkey, M. Townsend, and T. Zarzycki. 2007. Identification, definition, and quantification of goods and services provided by marine biodiversity: Implications for the ecosystem approach. Marine Pollution Bulletin 54:253–265.

Bottom, D.L., C.A. Simenstad, J. Burke, A.M. Baptista, D.A. Jay, K.K. Jones, E. Casillas, and M.H. Schiewe. 2005. Salmon at river's end: the role of the estuary in the decline and recovery of Columbia River salmon. U.S. Department of Commerce, NOAA Technical Memo NMFS-NWFSC-68, 246 pp.

Davis, M. J., I. Woo, C. S. Ellings, S. Hodgson, D. A. Beauchamp, G. Nakai, and S. De La Cruz. 2018. Integrated diet analyses reveal contrasting trophic niches for wild and hatchery juvenile Chinook salmon in a large river delta. Transactions of the American Fisheries Society 147:818–841.

Davis, M. J., I. Woo, C. S. Ellings, S. Hodgson, D. A. Beauchamp, G. Nakai, and S. De La Cruz. 2019. Freshwater tidal forests and estuarine wetlands may confer early-life growth advantages for delta-rearing Chinook salmon. Transactions of the American Fisheries Society. DOI: 10.1002/tafs.10134

Dybala, K.E., M.E. Reiter, C.M. Hickey, W.D. Shuford, K.M. Strum, and G.S. Yarris. 2017. A bioenergetics approach to setting conservation objectives for non-breeding shorebirds in California's central valley. San Francisco Estuary Watershed Science 15:1–28.

Ellings, C.S., M.J. Davis, E.E. Grossman, I. Woo, S. Hodgson, K. Turner, G. Nakai, J.E. Takekawa, and J.Y. Takekawa. 2016. Changes in habitat availability for outmigrating juvenile salmon (Oncorhynchus spp.) following estuary restoration. Restoration Ecology 24:415–427.

Galbraith, H., R. Jones, R. Park, J. Clough, S. Herrod-Julius, B. Harrington, and G. Page. 2002. Global climate change and sea level rise: potential losses of intertidal habitat for shorebirds. Waterbirds 25:173–183.

Geselbracht, L., K. Freeman, E. Kelly, D.R. Gordon, and F.E. Putz. 2011. Retrospective and prospective model simulations of sea level rise impacts on Gulf of Mexico coastal marshes and forests in Waccasassa Bay, Florida. 107:35–57.

Gray, A. 2005. The Salmon River estuary: restoring tidal inundation and tracking ecosystem response. Doctoral Dissertation. University of Washington, Seattle, USA.

Gregory, S.V., and P.A. Bisson. 1997. Degradation and loss of anadromous salmonid habitat in the Pacific Northwest. In D.J. Stouder, P.A. Bisson, R.J. Naiman (eds.) Pacific Salmon & Their Ecosystems. Springer, New York, USA.

Gustafson, R.G., R.S. Waples, J.M. Myers, L.A. Weitkamp, G.J. Bryant, O.W. Johnson, and J.J. Hard. 2007. Pacific salmon extinctions: quantifying lost and remaining diversity. Conservation Biology. 21:1009–1020.

Healey, M.C. 1991. Life history of Chinook salmon (*Oncorhynchus tshawytscha*) p. 313–393. In C. Groot and L. Margolis (eds.), Pacific Salmon Life Histories. UBC Press, Vancouver, Canada.

Healey, M.C. 2009. Resilient salmon, resilient fisheries for British Columbia, Canada. Ecology and Society 14:2.

Jeffres, C.A., J.J. Opperman, and P.B. Moyle. 2008. Ephemeral floodplain habitats provide best growth conditions for juvenile Chinook salmon in a California river. Environmental Biology of Fishes 83:449–458.

Kirwan, M.L., G.R. Guntenspergen, A. D'Alpaos, J.T. Morris, S.M. Mudd, and S. Temmerman. 2010. Limits on the adaptability of coastal marshes to rising sea level. Geophysical Research Letters 37:L23401.

Levin, P.S., and M.H. Schiewe. 2001. Preserving salmon biodiversity: the number of Pacific salmon has declined dramatically, but the loss of genetic diversity may be a bigger problem. American Scientist 89:220–227.

Magnusson, A., and R. Hilborn. 2003. Estuarine influence on survival rates of coho (Oncorhynchus kisutch) and Chinook salmon (Oncorhynchus tshawytscha) released from hatcheries on the U.S. Pacific Coast. Estuaries. 26:1094–1103.

Maier, G.O., and C.A. Simenstad. 2009. The role of marsh-derived macrodetritus to the food webs of juvenile Chinook salmon in a large altered estuary. Estuaries and Coasts. 32:984–998.

McLusky, D.S., and M. Elliot. 2004. The estuarine ecosystem: ecology, threats, and management. Oxford University Press, New York, New York, USA.

Morris, J.T., P.V. Sundareshwar, C.T. Nietch, B. Kjerfve, and D.R. Cahoon. 2002. Responses of coastal wetlands to rising sea level. Ecology 83:2869–2877.

Nehlsen, W., J.E. Williams, and J.A. Lichatowich. 1991. Pacific salmon at the crossroads: stocks at risk from California, Oregon, Idaho, and Washington. Fisheries 16:4–21.

NRC (National Research Council). 1996. Upstream: salmon and society in the Pacific Northwest. National Academy Press, Washington, D.C., USA.

Roni, R., T.J. Beechie, R.E. Bilby, F.E. Leonetti, M.M. Pollock, and G.R. Pess. 2002. A review of stream restoration techniques and a hierarchical strategy for prioritizing restoration in Pacific Northwest watersheds. North American Journal of Fisheries Management. 22:1–20.

Schindler, D.E., J.B. Armstrong, and T.E. Reed. 2015. The portfolio concept in ecology and evolution. Frontiers in Ecology and the Environment 13:257–263.

Semmens, B.X. 2008. Acoustically derived fine-scale behaviors of juvenile Chinook salmon (Oncorhynchus tshawytscha) associated with intertidal benthic habitats in an estuary. Canadian Journal of Fisheries and Aquatic Sciences. 65:2053–2062.

Simenstad, C.A., and J.R. Cordell. 2000. Ecological assessment criteria for restoring anadromous salmonid habitat in Pacific Northwest estuaries. Ecological Engineering 15:283–302.

Simenstad, C.A., K.L. Fresh, and E.O. Salo. 1982. The role of Puget Sound and Washington coastal estuaries in the life history of Pacific salmon: an unappreciated function. In: Kennedy, V.S. (ed.), Estuarine Comparisons. Academic Press, New York, New York, USA pp. 343–364.

Simenstad, C.A., W.G. Hood, R.M. Thom, D.A. Levy, and D.L. Bottom. 2000. Landscape structure and scale constraints on restoring estuarine wetlands for Pacific Coast juvenile fishes, p. 597–630. In M.P. Weinstein and D.A. Kreeger (eds.), Concepts and Controversies in Tidal Marsh Ecology. Kluwer Academic, Dordrecht, The Netherlands.

Thorne, K.M., B.D. Dugger, K.J. Buffington, C.M. Freeman, C.N. Janousek, K.W. Powelson, G.R. Gutenspergen, and J.Y. Takekawa. 2015. Marshes to mudflats — effects of sea level rise on tidal marshes along a latitudinal gradient in the Pacific Northwest. USGS Open File Report 2015-1204. U.S. Geological Survey, Reston, VA, USA.

Thorpe, J.E. 1994. Salmonid fishes and the estuarine environment. Estuaries 17:76–93.

Vandenbruwaene, W., T. Maris, T.J.S. Cox, D.R. Cahoon, P. Meire, and S. Temmerman. 2011. Sedimentation and response to sea-level rise of a restored marsh with reduced tidal exchange: comparison with a natural tidal marsh. Geomorphology 130:115–126.

Volk, E.C., D.L. Bottom, K.K. Jones, and C.A. Simenstad. 2010. Reconstructing juvenile Chinook salmon life history in the Salmon River estuary, Oregon, using otolith microchemistry and microstructure. Transactions of the American Fisheries Society 139:535–549.

Chapter 2

Integrated diet analyses reveal contrasting trophic niches for wild and hatchery juvenile Chinook salmon in a large river delta

Abstract

Hatchery programs have been used as a conservation tool to bolster declining Chinook salmon (*Oncorhynchus tshawytscha*) populations along much of the North American Pacific coast. In many watersheds, hatchery stock are released concurrently with the wild population, thus raising the potential for density-dependent effects. Competition for prey resources during the critical period for early marine growth and survival may diminish the foraging capacity and growth potential of wild Chinook salmon, highlighting the importance of a diverse and productive delta habitat mosaic. We used an integrated diet approach with stomach content and stable isotope analyses to evaluate contrasting patterns of habitat use and prey consumption in a fall run population of juvenile Chinook salmon from the Nisqually River delta in Puget Sound, Washington, USA. We examined size class and origin-level differences throughout a gradient of delta habitat types. Wild (unmarked) and hatchery juveniles exhibited distinct habitat use patterns, whereby unmarked fish were captured more frequently in tidally influenced freshwater and mesohaline emergent marsh, while hatchery fish were caught more often in the nearshore intertidal zone. Consequently, hatchery fish were less likely to consume the energy-dense terrestrial insects that were more common in freshwater and brackish marshes. Stable isotope signatures from muscle and liver tissues corroborated this finding, showing that unmarked juvenile Chinook had derived 24–31% of their diets from terrestrially sourced prey, while terrestrial insects only made up 2–8% of hatchery fish diets. This may have explained why

unmarked fish were in better condition and had stomach contents that were 15% more energy-rich than hatchery fish. We did not observe strong evidence for trophic overlap in juvenile Chinook salmon of different rearing origins, but our results suggest that hatchery juveniles could be more sensitive to diet-mediated effects on growth and survival.

Introduction

Anadromous Pacific salmon (*Oncorhynchus* spp.) use numerous life history strategies, including variation in freshwater and marine residence times, breeding seasons, size at ocean entry, and prey selection (Simenstad et al. 1982; Healey 1991; Schindler et al. 2010). Strategies can vary widely among species, populations, and watersheds, but the potential "portfolio effect" gained from this life history diversity has not been enough to prevent widespread decline along the North American coast (Nehlsen et al. 1991; Levin and Schiewe 2001; Quinn 2005; Gustafson et al. 2007). While several evolutionarily significant units (ESUs) of each species have been listed under the U.S. Endangered Species Act (16 U.S.C. §§ 1531–1544), Chinook salmon (*O. tshawytscha*) have experienced substantial population deterioration in the United States. Five ESUs are currently listed in the Columbia River Basin along with most of the Puget Sound stock (National Marine Fisheries Service 1999; Weitkamp et al. 2015). A number of factors have been attributed to the decline of Chinook salmon along the Pacific coast, but the loss of freshwater and estuarine rearing habitat is considered a major driver, since this species can spend several months in transitional waters during its out-migration (Nehlsen et al. 1991; Thorpe 1994; Kareiva et al. 2000; Gustafson et al. 2007).

Hatcheries, which were frequently operated for supporting recreational and commercial salmon fisheries, are now considered an important conservation tool. Approximately 140 million

hatchery salmon are released into the Columbia River Basin each year (Weitkamp et al. 2015), and hatchery stocks comprise a sizable proportion of Chinook salmon in Puget Sound (44–98%; Duffy et al. 2005) and the California Central Valley (90%; Barnett-Johnson et al. 2007; O'Farrell et al. 2013). In practice, hatchery stocks have successfully bolstered some depleted populations of juvenile Chinook salmon, but concerns over the spread of disease, loss of genetic fitness, and behavioral deficits in hatchery juveniles have been raised in recent years (Reisenbichler and Rubin 1999; Weber and Fausch 2005; Naish et al. 2008; Daly et al. 2012). Competition between wild and hatchery stocks has been postulated as a contributor to Chinook salmon decline because hatchery fish are released at a larger size and at elevated densities over a shorter timeframe (Weber and Fausch 2003; Weber and Fausch 2005; Tatara and Berejikian 2012). The strength of competitive forces during the out-migration season is likely dictated by composite densities of wild *and* hatchery fish, so the availability of optimal nursery habitat may serve as a mediating force in reducing negative density-dependent effects. The productivity of brackish (mesohaline) and saline (poly- or euhaline) emergent marsh is believed to provide profitable foraging for juvenile Chinook salmon (Simenstad et al. 1982; Wissmar and Simenstad 1998; Gray et al. 2002), but the complexity of the delta habitat mosaic as a whole should not be overlooked, especially considering within-species variation in life history traits.

Juvenile Chinook salmon habitat use has been well studied with respect to diet, growth, and residence times in coastal habitats (Simenstad et al. 1982; Neilson et al. 1985; Levings et al. 1986; Simenstad and Cordell 2000; Magnusson and Hilborn 2003), but there remains a gap in knowledge as to how each habitat within the delta mosaic contributes to its total foraging capacity. Furthermore, studies to-date have observed mixed results concerning differences in habitat use and prey consumption for juvenile Chinook salmon of different rearing origins,

although hatchery salmon appear to spend less time in estuaries than their wild counterparts (Levings et al. 1986; David et al. 2014; Weitkamp et al. 2015). Data gleaned from stomach content analyses have not shown dietary differences between hatchery and unmarked (i.e., assumed wild) individuals captured in the same habitat type (Cordell et al. 2011; David et al. 2014; Chittenden et al. 2018), yet wild fish appear to excel in terms of growth and energy consumption when compared to hatchery fish of the same cohort (Davis et al. 2018). Evidence for differential habitat use suggests there may be undetected ontogenetic aspects that reduce growth rates for hatchery stocks after they are released (Goertler et al. 2016).

The majority of studies examining dietary differences between wild and hatchery fish have focused on stomach contents. While stomach content analyses offer local specificity in determining what individuals consume, they cannot account for longer-term dietary shifts due to frequent movement among habitat types. Stable isotope analyses offer a robust alternative because the bulk stable isotopes of carbon, nitrogen, and sulfur are indicative of diets integrated over several weeks or months, and when used together they can provide additional information on trophic structure and site fidelity (Hesslein et al. 1991; Connolly et al. 2004; Heady and Moore 2013; Vander Zanden et al. 2015). Assimilated stomach content and stable isotope analyses have been used successfully to measure ontogenetic diet shifts in juvenile salmon, but they have not been used to evaluate origin-level (i.e., wild vs. hatchery) differences (Rine et al. 2016; Adams et al. 2017; Litz et al. 2017; Chittenden et al. 2018). Therefore, the combined use of these two approaches offers an opportunity to elucidate ontogenetic patterns of habitat use and energy consumption during a “critical period” of growth and survival (Beamish and Mahnken 2001; Duffy and Beauchamp 2011).

For our study, we used a cohesive analysis of short-term (stomach contents) and long-term (stable isotopes) datasets to elucidate where juvenile salmon were foraging within the delta habitat mosaic, the types of prey they were consuming, and the energetic quality of their diets with respect to habitat use. We expected to see clear differences between what we observed in stomach contents and the dietary contributions predicted from the temporally-integrative stable isotope analysis, because juvenile Chinook salmon exhibit variable residence times in habitats throughout the out-migration sequence (Healey 1991; Bottom et al. 2005; Volk et al. 2010). Overall, we anticipated that dietary composition would be dictated by habitat type such that the proportion of time spent in each habitat and the size class distribution of the individuals therein would be indicative of prey consumption patterns. We also hypothesized that because hatchery fish are reared on hatchery food and released at a larger size than their wild counterparts, their stable isotope signatures would demonstrate marked differences in diet earlier in the out-migration season, even if differences in stomach contents were not evident. The novel analysis described herein provides valuable information for habitat managers, because it evaluates the delta habitat mosaic as a whole in order to identify where wild and hatchery juvenile Chinook salmon are deriving the majority of their energy needed for growth and survival.

Methods

Study area

We used the Nisqually River delta in Puget Sound, Washington, USA (47.08°N 122.70°W) as our study site (Fig. 2.1). The glacial headwaters of the Nisqually River flow from Mount Rainier, merging with several rain-fed watersheds to form the largest river complex in southern Puget Sound. Adult Chinook salmon return to the Nisqually mainstem and its tributaries each fall to

spawn, with estimated runs of 500–3,000 wild individuals intermixed with 250–400 hatchery strays. The following winter, 50,000–400,000 juveniles begin to migrate through the delta, and in early May an additional 3.4–4.3 million hatchery fish are released from Clear Creek and Kalama Creek hatcheries.

The concurrent out-migration of wild and hatchery Chinook salmon through a diverse matrix of habitat types in the Nisqually River delta has provided us with a valuable opportunity to satisfy our aforementioned research objectives. Tidal influence permeates several kilometers upstream, where forested tidal freshwater habitat is characterized by pulses of oligohaline water, dense canopy cover, and swiftly moving flows. Water levels can fluctuate several meters depending on tidal regime, snowmelt, and rainfall. As juvenile salmon move toward the sea, they encounter transitional mesohaline emergent marsh, where salinities range from 5–18 PSU and high tides (3–4 m NAVD88) frequently inundate the marsh plain. Tall, overhanging vegetation such as cattails (*Typha latifolia*), Lyngbye's sedge (*Carex lyngbyei*), and rushes (*Juncus* sp.) line the edges of brackish channels and riverbanks (Belleveau et al. 2015). Transitional marsh gradually shifts to polyhaline emergent salt marsh as salinity increases. Higher channel elevations relative to mean tidal level (1.34 m NAVD88) and diminished riverine influence result in some channels being completely dewatered at low tide (Ellings et al. 2016), but the interconnectivity of the terrestrial-aquatic interface also supports inputs of prey drift from invertebrates in saltgrass (*Distichlis spicata*) and pickleweed (*Salicornia pacifica*). At the mouth of the river, euhaline intertidal delta mudflats and nearshore habitat feed into Puget Sound. These areas can have sandy or silty sediment substrates, and are largely unvegetated with the exception of several eelgrass (*Zostera marina*) beds at the northeast and northwest corners of the estuary (Davenport et al. 2017).

Field sampling

We collected juvenile Chinook salmon for stomach content and stable isotope analyses at 19 sampling stations positioned throughout a matrix of delta habitat types (Fig. 2.1). We captured fish using a standard beach seine measuring 37 m x 2 m with a 2.4-m bag of 6-mm mesh. The seine was set by boat and hauled to shore by hand at mid to high tide during daylight hours, with one set completed at each sampling station twice per-month. We sacrificed up to ten juvenile Chinook salmon at each station during sampling events, and 244 juveniles captured between March and July (2014–2015) were set aside for study purposes (Table A2.1). Of these samples, 156 from 2014 and 88 from 2015 were analyzed for stomach contents, but only fish captured in 2015 (68 samples total) were used for stable isotope analysis. Each individual was measured for fork length (FL), weighed, and checked for adipose fin clips and coded wire tags (CWT) to determine rearing origin. We assumed unmarked individuals were wild fish, as the average marking rate for Chinook salmon from Nisqually hatcheries is 95% (Regional Mark Information System; http://www.rmpc.org/home.html). Stomachs were removed in the field, stored in ethanol, and shipped to the USGS San Francisco Bay Estuary Field Station (SFBE) or the University of Washington (UW) for stomach content analysis. In 2015, we froze the remaining carcasses at -20˚C for stable isotope tissue preparation.

We also collected muscle and liver samples from 28 juvenile Chinook salmon captured in nearshore intertidal habitat (Fig. 2.1). These samples were used to test for differences in diet integration rates among tissues, and to account for potential temporal mismatches in habitat use and stable isotope signals due to rapid ontogenetic changes in habitat and diet (Heady and Moore 2013; Hussey et al. 2014; Hertz et al. 2016). A lampara net was used to sample these fish from

eight additional nearshore stations, which were farther from shore and too deep to sample by beach seine (Fig. 2.1). A 50 m lampara net (top rope 46 m, bottom rope 40 m) with a 6-m bag and 12.7-mm mesh was set by two boats and retrieved in an oval. Each station was sampled twice per-month from May to August during daylight hours; however, we only analyzed a subset of individuals captured in June 2015. Lampara samples were handled as described above, but carcasses were sent to USGS Western Fisheries Research Center (WFRC) for tissue preparation.

We conducted prey field (i.e., source) sampling efforts between May and July 2015 to overlap with juvenile salmon tissue collection. Benthic, terrestrial, and pelagic invertebrates were collected in five delta habitat types (forested tidal freshwater: FOR, mesohaline transitional emergent marsh: EFT, polyhaline emergent salt marsh: EEM, intertidal delta mudflat: DMF, and eelgrass: EEL; Fig. 2.1). Collection efforts were distributed throughout each sampling location to account for spatial heterogeneity in prey isotopes. We sampled benthic invertebrates at low tide using a 10 cm diameter by 10 cm depth PVC clam gun to extract stratified sediment cores. We rinsed each core through a 0.5 mm sieve in the field to separate invertebrates from the benthic substrate. The resultant matter was then washed with ocean water or gently moved with tweezers into a 250 ml jar. At FOR, EFT, and EEM we used a muslin sweep net to capture terrestrial invertebrates in vegetation adjacent to the channel edge. Live prey items were carefully transferred from the net to an inflated plastic bag while in the field to prevent crushing. To collect pelagic invertebrates from the water column, we towed a 1.5 m long, 150 μm neuston net from the edge of a boat for up to 10 minutes. We rinsed the cod-end into a 250 ml jar with sufficient ocean water to keep all invertebrates submerged. We obtained epifaunal invertebrate samples at EEL by picking eelgrass shoots by hand and transferring them to a 250 ml jar of

ocean water. All samples were kept on ice while in the field to prevent decomposition, and stored at 5˚C in a laboratory refrigerator upon our return.

Stomach content analysis

We identified, enumerated, and weighed stomach contents for 244 subyearling juvenile Chinook salmon with FL ranging 38–124 mm. We used stereo-dissection microscopes at a magnification range of 7–45 X to identify prey items to the lowest possible taxonomic level. Stomach contents were quantified as wet weight biomass (WWB) or dry weight biomass (DWB), which was estimated for each sample by separating identifiable taxa and weighing them on a 0.01 mg precision scale. For DWB, we dried identifiable taxa in a laboratory oven for 24 hours at 80˚C before weighing. To evaluate the relative energetic contribution of each taxon in a sample, we calculated its total energetic value (kJ) as its WWB (g) multiplied by its literature-derived energy density (kJ/g WWB; Table 2.1). A DWB to WWB conversion factor was used when WWB was not available. Unknown organisms and inorganic materials were also weighed, but were not included in our multivariate analyses. Likewise, fish with empty stomachs (n=14) were omitted from analyses of diet and stomach fullness.

We observed 71 different prey taxa, which were grouped to 13 broader taxonomic levels to capture general dietary patterns (Table 2.1). In order to discern dietary differences among juvenile Chinook salmon, we conducted multivariate analyses, omitting rare (<2.5% occurrence) taxonomic groups. We tested for dietary differences among juvenile salmon of different size classes and origins (hatchery or unmarked) using a permutational analysis of variance (PERMANOVA) and nonmetric multidimensional scaling (NMDS). Size class was subdivided into five categorical groups based on length: ≤ 60 mm, 61–80 mm, 81–90 mm, 91–100 mm, and

> 100 mm. We also tested for between-year and among-site differences in diet to account for habitat-specific variability in the prey field.

We used the "vegan" package in R 3.4.1 (R Core Development Team 2017) to perform multivariate analyses on arcsine square root-transformed gravimetric data. Prior to analysis, checked the coefficient of variation for each taxa to ensure that standardization was not necessary. A PERMANOVA procedure was employed on a Bray-Curtis dissimilarity matrix to compare groups in multivariate space (Anderson 2001). We ran 1,000 model permutations to calculate an *F* statistic and associated *P* value, which were used to test the null hypothesis that the gravimetric composition of stomach contents *did not* differ among groups. Several candidate models including year, month, origin, habitat type, and size class as explanatory variables were tested using a forward stepwise model selection process. We used similarity percentages (SIMPER) to identify taxa that contributed to among-group differences.

To corroborate significant groupings, we also conducted an NMDS ordination on a Bray-Curtis dissimilarity matrix, with stress < 0.2 as a measure of model fit (Clarke 1993). We calculated significant taxonomic loadings by conducting a linear regression analysis between each taxon and the scores from each NMDS axis, applying a permutation test of 1,000 replicates to assess statistical significance. To visualize potential size-related differences, the "ordisurf" function was used to plot fork length in relation to the NMDS output as a smoothed surface in multidimensional space.

Stable isotope analysis

We prepared all juvenile Chinook tissues at the USGS Nisqually Field Station (NNWR) before shipping them to the Northern Arizona University Colorado Plateau Stable Isotope Laboratory

(CPSIL) for C^{13}, N^{15}, and S^{34} stable isotope processing. We used a scalpel cleaned with 5% HCl solution to separate muscle tissue from bone, skin, and scales. Muscle was preferentially collected from above the lateral line, but for smaller fish we used the entire flank end with skin removed to ensure the sample was large enough. Liver tissue was processed concurrently with muscle tissue for an additional 28 hatchery fish to test for differences in the isotopic turnover rate of different tissue types. We targeted fish that were captured in nearshore habitat in June because we felt their isotopic signatures would be more reflective of estuarine foraging in the weeks and months prior to capture. All tissue samples were stored in a labeled whirl-pak® bag and frozen at -20˚C before they were shipped on dry ice to CPSIL.

We enumerated and processed terrestrial invertebrates at NNWR within 24 hours, while benthic, pelagic, and epifaunal samples were processed at SFBE within three days of collection. Presumably, this was enough time to facilitate gut evacuation, although there may have been minimal contamination from digested stomach contents. Prior to identification, we used forceps or tweezers to separate whole invertebrates from organic debris and rinsed each sample with distilled water. We used a 5% HCl acid solution to wash all equipment between handling each sample to prevent cross-contamination. Sources were initially grouped into 39 taxonomic categories using a stereo-dissection microscope at a magnification range of 7–45 X. We attempted to collect at least three source replicates at each sampling site; however, for very small or uncommon taxa it was difficult to gather enough biomass for separate replicates. In this case, stable isotope signatures were either pooled into broader source categories (Table A2.2) or omitted from the analysis.

We shipped all samples on dry ice to CPSIL, where they were processed for C^{13}, N^{15} and S^{34}. Each sample was dried in a laboratory oven at 80˚C for 24 hours, after which it was

pulverized using a ball mill grinder or mortar and pestle. Up to 6 mg of dried tissue (0.6–1.2 mg for C^{13} and N^{15}, 4–6 mg for S^{34}) was weighed on a 0.01 mg accuracy scale and packed into a 4 mm x 6 mm tin capsule. Tissue samples and international standards (IAEA-N1, N2, CH6, and CH7) were combusted at 1020˚C using a Thermo-Finnigan Delta^{plus} Advantage gas isotope-ratio mass spectrometer interfaced with a Costech Analytical ECS4010 elemental analyzer (more information at: http://www.isotope.nau.edu/index.html). Stable isotopes of carbon, nitrogen, and sulfur were expressed in standard delta notation ($\delta^{13}C$, $\delta^{15}N$, and $\delta^{34}S$):

$$\delta^{H}\mathrm{X} = \left(\frac{R_{sample}}{R_{standard}} - 1\right) \times 1000$$

where *R* is the ratio of heavy and light isotopes in a sample (C^{13}:C^{12}, N^{15}:N^{14}, and S^{34}:S^{32}). We expressed stable isotope ratios as part per mil (‰) differences relative to international standards: Pee Dee Belemnite (PDB) for $\delta^{13}C$, atmospheric nitrogen for $\delta^{15}N$, and Vienna Canyon Diablo Troilite (VCDT) for $\delta^{34}S$. None of the fish muscle tissue had a C/N ratio > 3.5; however, some fish liver samples and most invertebrate prey samples did exceed this threshold for lipid correction (Post et al. 2007). Consequently, we used the equation:

$$\delta^{13}C_{normalized} = \delta^{13}C_{untreated} - 3.32 + 0.99 \times C{:}N$$

to manually correct for depleted $\delta^{13}C$ values in affected samples.

We used a Bayesian mixing model to derive posterior estimates of juvenile Chinook salmon diet (Phillips and Gregg 2003; Parnell et al. 2010). A K-means learning algorithm was used to cluster paired $\delta^{13}C$/ $\delta^{15}N$, $\delta^{13}C$/ $\delta^{34}S$, and $\delta^{15}N$/ $\delta^{34}S$ invertebrate tissue signatures from 176 samples. We used these groupings, along with data on habitat and taxonomy, to inform the aggregation of invertebrate prey into six functional sources that were both biologically meaningful and separated in isotopic space (Table 2.2; Table A2.2). Stable isotope signatures from hatchery food (Clear Creek Hatchery) were also included as a source when we analyzed

hatchery fish. We calculated Trophic Enrichment Factors (TEF) for $\delta^{13}C$, $\delta^{15}N$, and $\delta^{34}S$ by comparing mean and standard deviation stable isotope signatures between juvenile Chinook salmon that were caught from rearing ponds at Clear Creek Hatchery (n=11; Olympia, Washington, USA) and hatchery food samples (n=3; Fig. A2.1). This was a valid way to calculate trophic level differences in stable isotope signatures, because Clear Creek hatchery fish were reared exclusively on hatchery food (barring infrequent, external inputs from invertebrate drift) and were likely to have reached isotopic equilibrium over the course of several months. Final mean ± SD TEF values were -0.21 ± 0.20 ‰ for $\delta^{13}C$, 2.91 ± 0.38 ‰ for $\delta^{15}N$, and -0.20 ± 0.29 ‰ for $\delta^{34}S$. These are comparable to standard TEF values observed in the literature (Vander Zanden and Rasmussen 2001).

We used the "simmr" package in R to derive posterior estimates of juvenile salmon diets. The package uses a Bayesian framework to solve stable isotope mixing equations with consumer groups, multiple sources, and trophic enrichment factors (Parnell et al. 2013). We grouped fish by origin, size class, and date of capture — all of which demonstrated significant, among-group differences in stable isotope signatures according to a PERMANOVA of Euclidean distances ($F_{1,68}$ = 29.87, P < 0.001; $F_{2,68}$ = 3.06, P = 0.020; $F_{2,68}$ = 5.39, P = 0.002; Table 2.2). Models were run separately for unmarked and hatchery fish because hatchery food was only a viable prey source for hatchery fish. We ran each model for 500,000 iterations with a burn in of 50,000, initially using an uninformative prior for all model runs. Stomach content data for each individual was also used as an informative prior to confirm the validity of the mixing model. Output is not reported here, as diet data are unlikely to be reflected in stable isotope tissues due to aforementioned discrepancies in tissue turnover.

We used a complementary analysis of muscle and liver tissue to evaluate turnover rates in stable isotope signatures. Because the tissues from lampara samples had been stored in ethanol before processing, we tested for an ethanol effect by comparing juvenile Chinook muscle tissue that had been frozen to muscle tissue from the same fish that had been submerged in ethanol for one month. We used a paired *t*-test to compare $\delta^{13}C$, $\delta^{15}N$ and $\delta^{34}S$ between treatments. All three isotopes exhibited significant ($P < 0.05$), small-magnitude differences in isotopic signatures between frozen and ethanol-preserved muscle tissue (95% CI: $\delta^{13}C$ = 0.41–1.33 ‰, $\delta^{15}N$ = 0.05–0.87 ‰, $\delta^{34}S$ = 0.53–1.40 ‰). As such, we used the mean differences among treatments as correction factors in our mixing model for liver tissue.

Stable Isotope Bayesian Ellipses in R ("SIBER") was used to compare the isotopic niche widths of unmarked and hatchery juvenile Chinook salmon of different sizes and catch dates. The SIBER model incorporates data and prior information with Bayesian inference to simulate a posterior covariance matrix for communities and groups within communities (Jackson et al. 2011). Posterior values of the means and a covariance matrix are used to derive standard ellipse metrics, including the standard ellipse area (SEA_B) and ellipse area for small sample sizes (SEA_C). We derived $\delta^{13}C$/ $\delta^{15}N$, $\delta^{13}C$/ $\delta^{34}S$, and $\delta^{15}N$/ $\delta^{34}S$ ellipse metrics for each community/group analysis. We also compared trophic niche widths between muscle and liver samples under the assumption that liver tissue was a more recent (~ 2 weeks) representation of diet than muscle tissue (1–2 months; Heady and Moore 2013).

Juvenile salmon migration patterns, body condition, and habitat use

To assess the relationship between ontogeny and physiology, we analyzed several measures of juvenile Chinook salmon habitat use and body condition. Habitat use was analyzed for the 2014

and 2015 sampling seasons by calculating the catch per-unit effort (CPUE; i.e., catch-per-set) at each sampling station during each set. We used a linear mixed effects model with sampling station as a random effect and origin, habitat type, year, and month as fixed effects to evaluate the CPUE of unmarked and hatchery fish. We applied a forward stepwise model selection procedure to determine which of these fixed effects were related to CPUE, where the lowest Akaike's Information Criterion (AIC) value was indicative of the best-fit model (Burnham and Anderson 2002).

We calculated the stomach fullness (%), mean dietary energy density (kJ/g WWB), and total dietary energy content (kJ) of each fish as metrics related to short-term consumption (i.e., stomach contents). Stomach fullness was defined as:

$$\frac{stomach\ content\ weight\ (g)}{total\ fish\ weight\ (g) - stomach\ content\ weight\ (g)}\ x\ 100$$

Even though this metric can be sensitive to diel feeding cycles (Sagar and Glova 1988; Schabetsberger et al. 2003), we conducted regular beach seining efforts on a mid to high tide, usually between hours 0800 and 1200. Given our consistent sampling schedule, this estimate of stomach fullness is a fairly reliable indicator of instantaneous ration after the peak dawn foraging hours for juvenile Chinook salmon.

Mean dietary energy density (ED) was calculated as:

$$ED_{tot} = \sum p_i ED_i$$

where p_i was the gravimetric contribution of prey taxon i to the WWB of all stomach contents, and ED_i was the energy density of taxon i (Table 2.1). The total dietary energy content (TEC) of each fish was calculated by multiplying its ED by the total WWB of its stomach contents, including unidentifiable material.

We used a condition index, calculated using the residuals from the linear regression of ln-transformed FL and mass (Brodeur et al. 2004), as a metric likely correlated to long-term consumption (i.e., stable isotope analysis). Condition indices derived from length-weight relationships are generally correlated with markers of salmonid body condition, despite being sensitive to water mass (Trudel et al. 2005).

We compared each body condition metric as described above for CPUE, using a linear mixed effects model with sampling station as a random effect. For TEC, we included fork length as a covariate to account for size differences. When appropriate, we conducted among group post-hoc comparisons using a Tukey's Honestly Significant Difference (HSD) test. All response variables were tested for the assumption of normality prior to analysis using a Shapiro-Wilk test and a Q-Q plot of residuals. CPUE, stomach fullness, and TEC were log-transformed to meet the assumption of normality.

Results

Stomach content analysis

Habitat type and rearing origin drove significant among-group differences in juvenile Chinook salmon stomach contents (PERMANOVA; Table 2.3). Insects, insect larvae, amphipods, and other crustaceans accounted for more than 50% of the dietary variation between unmarked and hatchery fish across both sampling seasons (SIMPER). In freshwater forested habitat (FOR), more than 95% of stomach contents were comprised of dipterans, non-dipteran insects, and insect larvae regardless of size class (Fig. 2.2). Diets of fish captured in mesohaline transitional marsh (EFT) reflected its intermediate location between FOR and the euhaline intertidal mudflats (DMF), with a roughly 50/50 mix of terrestrial insects and planktonic crustaceans. Mysids,

isopods, and amphipods were the most prevalent taxa in the diets of fish captured in emergent salt marsh (EEM) and DMF, with the exception of fish under 60 mm, which consumed mostly terrestrial insects. The stomach contents of fish captured in eelgrass beds (EEL), and nearshore intertidal areas (NS) were characterized by decapods and other crustaceans infrequently observed in the other four habitat types.

These results were corroborated by NMDS output. The three-dimensional ordination converged with a stress value of 0.11, indicating good fit. Crustaceans, decapod larvae, isopods, mysids, dipterans, non-dipteran insects, and insect larvae had highly significant ($P < 0.001$) loadings on the first and second axes, while amphipods had significant loadings on the third axis. Ordination biplots clearly demonstrated the importance of dipterans, non-dipteran insects, and their larvae at FOR; mysids and isopods at EFT, EEM, and DMF; and decapod larvae and other crustaceans at EEL and NS (Fig. 2.3). Size class was not determined to be a significant variable when habitat type was included in the PERMANOVA; however, the ordisurf procedure clearly identified dietary partitioning related to fork length, whereby larger individuals (>81 mm) consumed greater proportions of mysids, isopods, decapod larvae, and other crustaceans.

Stable isotope analysis

Juvenile Chinook salmon $\delta^{13}C$, $\delta^{15}N$, and $\delta^{34}S$ signatures fell within the isotopic mixing space defined by the seven prey sources after trophic fractionation was accounted for with TEF correction values (Fig. 2.4; Fig. A2.1). $\delta^{13}C$, $\delta^{15}N$, and $\delta^{34}S$ increased along a freshwater-to-marine gradient, and terrestrial insects tended to be more depleted in $\delta^{13}C$ and $\delta^{34}S$ than benthic and pelagic prey, regardless of habitat type (Table 2.2). Hemipterans, hymenopterans, arachnids, and coleopterans captured in forested habitat had some of the most depleted $\delta^{13}C$, $\delta^{15}N$, and $\delta^{34}S$

values ($\delta^{13}C$ = -26.05 ± 2.09, $\delta^{15}N$ = 2.35 ± 2.14, $\delta^{34}S$ = 6.23 ± 2.64), while delta benthic and pelagic prey, including amphipods, decapod larvae, harpacticoid copepods, and polychaetes were the most isotopically enriched ($\delta^{13}C$ = -13.98 ± 1.30, $\delta^{15}N$ = 12.39 ± 1.81, $\delta^{34}S$ = 16.31 ± 2.01).

Unmarked and hatchery fish exhibited distinct differences in stable isotope signatures and mixing model output (Fig. 2.4). Specifically, isotopes from hatchery fish were dominated by recent energetic contributions from hatchery food, which made up more than 70% of predicted diet for individuals under 100 mm and individuals that were captured in May or June (Fig. 2.5). The predominance of hatchery food signal was strongly indicative of isotopic disequilibrium, but in larger, late-season fish the hatchery food signal was dampened, and delta benthic and pelagic invertebrates comprised 47% of predicted dietary composition. Unmarked fish exhibited greater predicted contributions from tidal freshwater habitat (19–23%) as compared to hatchery fish (1–4%), but the most notable differences were associated with consumption of terrestrial prey. Unmarked fish were more likely to consume terrestrial insects such as adult dipterans, hemipterans, hymenopterans, arachnids, and coleopterans (24–31%) than hatchery fish (2–8%), even later in the season after the estimated assimilation of hatchery food had subsided.

Unmarked juvenile Chinook salmon also consistently exhibited broader trophic ellipse areas than hatchery salmon (Fig. 2.6). Smaller (< 90 mm) unmarked juveniles had an ellipse area of 6.33 $‰^2$, while the ellipse area was only 0.42 $‰^2$ for hatchery fish. Similarly, for medium-sized (91–100 mm) juveniles the ellipse area of unmarked fish was 7.23 $‰^2$ but only 0.41 $‰^2$ for hatchery fish. In both instances, the trophic ellipses of hatchery fish were completely enveloped within the ellipses of unmarked fish. Large (> 100 mm) hatchery fish had a slightly broader ellipse area of 2.12 $‰^2$ as compared to an ellipse area of 5.93 $‰^2$ for unmarked fish. Even after correcting for the legacy effect of hatchery feeding, trophic ellipses of large unmarked and

hatchery fish did not overlap, and hatchery fish had greater (~ 2 ‰) $\delta^{15}N$ values, suggesting they were feeding higher on the food chain.

When we compared muscle and liver tissues, liver was 0.42–0.71 ‰ more enriched in $\delta^{13}C$ than muscle (paired t-test; 95% CI; $df = 27$, $t = 7.98$, $P < 0.001$) and 1.15–1.57 ‰ more depleted in $\delta^{15}N$ ($df = 27$, $t = -13.42$, $P < 0.001$), whereas $\delta^{34}S$ did not differ significantly between liver and muscle ($df = 27$, $t = -1.35$, $P = 0.188$). These isotopic differences reflected temporal discrepancies in dietary composition. Liver samples predicted 13.7% dietary composition from hatchery food, 55.8% from marsh benthic and pelagic invertebrates, and 10.7% from delta benthic and pelagic invertebrates. In contrast, muscle samples predicted 51.2% dietary composition from hatchery food, 12.4% from marsh benthic and pelagic invertebrates, and 22.9% from delta benthic and pelagic invertebrates. Contributions from tidal freshwater and terrestrially sourced invertebrate prey remained low in this cohort of hatchery fish (Freshwater prey: liver = 9.7%, muscle = 5.0%; Terrestrial prey: liver = 12.5%, muscle = 6.2%).

Juvenile salmon migration patterns, body condition, and habitat use

Juvenile Chinook salmon out-migration timing depended on rearing origin (mixed-effects model; $F_{4,366} = 102.54$, $P < 0.001$; Table 2.4), with unmarked catches peaking in March and April before slowly tapering off throughout the summer, and hatchery catches peaking sharply in May (Fig. 2.7). Juveniles were more likely to be captured in emergent salt marsh, delta mudflat, and intertidal nearshore areas regardless of origin ($F_{4,366} = 3.73$, $P = 0.005$); however, we noted an interaction with habitat type whereby unmarked Chinook were only captured in 24 of 68 sampling events at nearshore sites as opposed to 64 of 68 sampling events for hatchery salmon ($F_{4,366} = 4.74$, $P = 0.001$). The opposite was true at the forested sites, where unmarked juvenile

Chinook were observed in 21 of 23 sampling events, but hatchery juveniles were only observed in 9 of 23 sampling events.

Stomach fullness and TEC were also related to rearing origin, where the stomachs of unmarked fish were twice as full (mean ± SD; unmarked: 2.18 ± 3.58%, hatchery: 1.16 ± 2.80%; $F_{1,238} = 13.02$, $P < 0.001$) and contained 15% more energy than hatchery fish ($F_{1,244} = 3.48$, $P < 0.001$; Fig. A2.2). Regardless of origin, fish captured in June consumed 0.8–4.5 times more energy than individuals captured in any other month ($F_{4,244} = 5.22$, $P < 0.001$). TEC was correlated with stomach fullness ($R^2 = 0.87$, $P < 0.001$) and fork length ($R^2 = 0.08$, $P < 0.001$), but not ED. A habitat-specific trend in TEC showed greater energy consumption at EFT (0.51 ± 0.59 kJ), EEM (0.40 ± 0.73 kJ), and DMF (0.62 ± 0.75 kJ) than at FOR (0.28 ± 0.45 kJ), EEL (0.20 ± 0.18 kJ), or NS (0.19 ± 0.24 kJ). Meanwhile, ED did not differ across habitats (i.e., $P > 0.05$ for all Tukey comparisons), except at FOR, where it was 50% to 100% higher than any other habitat type (7.55 kJ/g as opposed to 3.74–5.02 kJ/g; $P < 0.05$). The trend in origin-level differences continued, where unmarked juveniles had diets that were 19% more energy dense than hatchery juveniles (unmarked: 5.32 ± 2.94 kJ/g, hatchery: 4.47 ± 2.62 kJ/g; $F_{1,244} = 8.25$, $P = 0.004$).

Condition index, which we used as a measure of longer-term physiological effects, was related only to origin and year, with unmarked fish showing marginally positive deviations from a standardized length-weight regression (0.012 ± 0.323) while hatchery fish exhibited negative deviations (-0.013 ± 0.299; $F_{1,244} = 6.19$, $P = 0.014$). Condition was also generally better in 2015 than in 2014 (2014 = -0.008 ± 0.333, 2015 = 0.014 ± 0.260; $F_{1,244} = 5.31$, $P = 0.022$).

Discussion

Our study has demonstrated the utility of an integrated approach when analyzing consumption patterns for species such as Chinook salmon, which may exhibit varied life history strategies within a single watershed (Simenstad et al. 1982; Healey 1991). We perceived prevalent ontogenetic differences in diet, physiology, and habitat use, but the most noticeable dissimilarities were observed between unmarked and hatchery fish. Unmarked juveniles consistently ate greater quantities of energy-dense prey and were in better condition than their hatchery-origin counterparts. These physiological effects were at least partially associated with habitat occupancy and dietary composition, as revealed via cohesive stomach content and stable isotope analyses.

Prey consumption is generally determined by the availability, energy richness, and detectability of prey (Werner and Mittelbach 1981; Townsend and Winfield 1985). It follows that the composition of the prey field and the amount of time spent foraging in different parts of the delta habitat mosaic would affect juvenile salmon diets at different temporal scales. Stomach content analyses showed that hatchery fish had a greater proportion of decapods and miscellaneous crustaceans in their diets compared to unmarked fish, which were more likely to consume mysids. Hatchery fish were also captured in the nearshore intertidal zone (where decapod larvae were prevalent) twice as frequently as unmarked fish. While mysids and decapod larvae have similar energy densities (Gray 2005), mysids can grow more than 10 times larger in terms of WWB, and thus provide greater total energy. As such, disproportionate mysid consumption in emergent marsh and delta mudflats may have been one reason why unmarked juvenile salmon had stomachs that were twice as full and contained up to 15% more energy than hatchery fish stomachs.

The importance of mysid and decapod prey in Nisqually's salt marsh, mudflat, and nearshore intertidal zones is consistent with other studies, which have observed a predominance of crustaceans in the stomachs of subyearling Chinook salmon in southern Puget Sound (Pearce et al. 1982; Duffy et al. 2010; David et al. 2014; Davis et al. 2018). In contrast, fish captured in transitional and freshwater tidal marshes (the majority of which were unmarked) demonstrated a greater reliance on terrestrial insects and their larvae. Almost all Chinook salmon captured in tidal riverine habitat had diets that were comprised of dipterans, insects, and insect larvae, regardless of fork length. Meanwhile in emergent salt marsh and delta mudflat, salmon greater than 60 mm consumed mysids, isopods, and amphipods, while fish smaller than 60 mm had diets that were more similar to those in tidal riverine areas. Terrestrial insects can have energy densities up to four times greater than benthic and pelagic crustaceans (Gray 2005). Assuming that the literature values we used for ED (Gray 2005; David et al. 2014) were representative of Nisqually River delta invertebrates, salmon captured in forested habitat had stomach content ED averaging 7.55 kJ/g, while the ED values of individuals captured in emergent salt marsh and delta mudflat ranged between 3.74 and 4.55 kJ/g. Juvenile salmon of larger size classes (> 81 mm) were more likely to consume crustaceans, but increased gape size also allowed them to ingest an overall greater *quantity* of prey (Brodeur 1991; Scharf et al., 2000). Nisqually Chinook salmon devoured an additional 2.1% of dietary energy (in kJ) per mm increase in size.

In addition to the energy-dense terrestrial prey found in the forested tidal freshwater area, piscivory is believed to bolster early marine growth and survival (David et al. 2014; Litz et al. 2017). This behavior is commonplace in subyearling salmon (Brodeur 1991), but digested fish were detected in only two of our 244 stomach samples. We suspect that the lack of piscivory is indicative of reduced availability of fish larvae and small forage fish in the Nisqually River delta,

since juvenile Chinook salmon as small as 75 mm have been known to consume other fish (Daly et al. 2009; Duffy et al. 2010). Woo et al. (2018) did not observe surf smelt (*Hypomesus pretiosus*), Pacific herring (*Clupea pallasii*), or other forage fish when they sampled the Nisqually prey field during the 2010, 2011, and 2012 out-migration seasons. Conversely, Duffy et al. (2010) found that fish comprised up to 25% of diets in subyearling and yearling Chinook salmon captured in southern Puget Sound nearshore habitats in 2001 and 2002, although piscivory was more common in yearlings and large (> 130 mm) subyearlings. A more thorough analysis relating Puget Sound juvenile salmon diets to the historic, seasonal prevalence of forage fish and fish larvae would be needed to determine the relationship between piscivory and prey availability. Such an analysis would represent a pivotal scientific contribution to the salmonid literature, as there is currently little historic data to draw upon in the Pacific Northwest.

Our findings concerning the relative importance of terrestrial and aquatic prey in unmarked and hatchery fish stomach contents were corroborated by stable isotope analyses. We found that $\delta^{13}C$, $\delta^{15}N$ and $\delta^{34}S$ signatures in unmarked fish muscle tissue were influenced by contributions from a wider variety of prey. Smaller (< 90 mm) unmarked individuals produced an estimated 30% of their biomass from terrestrial insects and more than 37% of their biomass from freshwater habitats, while larger (> 100 mm) unmarked individuals derived roughly 24% of their biomass from terrestrial insects and 31% from freshwater habitats. Hatchery food signal dominated stable isotope signatures for hatchery fish less than 100 mm long, but larger individuals (which demonstrated less than 18% hatchery food signal in muscle tissue) appeared to obtain most of their energy from crustacean prey in delta mudflats and emergent marsh. The analysis of liver tissue, which has a faster isotopic turnover rate (Heady and Moore 2013), did not show a greater contribution of terrestrial or freshwater sources assimilated by hatchery fish.

In fish greater than 100 mm, up to 69% of diet could still be attributed to the consumption of aquatic crustaceans in marsh and delta habitats. Because hatchery fish spent less time in forested and transitional habitat and did not derive as much of their diet from terrestrial prey, their realized trophic niche space (SEA_C) was 64% smaller than their unmarked counterparts, even when the assimilation of hatchery food was low. Smaller SEA_C may be indicative of reduced foraging capacity, since having a broader trophic niche is an adaptive characteristic that allows fish to benefit from a variety of food resources as they become available (Bearhop et al. 2004).

These integrated analyses reveal early life benefits for wild fish foraging in forested habitat, especially in the absence of piscivory. Freshwater systems are generally postulated to be less nutrient rich, and thus less productive, than coastal marine systems due to their turbidity, reliance on longitudinal organic matter inputs, and lack of vertical mixing (Leith 1978; Gross et al. 1988; Townsend 1996). Nevertheless, the interconnectivity of the terrestrial-aquatic interface in tidally influenced, forested habitat contributed to the availability of energy-rich terrestrial drift, which unmarked juvenile Chinook salmon readily consumed during their out-migration. Meanwhile, hatchery fish were less likely to be captured in freshwater tidal forested areas. This was probably a result of their larger size at release, since movement among habitats is determined by ingrained life history strategies, developmental benchmarks, and environmental cues (Simenstad et al. 1982; Healey 1991; Quinn 2005). Origin-level differences in diet and habitat use also suggested there were clear benefits to longer residency in emergent marsh and delta mudflat before moving to the nearshore. As previously mentioned, these benefits were likely derived from the disproportionate consumption of mysids, a trend that is uncommon in other Puget Sound estuaries (Duffy et al. 2010).

This study is not the first to demonstrate foraging differences in wild and hatchery-origin Pacific salmon (Olla et al. 1998; Weber and Fausch 2003), but our integration of short-term stomach content and long-term isotope data with physiological markers has provided novel insight into how these cohorts use delta habitats differently as they out-migrate. This has implications for density-dependent effects driven by hatchery release, which are a growing issue in hatchery management (Tatara and Berejikian 2012). In the Nisqually River delta up to 4 million hatchery juveniles are released each spring. It appears that volitional release might lead to a short (~ 2 week) pulse of intense competition in May, whereby many individuals are foraging for crustacean prey in emergent marsh, delta mudflat, and nearshore habitats. Meanwhile, terrestrial insects in freshwater and mesohaline marsh may remain underutilized except by wild salmon. As fish grow larger in June and July, trophic overlap between the two cohorts separates because wild fish likely reside longer in the estuary before moving to the nearshore (Davis et al. 2018). The broader trophic niche and longer delta residence times of wild juvenile Chinook salmon may allow them to exploit resources better, and thus have higher bioenergetic growth potentials. Additional research comparing measured growth rates to modeled growth potential estimates under variable fish densities would help us to identify potential density-dependent effects in delta habitat.

We found strong evidence for foraging benefits in freshwater and estuarine habitats, which were related to differences in diet and body condition. Although our results are specific to the Nisqually River delta, recent studies have observed prolonged estuarine residence times and better body condition in wild salmon, despite minimal within-site differences in realized dietary composition (Daly et al. 2012; Weitkamp et al. 2015; Chittenden et al. 2018; Davis et al. 2018). Stable isotopes determined that long-term prey contributions and patterns of residency were at

least partially responsible for these physiological differences. Hatchery-origin salmon continue to perform worse in terms of early marine growth and ocean survival than concurrently out-migrating wild populations (Beamish et al. 2012; Zimmerman et al. 2015). Bolstered prey productivity through the targeted enhancement of delta habitats may offset large-scale habitat loss that has occurred in Puget Sound and along most of the North American Pacific coast (David et al. 2016), thereby allowing juvenile Pacific salmon of different rearing origins and stocks to successfully cohabitate.

Acknowledgments

This research was conducted as a collaborative effort with the Nisqually Indian Tribe, Billy Frank Jr. Nisqually National Wildlife Refuge, and the Nisqually River Foundation. Science support came from the USGS Ecosystem Mission Area and Estuary and Salmon Restoration Program funds (ESRP Project #13-1583P) awarded to the U.S. Geological Survey Western Ecological Research Center (USGS WERC). We thank Z. Zhu, J. Schmerfeld, and S. Covington for supporting additional isotopic analyses and staff support through the USGS Biologic Carbon Sequestration Program and USFWS Coastal Program. This study benefited from USGS internship programs (Students in Support of Native American Relations, National Association of Geoscience Teachers, Youth and Education in Science) and WERC program funds. The authors are thankful for the help of numerous USGS and Tribal biologists, including W. Duval, E. Perez, J. Donald, Y. Chan, C. Norton, H. Mittelstaedt, C. Freeman, L. Shakeri, S. Blakely, A. Munguia, A. Hissem, and L. Lamere, who were largely responsible for the success of the 2014/2015 field seasons. Any use of trade, firm, or product names is for descriptive purposes only, and does not imply endorsement by the U.S. Government.

References

Adams, J. N., R. D. Brodeur, E. A. Daly, and T. W. Miller. 2017. Prey availability and feeding ecology of juvenile Chinook (*Oncorhynchus tshawytscha*) and coho (*O. kisutch*) salmon in the northern California Current ecosystem, based on stomach content and stable isotope analyses. Marine Biology 164:98.

Anderson, M. J. 2001. A new method for non-parametric multivariate analysis of variance. Austral Ecology 32–46.

Barnett-Johnson, R., C. B. Grimes, C. F. Royer, and C. J. Donohoe. 2007. Identifying the contribution of wild and hatchery Chinook salmon (*Oncorhynchus tshawytcha*) to the ocean fishery using otolith microstructure as natural tags. Canadian Journal of Fisheries and Aquatic Sciences 64:1683–1692.

Beamish, R. J., and C. Mahnken. 2001. A critical size and period hypothesis to explain natural regulation of salmon abundance and the linkage to climate and climate change. Progress in Oceanography 49:423–437.

Beamish, R. J., R. M. Sweeting, C. M. Neville, K. L. Lange, T. D. Beacham, and D. Preikshot. 2012. Wild Chinook salmon survive better than hatchery salmon in a period of poor production. Environmental Biology of Fishes 94:135–148.

Bearhop, S., C. E. Adams, S. Waldron, R. A. Fuller, and H. Macleod. 2004. Determining trophic niche width: a novel approach using stable isotope analysis. Journal of Animal Ecology 73: 1007–1012.

Belleveau, L. J., J. Y. Takekawa, I. Woo, K. L. Turner, J. B. Barham, J. E. Takekawa, C. S. Ellings, and G. Chin-Leo. 2015. Vegetation community response to tidal marsh restoration of a large river estuary. Northwest Science 89:136–147.

Bottom, D. L., C. A. Simenstad, J. Burke, A. M. Baptista, D. A. Jay, K. K. Jones, E. Casillas, and M. H. Schiewe. 2005. Salmon at river's end: the role of the estuary in the decline and recovery of Columbia River salmon. U.S. Department of Commerce, NOAA Technical Memo NMFS-NWFSC-68.

Brodeur, R. D. 1991. Ontogenetic variations in the type and size of prey consumed by juvenile coho, *Oncorhynchus kisutch*, and Chinook, *O. tshawytcha*, salmon. Environmental Biology of Fishes 30:303–315.

Brodeur, R. D., J. P. Fisher, D. J. Teel, R. L. Emmett, E. Casillas, and T. W. Miller. 2004. Juvenile salmonid distribution, growth, condition, origin, environmental and species in the northern California current. Fisheries Bulletin 102:25–46.

Burnham, K., and D. Anderson. 2002. Model selection and multimodel inference: a practical information-theoretic approach. Colorado State University, Fort Collins. Springer, New York, New York, USA.

Chittenden, C. M., R. Sweeting, C. M. Neville, K. Young, M. Galbraith, E. Carmack, S. Vagle, M. Dempsey, J. Eert, and R. J. Beamish. 2018. Estuarine and marine diets of out-migrating Chinook salmon smolts in relation to local zooplankton populations, including harmful algal blooms. Estuarine, Coastal and Shelf Science 200:335–348.

Clarke, K. R. 1993. Non-parametric multivariate analyses of changes in community structure. Austral Ecology 18:117–143.

Connolly, R. M., M. A. Guest, A. J. Meville, and J. M. Oakes. 2004. Sulfur stable isotopes separate producers in marine food-web analysis. Oecologia 138:161–167.

Cordell, J. R., J. D. Toft, A. Gray, G. T. Ruggerone, and M. Cooksey. 2011. Functions of restored wetlands for juvenile salmon in an industrialized estuary. Ecological Engineering 37:343–353.

Daly, E. A., R. D. Brodeur, and L. A. Weitkamp. 2009. Ontogenetic shifts in diet of juvenile and subadult coho and Chinook salmon in coastal marine waters: important for marine survival? Transactions of the American Fisheries Society 138:1420–1438.

Daly, E. A., R. D. Brodeur, J. P. Fisher, L. A. Weitkamp, D. J. Teel, and B. R. Beckman. 2012. Spatial and trophic overlap of marked and unmarked Columbia River Basin spring Chinook salmon during early marine residence with implications for competition between hatchery and naturally produced fish. Environmental Biology of Fishes 94:117–134.

Davenport, A. E., J. D. Davis, I. Woo, E. E. Grossman, J. Barham, C. S. Ellings, and J. Y. Takekawa. 2017. Comparing automated classification and digitation approaches to detect change in eelgrass bed extent during restoration of a large river delta. Northwest Science 91:272–282.

David, A. T., C. S. Ellings, I. Woo, C. A. Simenstad, J. Y. Takekawa, and K. L. Turner. 2014. Foraging and growth potential of juvenile Chinook salmon after tidal restoration of a large river delta. Transactions of the American Fisheries Society 143:1515–1529.

David, A. T., C. A. Simenstad, J. R. Cordell, J. D. Toft, C. S. Ellings, A. Gray, and H. B. Berge. 2016. Wetland loss, juvenile salmon foraging performance, and density dependence in Pacific Northwest estuaries. Estuaries and Coasts 39:767–780.

Davis, M. J., C. S. Ellings, I. Woo, S. Hodgson, K. Larsen, G. Nakai, and S. de la Cruz. 2018. Gauging resource exploitation by juvenile Chinook salmon (*Oncorhynchus tshawytcha*) in restoring estuarine habitat. Restoration Ecology 26:976–986.

Duffy, E. J., and D. A. Beauchamp. 2011. Rapid growth in the early marine period improves the marine survival of Chinook salmon (*Oncorhynchus tshawytscha*) in Puget Sound, Washington. Canadian Journal of Fisheries and Aquatic Sciences 68:232–240.

Duffy, E. J., D. A. Beauchamp, and R. M. Buckley. 2005. Early marine life history of juvenile Pacific salmon in two regions of Puget Sound. Estuarine, Coastal and Shelf Science 64:94–107.

Duffy, E. J., D. A. Beauchamp, R. M. Sweeting, R. J. Beamish, and J. S. Brennan. 2010. Ontogenetic diet shifts of juvenile Chinook salmon in nearshore and offshore habitats of Puget Sound. Transactions of the American Fisheries Society 139:803–823.

Ellings, C. S., M. J. Davis, E. E. Grossman, I. Woo, S. Hodgson, K. L. Turner, G. Nakai, J. E. Takekawa, and J. Y. Takekawa. 2016. Changes in habitat availability for outmigrating juvenile salmon (*Oncorhynchus* spp.) following estuary restoration. Restoration Ecology 24: 415–427.

Goertler, P. A. L., M. D. Scheuerell, C. A. Simenstad, and D. L. Bottom. 2016. Estimating common growth patterns in juvenile Chinook salmon (*Oncorhynchus tshawytsha*) from diverse genetic stocks and a large spatial extent. PLoS ONE 11:e0162121.

Gray, A., C. A. Simenstad, D. L. Bottom, and T. J. Cornwell. 2002. Contrasting functional performance of juvenile salmon habitat in recovering wetlands of the Salmon River Estuary, Oregon, U.S.A. Restoration Ecology 10:514–526.

Gray, A. 2005. The Salmon River Estuary: restoring tidal inundation and tracking ecosystem response. Graduate dissertation. University of Washington, Seattle, Washington, USA.

Gross, M. R., R. M. Coleman, and R. M. McDowall. 1988. Aquatic productivity and the evolution of diadromous fish migration. Science 239:1291–1293.

Gustafson, R. G., R. S. Waples, J. M. Myers, L. A. Weitkamp, G. J. Bryant, O. W. Johnson, and J. J. Hard. 2007. Pacific salmon extinctions: quantifying lost and remaining diversity. Conservation Biology 21:1009–1020.

Heady, W. N., and J. W. Moore. 2013. Tissue turnover and stable isotope clocks to quantify resource shifts in anadromous rainbow trout. Oecologia 172:221–34.

Healey, M. C. 1991. Life history of Chinook salmon (*Oncorhynchus tshawytscha*). In: C Groot and L. Margolis (eds) Pacific Salmon Life Histories. University of British Columbia Press, Vancouver, British Columbia, Canada.

Hertz, E., M. Trudel, R. El-Sabaawi, S. Tucker, J. F. Dower, T. D. Beacham, A. M. Edwards, and A. Mazumder. 2016. Hitting the moving target: modelling ontogenetic shifts with stable isotopes reveals the importance of isotopic turnover. Journal of Animal Ecology 85:681–691.

Hesslein, R. H., M. J. Capel, D. E. Fox, and K. A. Hallard. 1991. Stable isotopes of sulfur, carbon, and nitrogen as indicators of trophic level and fish migration in the lower Mackenzie River Basin, Canada. Canadian Journal of Fisheries and Aquatic Sciences 48:2258–2265.

Hussey, N. E., M. A. MacNeil, B. C. McMeans, J. A. Olin, S. F. J. Dudley, G. Cliff, S. P. Wintner, S. T. Fennessy, and A. T. Fisk. 2014. Rescaling the trophic structure of marine food webs. Ecology Letters 17:239–250.

Jackson, A. L., R. Inger, A. C. Parnell, and S. Bearhop. 2011. Comparing isotopic niche width among and within communities: SIBER — Stable Isotope Bayesian Ellipses in R. Journal of Animal Ecology 80:595–602.

Kareiva, P., M. Marvier, and M. McClure. 2000. Recovery and management options for spring/summer Chinook salmon in the Columbia River Basin. Science 290:977–979.

Leith, H. 1978. Primary productivity in ecosystems: comparative analysis of global patterns. In: H. Leith (ed) Patterns of Primary Production in the Biosphere. Benchmark Papers in Ecology 8. Dowden, Hutchinson & Ross, Stroudsburg, Pennsylvania, USA.

Levin, P. S., and M. H. Schiewe. 2001. Preserving salmon biodiversity: the number of Pacific salmon has declined dramatically, but the loss of genetic diversity may be a bigger problem. American Scientist 89:200–227.

Levings, C. D., C. D. McAllister, and B. D. Chang. 1986. Differential use of the Campbell River Estuary, British Columbia by wild and hatchery-reared juvenile Chinook salmon (*Oncorhynchus tshawytscha*). Canadian Journal of Fisheries and Aquatic Sciences 43:1386–1397.

Litz, M. N. C., J. A. Miller, L. A. Copeman, D. J. Teel, L. A. Weitkamp, E. A. Daly, and A. M. Claiborne. 2017. Ontogenetic shifts in the diets of juvenile Chinook salmon: new insight from stable isotopes and fatty acids. Environmental Biology of Fishes 100:337–360.

Magnusson, A., and R. Hilborn. 2003. Estuarine influence on survival rates of coho (*Oncorhynchus kisutch*) and Chinook salmon (*Oncorhynchus tshawytscha*) released from hatcheries on the U.S. Pacific coast. Estuaries 26:1094–1103.

Naish, K. A., J. E. Taylor, P. S. Levin, T. P. Quinn, J. R. Winton, D. Huppert, and R. Hilborn. 2008. An evaluation of the effects of conservation and fishery enhancement hatcheries on wild populations of salmon. Advances in Marine Biology 53:61–194.

National Marine Fisheries Service. 1999. Endangered and threatened species: threatened status for three Chinook salmon evolutionarily significant units (ESUs) in Washington and Oregon, and endangered status for one Chinook salmon ESU in Washington. Federal Register 64:14308–14328.

Nehlsen, W. J., J. E. Williams, and J. A. Lichatowich. 1991. Pacific salmon at the crossroads: stocks at risk from California, Oregon, Idaho, and Washington. Fisheries 16:4–21.

Neilson, J. D., G. H. Geen, and D. Bottom 1985. Estuarine growth of juvenile Chinook salmon (*Oncorhynchus tshawytscha*) as inferred from otolith microstructure. Canadian Journal of Fisheries and Aquatic Sciences 42:899–908.

O'Farrell, M. R., M. S. Mohr, M L. Palmer-Zwahlen, and A. M. Grover. 2013. The Sacramento Index (SI). NOAA Technical Memorandum NMFS-SWFSC-512, National Marine Fisheries Service, Santa Cruz, California, USA.

Olla, B. L., M. W. Davis, and C. H. Ryer. 1998. Understanding how the hatchery environment represses or promotes the development of behavioral survival skills. Bulletin of Marine Science 62:531–550.

Parnell, A. C., R. Inger, S. Bearhop, and A. L. Jackson. 2010. Source partitioning using stable isotopes: coping with too much variation. PLoS One 5:e9672.

Parnell, A. C., D. L. Phillips, S. Bearhop, B. X. Semmens, E. J. Ward, J. W. Moore, A. L. Jackson, J. Grey, D. J. Kelly, and R. Inger. 2013. Bayesian stable isotope mixing models. Environmetrics 24:387–399.

Pearce, T. A., J. H. Meyer, and R. S. Boomer. 1982. Distribution and food habits of juvenile salmon in the Nisqually Estuary, Washington, 1979–1980. U.S. Fish and Wildlife Service, Olympia, Washington, USA.

Phillips, D. L., and J. W. Gregg. 2003. Source partitioning with stable isotopes: coping with too many sources. Oecologia 136:261–269.

Post, D. M., C. A. Layman, D. A. Arrington, G. Takimoto, J. Quattrochi, and G. Montana. 2007. Getting to the fat of the matter: models, methods, and assumptions for dealing with lipids in stable isotope analyses. Oecologia 152:179–189.

Quinn, T. P. 2005. The behavior and ecology of Pacific salmon and trout. University of Washington Press, Seattle, Washington, USA.

Reisenbichler, R. R., and S. P. Rubin. 1999. Genetic changes from artificial propagation of Pacific salmon affect the productivity and viability of supplemented populations. ICES Journal of Marine Science 56:459–466.

Ricardi, A., and E. Bourget. 1998. Weight-to-weight conversion factors for marine benthic macroinvertebrates. Marine Ecology Progress Series 163:245–251.

Rine, K. M., M. S. Wipfli, E. R. Schoen, T. L. Nightengale, and C. A. Stricker. 2016. Trophic pathways supporting juvenile Chinook and coho salmon in the glacial Susitna River, Alaska: patterns of freshwater, marine, and terrestrial food resource use across a seasonally dynamic habitat mosaic. Canadian Journal of Fisheries and Aquatic Sciences 73:1626–1641.

Sagar, P. M., and G. J. Glova. 1988. Diel feeding periodicity, daily ration and prey selection of a riverine population of juvenile Chinook salmon, *Oncorhynchus tshawytscha* (Walbaum). Journal of Fish Biology 33:643–653.

Sage, R. D. 1982. Wet and dry-weight estimates of insects and spiders based on length. American Midland Naturalist 108:407–411.

Schabetsberger, R., C. A. Morgan, R. D. Brodeur, C. L. Potts, W. T. Peterson, and R. L. Emmett. 2003. Prey selectivity and diel feeding chronology of juvenile Chinook (*Oncorhynchus*

tshawytscha) and coho (*O. kisutch*) salmon in the Columbia River plume. Fisheries Oceanography 12:523–540.

Scharf, F. S., F. Juanes, and R. A. Rountree. 2000. Predator size – prey size relationships of marine fish predators: interspecific variation and effects of ontogeny and body size on trophic-niche breadth. Marine Ecology Progress Series 208:229–248.

Schindler, D. E., R. Hilborn, B. Chasco, C. P. Boatright, T. P. Quinn, L. A. Rodgers, and M. S. Webster. 2010. Population diversity and the portfolio effect in an exploited species. Nature 465:609–612.

Simenstad, C. A., and J. R. Cordell. 2000. Ecological assessment criteria for restoring anadromous salmonid habitat in Pacific Northwest estuaries. Ecological Engineering 15: 283–302.

Simenstad, C. A., K. L. Fresh, and E. O. Salo. 1982. The role of Puget Sound and Washington coastal estuaries in the life history of Pacific salmon: an unappreciated function. In: V. S. Kennedy (ed) Estuarine Comparisons. Academic Press, New York, USA.

Tatara, C. P., and B. A. Berejikian. 2012. Mechanisms influencing competition between hatchery and wild juvenile anadromous Pacific salmonids in fresh water and their relative competitive abilities. Environmental Biology of Fishes 94:7–19.

Thorpe, J. E. 1994. Salmonid fishes and the estuarine environment. Estuaries 17:76–93.

Townsend, C. R. 1996. Concepts in river ecology: pattern and process in the catchment hierarchy. Archiv fur Hydrobiologie, Supplement 113, Large Rivers 10:3–21.

Townsend, C. R., and I. J. Winfield. 1985. The application of optimal foraging theory to feeding behavior in Fish. In: P. Tytler and P. Calow (eds) Fish Energetics. Springer, Dordrecht, the Netherlands.

Trudel, M., S. Tucker, J. F. T. Morris, D. A. Higgs, and D. W. Welch. 2005. Indicators of energetic status in juvenile coho salmon and Chinook salmon. North American Journal of Fisheries Management 25:374–390.

Vander Zanden, M. J., and J. B. Rasmussen. 2001. Variation in $\delta^{15}N$ and $\delta^{13}C$ trophic fractionation: implications for aquatic food web studies. Limnology and Oceanography 46:2061–2066.

Vander Zanden, M. J., M. K. Clayton, E. K. Moody, C. T. Solomon, and B. C. Weidel. 2015. Stable isotope turnover and half-life in animal tissues: a literature synthesis. PLoS One 10:e0116182.

Volk, E. C., D. L. Bottom, K. K. Jones, and C. A. Simenstad. 2010. Reconstructing juvenile Chinook salmon life history in the Salmon River estuary, Oregon, using otolith microchemistry and microstructure. Transactions of the American Fisheries Society 139:535–549.

Weber, E. D., and K. D. Fausch. 2003. Interactions between hatchery and wild salmonids in streams: differences in biology and evidence for competition. Canadian Journal of Fisheries and Aquatic Sciences 60:1018–1036.

Weber, E. D., and K. D. Fausch. 2005. Competition between hatchery-reared and wild juvenile Chinook salmon in enclosures in the Sacramento River, California. Transactions of the American Fisheries Society 134:44–58.

Weitkamp, L. A., D. J. Teel, M. Liermann, S. A. Hinton, D. M. Van Doornik, and P. J. Bentley. 2015. Stock-specific size and timing at ocean entry of Columbia River juvenile Chinook salmon and steelhead: implications for early ocean growth. Marine and Coastal Fisheries: Dynamics, Management, and Ecosystem Science 7:370–392.

Werner, E. E., and G. G. Mittelbach. 1981. Optimal foraging: field tests of diet choice and habitat switching. Integrative and Comparative Biology 21:813–829.

Wissmar, R. C., and C. A. Simenstad. 1998. Variability of riverine and estuarine ecosystem productivity for supporting pacific salmon. In: G. R. McMurray and R. J. Bailey (eds.) Change in Pacific Northwest Coastal Ecosystems. NOAA Coastal Ocean Program Decision Analysis Series No. 11. National Oceanic and Atmospheric Administration, Silver Spring, Maryland, USA.

Woo, I., M. J. Davis, C. S. Ellings, G. Nakai, J. Y. Takekawa, and S. De La Cruz. 2018. Enhanced invertebrate prey production following estuarine restoration supports foraging for multiple species of juvenile salmonids (*Oncorhynchus* spp.). Restoration Ecology 26:964–975.

Zimmerman, M. S., J. R. Irvine, M. O'Neill, J. H. Anderson, C. M. Greene, J. Weinheimer, M. Trudel, and K. Rawson. 2015. Spatial and temporal patterns in smolt survival of wild and hatchery coho salmon in the Salish Sea. Marine and Coastal Fisheries 7:116–134.

Tables

Table 2.1. Table of prey taxa observed in juvenile Chinook salmon stomach contents. Percent occurrence is the proportion of diet samples in which each taxon was observed. Biomass conversion factors (Sage 1982; Ricardi and Bourget 1998) and mean energy density values (Gray 2005; David et al. 2014) are shown in the right hand columns.

Taxon	Percent occurrence (%)	DWB to WWB	ED conversion (kJ/WW g)
Amphipoda			
Unidentified	21.72	20	3.07
Americorophium sp.	10.00	20	3.07
Americorophium spinicorne	0.71	20	3.07
Amphithoidae	0.71	20	2.97
Corophiidae	5.71	20	3.07
Corophium sp.	9.29	20	3.07
Eogammarus sp.	15.71	20	2.88
Hyperiidae	2.46	20	2.46
Monocorophium sp.	0.71	20	3.07
Crustacea			
Unidentified	28.69	20	3.37
Copepoda: Calanoida	0.71	20	4.62
Copepoda: Harpacticoida	4.29	20	4.62
Cumacea	6.43	17.2	3.37
Euphausiidae	1.23	20	3.37
Ostracoda	0.71	20	3.37
Paguoridea megalopa	0.71	25.4	3.36
Peracarida	2.05	20	3.37
Tanaidacea: *Leptochelia* sp.	2.86	20	3.37
Tanaidacea*: Sinelobus* sp.	1.43	20	3.37
Decapoda			
Decapoda megalopa	18.03	25.4	3.36
Decapoda zoea	19.67	25.4	3.36
Isopoda			
Gnorimosphaeroma oregonensis	4.69	20.7	2.96
Mysida			
Unidentified	21.31	18	3.55
Mysida larva	0.71	18	3.55
Neomysis mercedis	18.57	18	3.55
Cirripedia			
Cirripedia larvae	1.43	6.5	2.16
Platyhelminthes			
Trematoda	0.71	19.8	1.98
Polychaeta			
Unidentified	4.10	19.8	1.98
Arachnida			
Unidentified	3.69	3.07	5.32
Araneae	0.71	3.07	5.32
Diptera			

Unidentified adult	13.93	2.7	8.92
Asilidae	2.14	2.7	8.92
Brachycera	5.33	2.7	8.92
Chironomidae	9.29	2.7	3.83
Dolichopodidae	2.86	2.7	6.20
Ephydridae	2.14	2.7	8.92
Nematocera	9.62	2.7	8.92
Insecta			
Unidentified adult	32.38	2.6	10.93
Aphididae	0.71	2.7	10.93
Cercopidae	0.71	2.7	10.93
Cicadellidae	1.43	2.7	10.93
Coccinellidae	0.71	2.3	7.97
Corixidae	0.71	2.3	7.97
Formicidae	0.71	2.6	5.69
Hemiptera	4.51	2.6	10.93
Hymenoptera	6.56	2.7	12.67
Orthoptera	0.71	2.6	7.97
Psyllidae	0.71	2.6	10.93
Salididae	0.71	2.6	10.93
Staphylinidae	0.71	2.6	7.97
Thysanoptera	0.71	2.6	10.93
Insecta larvae			
Unidentified larva	10.25	4.6	7.41
Unidentified pupa	4.10	4.6	3.83
Ceratopogonidae larva	0.71	4.6	2.58
Ceratopogonidae pupa	0.71	4.6	3.83
Chironomidae larva	11.43	4.6	2.58
Chironomidae pupa	20.71	4.6	3.83
Coleoptera larva	4.29	6.5	2.41
Diptera larva	1.43	4.6	2.58
Dolichopodidae larva	0.71	4.6	2.58
Ephemeroptera larva	6.56	4.6	3.66
Ephydridae pupa	2.14	4.6	3.83
Hemiptera larva	0.71	4.6	7.41
Nematocera larva	0.71	4.6	2.58
Nematocera pupa	0.71	4.6	3.83
Odonata larva	2.14	4.6	3.66
Psychodidae larva	0.71	4.6	2.58
Psychodidae pupa	0.71	4.6	3.83
Psyllidae pupa	0.71	4.6	3.83
Trichoptera larva	0.71	4.6	2.58
Actinopterygii			
Fish larva	0.82	-	6.83

Table 2.2. Juvenile Chinook salmon and invertebrate source group mean ± SD stable isotope signatures for carbon, nitrogen, and sulfur.

Size and Origin	Mean $\delta^{13}C$	SD $\delta^{13}C$	Mean $\delta^{15}N$	SD $\delta^{15}N$	Mean $\delta^{34}S$	SD $\delta^{34}S$
Small/Unmarked	-20.12	2.62	11.64	1.11	12.27	3.73
Medium/Unmarked	-19.01	1.42	11.00	1.35	12.22	4.18
Large/Unmarked	-16.83	2.16	12.17	1.10	12.62	2.70
Small/Hatchery	-19.36	0.39	12.36	0.31	15.43	1.07
Medium/Hatchery	-19.08	0.80	12.28	0.24	15.97	0.26
Large/Hatchery	-17.09	1.14	13.32	0.73	15.82	0.35

Month and Origin	Mean $\delta^{13}C$	SD $\delta^{13}C$	Mean $\delta^{15}N$	SD $\delta^{15}N$	Mean $\delta^{34}S$	SD $\delta^{34}S$
May/Unmarked	-20.49	1.25	11.10	1.11	11.39	5.22
June/Unmarked	-19.12	2.71	12.07	0.75	14.22	2.82
July/Unmarked	-18.70	1.46	10.37	1.36	9.36	2.55
May/Hatchery	-19.37	0.17	12.21	0.32	15.62	1.08
June/Hatchery	-19.16	0.65	12.34	0.17	15.77	0.52
July/Hatchery	-16.57	0.49	13.59	0.43	15.90	0.38

Source Group	Mean $\delta^{13}C$	SD $\delta^{13}C$	Mean $\delta^{15}N$	SD $\delta^{15}N$	Mean $\delta^{34}S$	SD $\delta^{34}S$
Freshwater insects	-26.04	2.09	2.35	2.14	6.23	2.64
Freshwater benthic/pelagic	-27.53	3.42	7.32	1.79	9.41	1.92
Transitional invertebrates	-21.82	1.55	9.05	1.58	15.89	2.61
Marsh insects	-21.30	1.28	7.98	1.28	10.21	2.35
Marsh benthic/pelagic	-16.64	2.28	8.78	1.57	16.38	2.44
Delta benthic/pelagic	-13.98	1.30	12.39	1.81	16.31	2.01
Hatchery food	-19.23	0.13	9.39	0.11	15.78	0.06

Table 2.3. Model output for a PERMANOVA procedure analyzing gravimetric measurements of juvenile Chinook salmon stomach contents by year (2014, 2015), origin (unmarked, hatchery), habitat type (FOR, EFT, EEM, DMF, EEL, NS), and size class (≤ 60 mm, 61–80 mm, 81–90 mm, 91–100 mm, > 100 mm). The AIC model selection criterion was calculated using the equation $k + n * (\ln\left(2\pi * (\frac{RSS}{n-k})\right) + 1)$ where *k* is the model degrees of freedom (*df*), *n* is the number of observations, and *RSS* is the residual sum of squares. The best-fit candidate model (Habitat*Origin) was only slightly better in fit than the additive model (Habitat + Origin; ΔAIC > 2).

Model	df	RSS	AIC	ΔAIC	Parameter	*F*	*P*
Year	1	80.88	412.75	43.95	Habitat	11.7	< 0.001
Origin	1	79.74	409.52	40.72	Origin	5.89	< 0.001
Habitat	5	66.09	374.76	5.96	Habitat*Origin	2.42	0.002
Size class	4	79.34	414.39	45.59			
Habitat + Year	6	65.82	375.83	7.03			
Habitat + Origin	6	64.43	370.99	2.19			
Habitat + Size class	9	63.75	374.68	5.88			
Habitat + Origin + Year	7	64.04	371.64	2.84			
Habitat + Origin + Size class	10	62.71	372.96	4.16			
Habitat + Origin + Size class + Year	11	62.08	372.71	3.91			
Habitat*Origin	11	61.03	368.80	0.00			
Habitat*Origin + Size class	15	58.96	369.18	0.38			
Habitat*Origin*Size class	44	48.95	389.15	20.35			

Table 2.4. Candidate linear mixed effects models analyzing catch per-unit effort (CPUE), stomach fullness (%), dietary energy density (ED; kJ/g), energy content (TEC; kJ), and condition index in unmarked and hatchery Chinook salmon. Sampling station was included as a random effect for all models, and fork length (mm) was a covariate for TEC. The best-fit model(s) had a ΔAIC value < 2 (italics).

		CPUE		Stomach fullness		ED	
Model	df	AIC	ΔAIC	AIC	ΔAIC	AIC	ΔAIC
Year	1	1352.85	226.80	526.09	11.91	392.92	4.82
Year*Month	8	1336.55	210.50	528.94	14.76	405.52	17.42
Habitat	5	1350.33	224.28	531.98	17.80	399.92	11.82
Origin	1	1314.59	188.54	*514.18*	*0.00*	*388.10*	*0.00*
Origin + Habitat	6	1315.03	188.98	524.27	10.09	399.21	11.11
Origin + Year	2	1318.32	192.27	517.27	3.09	392.34	4.24
Origin + Month	5	1297.73	171.68	*515.93*	*1.75*	401.64	13.54
Origin + Year*Month	9	1299.02	172.97	518.90	4.72	404.06	15.96
Origin*Habitat	11	1294.48	168.43	522.53	8.35	410.13	22.03
Origin*Year	3	1313.84	187.79	520.74	6.56	391.98	3.88
Origin*Month	9	1160.58	34.53	518.17	3.99	399.61	11.51
Origin*Year*Month	17	1163.15	37.10	524.07	9.89	406.32	18.22
Origin*Month*Habitat	59	*1126.05*	*0.00*	522.85	8.67	424.82	36.72

		TEC		Condition index	
Model	df	AIC	ΔAIC	AIC	ΔAIC
Year	1	1070.79	72.52	*-422.19*	*0.99*
Year*Month	8	1061.24	62.97	-378.22	44.96
Habitat	5	1071.42	73.15	-393.03	30.15
Origin	1	1058.36	60.09	*-423.18*	*0.00*
Origin + Habitat	6	1060.42	62.15	-387.30	35.88
Origin + Year	2	1060.65	62.38	-419.40	3.78
Origin + Month	5	1049.47	51.20	-389.64	33.54
Origin + Year*Month	9	1048.04	49.77	-374.57	48.61
Origin*Habitat	11	1054.33	56.06	-356.14	67.04
Origin*Year	3	1060.34	62.07	-411.99	11.19
Origin*Month	9	1045.57	47.30	-378.52	44.66
Origin*Year*Month	17	1043.49	45.22	-350.95	72.23
Origin*Month*Habitat	59	*998.27*	*0.00*	-229.10	194.08

Figures

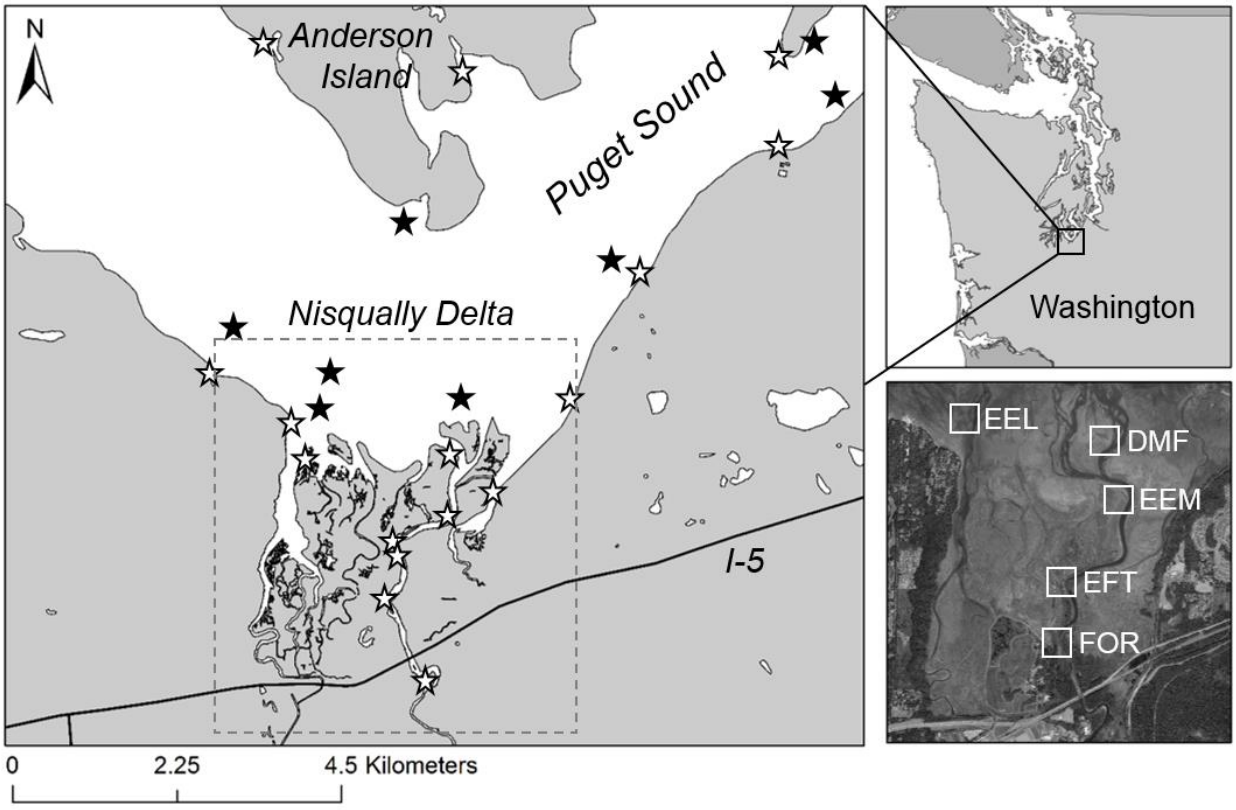

Figure 2.1. Map showing 2014/2015 beach seine (white stars) and lampara net (black stars) sampling stations for juvenile Chinook salmon in the Nisqually River delta, Washington, USA. Fish captured in beach seines were used for stomach content analysis and stable isotopes. Fish captured in lampara nets were used for stable isotopes only. Inset at bottom right shows stable isotope sampling locations for invertebrate prey sources in forested (FOR), transition (EFT), emergent salt marsh (EEM), delta mudflat (DMF), and eelgrass (EEL) habitats.

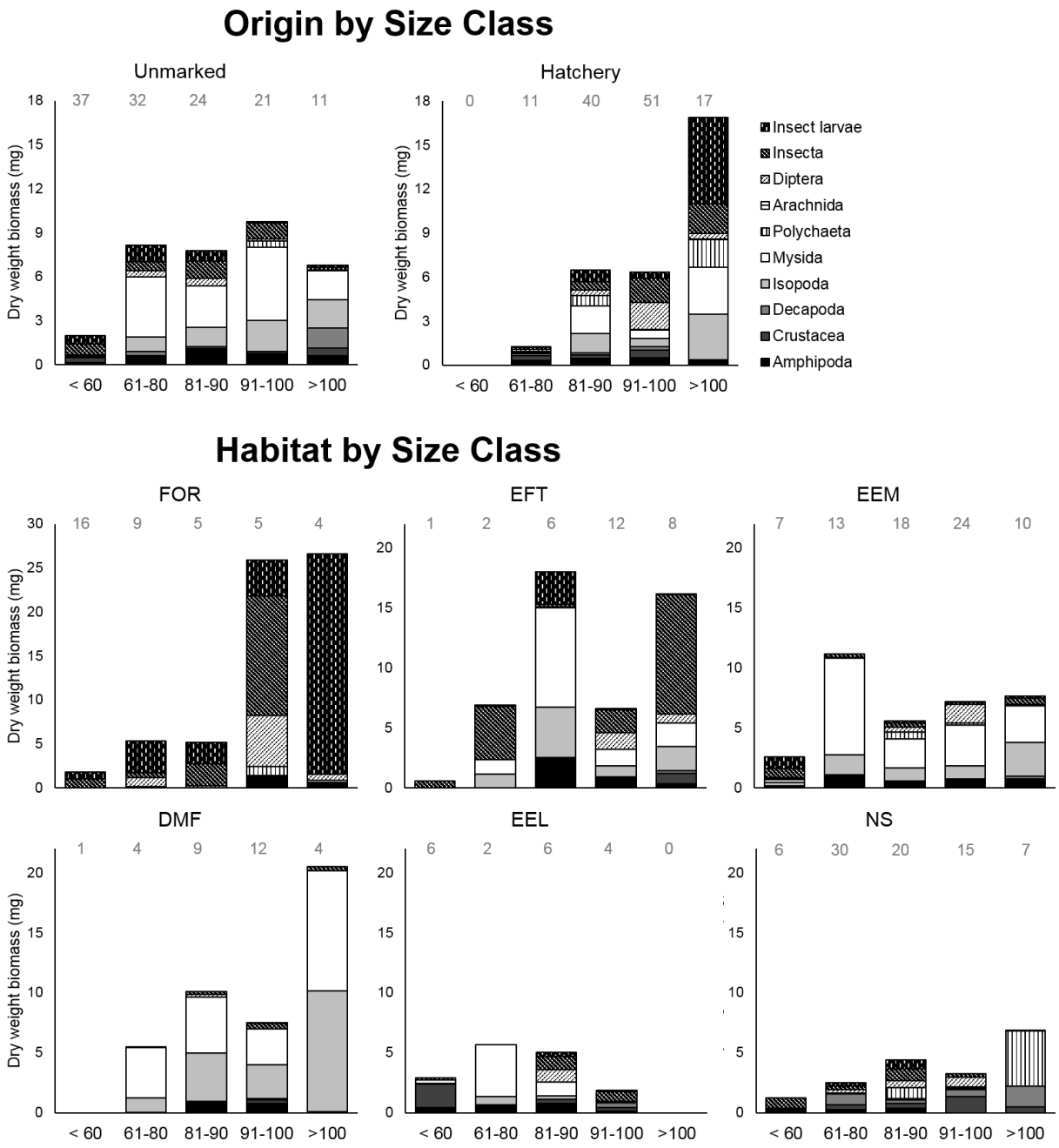

Figure 2.2. Bar plots showing juvenile Chinook salmon gravimetric diet composition by origin and size class (top), and habitat and size class (bottom). Data are presented as proportion dry weight biomass (DWB), with values averaged across stomach samples (gray numbers across top).

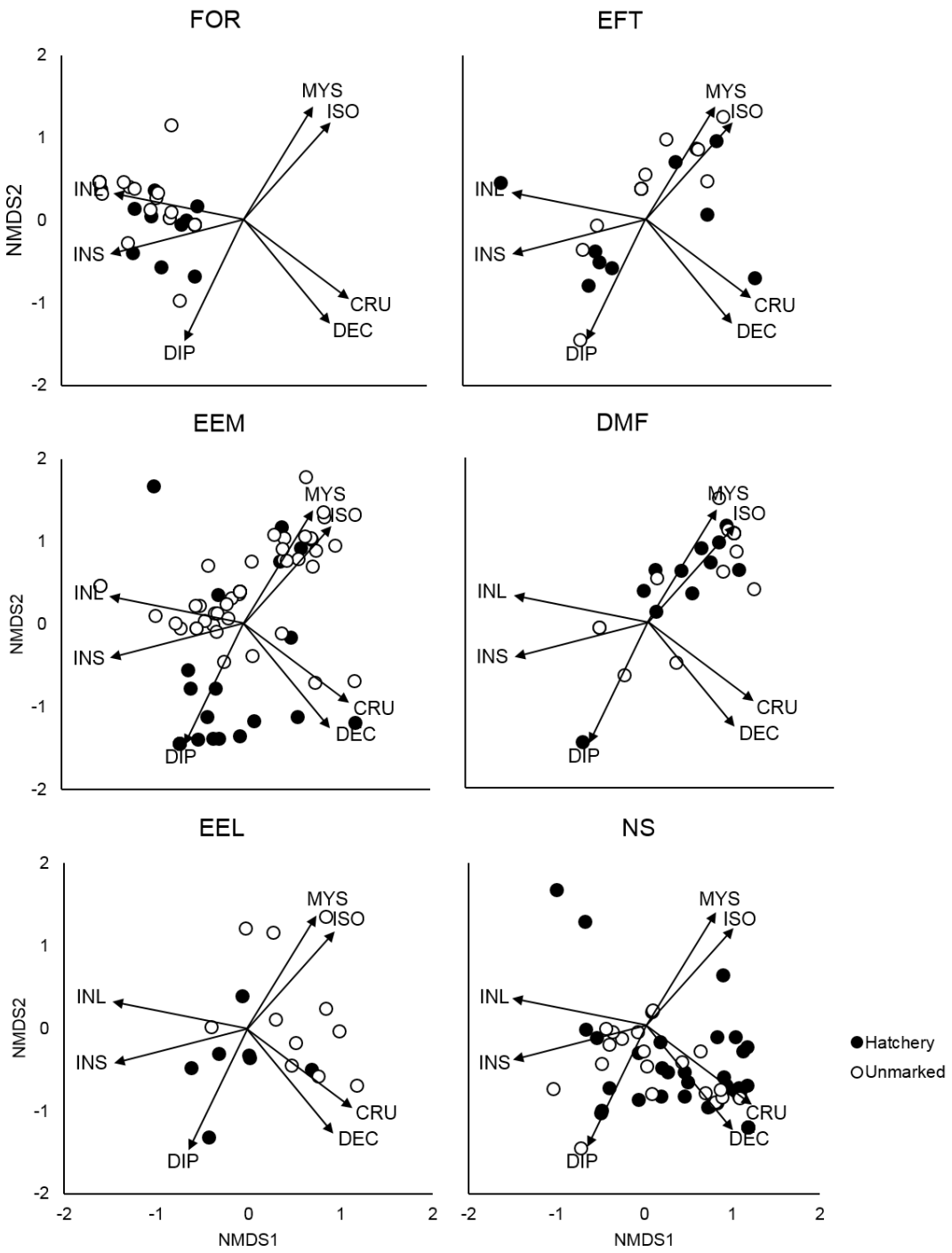

Figure 2.3. NMDS ordination biplots showing the position of unmarked and hatchery diets in ordinated space. Plots are split by habitat for ease of visualization. Species labels show taxa with significant ($P < 0.001$) loadings on NMDS axes 1 and 2, including dipterans (DIP), non-dipteran insects (INS), insect larvae (INL), mysids (MYS), isopods (ISO), decapod larvae (DEC) and crustaceans (CRU).

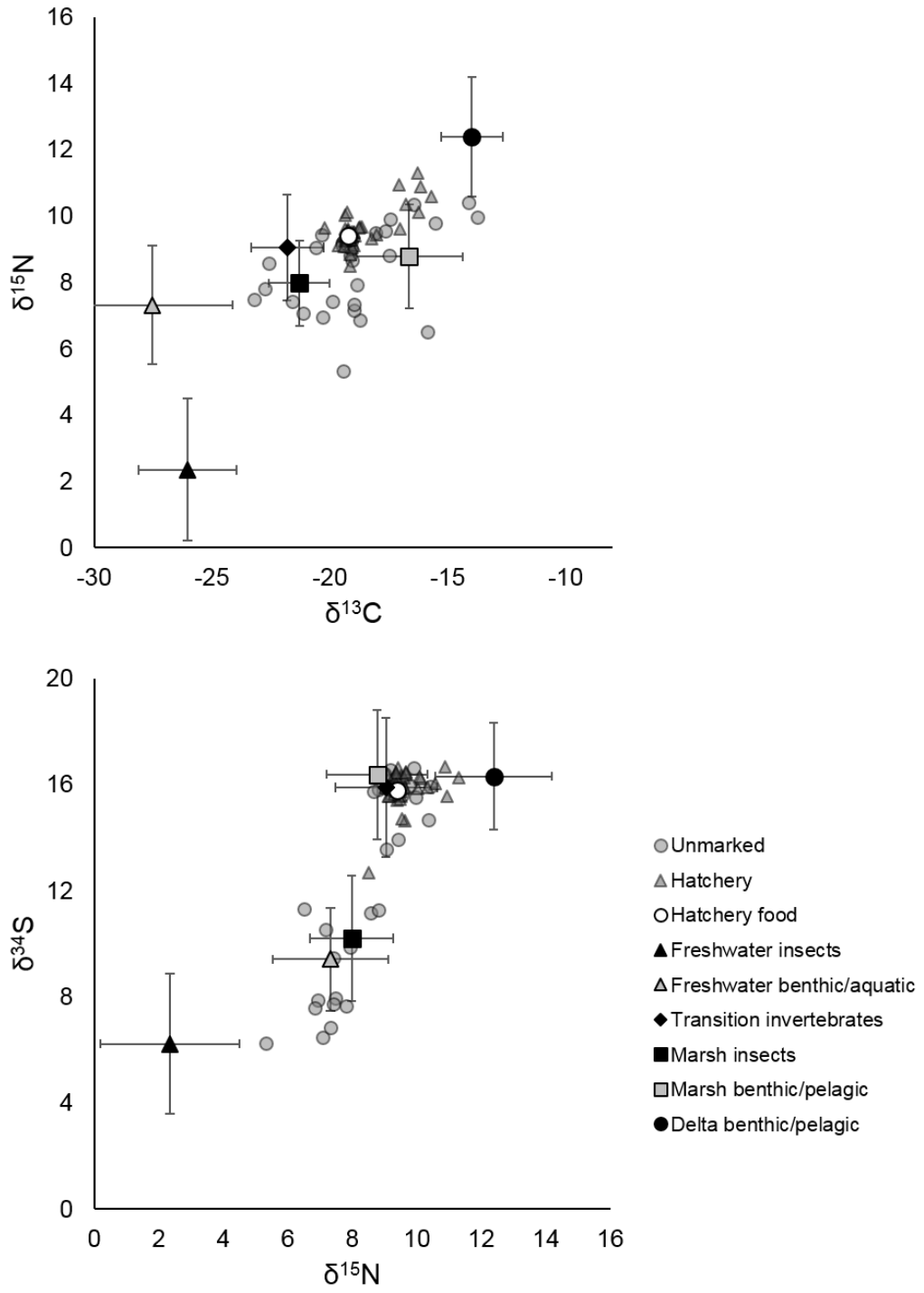

Figure 2.4. Mean ± SD stable isotope signatures of prey sources and individual unmarked (n = 32) and hatchery (n = 36) juvenile Chinook salmon. The top plot shows $\delta^{13}C$ and $\delta^{15}N$. The bottom plot shows $\delta^{15}N$ and $\delta^{34}S$. Source groupings can be found in Table A2.2.

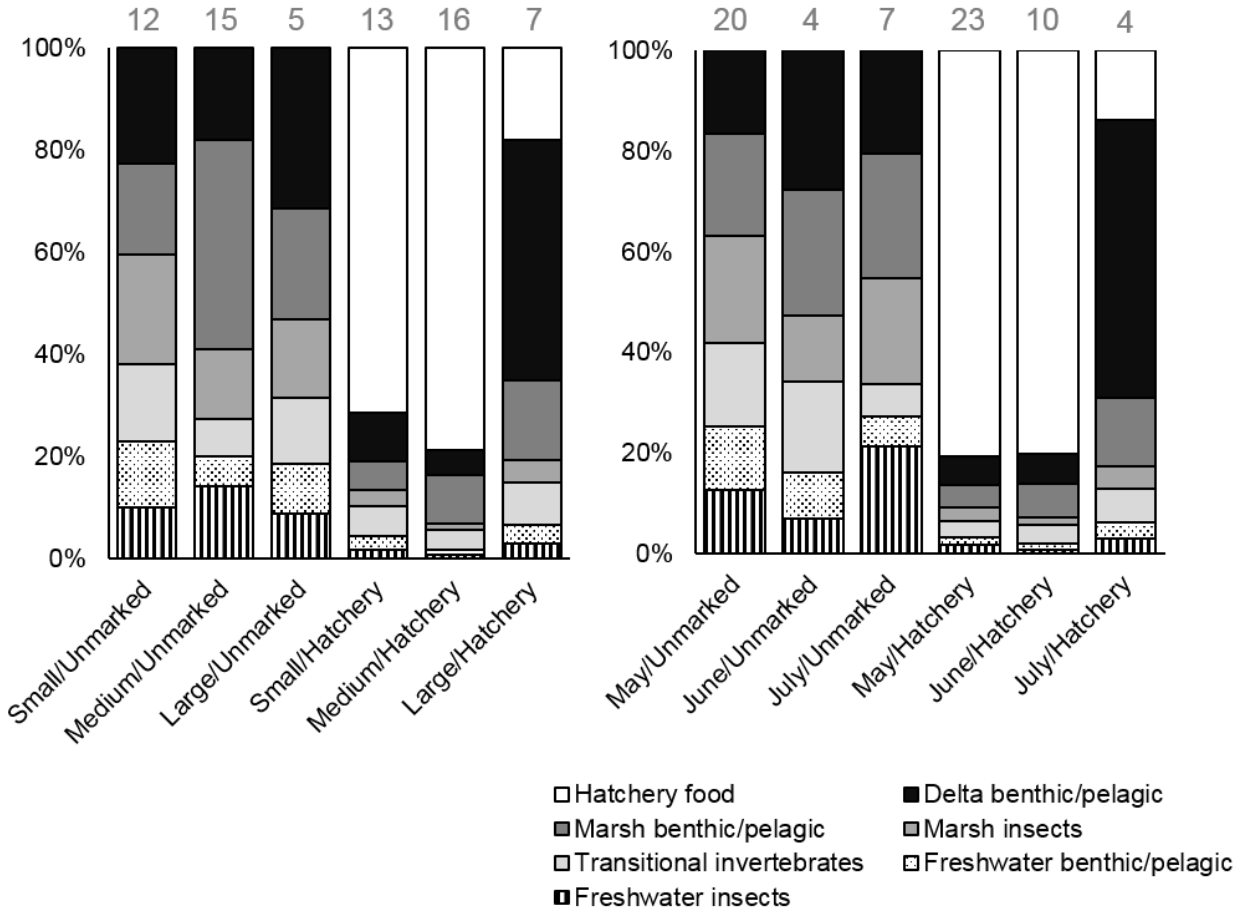

Figure 2.5. Proportion dietary composition as predicted from a stable isotope mixing model for juvenile Chinook salmon grouped by origin and size (small: < 90 mm, medium: 91–100 mm, large: > 100 mm; left), and origin and month of capture (right). Sample sizes are denoted as gray numbers at the top of each bar.

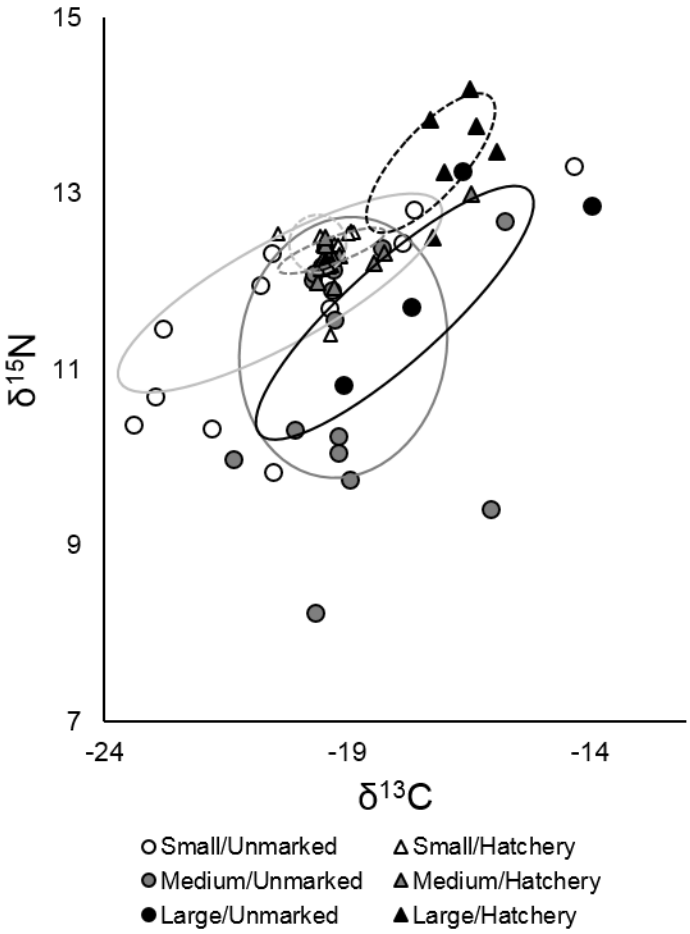

Figure 2.6. Trophic ellipse areas (SEA_C; ‰^{2}) for small (< 90 mm), medium (91–100 mm), and large (> 100 mm) juvenile Chinook salmon. Unmarked fish are represented by solid-lined ellipses and hatchery fish are represented by dashed ellipses. Points represent $\delta^{13}C$ and $\delta^{15}N$ values for individual fish. Metrics were calculated using the "SIBER" package in R 3.4.1.

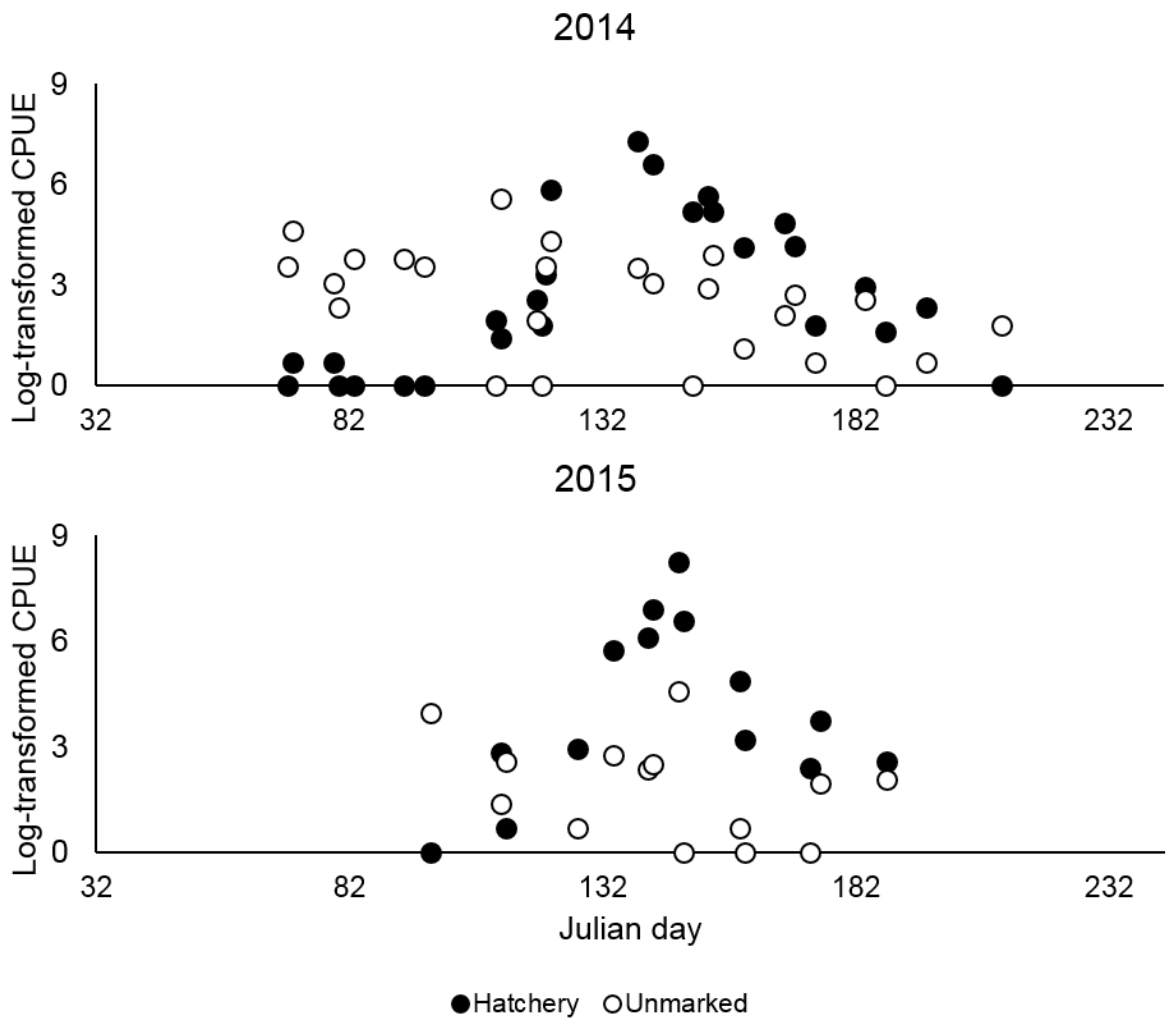

Figure 2.7. Total catch-per-set (CPUE) by sampling date of unmarked and hatchery juvenile Chinook salmon in 2014 (top) and 2015 (bottom).

Appendix: Additional tables and figures

Table A2.1. Sample sizes for unmarked and hatchery juvenile Chinook salmon across years, months, and habitat types. The number of fish analyzed is shown for diet and body condition (top), and stable isotopes (bottom).

	2014					2015				
Habitat	March	April	May	June	July	March	April	May	June	July
Unmarked										
FOR	7	2	8	9	2	0	0	0	0	0
EFT	1	0	0	3	1	0	0	4	0	0
EEM	7	3	2	1	12	0	0	13	1	5
DMF	0	5	1	0	2	0	0	1	3	2
EEL	6	0	4	0	0	0	0	1	0	0
NS	6	2	5	5	0	0	0	1	0	0
Hatchery										
FOR	0	0	1	9	0	0	0	0	1	0
EFT	0	0	2	1	0	0	0	10	2	0
EEM	0	0	14	4	0	0	0	9	1	0
DMF	0	0	1	2	1	0	0	7	5	0
EEL	0	0	4	1	0	0	0	1	1	0
NS	0	0	10	12	0	0	0	16	3	1

Size and Origin	N	Month and Origin	N
Small/Unmarked	12	May/Unmarked	20
Medium/Unmarked	15	June/Unmarked	4
Large/Unmarked	5	July/Unmarked	7
Small/Hatchery	13	May/Hatchery	23
Medium/Hatchery	16	June/Hatchery	10
Large/Hatchery	7	July/Hatchery	4*

*Includes three hatchery individuals captured on 6/24/2015, which is temporally distinct from June samples, the majority of which were captured on 6/8/2015.

Table A2.2. Stable isotope source groupings, including number of invertebrate samples processed and location of capture.

Taxon	FOR	EFT	EEM	DMF	EEL
Freshwater insects					
Aphidae	2				
Araneae	1				
Cicadellidae	1		1		
Coccinellidae	1				
Coleoptera	1				
Hymenoptera	2				
Lepidoptera	1				
Sciomyzidae	1				
Freshwater benthic/pelagic					
Ampithoe sp.	1				
Araneae	1				
Brachycera	2				
Chironomidae	4	1			
Cicadellidae		1			
Ephydridae	1	4			
Fish larvae	1				
Lepidoptera		1			
Neanthes sp.	3				
Neomysis mercedis	2				
Trichoptera larvae	1				
Transitional invertebrates					
Ampithoe sp.		2	1		
Araneae		2	1		
Corophiidae		3			
Dolichopodidae		1			
Gnorimosphaeroma oregonensis		2			
Lygaeidae		1			
Neanthes sp.		2			
Saldidae			1		
Marsh insects					
Ceraptogonidae pupae		1			
Chironomidae larvae	2	2			
Cicadellidae			1		
Corophiidae	1				
Dolichopodidae	8	1	2		
Ephydridae	2		4		
Muscidae		1			
Neanthes sp.	1				
Saldidae	2				
Tipulidae		1	1		
Trichoptera larvae	3				
Marsh benthic/pelagic					
Ampithoe sp.		1	4	1	3

Ceraptogonidae larvae		1			
Chironomidae larvae		1			
Corophiidae		1	3	1	1
Cumacea		1			2
Dolichopodidae larvae		1			
Gnorimosphaeroma oregonensis		1	3		
Harpacticoida			1		
Neanthes sp.		1	1		
Neomysis mercedis	1				
Spionidae				2	
Tanaidacea					1
Delta benthic/pelagic					
Ampithoe sp.				1	
Corophiidae	1		3	2	2
Crangon nigricauda					3
Eogammarus sp.					1
Eteone sp.				5	1
Glycera nana					2
Goniada brunea					2
Harpacticoida					1
Neanthes sp.				2	1
Neomysis mercedis	4	4	3	6	2
Phyllodocidae					1
Sabellidae					1
Spionidae				3	

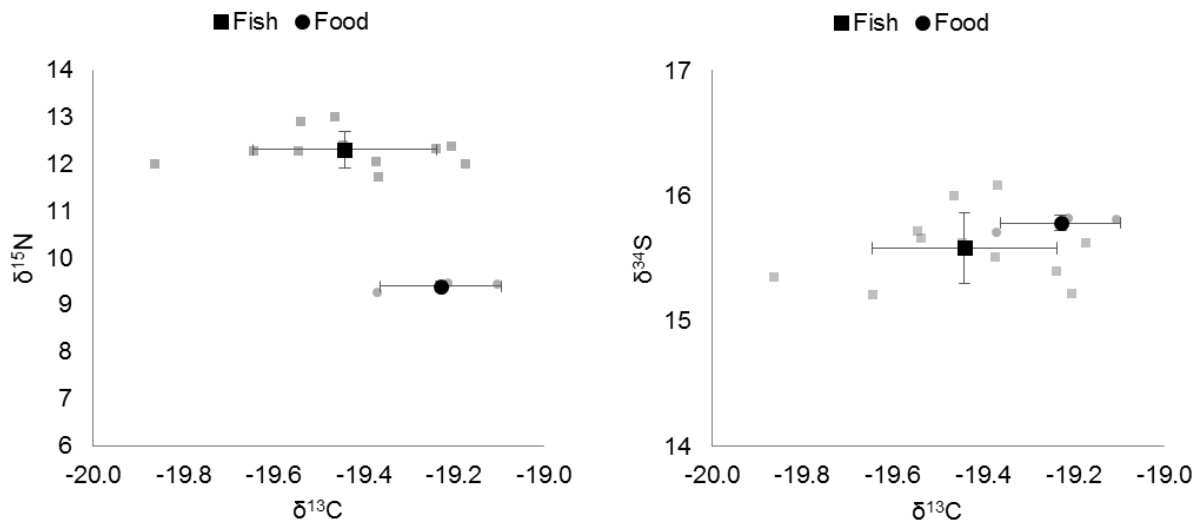

Figure A2.1. Scatterplots of $\delta C^{13}/\delta N^{15}$ (left) and $\delta C^{13}/\delta S^{34}$ (right) signatures for juvenile Chinook salmon captured in Clear Creek hatchery ponds and their food. Gray dots represent raw data and black dots represent group means ± SD. Because hatchery fish are reared exclusively on hatchery food, we used the magnitude of differences between carbon, nitrogen, and sulfur signatures to derive trophic enrichment factors (TEFs).

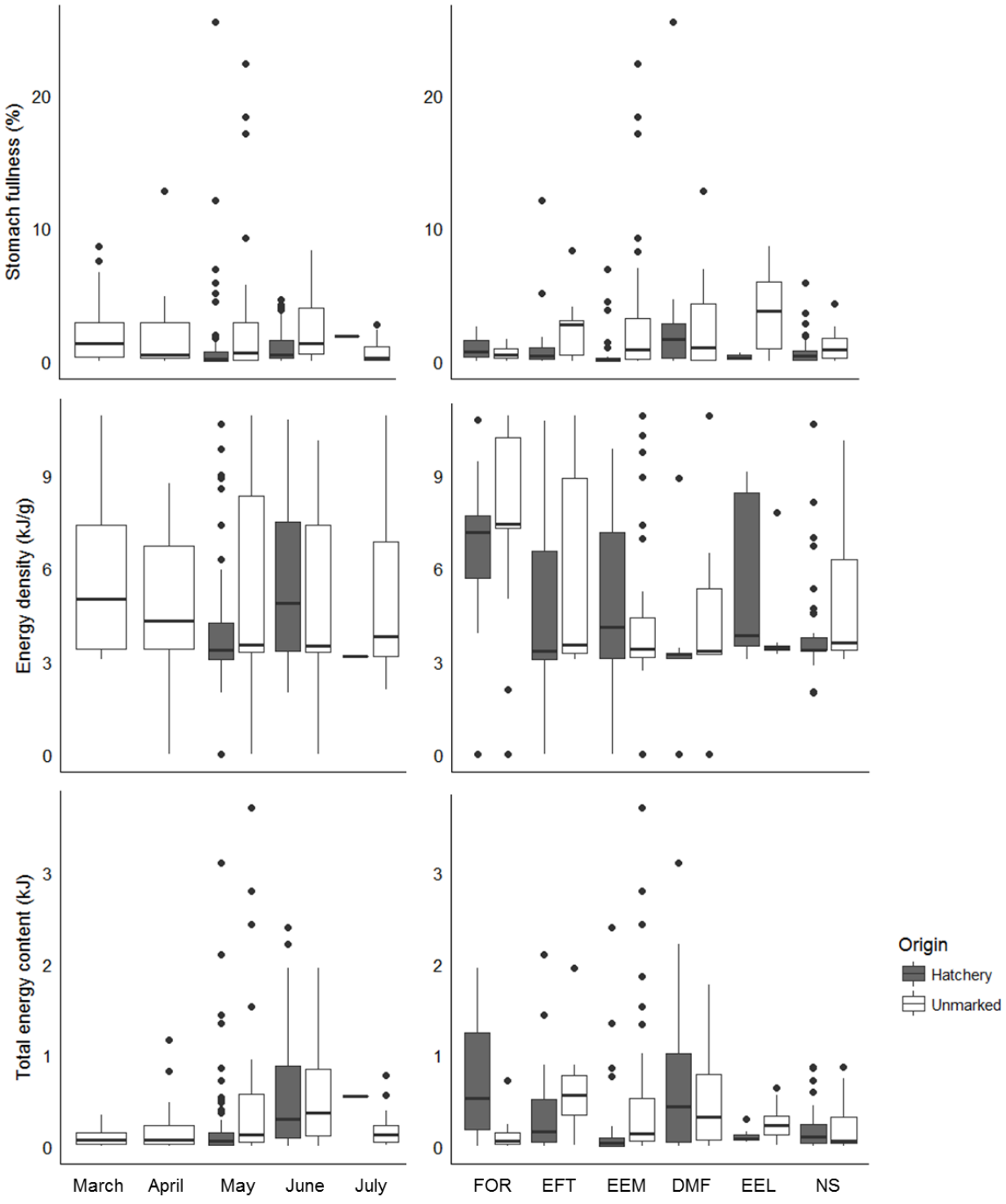

Figure A2.2. Box and whisker plot of juvenile Chinook salmon stomach fullness (%), dietary energy density (ED; kJ/g), and total energy content (TEC; kJ) by month (left) and habitat type (right). Values are averaged across years.

Chapter 3

Freshwater tidal forests and estuarine wetlands may confer early-life growth advantages for delta-rearing Chinook Salmon

Abstract

Large river deltas are complex ecosystems that are believed to play a pivotal role in promoting the early marine growth and survival of threatened Chinook Salmon *Oncorhynchus tshawytscha*. We used a fish bioenergetics model to assess the functional role of multiple delta habitats across a gradient of salinities and vegetation types, where consumption and growth rate potential (GRP) were considered as proxies for habitat quality. We subsequently compared our model output to empirical, or *realized*, growth estimates from scale circuli. In terms of consumption, prey energy density (ED_{prey}) was 46–86% higher in tidal freshwater forest than in any other habitat type, while estimated consumption rates (expressed as proportion of maximum daily consumption; P_{cmax}) were positively correlated with fork length. These size-related differences in P_{cmax} led to a noticeable increase along a freshwater-to-saline gradient from roughly 0.25 in tidal freshwater forest to 0.55 in the offshore subtidal zone, yet despite higher observed P_{cmax} values in nearshore and offshore habitats, the tidal freshwater forest and emergent salt marsh demonstrated the highest modeled GRP values. Similarly, realized growth rates for fish caught in tidal freshwater forest were up to 0.5% higher per-day than for fish caught in the offshore area, but habitat-level differences were overshadowed by allometry and rearing origin. Scales from unmarked fish (assumed to be of wild origin) indicated that they grew 11% faster on average than hatchery fish; however, these differences were subtle and were more obvious at fork lengths < 100 mm. Our results suggest that tidal forests and emergent marshes may offer early-life growth advantages

for wild Chinook Salmon, but that wild and hatchery fish can compensate as they move seaward by opportunistically consuming greater quantities of low-ED prey, taking advantage of pulses of larval forage fish, or by spending time in multiple interconnected habitat types.

Introduction

Juvenile Pacific Salmon *Oncorhynchus* spp. must overcome multiple physiological hurdles to survive their first year of life. One of the most important of these hurdles is the early marine "critical period" for growth and survival (Beamish and Mahnken, 2001). Juveniles that cannot achieve a sufficient size during their migration to the sea are more susceptible to predation and are less likely to make it through their first winter (Healey 1982; Beamish et al. 2004; Cross et al. 2008). For many federally-endangered subpopulations of Chinook Salmon *O. tshawytscha*, much of this critical period is spent in coastal habitats such as nearshore intertidal zones, emergent marshes, and other estuarine tidal wetlands (Healey 1991; Thorpe 1994; Magnusson and Hilborn 2003). As such, shoreline modifications and the loss of wetlands to urban development, agriculture, and engineered barriers along the Pacific coast represent a tangible threat to the viability of the Chinook Salmon (Simenstad and Cordell 2000; Greene et al. 2012; David et al. 2016).

Practitioners have recognized the need to restore and enhance suitable nursery habitats for salmon and other ecologically important fishes. This is especially true for productive delta and estuarine ecosystems, which play a vital role in transporting nutrients, allochthonous prey resources, and fish from land to sea (Simenstad and Cordell 2000; Simenstad et al. 2002; Sheaves 2009). In coastal river deltas, management efforts are often focused on emergent salt marshes, even though riverine floodplains, freshwater tidal areas, eelgrass beds, and nearshore

beaches also provide unique nursery benefits for juvenile Chinook Salmon (Sommer et al. 2001; Semmens 2008; Marin et al. 2009; Sheaves et al. 2015; Davis et al. 2018*a*). These habitat types are rarely studied concurrently with regard to their accessibility, thermal range, prey availability, and potential for conspecific or interspecific competition (Simenstad et al. 2002; Fig. 3.1). Furthermore, the uncertainty surrounding each habitat type's relative utility as nursery habitat is compounded by the remarkable life history diversity of the juvenile Chinook Salmon, which exhibits yearly variation in migration timing and habitat use depending on environmental conditions (Healey 1991; Simenstad et al. 1982; Schindler et al. 2010; Bourret et al. 2016). Despite advances, more information is needed to establish how a diverse gradient of estuarine habitat types contributes to the growth of a population of Chinook Salmon as it moves through its natal river delta.

For fish, growth is determined by the quantity of prey consumed, the energetic quality of those prey, and thermal constraints on respiration and metabolism (Kitchell et al. 1977; Neilson et al. 1985; Boisclair and Leggett 1989; Beauchamp 2009). Juvenile Chinook Salmon can opportunistically eat terrestrial insects, benthic and pelagic crustaceans, and other fish, all of which vary widely in abundance and energy content (Pearce et al. 1982; Gray et al. 2002; Duffy et al. 2010). Consequently, the quality of their diet is dependent on the type and quantity of prey in their surrounding environment (Davis et al. 2018*b*). Insects tend to have the highest energy densities (~8,000–13,000 J/g; Gray 2005; David et al. 2014), but they are only available when they enter the water column as they emerge from their pupal stages or as drift after falling from the terrestrial realm above the surface. Conversely, aquatic crustaceans are more easily accessible in the benthic and pelagic zone, with greater productivity in saline environments; however, their energy densities are far lower (2,500– 4,500 J/g). Juvenile Chinook Salmon may

encounter these consumption tradeoffs as they forage in different habitats (Fig. 3.1). For example, terrestrial insects may be found more frequently in tidal marshes with overhanging riparian vegetation and a connected terrestrial-aquatic interface, where a shady canopy helps regulate late-season temperatures (Balling and Resh 1991; Romanuk and Levings 2003; Broadmeadow et al. 2011). Meanwhile, open mudflats and nearshore intertidal zones might produce large quantities of aquatic crustaceans over a broader spatial extent and have areas that are still accessible at low tide (Levy and Northcote 1982; Soetaert and Rijswijk 1993; Chittenden et al. 2018). As such, differences in how juvenile Chinook Salmon forage throughout the delta habitat mosaic may have important, long-term consequences for their growth and survival.

Although a comprehensive assessment is difficult, some of these tradeoffs among different delta habitat types can be evaluated using bioenergetics models. Bioenergetics modeling incorporates empirical values of temperature and diet to calculate a growth rate potential (GRP) for fish using given habitat conditions (Kitchell et al. 1977; Hanson et al. 1997). Such modeling can inform estimates of relative habitat quality for fish of different size classes, rearing origins (i.e., wild or hatchery origin), and life history strategies. We used a bioenergetics model combined with empirical measurements of somatic growth to assess the relative contribution of multiple habitat types to the composite functional capacity of the Nisqually River delta in southern Puget Sound, Washington, USA.

The Nisqually River delta is part of one of the largest, most diverse, and most protected watersheds in Puget Sound, making it an optimal site at which to conduct our analyses. It is also the location of a ~360 ha estuarine restoration project, with newly-restored tidal marsh adding to a varied mosaic of delta habitats (see Ellings et al. 2016, Davis et al. 2018*a*). Previous studies in the restoring and unaltered tidal marshes have suggested that areas where the terrestrial-aquatic

interface is most connected may produce the highest salmon GRP (David et al. 2014; Davis et al. 2018*b*; Woo et al. 2018). We also expected that growth measured from scale circuli would serve as a mechanism to assess the functional capacity of the delta based on the amalgamated use of multiple delta habitat types over several days. Below we describe our expanded analyses, which identify high-priority areas for promoting the growth and survival of juvenile Chinook Salmon, and may inform management decisions related to the restoration and enhancement of coastal habitats.

Methods

Field sampling

The Nisqually Indian Tribe and partners conduct biweekly fish surveys each year in the Nisqually River delta as part of a standard monitoring protocol (Hodgson et al. 2016). We collected juvenile Chinook Salmon from 29 sites that were consistently surveyed by the Tribe in 2014 and 2015. We focused our efforts on juveniles captured during the height of the out-migration season (March–July) when salmon densities were highest. We used a beach seine or lampara net to capture fish in habitats positioned along a freshwater-to-saltwater gradient, including tidal freshwater forest, brackish transitional marsh, emergent salt marsh, delta mudflats, and intertidal nearshore areas (Fig. 3.2). Additionally, as part of the Salish Sea Marine Survival Project, we supplemented biweekly surveys with samples collected from the offshore subtidal zone using a purse seine. Survey methods are described in detail in Davis et al. 2018*a* and Gamble et al. (2018).

We counted all fish captured (including non-target species), but we limited lethal samples to ten unmarked and ten hatchery-marked juvenile Chinook Salmon from each set. After capture,

we recorded each fish's fork length, weight, and rearing origin. Rearing origin was determined using fin clips, coded wire tags, and thermal otolith marks. These markings are used as indications of rearing origin with an average accuracy of 97.5% at Nisqually hatcheries (Regional Mark Information System; http://www.rmpc.org/home.html). Because there was a possibility of biasing our results by mis-representing an unmarked hatchery fish as a natural-origin fish, we categorized all unmarked individuals as "unmarked" rather than "wild" for our analyses.

Sample fish were euthanized with buffered tricaine methanesulfonate (MS-222) and stored on ice in the field. Upon return to the lab, we removed and stored whole stomachs in 70% ethanol and shipped them to the U.S. Geological Survey San Francisco Bay Estuary Field Station or the University of Washington for processing. The remaining carcasses were preserved in ethanol and frozen for scale, otolith, and genetic analyses. Overall, we processed 236 diet and 452 scale samples in 2014, and 81 diet and 64 scale samples in 2015 (Table A3.1). We limited our analysis to subyearling juvenile Chinook Salmon with fork lengths ranging between 40 mm and 140 mm. Likewise, any fish with a coded wire tag indicating that Nisqually was not its natal watershed was not used in our analysis (n=33).

Bioenergetics model

We used a Wisconsin bioenergetics model (Fish 4.0; Hanson et al. 1997; Deslauriers et al. 2017) to: 1) estimate the proportion of the maximum daily consumption rate (P_{cmax}) for each individual fish; 2) calculate a range of monthly GRP values using observed temperatures and varying P_{cmax} inputs; and, 3) simulate growth through time for juvenile salmon in a single habitat type. These

simulations integrated empirical measurements of water temperature, size, and prey quality to capture multiple facets of each habitat type with respect to its relative functional capacity.

The bioenergetics model relies on the mass balance equation $G = C - R - SDA - F - U$, where *G* is growth, *C* is the quantity and type of food consumed, *R* is respiration, *SDA* is specific dynamic action (the metabolic cost of processing food), *F* is egestion, and *U* is excretion. Consumption and respiration are dependent on thermal experience, prey energy density (ED_{prey}), consumer energy density (ED_{fish}), and the quantity of food consumed relative to fish body size (Ware 1978; Trudel et al. 2004). Egestion and excretion are expressed as a proportional value of consumption, and account for the total amount of indigestible material in fish diets. The model is usually run on a daily time step to estimate GRP or consumption rate. We input water temperature, fish weight, and ED_{prey} to solve for P_{cmax} and conduct the GRP simulations. We also input an ED_{fish} value of 4,085 J/g based on bomb calorimetry of 16 unmarked and hatchery juvenile Chinook Salmon from the Nisqually River delta (SD < 200 J/g; David et al. 2014). We used Stewart and Ibarra's (1991) parameter values, which were adapted for Chinook Salmon from a Coho Salmon bioenergetics model. Although these parameters were originally calibrated for adult fish, they have accurately predicted juvenile Chinook Salmon growth in laboratory and environmental settings (Brodeur et al. 1992; Madenjian et al. 2004). Recent studies have found that Stewart and Ibarra's (1991) parameters overestimate the metabolic consequences of higher temperatures on subyearling Chinook Salmon, so we used modified temperature-dependent consumption parameters (Plumb and Moffitt 2015) when simulation temperatures were > 18˚C to minimize parameter error (Table A3.2).

Water temperature

We used continuous temperature data from Solinst LTC Leveloggers® (Solinst, Georgetown, Ontario, Canada) to measure the thermal experience of juvenile Chinook Salmon from March 1 through July 31. One logger was installed in each habitat type except for in the offshore zone, where we used publicly available sea surface temperature data from an Oceanic Remote Chemical Analyzer (ORCA) buoy in Case Inlet (https://orca.ocean.washington.edu). We installed data loggers along the Nisqually River mainstem in tidal freshwater forest, in blind channels running through the transitional and emergent salt marshes, and at the southern edge of the mudflat and nearshore intertidal areas (Fig. 3.2). When processing the data, we removed extraneous temperature values and measurements that we interpreted to occur when the logger was exposed to the air or buried in sediment. Mean daily water temperature was estimated for the 2014 and 2015 out-migration seasons by calculating the average temperature over a 24-hour period, starting at midnight. We interpolated missing data using a regression of water temperature and air temperature (https://www.ncdc.noaa.gov/data-access/land-based-station-data). Such statistical methods are a simple, commonly used way of predicting water temperatures in lakes, rivers, and other bodies of water (Morril et al. 2005; Sharma et al. 2008).

Diet and individual consumption

We derived dietary inputs from juvenile Chinook Salmon stomach contents. We used a stereo-dissection microscope at a magnification range of 7–45× to identify and enumerate prey items from stomach samples to family, genus, or species. For each sample, we measured the wet weight biomass of identifiable taxa by weighing them separately on a 0.1-mg precision scale. We identified 71 taxa, which we grouped into 18 broader functional categories with similar ED_{prey} values for ease of analysis (Table 3.1). Detailed descriptions of habitat and rearing origin-level

dietary differences can be found in Davis et al. (2018*a*). Indigestible material was omitted from the bioenergetics analysis, and digested or unidentifiable material was assumed to have an equivalent gravimetric (i.e., proportional biomass) composition to the rest of the diet sample.

We analyzed the proportional gravimetric composition of juvenile Chinook Salmon stomach contents to derive information on ED_{prey}. We calculated the average energy density (J/g) of each fish's stomach contents as:

$$ED_{prey} = \sum p_i ED_i$$

where p_i is the proportional gravimetric contribution of prey taxon i to sample biomass and ED_i is the energy density of taxon i. To account for individual variation when calculating GRP curves, we averaged ED_{prey} by month, habitat type, and rearing origin. We also evaluated the stomach fullness, or instantaneous ration (IR), of each fish using the equation:

$$IR\ (\%) = 100 \times \frac{stomach\ contents\ (g)}{weight\ (g) - stomach\ contents\ (g)}$$

We estimated individual P_{cmax} values using the bioenergetics model, where model inputs included mean daily temperature on date of capture, weight, ED_{prey}, and scale-derived growth rate. Group averages of estimated individual P_{cmax} (hereafter referred to as P_{obs}) were analyzed as described below and used as inputs for the GRP simulations. Because unmarked and hatchery fish exhibit distinct differences in size, residence times, and diets (Chittenden et al. 2018; Davis et al. 2018*a*, 2018*b*), we grouped P_{obs} by rearing origin, habitat type, and month for calculating habitat-specific ranges of GRP (Table 2.2).

We used a linear mixed effects model to analyze trends in ED_{prey} and IR. Habitat type, rearing origin, year, and month were included as fixed effects, while sampling site was included as a random effect. We analyzed P_{cmax} using an analysis of variance (ANOVA) because the

random effect of sampling site was several magnitudes smaller than the residual error of the model, thus indicating that its inclusion would not improve model fit. We applied an exploratory stepwise model selection procedure to each response variable whereby additive and interactive terms were sequentially added to the model, avoiding four-way interactions which are difficult to biologically interpret. In some model iterations we added fork length or catch-per-set as covariates to account for size-specific dietary differences and density effects. We used pseudo R^2, root mean-square-error (RMSE), and Akaike's Information Criterion (AIC; Burnham and Anderson 2002) as model selection criteria such that an increase in model R^2, a decrease in RMSE, and/or a decrease in AIC > 2 was considered an improvement in model goodness of fit. For significant month and habitat effects, we used a Tukey's HSD post-hoc test to compare pairwise among-group differences. All statistical analyses were conducted in R 3.4.1 (R Core Development Team 2017), and linear mixed effects models were run using the "lme4" package.

Growth rate potential simulations

We calculated a range of GRP estimates ($g \cdot g^{-1} \cdot d^{-1}$) for unmarked and hatchery juvenile Chinook Salmon in each month/habitat group for which data were available from more than three fish (Table 2.2). We simulated GRP across a full range of observed daily temperatures (30–31 data points per simulation), using P_{cmax} values of 0.2, 0.4, 0.6, or P_{obs}. This allowed us to assess the effects of monthly temperature fluctuations and variable consumption rates on GRP, which we used as a broad indicator of habitat quality. We are confident that the diet and temperature inputs for our bioenergetics model of GRP were specific to each habitat type; however, we calculated P_{obs} using data from scales, which may reflect foraging in multiple habitat types over the course

of a single week prior to capture (Gamble et al. 2018). Therefore, we calculated GRP using several P_{cmax} values that were held constant across habitat types in addition to P_{obs}.

We also used the bioenergetics model to conduct a simulation exercise whereby fish weight was modeled on a daily time step from March 1 through July 31. We ran this exercise separately for each habitat type in each year. In our model, unmarked fish "entered" the delta on March 1 at a weight of 0.75 g, while hatchery fish were "released" on May 1 at 5 g. Instead of using habitat-specific monthly average values, we linearly interpolated ED_{prey} on a daily time step. For missing month/habitat combinations, we used average ED_{prey} for all fish sampled in that habitat. We ran the simulation separately for P_{cmax} values of 0.2, 0.4, 0.6, and P_{obs} to determine which habitats predicted optimal or realistic weights at the end of the out-migration season. We used these simulations to compare growth trajectories among habitat types, years (2014, 2015), and fish of different rearing origins.

Realized growth

Scale radii grow proportionally with respect to fish length, where circuli (rings) are added at a relatively constant rate through time during the growing season (Casselman 1990; Courtney et al. 2000; Cross et al. 2008). It follows that scales can be used to accurately measure relative somatic growth at specific intervals within a given population. We used back-calculated growth measurements from scales to estimate P_{obs} (as described above) and to compare to predicted GRP curves from our bioenergetics model. Scale samples were processed according to methods outlined in Gamble et al. (2018). We used the two most recent complete scale circuli to back-calculate the fork length and weight of each fish using the Fraser-Lee method (Pierce et al. 1996; Martinson et al. 2000). We then converted these back-calculated fork length estimates to weights

using a log-log regression equation (Fig. A3.1). This was assumed to be the true, or *realized*, amount of growth over the time it took to grow from the previous to most recent circulus. We calculated each fish's daily growth rate ($g \cdot g^{-1} \cdot d^{-1}$) using the equation:

$$G = \frac{\ln(W_t) - \ln(W_0)}{t}$$

where W_t is the back-calculated weight from the most recent circulus, W_0 is the back-calculated weight from the penultimate circulus, and t is the number of days (t=6) needed to grow from one circulus to the next (Gamble et al. 2018).

Realized growth was analyzed using an analysis of variance (ANOVA), where the model selection procedure was conducted as described above for consumption parameters. We included habitat type, rearing origin, year, month, and fork length as predictor variables. Prior to analysis, we used a Q-Q plot, Shapiro-Wilk test, and Levene's test for equal variance to ensure that model assumptions were satisfied. This data screening procedure confirmed that realized growth did not have to be transformed to fit model assumptions.

Results

Water temperature

Mean water temperatures varied among months and habitats, and between years (Table 3.3). The transitional marsh logger was washed away by large woody debris in 2014. We used temperature measurements from tidal freshwater forest as a substitution for missing data in transitional marsh since daily temperature values at these two sites were highly correlated (r = 0.96). Temperatures were 4–10% higher in 2015 than in 2014, with the greatest among-year differences observed in March, June, and July. In 2014, the offshore site was 0.5–1.7˚C cooler than any other site, while in 2015 both emergent salt marsh and offshore had the lowest temperatures. In contrast, the

nearshore site had the highest temperatures out of any habitat type in both years, particularly in the spring.

Diet and individual consumption

Adult insects and insect larvae were predominant in the stomachs of fish captured in tidal freshwater forest from March through July (see Davis et al. 2018*a*; Table 3.1). Insects were also common in the stomach contents of fish captured in transitional marsh; however, mysids and amphipods comprised 69–79% of dietary biomass in May and June. In the emergent salt marsh and delta mudflats, these two taxa were also the most prevalent (averaging 51–96% of dietary biomass), while crustaceans (copepods, cumaceans, and tanaids) and decapod larvae were more prevalent at nearshore sites. In the offshore sites furthest from the delta, fish made up the majority of subyearling Chinook Salmon diets in May, and decapod larvae encompassed 88.1% and 81.2% of dietary biomass in June and July, respectively.

The best-fit model for dietary energy density (ED_{prey}) indicated that it varied across month, habitat type, and rearing origin, with the diets of unmarked and hatchery fish captured in tidal freshwater forest containing 46–86% higher energy densities than in any other habitat type ($F_{6,278} = 2.87$, $P = 0.015$; Fig. 3.3, Table 3.4). On average, unmarked fish consumed prey that were more energy dense than hatchery fish (95% CI: unmarked = [4714 J/g, 5787 J/g], hatchery = [4374 J/g, 5516 J/g]), especially in the tidal freshwater forest. The monthly effect was such that the ED_{prey} of unmarked fish decreased from 5659 ± 2681 J/g in March to 4583 ± 2738 J/g in July, while the mean ED_{prey} of hatchery fish diets did not change monthly. Year was included as a fixed effect in the best-fit model, but was not significant ($F_{1,278} = 1.42$, $P = 0.235$).

Instantaneous ration (IR) also varied by month of capture, habitat type, and rearing origin (Table 3.4), with a significant interaction effect between origin and habitat ($F_{5,279}$ = 2.34, P = 0.042; Fig. 3.3). Unmarked fish had stomachs that were almost twice as full as hatchery fish (means ± SD: unmarked = 1.59 ± 2.28%, hatchery = 0.87 ± 1.29%), especially in the emergent salt marsh, delta mudflat, and nearshore habitat types. Stomachs were emptiest in the offshore zone regardless of rearing origin, with mean IR values of only 0.48 ± 0.67%. In general, IR declined from March through July, exhibiting a downward trend across all months (95% CI: March = [0.53%, 1.72%], April = [0.32%, 1.45%], May = [0.32%, 0.61%], June = [0.45%, 0.89%], July = [0.14%, 0.48%]).

Trends in individual consumption (P_{obs}), were best represented by an interaction effect between habitat and rearing origin ($F_{5,474}$ = 8.98, P < 0.001) and habitat and month ($F_{16,474}$ = 2.39, P = 0.001; Table 3.4). Overall, P_{obs} averaged 0.48 ± 0.14, but hatchery fish consumption was about 5% greater than for unmarked fish (95% CI: unmarked = [0.45, 0.49], hatchery = [0.48, 0.51]; Fig. 3.3). Consumption generally increased along a tidal freshwater to saline habitat gradient and from March through July, although this was likely related to a positive, allometric relationship between P_{obs} and fork length (r = 0.69, $F_{1,474}$ = 95.72, P < 0.001).

Growth rate potential simulations

Modeled GRP for juvenile Chinook Salmon was highly variable among months, habitat types, and rearing origins. When P_{cmax} was held at a constant value across simulations (0.2, 0.4, or 0.6), tidal freshwater forest consistently had the highest GRP, followed by transitional and emergent salt marsh (Fig. 3.4; Fig. A3.2). Simulated growth in the offshore was comparable to the other five habitat types in May but was substantially lower in June and July due to lower ED_{prey}. All

simulations using a P_{cmax} of 0.2 produced negative GRP values within the range of observed temperatures, regardless of month or habitat type. In contrast, a P_{cmax} of 0.4 resulted in consistently positive GRP estimates that were quite like those obtained using observed consumption rates. When P_{obs} was used to simulate the average observed habitat-specific feeding rates, estimated GRP was still highest in forested and emergent salt marsh for much of the out-migration season, with the exception of the delta mudflats in March and the offshore zone in May (Table 3.5). Because most of our hatchery samples were caught in May and June, we were only able to directly compare unmarked and hatchery fish in these two months, but our simulations showed that unmarked fish exhibited GRP values that were 5–10% higher than hatchery fish in May, and 1–2% lower than hatchery fish GRP in June. Because we did not vary size, ED_{prey}, or P_{cmax} between years, differences in GRP between sampling years were temperature driven and subtle, where GRP was less than 0.001 $g \cdot g^{-1} \cdot d^{-1}$ higher in 2014 than in 2015.

Simulations of weights through time demonstrated clear patterns that could not be predicted solely from monthly estimates of GRP. Average measured weights for fish captured at the end of July were 15.84 ± 7.23 g, but habitat-specific simulations using a P_{cmax} of 0.6 overestimated size estimates, especially in tidal freshwater forest, transitional marsh, and emergent salt marsh (as large as 466 g; Fig. 2.5). Conversely, simulations using a P_{cmax} of 0.2 produced negative growth later in the year in all habitat types. Simulations incorporating observed P_{cmax} values over- or underestimated observed weights depending on rearing origin. Specifically, for unmarked fish the bioenergetics model overestimated final weights in the offshore, underestimated final weights in the transitional marsh and nearshore, and produced similar estimates to observed weights in the tidal freshwater forest, emergent salt marsh, and

delta mudflats. For hatchery fish, the model overestimated final weights in all habitat types except for the delta mudflats. Despite starting at a smaller size, modeled unmarked fish growth outpaced hatchery fish growth from May–July except for in transitional and emergent salt marsh, especially at higher P_{cmax} values of 0.4 or 0.6 (Fig. 3.5). When P_{obs} was used in the simulation, final weights for hatchery fish were always greater, except for in the offshore zone. In general, final predicted weights were greater in 2014 than in 2015, but for offshore simulations using a P_{cmax} of 0.4 or 0.6, final weights were slightly higher in 2015 for unmarked fish.

Realized growth

Rearing origin, in conjunction with fork length ($F_{1,512} = 9.77$, $P = 0.002$; Table 3.4), was the predominant factor affecting realized growth rates derived from scale morphometry. On average, unmarked fish exhibited 11% faster growth when compared to hatchery fish of a similar size class, although this difference was minimal for subyearlings >100 mm (Fig. 3.6). Realized growth did not differ by year or month, but there was a significant origin by habitat effect that was not included in the best-fit model ($F_{5,504} = 2.85$, $P = 0.015$). This trend suggested that unmarked fish had realized growth rates that were, on average, 0.003 to 0.005 $g \cdot g^{-1} \cdot d^{-1}$ greater than hatchery fish in all habitat types except for EFT—an effect that was likely correlative with size (Table 3.5).

Discussion

We found that juvenile Chinook Salmon exhibited variable consumption and growth patterns as they out-migrated through a delta habitat mosaic. An abundance of energy-dense, terrestrial insect prey appeared to be particularly beneficial for unmarked and hatchery fish using the

estuarine wetlands. Both groups exhibited above average dietary energy densities if they consumed prey from the tidal freshwater forest, resulting in GRP estimates that were consistently elevated regardless of consumption rate. Realized growth measurements derived from scale morphometry highlighted how size also played a role in determining growth trends because observed growth rates declined allometrically with fork length. Larger subyearlings needed greater P_{cmax} values to achieve similar growth to smaller sized fish using the same habitat type. As a result, the consumption of small, low-energy crustaceans in the nearshore and offshore zones may have reduced growth efficiency in these habitats in June and July, when subyearlings were larger. This was especially true for the nearshore zone, where temperatures occasionally reached near-lethal levels.

Diet and individual consumption varied monthly among habitat types and were driven to some extent by the availability of high-energy prey (Davis et al. 2018*a*). Dietary energy density—an important input for the bioenergetics model—was influenced by the proportion of adult insects comprising juvenile Chinook Salmon diets. Adult dipterans, hemipterans, and hymenopterans were almost exclusively observed in the diets of fish from the tidal freshwater forest. As such, this habitat type generated dietary energy densities that were nearly twice as much as in the nearshore and offshore zones, where fish consumed greater proportions of crab larvae. Conversely, instantaneous ration (i.e., stomach fullness) was not noticeably higher in the tidal freshwater forest, but was greatest in the brackish transitional and emergent salt marshes and in the delta mudflats, especially for unmarked fish. This was likely driven by the disproportionate consumption of mysids such as *Neomysis mercedis*, a relatively large shrimp species (> 1 cm) that is frequently observed in Puget Sound, but is only common in the diets of juvenile salmon captured near Nisqually (Duffy et al. 2010; David et al. 2016; Davis et al.

2018*a*). Modeled individual P_{cmax} (P_{obs}) did not appear to follow consumption patterns that were derived from stomach content analyses. Instead, P_{obs} was directly related to allometry, where larger fish had to consume more to maintain somatic growth rates that were comparable to smaller fish using the same environment (Armstrong et al. 2010; Perry et al. 2015). Estimated P_{obs} values tended to increase along a salinity gradient, which may have resulted from subyearlings' larger body sizes and lower ED_{prey} in the nearshore and offshore environments. Size-related consumption mechanisms meant that among-habitat differences were dampened to some extent when P_{obs} was used in the bioenergetics growth model.

For GRP simulations, we observed notable trends related to rearing origin, habitat type, and month of capture. Monthly differences were most likely driven by fluctuations in temperature because the consumption and respiration rates of ectotherms, such as fish, are regulated by their thermal experience (Kitchell et al. 1977). For their temperature-dependent consumption curve, Stewart and Ibarra (1991) implemented a lower threshold of 5˚C and an upper threshold of 24˚C. These values changed little in Plumb and Moffitt's (2015) updated bioenergetics model for juvenile Chinook Salmon; however, the authors' adjusted parameter estimates increased the optimum temperature for maximum feeding from 15˚C to 20.93˚C. For the most part, water temperatures at each of our sites remained well within Plumb and Moffitt's (2015) estimated optimal thermal range, but Nisqually juvenile salmon had an average P_{cmax} of 0.48 ± 0.14, or about half of the maximum feeding rate. As a result, their thermal tolerance was likely constrained by several degrees at the upper and lower ends of the modeled temperature threshold. Average July temperatures did not exceed 24°C, but water loggers in the tidal freshwater forest, brackish transitional marsh, and nearshore areas recorded potentially lethal temperatures at several points throughout the summer. This occurred more frequently in 2015,

when we predicted slightly slower (< 0.001 $g \cdot g^{-1} \cdot d^{-1}$) GRP in all habitat types except for the cooler offshore area.

Water temperatures varied among habitat types, with emergent salt marsh and offshore areas experiencing cooler than average temperatures and nearshore areas exhibiting warmer than average temperatures. Nevertheless, differences in modeled GRP among unmarked and hatchery fish captured in different habitat types were clearly driven by diet and consumption. When P_{cmax} was held constant, model output predicted the highest GRP in tidal freshwater forest, brackish transitional marsh, and emergent salt marsh, while GRP was consistently predicted to be negative for fish captured in the nearshore and offshore areas. This tracks closely with trends in ED_{prey}, where the stomach contents of fish captured in the tidal freshwater forest were almost twice as energy rich as those from fish captured in the offshore subtidal zone. In contrast, when P_{obs} was used to calculate GRP, the effect of ED_{prey} became less apparent. Larger fish appeared to compensate for low-energy prey by eating greater quantities of crustaceans such as mysids, amphipods, and (to some extent) crab larvae.

The likelihood that fish will be able to access and benefit from high-energy insect prey is facilitated by allochthonous inputs of organic and inorganic material, overhanging vegetation in distributary and backwater channels, and tidal fluxes that transport allochthonous material (Allan et al. 2003; Baxter et al. 2005; Doi 2009; Wipfli and Baxter 2010). This terrestrial-aquatic interface is one reason why floodplains, large river deltas, and estuaries are postulated to be crucial nursery habitat for juvenile Chinook Salmon and other fishes (Healey 1982; Simenstad et al. 1982; Bellmore et al. 2013). Previous studies have observed physiological benefits for juvenile salmon derived from the consumption of energy-rich terrestrial prey during delta residence. In the Nisqually River delta, Davis et al. (2018*a*) found that unmarked juvenile

Chinook Salmon were more likely than hatchery salmon to be observed in tidal riverine habitats, where the ingestion of adult insects was correlated with greater stomach fullness and body condition. Similarly, Sommer et al. (2001) observed enhanced growth and survival in juvenile Chinook Salmon that were released into floodplain habitats along the Sacramento River, USA. Fish using floodplain areas appeared to compensate for higher temperatures by ingesting greater quantities of terrestrial insects than the fish in the river. Terrestrial prey subsidies may also mitigate density dependent effects. Based on stable isotope analyses, Romanuk and Levings (2005) hypothesized that terrestrial inputs promoted prey partitioning and reduced competition among multiple species of juvenile Pacific Salmon in the Strait of Georgia, Canada. Of course, the likelihood of encountering terrestrially-sourced prey decreases as juvenile salmon migrate seaward (Odum 1988). Furthermore, the temporary dewatering of tidal channels and competition for limited terrestrial inputs among larger-bodied juvenile salmon may necessitate foraging in the nearshore and offshore environments, where aquatic prey are generally more productive.

Although plankton and aquatic macroinvertebrates can be highly abundant in nearshore and offshore areas, piscivory is believed to bolster salmonid growth by providing a large, high-energy alternative to smaller crustaceans such as amphipods and crab larvae (Brodeur 1991; Daly et al. 2009; Litz et al. 2017). Forage fish, which are a major source of prey for some Puget Sound Chinook Salmon as they move to the offshore (Duffy et al. 2010; Chamberlin et al. 2017), were scarcely observed in Nisqually diet samples except for in the offshore area in May. Consequently, this was the only month during which modeled GRP in the offshore habitat reached values that were equivalent to the tidal marshes, regardless of P_{cmax}. In the adjacent nearshore area, modeled growth through time reflected depressed monthly GRP estimates, which were presumably driven by the consumption of crustaceans and annelids in tandem with higher

than average temperatures. It must be noted that crustaceans also made up a large portion of diets in juveniles captured in emergent salt marsh and delta mudflats; however, fish from these sites had the fullest stomachs and had P_{obs} values ranging between 0.30 and 0.55. These factors resulted in modeled growth rates that were most likely to resemble empirical values and observed weights. July size estimates of 14 g in emergent salt marsh and 13–15 g in delta mudflats were closest to the observed weights of 15.84 ± 7.23 g for unmarked fish captured in July. For hatchery fish, only the delta mudflats scenario resulted in final weights that were like observed values.

Short-term realized growth rates fell into a range of values that was similar to predicted GRP, but we found less variability among habitat types. Even though our bioenergetics model predicted negative GRP later in the season, realized growth was almost always over 0.01 $g \cdot g^{-1} \cdot d^{-1}$. Empirical estimates for juvenile salmon caught in the offshore were ~0.005 $g \cdot g^{-1} \cdot d^{-1}$ less than in the tidal freshwater forest, but not significantly so. Alternatively, body size and rearing origin were more important determinants of realized growth, where fish < 60 mm grew fastest and unmarked fish < 100 mm had a growth advantage over similarly-sized hatchery fish. The faster growth rates of these smaller, unmarked fish when compared to their hatchery counterparts is indicative of growth advantages in tidal freshwater forest and emergent salt marsh habitats, which hatchery fish are less likely to use (Davis et al. 2018*a*). Meanwhile, in larger-sized subyearlings, the tighter range of realized growth values was likely reflective of unmarked and hatchery fish frequently moving from one habitat type to another during their delta residence (Miller and Sadro 2003; Bottom et al. 2005; Semmens 2008), selecting for high GRP microhabitats (Nislow et al. 1999, 2000), exhibiting compensatory feeding mechanisms during periods of low prey availability or intense competition (Damsgird and Dill 1998; Metcalfe and

Monaghan 2001; Ali et al. 2003), or falling victim to predation prior to capture if they were not able to reach a given size.

By comparing our bioenergetics model output to end-of-season weights and empirical growth rates from scales, we could identify areas where model output was unrealistic. For example, the model overestimated the GRP of the freshwater tidal and transitional habitats, and underestimated the GRP of the nearshore and offshore zones when P_{cmax} was 0.4 or 0.6, and underestimated GRP in most habitat types when P_{cmax} was 0.2. Bioenergetics models are subject to model sensitivity, especially with respect to consumption parameters, which tend to scale allometrically (Beauchamp et al. 1989, Bartell et al. 1986). We calculated P_{obs} and GRP from the same empirical dataset, resulting in GRP calculations that were somewhat logically circular. This is one reason why we modeled habitat-specific growth using both constant and observed P_{cmax} inputs. An additional caveat to our analysis is that we used stomach contents from fish captured in beach seines to calculate ED_{prey}, which may have only partially reflected foraging conditions at a given site. While we are confident that our sample size was large enough to capture intra- and inter-habitat variation, we recognize that juvenile salmon can move several kilometers in a day (Orsi et al. 2000), so diets (and consequently, growth) may not be completely representative of specific habitats. Modeled GRP spanned a similar (albeit less constrained) range of values when compared to realized growth rates from scales, which were reflective of movement among habitat types during the estimated 6-day span between the formation of the most recent circulus interval. Thus, even though the bioenergetics model may not be as accurate at fine spatiotemporal scales as it is for coarser-scale analyses, it is still an important measure of relative habitat quality.

Our habitat-specific analysis of modeled and observed growth rates in juvenile Chinook Salmon supports the conclusions of Davis et al. (2018*a*), demonstrating clear foraging advantages for fish in tidal wetlands, including freshwater forest areas and emergent marshes. Compared to hatchery fish, wild salmon appear to have longer delta residence times and are more likely to use estuarine tidal wetlands during their out-migration to the sea (Davis et al. 2018*a*, Chittenden et al. 2018) so a greater proportion of their somatic growth is derived from energy-rich, allochthonous prey. This may result in long-term physiological advantages during the early marine critical period. Fostering the restoration of freshwater, brackish, and saline emergent marshes is one possibility for increasing the functional capacity of the estuarine gradient, and represents a crucial mitigation option to prevent habitat loss from rising sea levels (Temmerman et al. 2013). On the other hand, these functional benefits appear to stem from the quantity and species composition of the prey community in addition to the structural characteristics of the habitat itself, indicating that there are comprehensive advantages to enhancing the terrestrial-aquatic interface and productivity of the delta habitat mosaic as a whole. This could be accomplished by removing engineered barriers to tidal exchange, encouraging the formation of tidal channel networks, increasing overhanging riparian vegetation, and improving environmental conditions for invertebrate productivity. Such management actions may provide valuable prey resources for juvenile salmon and other fishes, while also representing crucial steps toward protecting river deltas from degradation and functional loss.

Acknowledgments

This research was funded by the Washington State Estuary and Salmon Restoration Program (ESRP Project #13-1583P) with a grant awarded to the U.S. Geological Survey Western

Ecological Research Center (USGS WERC). Additional science support came from the Salish Sea Marine Survival Program, WERC program funds, the USGS Ecosystem Mission Area, the USGS Biologic Carbon Sequestration Program, the USFWS Coastal Program, and several USGS internship programs (Students in Support of Native American Relations, National Association of Geoscience Teachers, and Youth and Education in Science). This research represents a cooperative effort among federal, tribal, and non-profit partners, including the Nisqually Indian Tribe, Billy Frank Jr. Nisqually National Wildlife Refuge, and the Nisqually River Foundation. We are grateful for the input and assistance of USGS employees L. Shakeri, S. Blakely, A. Munguia, A. Hissem, L. Lamere, J. Donald, Y. Chan, C. Norton, and H. Mittelstaedt; Tribal employees W. Duval, E. Perez, and J. Moore; and University of Washington biologists K. Connelly, J. Gardner, and M. Gamble. Our thanks go out to Z. Zhu, J. Schmerfeld, and S. Covington for their financial and logistical support. Graduate student author M. Davis was supported by an American Dissertation Fellowship through the American Association of University Women, for which she is deeply appreciative. Government disclaimer: any use of trade, firm, or product names is for descriptive purposes only and does not imply endorsement by the U.S. Government.

References

Ali, M., A. Nicieza, and R. J. Wootton. 2003. Compensatory growth in fishes: a response to growth depression. Fish and Fisheries 4:147–190.

Allan, J. D., M. S. Wipfli, J. P. Caouette, A. Prussian, and J. Rodgers. 2003. Influence of streamside vegetation on inputs of terrestrial invertebrates to salmonid food webs. Canadian Journal of Fisheries and Aquatic Sciences 60:309–320.

Armstrong, J. B., D. E. Schindler, K. L. Omori, C. P. Ruff, and T. P. Quinn. 2010. Thermal heterogeneity mediates the effects of pulsed subsidies across a landscape. Ecology 91:1445–1454.

Balling, S., and V. Resh. 1991. Seasonal patterns in a San Francisco Bay, California salt-marsh arthropod community. Pan-Pacific Entomologist 67:138–144.

Bartell, S. M., J. E. Breck, R. H. Gardner, and A. L. Brenkert. 1986. Individual parameter perturbation and error analysis of fish bioenergetics models. Canadian Journal of Fisheries and Aquatic Sciences 43:160–168.

Baxter, C. V., K. D. Fausch, and W. C. Saunders. 2005. Tangled webs: reciprocal flows of invertebrate prey link streams and riparian zones. Freshwater Biology 50:201–220.

Beamish, R. J., and C. Mahnken. 2001. A critical size and period hypothesis to explain natural regulation of salmon abundance and the linkage to climate and climate change. Progress in Oceanography 49:423–437.

Beamish, R. J., C. Mahnken, and C. M. Neville. 2004. Evidence that reduced early marine growth is associated with lower marine survival of coho salmon. Transactions of the American Fisheries Society 133:26–33.

Beauchamp, D. A. 2009. Bioenergetic ontogeny: linking climate and mass-specific feeding to life-cycle growth and survival of salmon. Pages 53–72 *in*: Krueger C. C. and C. E. Zimmerman (eds.) American Fisheries Society Symposium 70, Bethesda, Maryland, USA.

Beauchamp, D. A., D. J. Stewart, and G. L. Thomas. 1989. Corroboration of a bioenergetics model for sockeye salmon. Transactions of the American Fisheries Society 118:597–607.

Bellmore, J. R., C. V. Baxter, K. Martens, and P. J. Connolly. 2013. The floodplain food web mosaic: a study of its importance to salmon and steelhead with implications for their recovery. Ecological Applications 23:189–207.

Boisclair, D., and W. C. Leggett. 1989. Among-population variability of fish growth: I. influence of the quantity of food consumed. Canadian Journal of Fisheries and Aquatic Sciences 46:457–467.

Bottom, D. L., K. K. Jones, T. J. Cornwell, A. Gray, C. and A. Simenstad. 2005. Patterns of Chinook salmon migration and residency in the Salmon River estuary (Oregon). Estuarine, Coastal and Shelf Science 64:79–93.

Bourret, S. L., C. C. Caudill, and M. L. Keefer. 2016. Diversity of juvenile Chinook salmon life history pathways. Reviews in Fish Biology and Fisheries 26:375–403.

Broadmeadow, S. B., J. G. Jones, T. E. L. Langford, P. J. Shaw, and T. R. Nisbet. 2011. The influence of riparian shade on lowland stream water temperatures in southern England and their viability for brown trout. River Research and Applications 27:226–237.

Brodeur, R. D. 1991. Ontogenetic variations in the type and size of prey consumed by juvenile coho, *Oncorhynchus kisutch*, and Chinook, *O. tshawytcha*, salmon. Environmental Biology of Fishes 30:303–315.

Brodeur, R. D., R. C. Francis, and W. G. Pearcy. 1992. Food consumption of juvenile coho (*Oncorhynchus kisutch*) and Chinook (*O. tshawytscha*) on the continental shelf off Washington and Oregon. Canadian Journal of Fisheries and Aquatic Sciences 49:1670–1685.

Burnham, K., and D. Anderson. 2002. Model selection and multimodel inference: a practical information-theoretic approach. Colorado State University, Fort Collins. Springer, New York, New York, USA.

Casselman, J. M. 1990. Growth and relative size of calcified structures of fish. Transactions of the American Fisheries Society 119:673–688.

Chamberlin, J. W., B. R. Beckman, C. M. Greene, C. A. Rice, and J. E. Hall. 2017. How relative size and abundance structures the relationship between size and individual growth in an ontogenetically piscivorous fish. Ecology and Evolution 7:6981–6995.

Chittenden, C. M., R. Sweeting, C. M. Neville, K. Young, M. Galbraith, E. Carmack, S. Vagle, M. Dempsey, J. Eert, and R. J. Beamish. 2018. Estuarine and marine diets of out-migrating Chinook salmon smolts in relation to local zooplankton populations, including harmful blooms. Estuarine, Coastal and Shelf Science 200:335–348.

Cordell, J. R., J. D. Toft, A. Gray, G. T. Ruggerone, and M. Cooksey. 2011. Functions of restored wetlands for juvenile salmon in an industrialized estuary. Ecological Engineering 37:343–353.

Courtney, D. L., D. G. Mortensen, and J. A. Orsi. 2000. Digitized scale and otolith microstructures as correlates of juvenile pink salmon size. North Pacific Anadromous Fish Commission Bulletin 2:337–345.

Cross, A. D., D. A. Beauchamp, K. W. Myers, and J. H. Moss. 2008. Early marine growth of pink salmon in Prince William Sound and the coastal Gulf of Alaska during years of low and high survival. Transactions of the American Fisheries Society 137:927-939.

Daly, E. A., R. D. Brodeur, and L. A. Weitkamp. 2009. Ontogenetic shifts in diet of juvenile and subadult coho and Chinook salmon in coastal marine waters: important for marine survival? Transactions of the American Fisheries Society 138:1420–1438.

Damsgird, B., and L. M. Dill. 1998. Risk-taking behavior in weight-compensating coho salmon, *Oncorhynchus kisutch*. Behavioral Ecology 9:26–32.

David, A. T., C. S. Ellings, I. Woo, C. A. Simenstad, J. Y. Takekawa, and K. L. Turner. 2014. Foraging and growth potential of juvenile Chinook salmon after tidal restoration of a large river delta. Transactions of the American Fisheries Society 143:1515–1529.

David, A. T., C. A. Simenstad, J. R. Cordell, J. D. Toft, C. S. Ellings, A. Gray, and H. B. Berge. 2016. Wetland loss, juvenile salmon foraging performance, and density dependence in Pacific Northwest estuaries. Estuaries and Coasts 39:767–780.

Davis, M. J., I. Woo, C. S. Ellings, S. Hodgson, D. A. Beauchamp, G. Nakai, and S. De La Cruz. 2018*a*. Integrated diet analyses reveal contrasting trophic niches for wild and hatchery juvenile Chinook salmon in a large river delta. Transactions of the American Fisheries Society 147:818–841.

Davis, M. J., C. S. Ellings, I. Woo, S. Hodgson, K. Larsen, and G. Nakai. 2018*b*. Gauging resource exploitation by juvenile Chinook salmon (*Oncorhynchus tshawytscha*) in restoring estuarine habitat. Restoration Ecology 26:976–986.

Deslauriers, D., S. R. Chipps, J. E. Breck, J. A. Rice, and C. P. Madenjian. 2017. Fish Bioenergetics 4.0: an R-based modeling application. Fisheries 42:586–596.

Doi, H. Spatial patterns of autochthonous and allochthonous resources in aquatic food webs. Population Ecology 51:57–64.

Duffy, E. J., D. A. Beauchamp, R. M. Sweeting, R. J. Beamish, and J. S. Brennan. 2010. Ontogenetic diet shifts of juvenile Chinook salmon in nearshore and offshore habitats of Puget Sound. Transactions of the American Fisheries Society 139:803–823.

Ellings, C. S., M. J. Davis, E. E. Grossman, I. Woo, S. Hodgson, K. L. Turner, G. Nakai, J. E. Takekawa, and J. Y. Takekawa. 2016. Changes in habitat availability for outmigrating juvenile salmon (*Oncorhynchus* spp.) following estuary restoration. Restoration Ecology 24: 415–427.

Gamble, M. M., K. A. Connelly, J. R. Gardner, J. W. Chamberlin, K. I. Warheit, and D. A. Beauchamp. 2018. Size, growth, and size-selective mortality of subyearling Chinook

salmon during early marine residence in Puget Sound. Transactions of the American Fisheries Society 147:370–389.

Gray, A. 2005. The Salmon River Estuary: restoring tidal inundation and tracking ecosystem response. Graduate dissertation. University of Washington, Seattle, Washington, USA.

Gray, A., C.A. Simenstad, D. L. Bottom, and T. J. Cornwell. 2002. Contrasting functional performance of juvenile salmon habitat in recovering wetlands of the Salmon River Estuary, Oregon, USA. Restoration Ecology 10:514–526.

Greene, C. M., D. W. Jensen, G. R. Pess, E. A. Steel, and E. Beamer. 2012. Effects of environmental conditions during stream, estuary, and ocean residency on Chinook salmon return rates in the Skagit River, Washington. Transactions of the American Fisheries Society 134:1562–1581.

Hanson, P. C., T. B. Johnson, D. E. Schindler, and J. K. Kitchell. 1997. Fish bioenergetics 3.0. University of Wisconsin Madison Center for Limnology and University of Wisconsin Sea Grant Institute. Madison, Wisconsin, USA.

Healey, M. C. 1991. Life history of Chinook salmon (*Oncorhynchus tshawytscha*). Pages 313–393 *in*: Groot, C., and L. Margolis (eds.) Pacific Salmon Life Histories. University of British Columbia Press, Vancouver, British Columbia, Canada.

Healey, M. C. 1982. Juvenile Pacific salmon in estuaries: the life support system. Pages 315–341 *in*: Kennedy, V. S. (ed.) Estuarine Comparisons. Academic Press, New York, USA.

Hodgson, S., C. S. Ellings, S. P. Rubin, M. C. Hayes, W. Duval, and E. E. Grossman. 2016. 2010–2015 Juvenile fish ecology in the Nisqually River Delta and Nisqually Reach Aquatic Reserve. Salmon Recovery Program Technical Report No. 2016-1, Nisqually Indian Tribe Department of Natural Resources, Olympia, Washington, USA.

Kitchell, J. F., D. J. Stewart, and D. Weininger. 1977. Applications of a bioenergetics model to yellow perch (*Perca flavescens*) and walleye (*Stizostedion vitreum vitreum*). Journal of the Fisheries Research Board of Canada 34:1910–1921.

Levy, D. A., and T. G. Northcote. 1982. Juvenile salmon residency in a marsh area of the Fraser River estuary. Canadian Journal of Fisheries and Aquatic Sciences 39:270–276.

Litz, M. N. C., J. A. Miller, L. A. Copeman, D. J. Teel, L. A. Weitkamp, E. A. Daly, and A. M. Claiborne. 2017. Ontogenetic shifts in the diets of juvenile Chinook salmon: new insight from stable isotopes and fatty acids. Environmental Biology of Fishes 100:337–360.

Madenjian, C. P., D. V. O'Connor, S. M. Chernyak, R. R. Rediske, and J. P. O'Keefe. 2004. Evaluation of a Chinook salmon (*Oncorhynchus tshawytscha*) bioenergetics model. Canadian Journal of Fisheries and Aquatic Sciences 61:627–635.

Magnusson, A., and R. Hilborn. 2003. Estuarine influence on survival rates of coho (*Oncorhynchus kisutch*) and Chinook salmon (*Oncorhynchus tshawytscha*) released from hatcheries on the U.S. Pacific coast. Estuaries 26:1094–1103.

Marin Jarrin, J. R., A. L. Shanks, and M. A. Banks. 2009. Confirmation of the presence and use of sandy beach surf-zones by juvenile Chinook salmon. Environmental Biology of Fishes 85:119–125.

Martinson, E. C., M. M. Masuda, and J. H. Helle. 2000. Back-calculated fish lengths, percentages of scale growth, and scale measurements for two scale measurement methods used in studies of salmon growth. North Pacific Anadromous Fish Commission Bulletin 2:331–336.

Metcalfe, N. B., and P. Monaghan. 2001. Compensation for a bad start: grow now, pay later? Trends in Ecology and Evolution 16:254–260.

Miller, B. A., and S. Sadro. 2003. Residence time and seasonal movements of juvenile coho salmon in the ecotone and lower estuary of Winchester Creek, South Slough, Oregon. Transactions of the American Fisheries Society 132:546–559.

Morril, J. C., R. Bales, and M. H. Conklin. 2005. Estimating stream temperature from air temperature: implications for future water quality. Journal of Environmental Engineering 131:139–146.

Neilson, J. D., G. H. Green, and D. Bottom. 1985. Estuarine growth of juvenile Chinook salmon (*Oncorhynchus tshawytscha*) as inferred from otolith microstructure. Canadian Journal of Fisheries and Aquatic Sciences 42:899–908.

Nislow, K. H., C. L. Folt, and D. L. Parrish. 1999. Favorable foraging locations for age-0 Atlantic salmon: application to the restoration of populations and habitats. Ecological Applications 9:1085–1099.

Nislow, K. H., C. L. Folt, and D. L. Parrish. 2000. Spatially explicit bioenergetics analysis of habitat quality for age-0 Atlantic salmon. Transactions of the American Fisheries Society 129:1067–1081.

Odum, W. E. 1988. Comparative ecology of tidal freshwater and salt marshes. Annual Review of Ecological Systems 19:147–176.

Orsi, J. A., M. V. Sturdevant, J. M. Murphy, D. G. Mortensen, and B. L. Wing. 2000. Seasonal habitat use and early marine ecology of juvenile Pacific salmon in Southeastern Alaska. North Pacific Anadromous Fish Commission Bulletin 2:111–122.

Pearce, T. A., J. H. Meyer, and R. S. Boomer. 1982. Distribution and food habits of juvenile salmon in the Nisqually Estuary, Washington, 1979–1980. U.S. Fish and Wildlife Service Fisheries Assistance Office, Olympia, Washington, USA.

Perry, R. W., J. M. Plumb, and C. W. Huntington. 2015. Using a laboratory-based growth model to estimate mass- and temperature-dependent growth parameters across populations of juvenile Chinook salmon. Transactions of the American Fisheries Society 144:331–336.

Pierce, C. L., J. B. Rasmussen, and W. C. Leggett. 1996. Back-calculation of fish length from scales: empirical comparison of proportional methods. Transactions of the American Fisheries Society 125:889–898.

Plumb, J. M., and C. M. Moffitt. 2015. Re-estimating temperature-dependent consumption parameters in bioenergetics models for juvenile Chinook salmon. Transactions of the American Fisheries Society 144:323–330.

R Core Development Team. 2017. R: A language and environment for statistical computing. R Foundation for Statistical Computing, Vienna, Austria.

Romanuk, T. N., and C. D. Levings. 2003. Associations between arthropods and the supralittoral ecotone: dependence of aquatic and terrestrial taxa on riparian vegetation. Environmental Entomology 32:1343–1353.

Romanuk, T. N., and C. D. Levings. 2005. Stable isotope analyses of trophic position and terrestrial vs. marine carbon sources for juvenile Pacific salmonids in nearshore marine habitats. Fisheries Management and Ecology 12:113–121.

Schindler, D. E., R. Hilborn, B. Chasco, C. P. Boatright, T. P. Quinn, L. A. Rodgers, and M. S. Webster. 2010. Population diversity and the portfolio effect in an exploited species. Nature 465:609–612.

Semmens, B. X. 2008. Acoustically derived fine-scale behaviors of juvenile Chinook salmon (*Oncorhynchus tshawytscha*) associated with intertidal benthic habitats in an estuary. Canadian Journal of Fisheries and Aquatic Sciences 65:2053–2062.

Sharma, S., S. C. Walker, and D. A. Jackson. 2008. Empirical modelling of lake water-temperature relationships. A comparison of approaches. Freshwater Biology 53: 897–911.

Sheaves, M. 2009. Consequences of ecological connectivity: the coastal ecosystem mosaic. Marine Ecology Progress Series 391:107–115.

Sheaves, M., R. Baker, I. Nagelkerken, and R. M. Connolly. 2015. True value of estuarine and coastal nurseries for fish: incorporating complexity and dynamics. Estuaries and Coasts 38:401–414.

Simenstad, C. A., and J. R. Cordell. 2000. Ecological assessment criteria for restoring anadromous salmonid habitat in Pacific Northwest estuaries. Ecological Engineering 15: 283–302.

Simenstad, C. A., K. L. Fresh, and E. O. Salo. 1982. The role of Puget Sound and Washington coastal estuaries in the life history of Pacific salmon: an unappreciated function. Pages 343–364 *in*: Kennedy, V. S. (ed.) Estuarine Comparisons. Academic Press, New York, USA.

Simenstad, C. A., W. G. Hood, R. M. Thom, D. A. Levy, and D. L. Bottom. 2002. Landscape structure and scale constraints on restoring estuarine wetlands for Pacific coast juvenile fishes. Pages 597–630 *in*: Weinstein, M. P., and D. A. Kreeger (eds.) Concepts and Controversies in Tidal Marsh Ecology. Springer, Dordrecht, the Netherlands.

Soetaert, K., and P. V. Rijswijk. 1993. Spatial and temporal patterns of the zooplankton in the Westerschelde estuary. Marine Ecology Progress Series 97:47–59.

Sommer, T. R., M. L. Nobriga, W. C. Harrell, W. Batham, and W. J. Kimmerer. 2001. Floodplain rearing of juvenile Chinook salmon: evidence of enhanced growth and survival. Canadian Journal of Fisheries and Aquatic Sciences 58:325–333.

Stewart, D. J., and M. Ibarra. 1991. Predation and production by salmonine fishes in Lake Michigan, 1978–88. Canadian Journal of Fisheries and Aquatic Sciences 48:909–922.

Temmerman, S., P. Meire, T. J. Bouma, P. M. J. Herman, T. Ysebaert, and H. J. De Vriend. 2013. Ecosystem-based coastal defence in the face of global change. Nature 504:79–83.

Thornton, K. W., and A. S. Lessem. 1978. A temperature algorithm for modifying biological rates. Transactions of the American Fisheries Society 107:284–287.

Thorpe, J. E. 1994. Salmonid fishes and the estuarine environment. Estuaries 17:76–93.

Trudel, M., D. R. Geist, and D. W. Welch. 2004. Modeling the oxygen consumption rates in Pacific salmon and steelhead: an assessment of current models and practices. Transactions of the American Fisheries Society 133:326–348.

Ware, D. W. 1978. Bioenergetics of pelagic fish: theoretical change in swimming speed and ration with body size. Journal of the Fisheries Research Board of Canada 34:220–228.

Wipfli, M. S., and C. V. Baxter. 2010. Linking ecosystems, food webs, and fish production: subsidies in salmonid watersheds. Fisheries 35:373–387.

Woo, I., M. J. Davis, C. S. Ellings, G. Nakai, J. Y. Takekawa, and S. De La Cruz. 2018. Enhanced invertebrate prey production following estuarine restoration supports foraging for multiple species of juvenile salmonids (*Oncorhynchus* spp.). Restoration Ecology 26:964–975.

Tables

Table 3.1. Proportion of juvenile Chinook Salmon dietary wet weight biomass (%) contributed by prey taxa in tidal freshwater forest (FOR), brackish transitional marsh (EFT), emergent salt marsh (EEM), delta mudflat (DMF), nearshore intertidal (NS), and offshore subtidal (OFF) habitat types. Data were averaged across the 2014 and 2015 out-migration seasons (March–July). Monthly contributions greater than 30% are highlighted with italics and major prey taxa are starred with an asterisk. Energy densities (J/g) for each taxonomic group are shown in the right hand column (see Gray 2005; Cordell et al. 2011; David et al. 2014).

	FOR					EFT					EEM					DMF					NS					OFF				
	M	A	M	J	J	M	A	M	J	J	M	A	M	J	J	M	A	M	J	J	M	A	M	J	J	M	A	M	J	J	ED (J/g)
*Crustacea				0.4				1.9	4.8		16.4		0.8	0.8	6.7	*41.4*	7.3	2.0	0.3	7.4	*46.4*	*32.0*	20.3	9.7				2.9	2.6	5.3	3370
*Amphipoda	5.4	1.6	2.7	15.6				21.9	19.9		6.1	*60.4*	15.6	0.4	*39.5*	11.1	1.4	13.7	1.1	*63.2*	*31.4*	3.9	6.5	6.6				4.1	3.1	11.6	3065
*Decapoda									3.9				0.7	5.8	13.0			6.3				*52.7*	26.8	26.9				2.8	*88.1*	*81.2*	3360
Euphausiidae																		1.7	3.2				0.3	22.0				2.6	0.6	1.3	3370
Isopoda								10.5					0.5					0.2		2.8		1.0	2.3								2960
*Mysida								*57.0*	*49.4*	*64.1*	*50.8*		*62.1*	*79.8*	*34.5*	*39.6*	*61.4*	*74.1*	*94.7*	18.9		0.3	0.6	0.0				0.9	1.9	0.5	3550
Annelida	5.4		7.8		*98.3*								7.7										27.4	22.4					0.3		1980
Diptera	0.8		0.2	10.2				1.4	5.7		8.1		3.5	8.8	0.3	3.1	2.2	0.1	0.5		3.2	10.0	1.7	2.3				0.5	0.2		8920
Diptera lar.	4.0		4.0	0.6	0.7			2.8				3.7			0.2			0.0					0.5							2580
Diptera pup.	15.2	2.0	7.6	0.7				0.2	0.1			14.3	0.1	0.0	1.8			0.1						1.4							3830
*Insecta	18.2	*34.5*	*74.3*	8.6	1.0			3.8	9.2	*33.6*	10.0	3.5	3.1	1.3	3.0	3.7		0.2		2.7	16.4		2.1	0.8				0.2		0.0	10930
Insect larvae	16.2	*34.3*	3.2	20.2				0.3	0.0	1.6	1.7	10.4	3.5	0.8	0.6	0.0		0.2					0.2	0.2							7412
Insect pupae	12.7			0.9					0.1									0.1						3.2							3830
Arachnida				0.2								7.6	0.0		0.2			0.1					0.0	0.2				0.1	0.3		5320
Hemiptera			0.3	13.4					0.4						0.2			0.2	0.0	0.1			0.1	0.5					1.3		10930
Hymenoptera								0.1	6.6	0.6			1.5	0.7				1.0	0.2	4.9			0.2	0.1					0.0		12670
Palaeoptera	22.0	27.5		29.1							7.0		1.0	1.6		1.2													0.0		7970
Fish																	27.6				2.7		11.5	3.3				*85.8*	1.4		6830

Table 3.2. Model input for unmarked and hatchery fish growth simulations, including weight, ED_{prey}, and P_{obs}. Growth rate potential was only calculated when more than three diet samples were available for a given month/habitat group.

	Unmarked						Hatchery					
Month	FOR	EFT	EEM	DMF	NS	OFF	FOR	EFT	EEM	DMF	NS	OFF
Weight (g)												
March	0.9		1.4	1.2	0.7							
April	1.6		1.5	3.9	3.0							
May	3.1	8.6	6.4	5.6	5.8	8.8		8.3	6.9	7.9	7.3	7.6
June	3.2	8.4	6.4	8.6	7.2	14.1	9.3	10.7	11.5	11.0	9.3	14.4
July			10	9.0		20						16.8
ED_{prey} (J/g)												
March	7139		5305	5383	4945							
April	6002		4003	3947	2707							
May	9084	6489	5005	2854	5268	5617		4123	5244	4822	3915	4789
June	8486	3322	3742	4585	3944	3510	7297	8177	6817	4165	4295	3286
July			4613	4479		3196						3290
P_{obs}												
March	0.24		0.47	0.52	0.33							
April	0.23		0.35	0.38	0.37							
May	0.24	0.29	0.44	0.44	0.41	0.55		0.47	0.34	0.44	0.49	0.47
June	0.24	0.37	0.35	0.37	0.47	0.58	0.33	0.41	0.39	0.43	0.57	0.55
July			0.43	0.48		0.65						0.57

Table 3.3. Mean ± SD monthly temperatures (˚C) in each habitat type. Bioenergetics model simulations for growth were run separately in 2014 and 2015. The transitional marsh logger was washed away by large woody debris in 2014, so we used tidal freshwater forest temperature measurements as a substitution for March–July 2014 and March–May 2015.

	FOR		EFT		EEM	
Month	2014	2015	2014	2015	2014	2015
March	6.9 ± 0.6	8.3 ± 1.3	6.9 ± 0.6	8.3 ± 1.3	7.2 ± 0.5	8.5 ± 0.8
April	9.2 ± 0.7	9.3 ± 1.2	9.2 ± 0.7	9.3 ± 1.2	9.2 ± 1.0	9.4 ± 0.9
May	12.0 ± 1.1	12.2 ± 1.3	12.0 ± 1.1	12.2 ± 1.3	11.4 ± 1.4	11.8 ± 1.1
June	14.2 ± 1.1	15.5 ± 2.0	14.2 ± 1.1	15.5 ± 1.9	13.2 ± 0.9	14.3 ± 1.6
July	16.3 ± 1.5	18.1 ± 1.5	16.3 ± 1.5	17.8 ± 1.1	15.2 ± 0.6	15.7 ± 0.5

	DMF		NS		OFF	
Month	2014	2015	2014	2015	2014	2015
March	7.8 ± 0.8	8.8 ± 1.8	9.3 ± 1.2	9.8 ± 1.4	8.0 ± 1.0	10.2 ± 0.2
April	9.9 ± 1.3	8.8 ± 1.4	10.6 ± 1.5	10.5 ± 1.4	9.7 ± 0.8	10.5 ± 0.4
May	11.8 ± 1.3	11.7 ± 1.6	12.8 ± 1.5	13.3 ± 1.4	10.8 ± 0.8	11.5 ± 0.6
June	12.6 ± 1.0	14.4 ± 1.6	13.8 ± 1.0	15.9 ± 1.5	12.2 ± 0.6	13.0 ± 0.8
July	15.0 ± 1.4	15.5 ± 1.3	16.3 ± 1.5	16.8 ± 1.4	13.6 ± 0.4	14.5 ± 0.3

Table 3.4. Candidate linear models for dietary energy density (ED_{prey}), instantaneous ration (IR), proportion of maximum consumption (P_{cmax}), and realized growth rate. We tested the effect of year of capture (Y), month of capture (M), habitat type (H), and rearing origin (O) as fixed effects, while sampling site was included as a random effect for ED_{prey} and IR. We also tested the suitability of fork length (L) and catch-per-set (C) as covariates. We conducted a stepwise exploratory data analysis, avoiding complex (more than 3-way) interaction effects. We used pseudo R^2, root mean-square-error (RMSE), and Akaike's Information Criterion (AIC) to assess relative model fit, where a $\Delta AIC > 2$ between the best-fit and next best-fit candidate models was indicative of strong support.

ED_{prey} (J/g)						IR (%)					
Model	df	R^2	RMSE	AICc	ΔAIC	Model	df	R^2	RMSE	AICc	ΔAIC
H × M × O + Y	43	0.35	1971.13	5233.63	0.00	M × H × O	42	0.26	1.31	1146.23	0.00
H × M × O + L	43	0.35	1966.93	5240.42	6.79	M × H × O + Y	43	0.26	1.31	1148.94	2.71
H × M × O	42	0.35	1968.65	5246.90	13.27	M × H × O + L	43	0.26	1.31	1155.76	9.53
H × M × Y	38	0.36	2008.43	5303.96	70.33	M × H × Y	38	0.20	1.34	1163.32	17.09
H × M + O	28	0.29	2063.17	5481.34	247.71	M × H + O	28	0.19	1.35	1169.15	22.92
H × M + Y	28	0.29	2074.85	5482.13	248.50	M × O	11	0.12	1.38	1169.33	23.10
H × M + L	28	0.29	2071.90	5487.88	254.25	M × Y	10	0.12	1.38	1169.47	23.23
H × M	27	0.29	2074.26	5494.30	260.67	M + O	8	0.11	1.39	1170.39	24.16
M × O + H + L	17	0.26	2158.18	5662.43	428.80	M × H	27	0.19	1.35	1170.39	24.16
M × O + H	16	0.25	2175.19	5673.31	439.67	H × O + M	18	0.19	1.38	1171.20	24.97
H × O	14	0.23	2214.84	5703.45	469.82	M	7	0.10	1.40	1172.13	25.90
H × Y	13	0.24	2210.55	5709.47	475.84	M × H + Y	28	0.18	1.35	1172.69	26.46
H + M	12	0.23	2203.03	5731.70	498.07	M + Y	8	0.10	1.40	1173.39	27.16
H + Y	9	0.23	2222.00	5772.07	538.44	M + H	12	0.14	1.39	1176.55	30.32
H + O	9	0.22	2220.48	5773.28	539.65	O	4	0.05	1.44	1177.22	30.99
H + L	9	0.22	2225.59	5779.51	545.87	M × H + C	28	0.19	1.35	1178.60	32.37
H + C	9	0.22	2226.43	5782.19	548.56	M × H + L	28	0.19	1.35	1179.41	33.18
H	8	0.22	2220.72	5784.40	550.77	L	4	0.06	1.44	1182.47	36.24
M	7	0.01	2195.56	5820.69	587.06	Null	3	-	1.47	1186.61	40.38
Y	4	0.00	2214.14	5860.23	626.60	H	8	0.07	1.47	1186.95	40.72
O	4	0.00	2215.10	5861.01	627.38	C	4	0.05	1.47	1188.40	42.17
L	4	0.01	2224.10	5866.20	632.57	Y	4	0.00	1.47	1189.75	43.52
C	4	0.00	2223.02	5869.71	636.08						
Null	3	-	2214.12	5872.65	639.01						

P_{cmax}						Realized growth ($g \cdot g^{-1} \cdot d^{-1}$)					
Model	df	R^2	RMSE	AIC	ΔAIC	Model	df	R^2	RMSE	AIC	ΔAIC
H × M × O + L	43	0.64	0.08	-1058.61	0.00	O × L	5	0.05	0.0070	-3651.47	0.00
H × M + L	28	0.62	0.09	-1037.48	21.12	O × L × Y	7	0.05	0.0070	-3650.25	1.21

H × M × Y + L	35	0.60	0.09	-1020.56	38.05	O × L + Y	6	0.05	0.0070	-3650.01	1.46
H + L	8	0.52	0.09	-963.47	95.13	O × L × M	18	0.07	0.0069	-3649.07	2.39
H × M + Y	28	0.54	0.09	-960.99	97.62	O × L + H	10	0.05	0.0070	-3645.04	6.42
H × M + O	28	0.53	0.09	-949.23	109.37	O × L + M	9	0.05	0.0070	-3644.26	7.20
H × M	27	0.52	0.09	-945.81	112.80	O + L	4	0.04	0.0071	-3643.74	7.72
H + M	11	0.50	0.10	-942.30	116.31	O × H	13	0.05	0.0070	-3640.91	10.56
M × O + L	11	0.49	0.10	-931.45	127.15	O	3	0.03	0.0071	-3640.36	11.11
H × O	13	0.48	0.10	-917.17	141.43	O × M	10	0.04	0.0070	-3639.88	11.59
H + O	8	0.43	0.10	-877.84	180.76	O + M	7	0.03	0.0071	-3639.82	11.64
H × Y	11	0.43	0.10	-874.86	183.75	O + Y	4	0.03	0.0071	-3638.64	12.83
H + Y	8	0.42	0.10	-872.02	186.59	O × Y	4	0.03	0.0071	-3638.61	12.86
H	7	0.42	0.10	-866.64	191.96	L	3	0.02	0.0071	-3637.83	13.63
L	3	0.39	0.11	-848.01	210.59	O + H	8	0.03	0.0071	-3636.92	14.55
M	6	0.24	0.12	-729.06	329.54	M	6	0.02	0.0071	-3634.05	17.42
Y	3	0.02	0.13	-601.00	457.61	O × L × H	25	0.05	0.0070	-3629.71	21.76
O	3	0.01	0.14	-596.00	462.60	H	7	0.01	0.0071	-3628.65	22.81
Null	2	-	0.14	-594.02	464.58	Y	3	0.00	0.0072	-3627.93	23.54
						Null	2	-	0.0072	-3627.17	24.30

Table 3.5. Minimum and maximum GRP estimates and mean ± SD realized growth rates (RG) for unmarked and hatchery juvenile Chinook Salmon in each month/habitat group. Simulated GRP values were derived using empirical measurements of mean daily water temperature, weight, ED_{prey}, and consumption (P_{obs}).

Habitat	Month	Unmarked			Hatchery		
		Min GRP ($g \cdot g^{-1} \cdot d^{-1}$)	Max GRP ($g \cdot g^{-1} \cdot d^{-1}$)	RG ($g \cdot g^{-1} \cdot d^{-1}$)	Min GRP ($g \cdot g^{-1} \cdot d^{-1}$)	Max GRP ($g \cdot g^{-1} \cdot d^{-1}$)	RG ($g \cdot g^{-1} \cdot d^{-1}$)
FOR	March	0.014	0.038	0.029 ± 0.017			
	April	0.014	0.021	0.034 ± 0.008			
	May	0.034	0.038	0.029 ± 0.007			0.022 ± NA
	June	0.014	0.033	0.026 ± 0.005	0.013	0.030	0.022 ± 0.007
	July			0.025 ± NA			
EFT	March						
	April						
	May	0.016	0.020	0.015 ± 0.002	0.017	0.021	0.029 ± 0.005
	June	-0.010	0.006	0.019 ± 0.010	0.031	0.047	0.021 ± NA
	July			0.037 ± NA			
EEM	March	0.026	0.055	0.026 ± 0.008			
	April	0.015	0.022	0.026 ± 0.003			
	May	0.025	0.029	0.028 ± 0.009	0.015	0.020	0.022 ± 0.005
	June	-0.001	0.010	0.018 ± 0.005	0.024	0.033	0.024 ± 0.008
	July	0.012	0.018	0.019 ± 0.003			
DMF	March	0.028	0.073	0.032 ± 0.016			
	April	0.009	0.017	0.023 ± 0.008			0.023 ± NA
	May	0.004	0.009	0.028 ± 0.008	0.022	0.025	0.021 ± 0.005
	June	0.004	0.016	0.021 ± 0.008	0.004	0.016	0.015 ± 0.007
	July	0.009	0.024	0.028 ± 0.017			
NS	March	0.022	0.038	0.026 ± 0.005			
	April	-0.002	0.006	0.017 ± NA			
	May	0.022	0.029	0.025 ± 0.006	0.014	0.022	0.020 ± 0.006
	June	0.002	0.020	0.023 ± 0.010	0.012	0.030	0.023 ± 0.008
	July			0.033 ± 0.004			0.023 ± 0.018
OFF	March						
	April						
	May	0.040	0.044	0.022 ± 0.009	0.026	0.028	0.023 ± 0.007
	June	0.014	0.019	0.022 ± 0.005	0.010	0.014	0.023 ± 0.006
	July	0.012	0.016	0.024 ± 0.006	0.010	0.014	0.022 ± 0.007

Figures

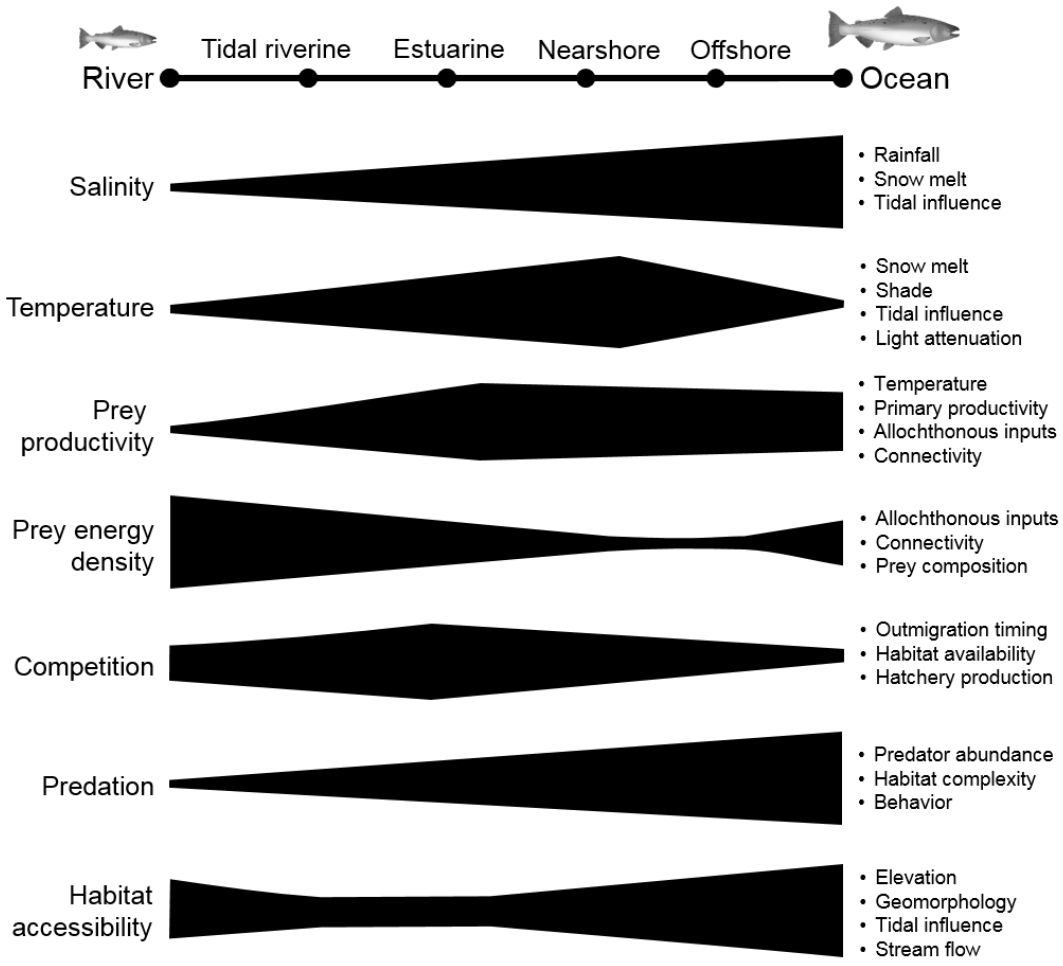

Figure 3.1. Juvenile Chinook Salmon use multiple habitat types as they migrate from river to sea. In coastal deltas, functional characteristics (left, roughly quantified by the width of the shaded regions) are determined by various physical and biological factors (right). This conceptual diagram demonstrates a hypothetical system where no single habitat type provides maximal benefits for resident juvenile salmon. For example, a tidal riverine habitat may have optimal water temperatures and very few predators, but there may also be greater competition for sparsely distributed prey. Conversely, higher prey productivity in the offshore zone might be offset by lower prey energy densities and fewer foraging opportunities due to the presence of predators. Although the shapes of these relationships likely vary through time and among watersheds, these functional tradeoffs show how each habitat type allows juvenile salmon to optimize their growth and survival by strategically using different habitats depending on environmental or ontogenetic limitations.

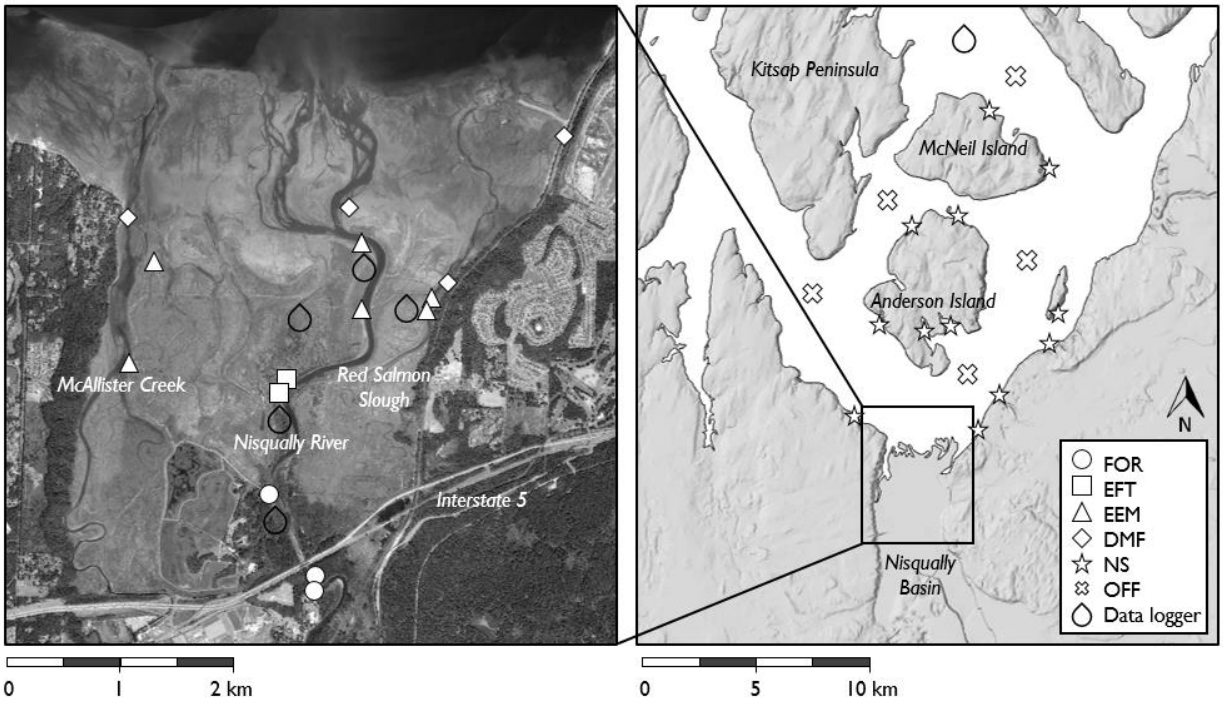

Figure 3.2. Map showing juvenile Chinook Salmon sampling sites in southern Puget Sound, Washington, USA. The panel on the left indicates beach seining efforts within the Nisqually River delta (aerial imagery: GeoTerra, Inc., Portland, Oregon, USA). The panel on the right shows lampara and purse seine locations further from shore. Shapes are representative of different habitat types: tidal freshwater forest (FOR), brackish transitional marsh (EFT), emergent salt marsh (EEM), delta mudflats (DMF), nearshore intertidal (NS), and offshore subtidal (OFF).

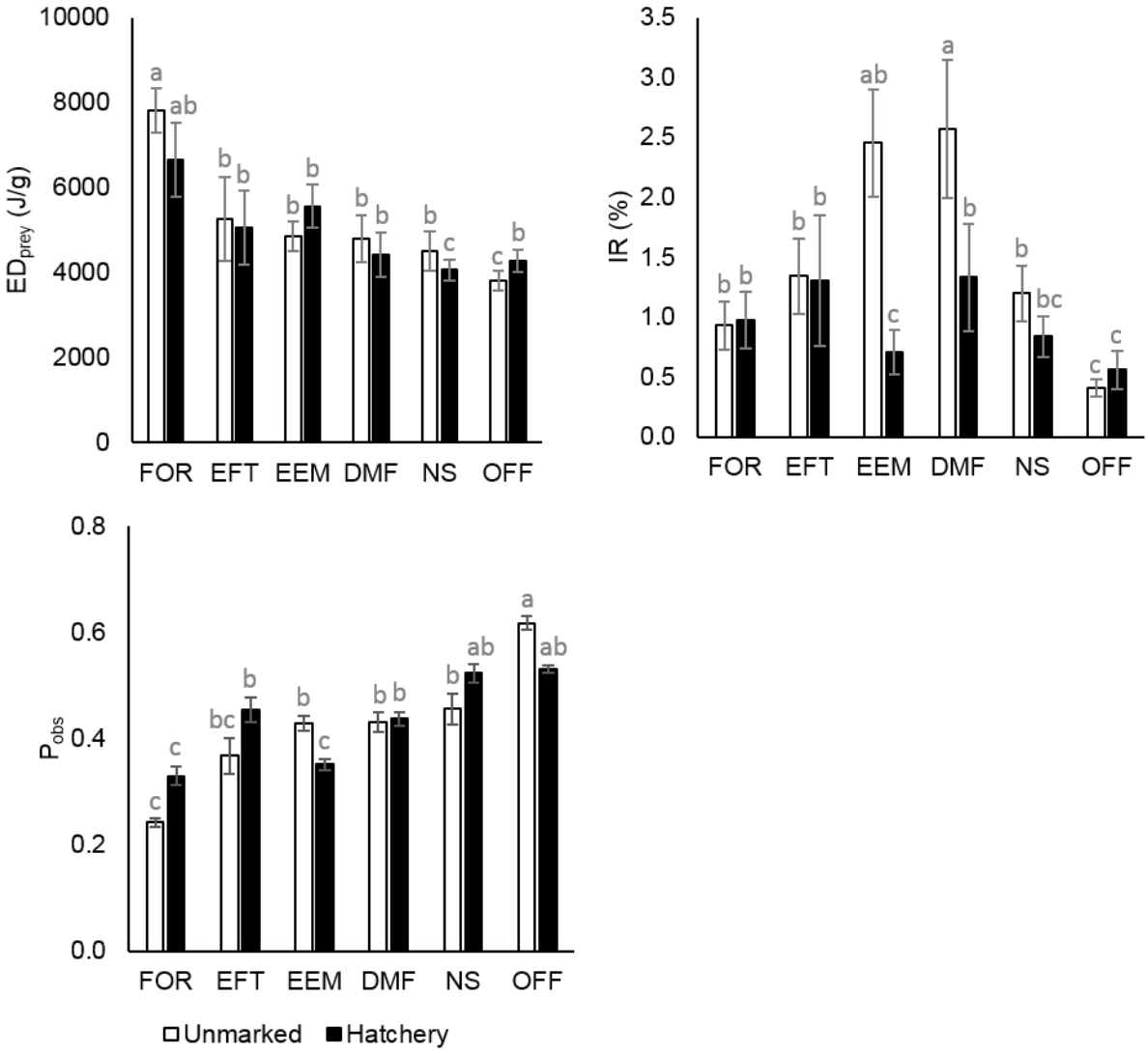

Figure 3.3. Mean dietary energy density (ED_{prey}; top left), instantaneous ration (IR; top right), and proportion of maximum consumption (P_{obs}; bottom left) for unmarked and hatchery juvenile Chinook Salmon. Tukey's HSD test was used to evaluate pairwise post hoc differences, and post-hoc groupings are denoted using letters above each bar. Error bars represent ± 1 SE.

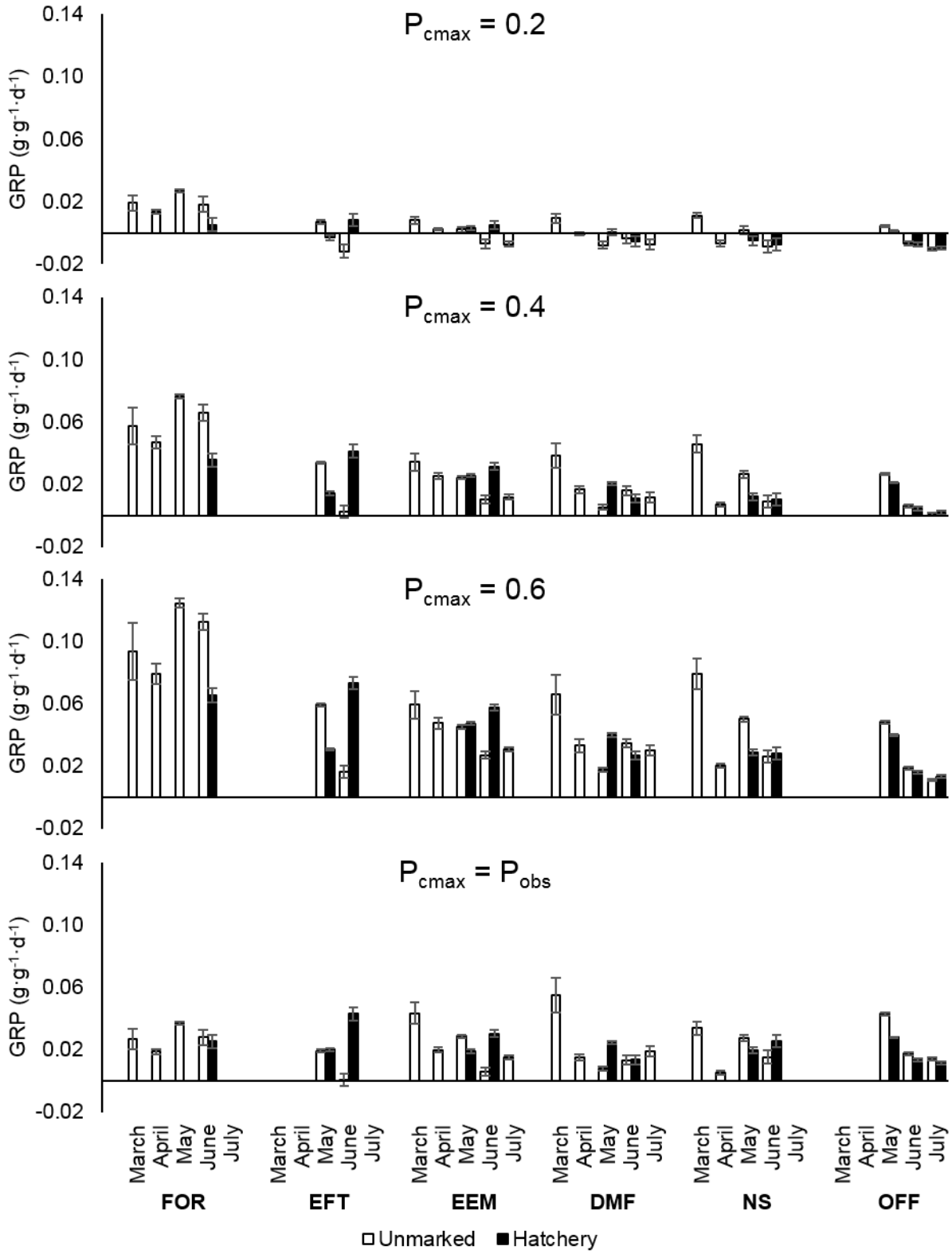

Figure 3.4. Mean ± SD simulated growth rate potential (GRP) for unmarked and hatchery juvenile Chinook Salmon captured in different months and habitat types.

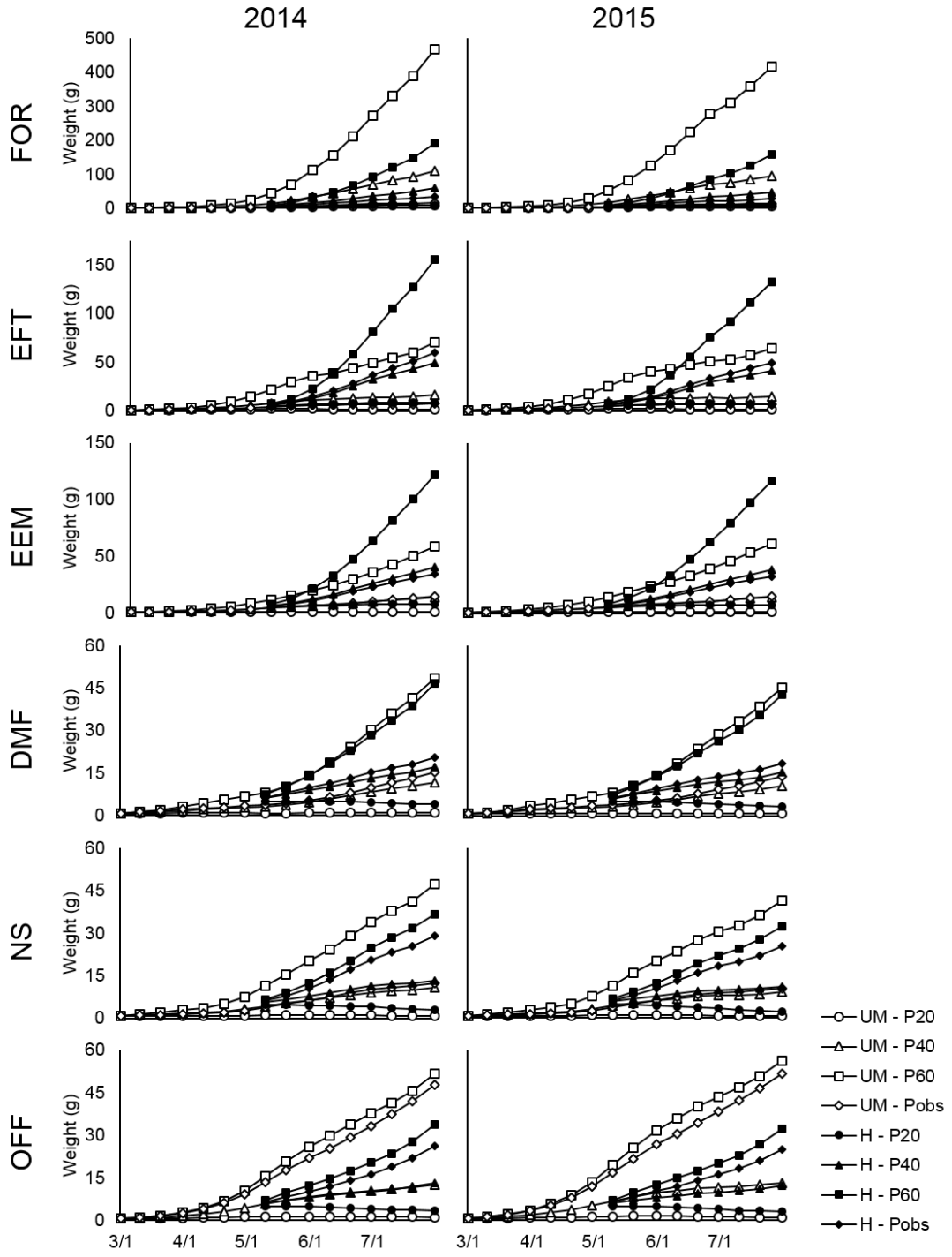

Figure 3.5. Output from habitat-specific bioenergetics simulations of unmarked (UM) and hatchery (H) juvenile Chinook Salmon. Weight (g) was calculated on a daily time step for P_{cmax} of 0.2, 0.4, 0.6, and P_{obs}. The simulation was run from May 1–July 31 for unmarked fish (0.75 g) and May 1–July 31 for hatchery fish (5 g).

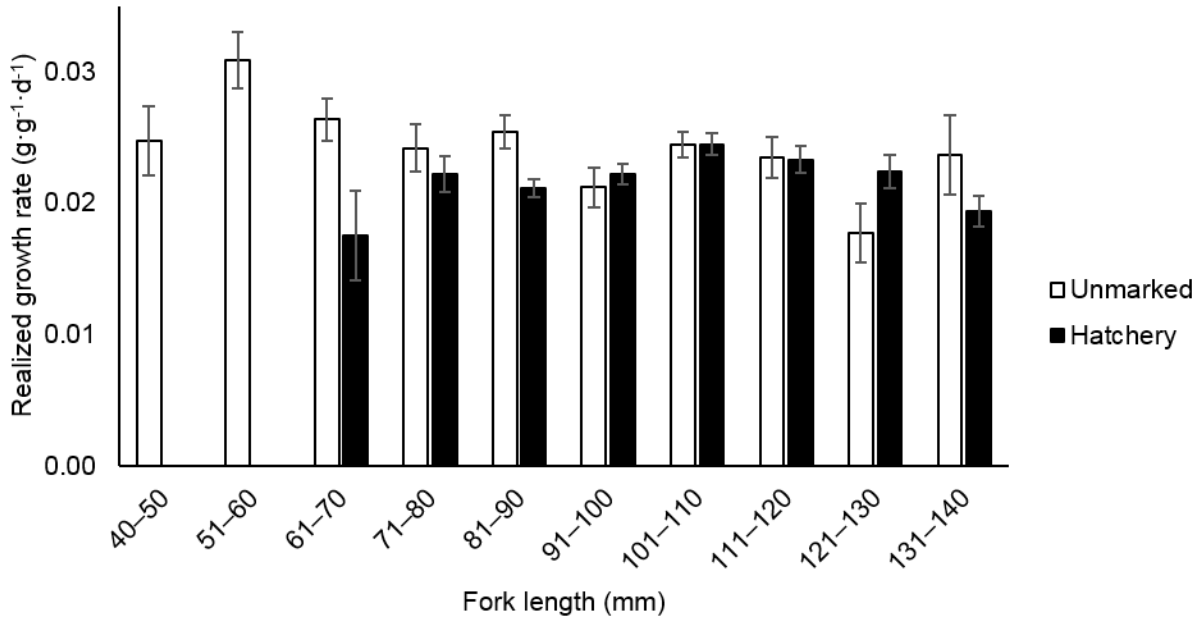

Figure 3.6. Relationship between realized growth rate and fork length for unmarked and hatchery juvenile Chinook Salmon. Realized growth was back-calculated from the two most recent scale circuli. Error bars represent ± 1 SE.

Appendix: Additional tables and figures

Table A3.1. Sample sizes for juvenile Chinook Salmon diet and scale samples by fork length, habitat type, month of capture, and rearing origin.

	Diets		Scales	
	Unmarked	Hatchery	Unmarked	Hatchery
Size				
40–50	28		11	
51–60	18		22	
61–70	16	1	20	2
71–80	22	12	27	20
81–90	33	51	36	77
91–100	25	59	24	78
101–110	12	17	30	60
111–120	6	8	18	37
121–130	5	1	5	28
131–140	2	1	4	17
Habitat				
FOR	32	11	28	11
EFT	8	13	7	4
EEM	47	30	33	30
DMF	27	20	36	28
NS	26	47	20	41
OFF	27	29	73	205
Month				
March	33		21	
April	16	1	19	1
May	51	93	53	133
June	44	51	52	133
July	23	5	52	52

Table A3.2. Wisconsin bioenergetics model equations and parameters for Chinook Salmon (Stewart and Ibarra 1991; Hanson et al. 1997; Plumb and Moffitt 2015). *Mass*, *Temp*, ED_{prey}, and ED_{fish} are inputs from empirical data (see Table 3.3). We used temperature-adjusted consumption parameters from Plumb and Moffitt (2015) when measured temperatures were > 18˚C.

Equation	Parameter	Value
$L_1 = e^{CG_1 \times (Temp - CQ)}$	CG_1	0.447[a], 0.389[b]
	CQ	5[a], 4.97[b]
$K_A = \frac{CK_1 \times L_1}{1 + CK_1 \times (L_1 - 1)}$	CK_1	0.360[a], 0.09[b]
$L_2 = e^{CG_2 \times (CTL - Temp)}$	CG_2	1.414[a], 1.209[b]
	CTL	24[a], 24.05[b]
$K_B = \frac{CK_4 \times L_2}{1 + CK_4 \times (L_2 - 1)}$	CK_4	0.010[a], 0.53[b]
$C_{scal} = K_A \times K_B$		
$C_{max} = CA \times Mass^{CB}$	CA	0.303
	CB	-0.275
$C_{prop} = C_{max} \times P_{cmax} \times C_{scal}$		
$C = C_{prop} \times ED_{prey}$		
$R_{scal} = RQ \times Temp$	RQ	0.068
$VEL = \begin{cases} if\ Temp > RTL, & RK_1 \times Mass^{RK_4} \\ if\ Temp < RTL, & A_{ACT} \times Mass^{RK_4 \times e^{B_{ACT} \times Temp}} \end{cases}$	RTL	25
	RK_1	1
	RK_4	0.13
	A_{ACT}	9.7
	B_{ACT}	0.041
$ACT = e^{RTO \times VEL}$	RTO	0.023
$R_{max} = RA \times Mass^{RB}$	RA	0.0026
	RB	-0.217
$Resp = R_{max} \times R_{scal} \times ACT$		
$R = Resp * 13{,}388$		
$PE = FA \times Temp^{FB} \times e^{FG \times P_{cmax}}$	FA	0.212
	FB	-0.222

	FG	0.631
$PF = \frac{PE - 0.1}{0.9} \times (1 - PFF) + PFF$	*PFF*	0.170
$F = PF \times C$		
$SDA = PSDA \times (C - F)$	*PSDA*	0.172
$U = UA \times (Temp^{UB}) \times e^{UG \times P_{cmax}} \times (C - F)$	*UA*	0.031
	UB	0.580
	UG	-0.299
$G = C - R - SDA - F - U$		

[a]Parameter values from Stewart and Ibarra (1991)

[b]Parameter values from Plumb and Moffitt (2015)

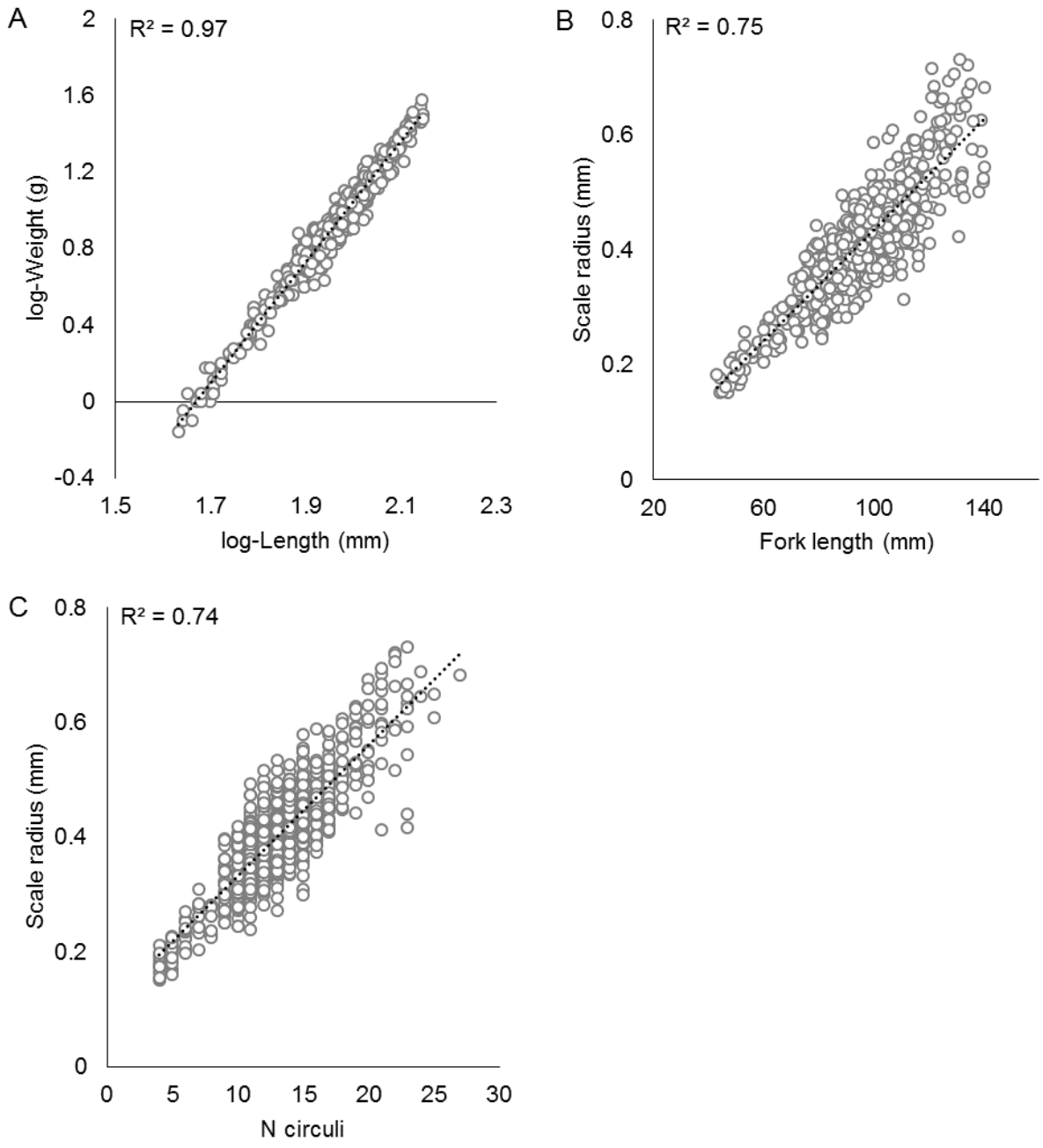

Figure A3.1. Modeled relationships between (A) log-fork length and log-weight, (B) length and scale radius, and (C) number of circuli and scale radius. The dashed line shows the predicted linear relationship between each set of variables. The direct association between somatic growth and scale growth was used to estimate the realized growth rates of subyearling Chinook Salmon in the Nisqually River delta.

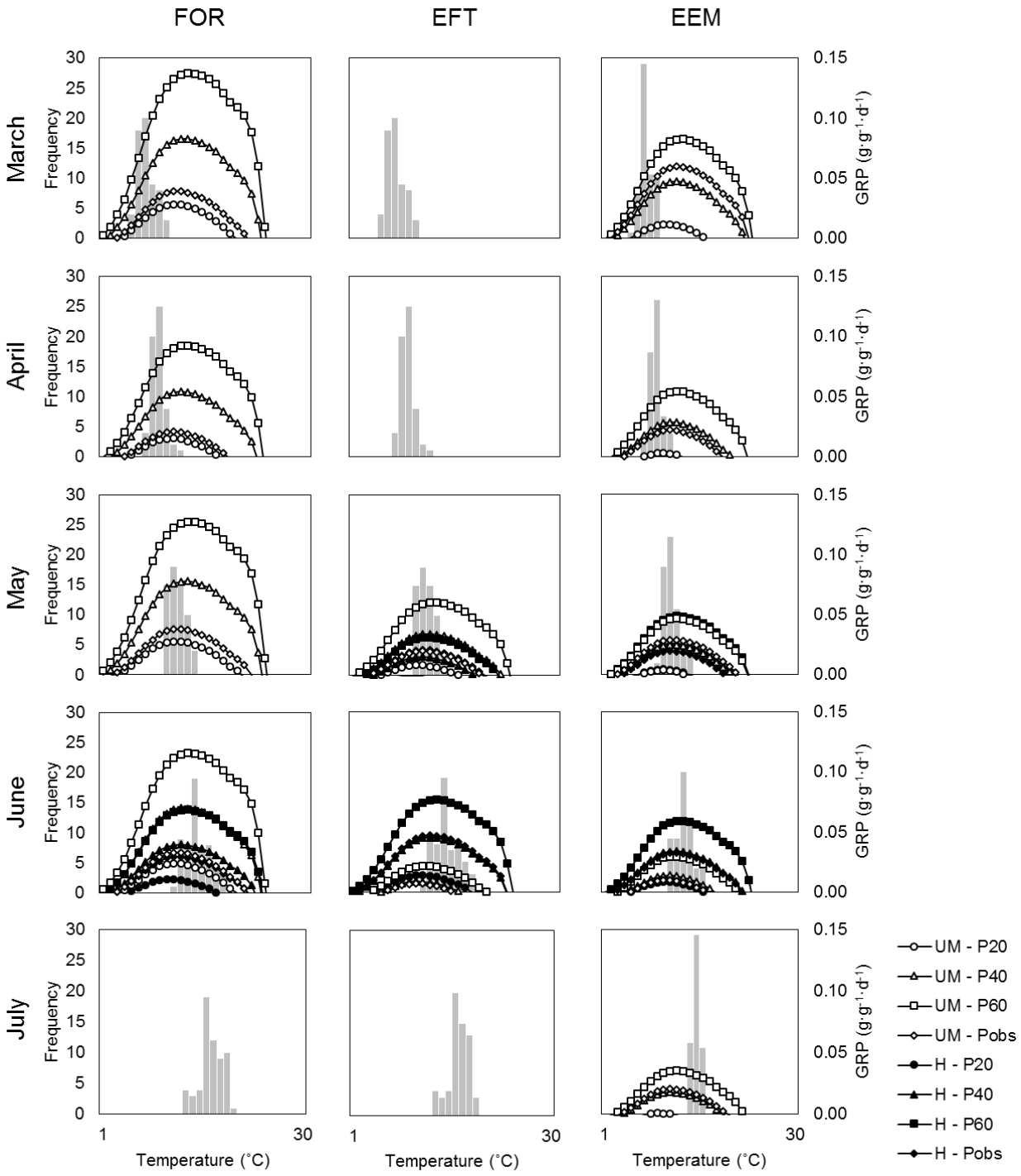
FOR
EFT
EEM
March
April
May
June
July
Frequency
GRP (g·g⁻¹·d⁻¹)
Temperature (°C)
1
30
0
5
10
15
20
25
0.00
0.05
0.10
0.15
UM - P20
UM - P40
UM - P60
UM - Pobs
H - P20
H - P40
H - P60
H - Pobs

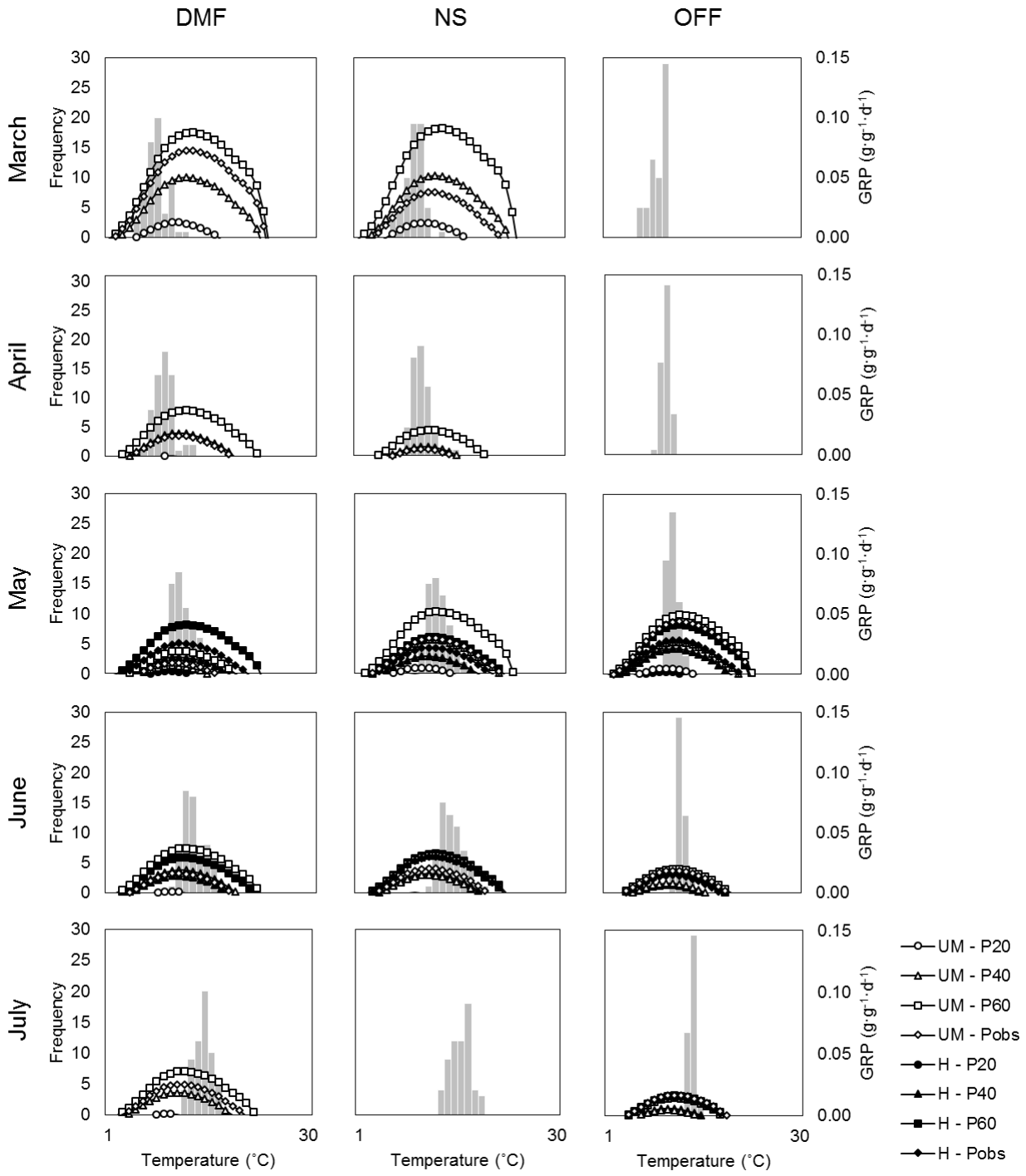

Figure A3.2. Modeled GRP curves by habitat type, month, rearing origin (unmarked = open points, hatchery = closed points), and proportion of maximum consumption (0.20, 0.40, 0.60, and P_{obs}). Size and ED_{prey} were held constant for each month based on inputs from Table 3.2. Gray bars represent frequency distributions of observed monthly temperatures.

Chapter 4

Development and implementation of an empirical habitat change model and decision support tool for estuarine ecosystems

Abstract

Widespread land use change in coastal ecosystems has led to a decline in the amount of habitat available for fish and wildlife, lower production of ecosystem goods and services, and loss of recreational and aesthetic value. This has prompted global efforts to restore the natural hydrologic regimes of developed shorelines, especially resource-rich estuaries, but the resilience of these restored ecosystems in the face of accelerated sea-level rise (SLR) remains uncertain. We implemented a Monitoring-based Simulation of Accretion in Coastal Estuaries (MOSAICS) to address uncertainty in the resilience of modified estuarine habitats, using the Nisqually River Delta in the Pacific Northwest USA as a case study. MOSAICS is a spatially explicit model with a numerical foundation that uses empirical monitoring datasets to forecast habitat change in response to rising tidal levels. Because it accounts for the crucial ecomorphodynamic feedbacks between tidal inundation, vegetative growth, and sediment accretion, MOSAICS can be used to determine whether alternative management scenarios, such as enhanced sediment inputs, will bolster estuarine resilience to SLR. Under moderate SLR (0.62 m), the model predicted that a two-fold increase in mean daily suspended sediment during the rainy season was sufficient to maintain Nisqually's emergent marshes through 2100, but under high SLR (1.35 m) MOSAICS indicated that greater sediment additions would be necessary to prevent submergence. A comparison between a restored marsh with subsided and high-elevation areas and a relict marsh demonstrated that the subsided restoration area was highly susceptible to SLR. Findings from the

MOSAICS model highlight the importance of a site's initial elevation, capacity for producing above and belowground biomass, and suspended sediment availability when considering management actions in estuaries and other coastal ecosystems.

Introduction

Estuaries and their associated tidal marshes connect freshwater riverine ecosystems to the open ocean, thereby playing a critical role in supporting marine ecosystem function (McLusky and Elliot 2004; Beaumont et al. 2007). They supply valuable economic, cultural, and ecological goods and services, including habitat for fish, waterbirds, and mammals (Simenstad and Cordell 2000; Greenberg et al. 2006; Barbier et al. 2011). Consequently, their preservation is a priority for coastal management. Over the coming century, global sea-level rise (SLR) is expected to diminish the extent of coastal wetlands by as much as 90%, converting productive tidal marshes into subtidal habitat (Nicholls et al. 1999; Galbraith et al. 2002; Craft et al. 2009; Crosby et al. 2016). Shoreline armoring, levees, and dams further compound the threat of SLR by removing many estuaries from tidal influence, preventing them from migrating inland, and reducing sediment accretion (Kirwan and Murray 2008; Jackson 2010). Major efforts are underway to eliminate unnecessary barriers to tidal exchange, but restored estuaries are often subject to degradation, which can reduce their resilience to SLR and other natural hazards (Callaway et al. 2007; Vandenbruwaene 2011).

Historically, estuarine tidal marshes have been able to counter the effects of SLR via an ecomorphodynamic feedback cycle whereby tidal inundation, vegetative growth, and sediment accumulation allow the marsh plain to keep pace with gradually increasing tidal levels (Kirwan et al. 2010; French 2006; Fitzgerald et al. 2008). Specifically, marsh vegetation traps suspended

sediment and slows the flow of water across the marsh surface, thereby facilitating sediment deposition and accretion (D'Alpaos et al. 2007, 2011). Habitat degradation due to disturbance, development, or management actions may inhibit this feedback cycle by facilitating erosion, hindering sediment delivery, or limiting above and belowground productivity (Syvitski et al. 2009; Vandenbruwaene 2011; Burdick and Roman 2012). Practitioners can augment the resilience of at-risk tidal marshes through the physical modification of sedimentation and subsidence rates, but there are often extrinsic (i.e., ecological, physical, or demographic) limitations to the continued stability of estuarine habitat (Kirwan and Megonigal 2013). Given these limitations, practitioners may benefit from a decision support tool that uses empirical data to identify vulnerable areas in a restored or degraded estuary, predicts changes to the estuarine habitat mosaic, and assesses the effects of alternative management actions given projected estimates of SLR.

Marsh accretion models can be used as a decision support tool to help managers determine a target estuary's long-term resilience, but most available models do not use empirically-derived datasets, are not spatially explicit, cannot directly incorporate management actions, or are "black box" simulations with respect to model calculations (Rybczyk and Callaway 2009; Mcleod et al. 2010*a*; Table 4.1). There is considerable breadth in the type and utility of marsh accretion models, ranging from generalized numerical equations (Kirwan et al. 2010) and simplified "bathtub" inundation simulations (Titus and Richman 2001), to spatially explicit, process-based models that lack a user interface and cost thousands of dollars to calibrate and run (Morris et al. 2016; Thorne et al. 2018). At present, stark tradeoffs between accuracy and simplicity demonstrate the need for a model that combines a transparent numerical foundation with localized, empirical data. Such an approach has already been used to predict water

temperature (Morrill et al. 2005, Sharma et al. 2008), phytoplankton productivity (Joint and Groom 2000; Barnes et al. 2011), marsh vegetation (Sanderson et al. 2001), and tidal channel formation (Hibma et al. 2004) in a variety of freshwater and marine ecosystems. Thus, there is reason to believe that the combined use of empirical datasets with numerical models may also be suitable for predicting estuarine responses to climate change.

This study evaluates the effects of rising tidal levels and modified sediment management strategies on estuarine habitat by developing a Monitoring-based Simulation of Accretion in Coastal Estuaries (MOSAICS). We calibrated and tested MOSAICS using seven years of post-restoration monitoring data from the Nisqually River Delta (NRD) in southern Puget Sound, Washington, USA. The NRD is a macro-tidal system comprised of a diverse habitat mosaic of upland tidal forests, freshwater, brackish, and saline emergent marshes, and intertidal mudflats. These attributes make it an ideal case study to evaluate habitat resilience to SLR and resultant changes in habitat distribution among historically managed and unaltered (relict) areas. Restoration actions conducted between 1996 and 2009 were led by Billy Frank Jr. Nisqually National Wildlife Refuge (hereafter "Refuge") and the Nisqually Indian Tribe (hereafter "Tribe"). The restored marshes have provided ample foraging and roosting sites for economically-valuable waterbirds and crucial nursery habitat for ESA-listed juvenile Chinook salmon (*Oncorhynchus tshawytscha*; Ellings et al. 2016; Davis et al. 2018; Woo et al. 2018). As such, state, federal, and tribal managers have a vested interest in maintaining the current extent of wetland habitat over the coming century.

Here we describe our steps in constructing, validating, and evaluating MOSAICS, which we used to evaluate long-term habitat trajectories in a subsided restoration area, a higher elevation restoration area, and a relict tidal marsh. Our overarching objectives for this study

were: 1) develop an empirical model to project long-term trajectories of elevation change and habitat distribution; 2) manipulate tidal level and sediment input parameters to determine how management scenarios may influence the estuarine habitat mosaic under impending SLR; and 3) compare estimated changes in the habitat mosaic for restored and relict sites. We anticipated that subsided restoration areas would exhibit less resilience to rising sea levels than the relict marsh due to lower initial elevations and a lack of vegetative biomass. Our approach demonstrates how monitoring data can play a crucial role in modeling efforts and can be used as part of a decision support tool to gauge the resilience of restored estuaries in the face of climate change.

Materials and methods

Study site

The Nisqually River originates from glacial discharge at the southwestern base of Mount Rainier, Washington, USA. From there the river meanders 130 km northward, where it empties into Puget Sound between the cities of Olympia and Tacoma (47.08°N 122.70°W), forming a large river delta with an areal extent of approximately 20 km^2. Between 1904 and 2009, roughly 5 km^2 of the delta's marshes were diked or leveed for agriculture, resulting in habitat loss for a variety of fish and wildlife species. Agricultural practices, including the drying of wetland soils, led to peat degradation and subsidence, with elevations behind the dikes subsiding up to 1.5 m lower than the surrounding marsh plain.

In 2009, the Refuge removed 8 km of dikes on the west side of the river, restoring over 3 km^2 of subsided marsh to tidal influence ("Restored Refuge"; Fig. 4.1). This major restoration project, along with several smaller restorations carried out by the Tribe on the east side of the river in 1996 (Pilot), 2002 (Phase I), and 2006 (Phase II; "Restored East"), represents the largest

composite estuary restoration in Puget Sound to-date. As of publication, the Restored Refuge sits at 0–2 m above mean tidal level (MTL = 1.34 m NAVD88), while Restored East is generally higher in elevation (1–3 m above MTL). Islands of relict salt marsh ("Relict Marsh") bound both restoration areas to the north and west, and are characterized by vegetated platforms (1–3 m above MTL) incised by a fractal network of tidal channels. In addition to its restored and relict marshes, the NRD consists of a diverse habitat mosaic including upland forests, freshwater and brackish tidal wetlands, intertidal mudflats, eelgrass (*Zostera marina*) beds, and nearshore subtidal areas (Belleveau et al. 2015; Ballanti et al. 2017; Davenport et al. 2017; Appendix A). A tidal range of more than 6 m during spring tides and frequent storm events throughout the autumn rainy season ensure that much of this mosaic is inundated at high tide.

The NRD was originally formed by infrequent volcanic events such as lahar flows (Pringle and Scott 2001), but regular inputs of inorganic sediment are crucial for maintaining the current extent and configuration of estuarine habitat. Each year, spring snow melt and autumn rainfall carry sediment to the NRD, where it is deposited or carried away by tidal currents. In 1945, construction of the Alder-LaGrande Dam complex was completed at river kilometer 65, trapping more than 42 million m^3 of sediment (Czuba et al. 2012*a*; Curran et al. 2016). As a result, the current quantity that is transported to the mouth of the Nisqually River is low compared to other, similarly-sized Puget Sound rivers (Czuba et al. 2011). Various tributaries feed into the main stem below the dam, but it is estimated that only 10% of the primary sediment load generated upstream reaches the mouth of the river (Nelson 1974; Czuba et al. 2012*a*). Consequently, it is important to consider the interplay among depleted inorganic sediment inputs, changing tidal regimes, and geological processes such as uplift and subsidence when assessing the response of the NRD to rising tidal levels.

Data collection

Post-restoration monitoring efforts were conducted throughout the NRD in 2010–2017 as part of a larger comprehensive monitoring plan. We collected data throughout restored and relict marshes with varying levels of freshwater and tidal input (Fig. 4.1; Table 4.2). When possible, we targeted sampling sites adjacent to tidal sloughs such that geomorphological and biological datasets overlapped spatially. We did not include sampling sites in areas that had been removed from tidal influence, including freshwater wetlands within the new dike or wetlands to the south of the I-5 highway barrier. All relevant datasets contributing to the construction and validation of MOSAICS are described in detail below.

Water level

We used barometrically-compensated water level data collected from a Solinst® LTC level logger located in a Relict Marsh channel (Fig. 4.1) to quantify inundation duration. Data were logged continuously at 6, 12, or 15-minute intervals between February 2010 and January 2015, and were converted from water level (m) to vertical elevation (m NAVD88) based on Real Time Kinematic Global Positioning System (RTK GPS) measured sensor height. We used the complete dataset to calculate a tidal datum for the NRD; MTL for the estuary was 1.34 m, with a mean high water level (MHW) of 2.82 m, a mean higher-high water level (MHHW) of 3.11 m, a mean low water level (MLW) of -0.11 m, and a mean lower-low water level (MLLW) of -1.00 m.

Vegetation surveys

We conducted vegetation surveys at 30 sites in September 2009–2015 (Fig. 4.1). At each site, we measured mean percent cover, canopy height, and stem density for all species observed within a 0.25-m^2 sampling quadrat. We sampled three quadrats per-site at locations 0-, 20-, and 40- m from the edge of an adjacent tidal slough to account for spatial variation in sediment distribution. We also noted local habitat characteristics such as water depth and overhead canopy cover. Associated soil pore salinity values (psu) were obtained for each surveyed quadrat by drawing out moisture from the top layer of marsh sediment and analyzing the extracted water with a refractometer.

Elevation change

We measured elevation change through time at a precision of up to 1 mm using rod Surface Elevation Tables (SETs; Cahoon et al. 2002) located at 14 restored and relict marsh sites (Fig. 4.1). We took an initial SET measurement immediately after the restoration in September 2009 and collected yearly measurements every spring thereafter through April 2017. Feldspar horizon markers and sediment pins at each site were used to measure corresponding sediment accretion rates, although due to scouring and obvious sediment redistribution at the northwest corner of the Restored Refuge, horizon markers were not considered to be an accurate measure of sediment deposition at these sites.

Suspended sediment

Because we did not collect empirical measurements of suspended sediment, we used a regression model to estimate sediment load to the NRD (Curran et al. 2016): $L = 0.00199 \cdot Q^{2.68} \cdot bcf$ where L is suspended sediment load in metric tons per day (t/d), Q is river discharge in cubic

meters per second (m^3/s), and *bcf* is a bias correction factor equal to 1.17. We obtained daily mean discharge estimates from a combination of water data reports and publicly-available water quality data (https://waterdata.usgs.gov/nwis). These data were then converted to mean daily suspended sediment loads using the transport curve equation for total yearly inputs and for the rainy season (October–March).

Spatial data

We used a 3-m resolution bare earth digital elevation model (DEM) acquired from airborne, topographic lidar collected in January 2011 (Watershed Sciences Inc., Portland, Oregon, USA) to determine initial elevation values for the spatially explicit model. These data were validated to a vertical accuracy of ± 3 cm using RTK GPS and boat-mounted bathymetric surveys. We hand-digitized channels and other water features on georeferenced aerial imagery flown in summer 2011 (Bergman Photographic Services Inc., Portland, Oregon, USA; Ellings et al. 2016).

We derived several spatial datasets using the 2011 DEM. For each 3 × 3-m cell, we analyzed least-cost path distances to the delta at MTL (i.e., marsh edge), the nearest freshwater source (Nisqually River or McAllister Creek), and the Nisqually River main stem using the "Path Distance" tool in ArcGIS 10.3 software (ESRI Inc., Redlands, California, USA). We used the "Euclidean Distance" tool in ArcGIS to measure the straight-line distance between each cell and the edge of the nearest tidal channel. All spatial datasets were georeferenced to the WGS84 coordinate system.

Data analysis

Model structure and parameterization

The MOSAICS model and decision support tool has a hierarchical structure based on multiple, numerical models that recognize the interdependency of inundation duration, vegetative biomass, sediment availability, and elevation change in tidal marshes (Morris et al. 2002; Temmerman et al. 2003; D'Alpaos et al. 2007; Kirwan and Murray 2007; Fig. 4.2). These models have shown that elevation change is an additive product of allochthonous mineral sediment settling on the marsh surface (E_{sed}), sediment captured by vegetation (E_{cap}), autochthonous organic matter deposition (E_{org}), tidal erosive forces (E_{er}), and compaction (D'Alpaos et al. 2011). Compaction and settling are generally assumed to have minimal effects on elevation change in most tidal marshes (French 1993; French 2006; but see Morris et al. 2016), while the geological processes of subsidence and uplift (E_{geo}) can significantly impact elevations at longer timescales (Verdonck 2006). We modeled elevation change (ΔE) as an iterative yearly time step (t) for each raster cell (x, y), with inundation duration ($I_{t,x,y}$), vegetative biomass ($V_{t,x,y}$), and suspended sediment (L_t) as primary drivers. We applied a maximum likelihood estimation procedure with the "bbmle" package in R 3.4.1 (R Core Development Team 2017) to parameterize each equation using the empirical monitoring datasets described below.

To model elevation change through time, we used an autoregressive framework based on D'Alpaos et al. (2011):

$$E_{t+1,x,y} = E_{t,x,y} + \Delta E_{t,x,y} \qquad (1)$$

$$\Delta E_{t,x,y} = E_{sed} + E_{cap} + E_{org} + E_{er} + E_{geo} \qquad (2)$$

with the assumption that E_{sed} is dependent upon L_t and $I_{t,x,y}$; E_{cap} is dependent upon L_t, $I_{t,x,y}$, and $V_{t,x,y}$; E_{org} is dependent upon $V_{t,x,y}$; E_{er} is dependent upon $I_{t,x,y}$; and E_{geo} is constant for the entire study area (0.5 mm/yr; Verdonck 2006). Suspended sediment concentrations decay exponentially with distance from the sediment source (Stumpf 1983; Christiansen et al. 2000). Because we did

not have spatially explicit data for L_t we used position on the marsh plain in relation to tidal channels as a proxy for spatial variation in sediment distribution, which is broadly recognized to influence accretion rates (Christiansen et al. 2000; D'Alpaos et al. 2007; Li and Yang 2009). Specifically, we modeled L_t as a linear function of a cell's path distance from the Nisqually River main stem ($Riv_{x,y}$) and as an exponentially decreasing function of its Euclidean distance from the nearest tidal channel edge ($Chan_{x,y}$). The relationship between $\Delta E_{t,x,y}$ and $I_{t,x,y}$ was modeled as an exponential decay function (increasing form) based on a preliminary analysis of the sediment pin and horizon marker data showing that E_{sed} leveled off asymptotically with increasing $I_{t,x,y}$. Thus, the mathematical form of each component was:

$$E_{sed} = L_t \cdot (1 - e^{-i_a \cdot I_{t,x,y}}) \cdot \left(int_1 + r_a \cdot Riv_{x,y} + c_a \cdot e^{-c_b \cdot Chan_{x,y}}\right) \quad (3)$$

$$E_{cap} = L_t \cdot V_{t,x,y} \cdot (1 - e^{-i_b \cdot I_{t,x,y}}) \cdot \left(int_2 + r_b \cdot Riv_{x,y} + c_d \cdot e^{-c_e \cdot Chan_{x,y}}\right) \quad (4)$$

$$E_{org} = v_a \cdot V_{t,x,y} \quad (5)$$

$$E_{er} = i_c \cdot (e^{-i_d \cdot I_{t,x,y}} - 1) \quad (6)$$

The interactive terms of the model were structured such that when L_t or $I_{t,x,y}$ were zero elevation change was dependent solely on organic matter accumulation (E_{org}), when $V_{t,x,y}$ was zero elevation change was dependent exclusively on mineral sedimentation and erosive forces (E_{sed}, E_{er}), and when all three were zero only geologic uplift and subsidence (E_{geo}) affected yearly elevation change.

The inputs for $I_{t,x,y}$ and $V_{t,x,y}$ were expressed as their own set of hierarchical equations. For $I_{t,x,y}$, we modeled the relationship between inundation duration and surface elevation as a cumulative distribution of the proportion of time a cell of elevation E was submerged by the tide during a given year t (Bockelmann et al. 2002; Temmerman et al. 2003). To incorporate changing sea levels, we used E relative to MTL, assuming MTL stayed relatively constant at

1.34 m NAVD88 between 2010 and 2015. We parameterized a cumulative distribution function on incrementally increasing elevation values representing the full range of elevations observed for the Nisqually estuary (-1–3.5 m relative to MTL):

$$I_{t,x,y} = \frac{1}{(1+a \cdot e^{-b \cdot E_{t,x,y}})^{\frac{1}{c}}} \qquad (7)$$

The function was given a lower asymptote of 0 and an upper asymptote of 1 to limit $I_{t,x,y}$ to proportional values, and the model was fit to the data by parameterizing *a*, *b*, and *c*.

We modeled $V_{t,x,y}$ as a function of $I_{t,x,y}$ and soil pore salinity ($S_{t,x,y}$). While we did not explicitly measure aboveground biomass using the vegetation quadrats, it is calculable as a function of several structural parameters, including stem density per unit area and mean plant height (Morris and Haskin 1990; Thursby et al. 2002). We calculated per-area standing biomass (g/m^2) for each species *j* observed in a sampling quadrat using the equation $V_j = 0.04 n_j h_j$, where n_j is the species' extrapolated stem density per m^2 and h_j is its average stem height. This equation was based on literature values and observed height-biomass relationships for *Carex lyngbyei*, *Distichlis spicata*, and *Salicornia pacifica* (USGS, unpublished data). The sum across all observed species was considered the total estimated vegetative biomass value for a given sampling quadrat, and was used as our input dataset for parameterizing $V_{t,x,y}$.

We modeled $V_{t,x,y}$ as a Gaussian function with respect to $I_{t,x,y}$. This was reflective of the polynomial relationship demonstrated by Morris et al. (2002), showing that productivity increases with greater elevations relative to MTL, but then starts to decrease again at a threshold height. We chose a Gaussian equation to keep $V_{t,x,y}$ above zero across the full range of $I_{t,x,y}$ values. We also included an interaction effect with $S_{t,x,y}$ because exploratory data analyses determined that biomass decreased with increasing soil salinities, leveling off around 50 psu. Our final model for predicting $V_{t,x,y}$ was:

$$V_{t,x,y} = N \cdot e^{-\delta \cdot S_{t,x,y}} e^{\frac{-(I_{t,x,y} - \mu)^2}{2 \cdot \sigma^2}} \quad (8)$$

where $I_{t,x,y}$ was determined from equation 7, $S_{t,x,y}$ was determined from equation 9 (below), and N, δ, μ, and σ were shape parameters.

Estimates of $S_{t,x,y}$ were necessary to calculate $V_{t,x,y}$ and to identify different estuarine habitat types. Soil salinity is governed by several environmental factors, including the frequency and duration of tidal inundation, distance from the nearest source of freshwater, and distance from the marsh edge (Odum 1988; Moffett et al. 2010). High elevation marshes tend to be more saline than low elevation marshes because evapotranspiration and infrequent tidal flushing can lead to the accumulation of salt within the soil (Callaway et al. 2007), while sites closer to riverine freshwater inputs tend to have lower salinities. An exploratory analysis suggested that the relationships between $S_{t,x,y}$, $I_{t,x,y}$, and a site's position on the marsh plain were highly complex, so we used an information theoretic approach to compare several non-linear candidate models for $S_{t,x,y}$ (Appendix B). An exponential decay function was used to define the asymptotic relationship between $S_{t,x,y}$ and $Riv_{x,y}$, and several additive and interactive functions including distance from the marsh edge ($Mar_{x,y}$) and $I_{t,x,y}$ were tested. We parameterized each candidate model using maximum likelihood estimation and selected the best-fit model using Akaike's Information Criterion (AIC; Burnham and Anderson 2002). We determined the best-fit model structure to be:

$$S_{t,x,y} = \alpha + \beta \cdot Mar_{x,y} + \left(C + \gamma \cdot I_{t,x,y}\right) \cdot \left(1 - e^{-k \cdot Riv_{x,y}}\right) \quad (9)$$

where $I_{t,x,y}$ was ascertained using equation 7 and α, β, γ, C, and k were shape parameters.

Our final step was to classify a given cell as a specific estuarine habitat type given model outputs ($H_{t,x,y}$). In most estuaries, habitat type is primarily related to inundation duration and soil pore salinity and is generally defined by the vegetation species occupying a particular tract of the

marsh plain. Species tolerances for inundation regimes and soil pore salinity can vary widely among regions and among estuaries (Pennings et al. 2005; Silvestri et al. 2005), so we used vegetation survey data and a clustering algorithm to define inundation and salinity ranges for each habitat type. Detailed methods along with a list of plant species observed in each habitat type are outlined in Appendix A.

We applied MOSAICS to the NRD by calculating $I_{t,x,y}$, $S_{t,x,y}$, $V_{t,x,y}$, $\Delta E_{t,x,y}$, and $H_{t,x,y}$ iteratively on an annual time step for each 3 × 3-m cell. The 2011 DEM was used for our initial elevation values and the spatial datasets described below were used as measurements of $Riv_{x,y}$, $Mar_{x,y}$, *and* $Chan_{x,y}$. All spatially explicit model analyses were conducted with the "rgdal" and "raster" packages in R.

Model validation

To validate the elevation change model, we conducted a sensitivity analysis using parameter space estimation in the R package "pse." We varied predictor variables over a range of uniformly or normally distributed realistic values including inundation duration ($I_{t,x,y}$; 0–1), suspended sediment input (L_t; mean ± SD: 300 ± 100 t/d), vegetative biomass ($V_{t,x,y}$; 0–5,000 g/m^2), path distance to the Nisqually River ($Riv_{x,y}$; 0–2,000 m), and Euclidean distance to the nearest channel edge ($Chan_{x,y}$; 0–300 m). We produced 3D surface plots of model output when parameter space was manipulated for two variables at a time to discern each variable's distinct influence on annual elevation change (mm).

The autoregressive structure of MOSAICS meant that model error was potentially propagated through time. We conducted a second, longitudinal sensitivity analysis, where elevation change was simulated through time (2011–2100) for a single hypothetical cell under

present day SLR. We tested initial elevations (E_0) of -1-, 0-, 1-, 2-, and 3-m relative to MTL, while *Riv* was held constant at 550 m, *Mar* was held constant at 550 m, *Chan* was held constant at 30 m, and L_t was set to 300 t/d. We varied $I_{t,x,y}$, $S_{t,x,y}$, $V_{t,x,y}$, and $\Delta E_{t,x,y}$ by ± 1 root-mean-squared error (RMSE) as a percentage of the full range of observed values. RMSE was determined from the maximum likelihood estimation procedure for model equations 7, 9, 8, and 2 respectively (Table 4.3).

Management scenarios

We used MOSAICS as a decision support tool to determine how SLR in the NRD might affect the elevation and habitat composition of its restored and relict marshes through the year 2100. Scenarios included present day SLR (2 mm/yr or 0.18 m by 2100; Bromirski et al. 2011), moderate SLR (0.62 m by 2100; NRC 2012), and high SLR (1.35 m by 2100). Additionally, we tested several management strategies for increasing the delivery and retention of suspended sediment in river deltas, including raising initial elevations through dredging or sediment augmentation, periodic riverine sediment pulses via altered reservoir practices, and dam removal (NRC 2011). Present day (2009–2016) mean suspended sediment loads for the NRD range between 100 and 550 t/d during the rainy season, with peaks of up to 10,000 t/d during major storm events (Curran et al. 2016). To simulate periodic sediment loads, we introduced spikes in suspended sediment (1,000 t/d) once every 10 years. To test the effects of a gradual increase in sediment delivery (i.e., through altered reservoir practices), we increased annual suspended sediment inputs two-fold from an average of 300 t/d to 600 t/d during the rainy season. To simulate unrestrained sediment input (i.e., dam removal), we increased mean seasonal sediment loads from 300 t/d to 3,000 t/d based on an estimated dam trap efficiency of 90% and an

estimated river retention rate of roughly 50% (Czuba et al. 2012*a*). We also tested a scenario where we raised initial elevations across the delta by 0.5 m, although realistically this strategy would only be viable at smaller spatial scales. We tested each sediment input scenario in tandem with moderate and high estimates of SLR (NRC 2012) to determine whether additional suspended sediment could mitigate potential habitat loss.

Results

Model structure and validation

We successfully parameterized each hierarchical component of MOSAICS ($I_{t,x,y}$, $S_{t,x,y}$, $V_{t,x,y}$, $\Delta E_{t,x,y}$) using the empirical datasets. Model RMSE was less than 16% of the range of observed values for each component (Table 4.3). For $\Delta E_{t,x,y}$, the parameters r_b in the sediment capture equation (E_{cap}) and v_a in the organic matter deposition equation (E_{org}) converged on zero, so they were omitted from the final model. This meant that E_{org} essentially had no effect on elevation change in the NRD. Instead, inorganic sediments (E_{sed}) were the predominant contributor to annual elevation change for all scenarios, although erosive processes (E_{er}) negated this contribution in areas that were inundated more than 50% of the time. Sediment capture by vegetation (E_{cap}) augmented annual elevation change by 0–70% within the range of marsh plant inundation tolerances, with peak contributions at an inundation duration of approximately 12%. As such, the greatest accretion rates were predicted to occur in areas that were inundated between 2% and 23% of the time.

The parameter space estimation procedure showed that most predicted model outcomes fell between -1 and 15 mm/yr — a realistic, albeit conservative estimate based on annual observed SET readings, which ranged between -58 mm and 90 mm/yr (mean ± SD: Restored

Refuge = 4.91 ± 20.07 mm/yr, Restored East = 6.91 ± 6.43 mm/yr, Relict Marsh = 2.45 ± 4.36 mm/yr). The sensitivity analysis also found that each predictor variable differed with respect to its relative effects on marsh accretion rates. Partial rank correlation coefficients indicated that positive accretion rates were more likely to occur further from the Nisqually River (mean ± SE PRCC = 0.90 ± 0.02) and with greater suspended sediment loads (0.68 ± 0.04), while negative accretion rates were more likely to occur in areas further from tidal channels (-0.37 ± 0.05). Vegetative biomass had a moderately positive relationship with increasing marsh elevations (0.31 ± 0.04). Three-dimensional surfaces produced from a pairwise manipulation of parameter space supported these findings and highlighted parameter values that were more likely to produce unrealistic model output (Fig. 4.3).

In addition to error that was potentially introduced by the spatial inputs (*Riv*, *Chan*), the longitudinal sensitivity analysis determined that model error was propagated through time; however, it appeared to have only a marginal effect regardless of a site's initial elevation. The RMSE of the inundation component was only 0.015, which was 1.5% of the total range of observed values (0–1). As such, the inclusion of such minor error had little effect on the model output than would otherwise be expected based on year-to-year variance in the sediment term (Fig. 4.4). Unremarkable findings were also observed for soil pore salinity and vegetation despite higher RMSE (~15%). The only component for which the propagation of error appeared to be a concern was for annual elevation change, where the inclusion of error resulted in a 5–35% decrease (-RMSE) or 3–13% increase (+RMSE) in the final predicted elevation depending on E_0.

Present day conditions

For the first decade after restoration (2011–2020), MOSAICS forecasted varying rates of elevation change throughout the delta with an overall trend toward elevation gain relative to MTL in the Restored Refuge (0.027 ± 0.026 m), Restored East (0.042 ± 0.047 m), and Relict Marsh sites (0.049 ± 0.051 m). The model classified the 2011 estuarine habitat mosaic as 43.2% subtidal, 6.4% eelgrass, 11.3% intertidal mudflats, 16.4% low-elevation salt marsh, 4.9% mid-elevation salt marsh, 9.3% high-elevation salt marsh, 4.9% brackish marsh, 0.3% freshwater marsh, and 3.5% upland habitat (Fig. 4.5). The most notable changes in habitat distribution between 2011 and 2020 were observed in the intertidal mudflats (-0.5%), mid-elevation salt marsh (-1.1%), and high-elevation salt marsh (+1.7%), with zero change in the extent of low-elevation salt marsh, freshwater, and upland habitats.

Management scenarios

Without additional suspended sediment inputs, MOSAICS projected that mean elevation relative to MTL would increase by 0.38 m in the Restored Refuge, 0.37 m at Restored East, and 0.43 m in the Relict Marsh by 2100 under present rates of SLR (Fig. 4.6). This led to a 225% increase in the areal extent of upland habitat, a 25% decrease in mudflat, and a 18% decrease in low salt marsh, which was primarily driven by the E_{geo} parameter (Fig. 4.7, Table 4.4). Under moderate SLR, elevations at all sites increased through 2050 before succumbing to rising tidal levels in 2100. As a result, elevation relative to MTL decreased by 0.12 m in the Restored Refuge and 0.02 m at Restored East, while elevations increased slightly by 0.04 m in the Relict Marsh. In this case, upland habitat decreased to half it's current areal extent as it was converted to high salt marsh and brackish marsh along the edge of the Nisqually River. The highest rates of SLR resulted in substantial submergence of marsh habitat throughout the NRD. All three study areas

experienced sharp declines in elevation, especially during the latter half of the century. The modeled elevation of the Restored Refuge decreased by 0.78 m, meaning it was inundated for 57% of the average tidal cycle. The elevations of Restored East and the Relict Marsh declined by 0.63 m and 0.56 m respectively. This led to delta-wide losses of low, mid-, and high salt marsh, and upland habitats. Salt marsh submergence was especially noticeable in the Restored Refuge, where almost all the low salt marsh was converted to intertidal mudflat by 2100, and only small swaths of high and brackish marsh remained along the edge of the Nisqually River.

Output from MOSAICS indicated that raising the initial marsh plain by 0.5 m was an effective buffer against SLR in the restored marshes. Under moderate SLR, mean elevations were 0.65 m higher than present day conditions in the Restored Refuge and 0.41 m higher at Restored East by the year 2100 (Fig. 4.6). Delta-wide, the extent of high marsh was doubled, while low and mid-salt marsh declined by 54% and 18% respectively (Fig. 4.7, Table 4.4). In 2100, the predominant habitat type predicted for both restoration areas was high salt marsh, with intermittent patches of brackish marsh and upland habitat. When high SLR rates were used in the model, the 0.5 m elevation buffer was enough to ensure that much of the subsided Restored Refuge was not submerged, and projected 2100 elevations and habitat distributions were similar to present day. Elevation relative to MTL was only 0.13 m less than present day conditions in the Restored Refuge and 0.11 m less at Restored East. Delta-wide, the extent of low and mid-salt marsh decreased slightly, while high salt marsh increased by 34%.

Intermittently increasing the mean daily suspended sediment load from 300 t/d to 1,000 t/d once every 10 years did little to stave off the effects of accelerated SLR according to model projections. Under moderate SLR, mean elevations were only 6–8 cm greater than those projected in 2100 without any additional sediment input (Fig. 4.6). A similar trend occurred

under high SLR, where 2100 elevations were projected to be only ~7 cm greater in the Restored Refuge, Restored East, and Relict Marsh than those estimated under the model scenario without additional sediment. Conversely, doubling the amount of sediment delivered to the NRD appeared to be the most effective strategy to prevent the submergence of emergent marsh and to maintain the estuarine habitat mosaic over the coming century. Under moderate SLR, MOSAICS projected that mean elevation relative to MTL would increase by 0.45 m in the Restored Refuge, 0.31 m at Restored East, and 0.41 m in the Relict Marsh. Under modeled conditions, the extent of delta mudflat habitat would decrease by 29%, while high salt marsh would increase by 52% (Fig. 4.7, Table 4.4). Under high rates of SLR, mean elevations would only decrease by 0.28 m in the Restored Refuge, 0.21 m at Restored East, and 0.10 m in the Relict Marsh. Given these rates of elevation change, the extent of low and mid-salt marsh would be halved, but high salt marsh would still increase by 23%.

With up to 42,000,000 m^3 of sediment trapped behind Alder Dam (Czuba et al. 2012*b*), the hypothetical scenario of dam removal would result in almost all the currently-existing marsh being converted to upland habitat by 2100, even after accounting for SLR (Fig. 4.7, Table 4.4). Under moderate SLR, mean elevation relative to MTL would increase by 1.5 m in the Restored Refuge, 0.61 m at Restored East, and 1.27 m in the Relict Marsh (Fig. 4.6). The model forecast similar conditions under high SLR, where elevation relative to MTL would increase by 1.3 m in the Restored Refuge, 0.66 m at Restored East, and 1.20 m in the Relict Marsh. Again, most of the delta would be predominated by subtidal and upland habitats by 2100, but eelgrass beds and high salt marsh were also expected to increase.

Discussion

Our study effectively demonstrates how empirical data can be used as part of a decision support tool to forecast differences in the long-term resilience of restored and relict estuaries when confronted with climate change. We evaluated the relative effects of alternative sediment management scenarios on the persistence and composition of estuarine habitats using a hierarchical numerical model (MOSAICS). Model predictions indicated that post-restoration marsh accretion in the NRD is occurring at a slow but steady rate and will likely continue to do so over the next 40 years if SLR does not accelerate. Short-term model output predicted roughly 3 cm of elevation gain relative to MTL in the subsided restoration area (Restored Refuge) and 5 cm of elevation gain in the higher elevation restoration area (Restored East) between 2011 and 2020. This is consistent with observations from SET readings, sediment pins, and RTK GPS surveys (USGS, unpublished data). Differences between projected habitat distributions in 2011 and 2020 were marginal, suggesting that post-disturbance vegetative succession rather than accretion-mediated habitat change is driving the ongoing transition from mudflat to salt marsh in the subsided restoration area.

Long-term scenarios of climate change demonstrated varying levels of resilience to predictions of rising sea levels. Under current estimated SLR rates of 2 mm/yr (Bromirski et al. 2011), the NRD continued to increase in elevation through the end of the 21st century. Restored and relict tidal marshes gained 0.38–0.43 m of elevation relative to MTL by 2100, and almost all of the subsided restoration area was converted from mudflat and low marsh to mid- and high marsh. Unfortunately, the current rates of SLR are likely to increase. NRC (2012) and IPCC (2014) estimates pin global SLR at 0.53–0.98 m, with projected ranges of 0.10–1.43 m along the Pacific Northwest coast. Moderate estimates for Seattle, Washington predict a 0.62 ± 0.29 m increase in tidal levels by 2100, but the upper limit of these projections is becoming more likely

as ice sheets in Antarctica and Greenland continue to melt (DeConto and Pollard 2016). Under the moderate SLR scenario, our model indicated that the relict tidal marsh would exhibit resilience to rising tidal levels, while the subsided restoration area would decrease 0.12 m in elevation and the higher elevation restoration area would decrease 0.02 m in elevation. If SLR approaches the higher end of forecasted trends, almost all the Restored Refuge is predicted to convert to intertidal mudflat habitat after sinking to approximately 0.07 m below MTL. Restored East would decrease from a mean elevation of 1.58 m to 0.94 m above MTL, becoming a mix of brackish marsh, salt marsh, and mudflat, while much of the Relict Marsh would also be converted to intertidal mudflat, especially at the northern end of the estuary.

This study highlights the importance of incorporating a variety of adaptive management scenarios into a decision support tool, because the submergence of tidal marsh is an undesirable outcome in most systems. Raising the initial marsh elevation by 0.5 m decreased the likelihood of marsh drowning by creating a higher baseline platform and promoting vegetative biomass. In the Mississippi River delta, as little as 10 cm of additional sediment has bolstered plant productivity and soil condition, thus protecting marshes against erosion and submergence (DeLaune et al. 1990; Slocum et al. 2005). Although we raised the entire delta in our simulation, realistically such a strategy would only be used on small swaths of land due to construction costs, logistics, and the risks of over-engineering a vulnerable ecosystem with permanent physical features (Elliott et al. 2016). Thin layers of sediment augmentation may provide the needed elevation capital for drowning marshes and cause less ecological disruption than large-scale dredging, but recovery may require repeated supplementation, and thus may be more appropriate for small areas with a nearby appropriate sediment source (McAtee 2018).

The addition of sediment through natural hydrologic processes or altered reservoir practices represents a more gradual and sustainable strategy, even with the risk of disruptive effects from increasing turbidity (Henley 2000; Thrush et al. 2004; NRC 2011). Output from the MOSAICS model showed that an intermittent sediment pulse with increased rainy season sediment inputs of 1,000 t/d every ten years did little to enhance the resilience of estuarine tidal marsh. Under moderate and high SLR scenarios, elevation relative to MTL was only 6–8 cm greater in 2100 than projected elevations for simulations without any sediment delivery at all. On the other hand, doubling the daily amount of sediment delivered to the delta during the rainy season had a considerable impact. Under moderate SLR, augmented sediment delivery resulted in a change in elevation relative to MTL of 0.44 m in the subsided Restored Refuge, 0.31 m at Restored East, and 0.41 m in the Relict Marsh. These modifications resulted in an estimated 50% expansion in the areal extent of high salt marsh. Under high SLR, elevations were still projected to decline, but only about a third as much as if there was no augmented sediment delivery at all. The elevation relative to MTL of the subsided restoration area would decrease by 0.29 m, the higher elevation restoration area would decrease by 0.21 m, and the relict marsh would decrease by 0.10 m. These changes resulted in a roughly 50% decrease in the extent of modeled low salt marsh and mid-salt marsh, and a modest increase in high salt marsh. While the loss of low and mid-salt marsh would not be ideal, it represents a potential improvement over inaction.

Our final model simulation mimicked the removal of the Alder-LaGrande dam complex by increasing rainy season sediment loads from 300 t/d to 3,000 t/d. The resultant model output showed a homogenized landscape of upland and subtidal habitat under moderate and high SLR scenarios. Because this concentration of suspended sediment was outside the range of observed measurements for the NRD, it is likely that model output overestimated the amount of sediment

that would be delivered directly to the existing marsh plain as opposed to nearshore subtidal zones. The Elwha dam removal on the nearby Olympic Peninsula offers a real-world (albeit short-term) example of how post-dam removal disturbance can physically and biologically alter a large river delta. In the months following the deconstruction of the Elwha and Glines Canyon dams, more than 7.5 million tons of sediment were released into the river (Gelfenbaum et al. 2015; Warrick et al. 2015). Sandy and muddy substrates were deposited at the mouth and nearby sea floor, primarily at subtidal elevations. This resulted in the seaward expansion of the estuary by over 0.28 km^2, with nearshore elevation gains of up to 5 m. Despite the expansion of intertidal beaches and river bars at the mouth of the river, the extent of vegetated habitat had declined by about 6% as of two years post-dam removal (Foley et al. 2017). This response is typical of large-scale disturbance, and habitat configurations are expected to change and recover as sediment conditions, river flow, and tidal currents stabilize.

Several management actions were not addressed in this study, including the active planting of marsh vegetation, increasing delta connectivity, and the purchase of adjacent land to foster inland migration. While vegetation clearly plays a vital role in capturing sediment and preventing erosive forces, active planting has not accelerated functional recovery trajectories in managed or restored wetlands when compared to successional growth (Moreno-Mateos et al. 2015). Increasing the connectivity of the river to its adjacent delta to augment the number of sediment pathways is a practical solution when flow regimes have been altered, but will not increase the total amount of suspended sediment delivered to the system (Elliott et al. 2016). The prevention of "coastal squeeze" through easements, land acquisition, or restrictions on development may be necessary in cases where estuaries are at a higher risk of drowning despite the implementation of one or more of the aforementioned management actions (Torio and

Chmura 2013). Estuarine expansion may be particularly challenging in urban environments where the surrounding area has already been heavily developed or where steep embankments prevent landward encroachment like in the San Francisco Bay, California (Stralberg et al. 2011; Thorne et al. 2018). Each focal system is faced with its own set of limitations and challenges, underscoring the need for more flexible, monitoring-based decision support tools.

Our empirical model projected a diverse set of outcomes when presented with different tidal level and sediment inputs; however, all models are abstractions of reality. In hierarchical models with an iterative time step, error may be propagated through time, especially when contemporary datasets are used to project long-term outcomes. Our model sensitivity analyses showed that distance from the Nisqually River had a magnifying effect on yearly elevational change, where iterations with higher sediment loads were likely to overestimate elevation change in areas further from the river and underestimate elevation change in areas closer to the river. Projections were also higher for highly vegetated areas within 10 m of the tidal channel edge, although they did not fall outside the range of observed SET measurements. Fortunately, the longitudinal sensitivity analysis indicated that error in the inundation, soil pore salinity, and vegetation components of MOSAICS was unlikely to propagate outside the range of variation that would otherwise be expected based on year-to-year fluctuations in suspended sediment. Only model error in the elevation change component itself appeared to have notable effect on the final predicted output.

The MOSAICS model provides a reasonable representation of future habitat conditions despite potential spatial and temporal errors because its output is intermediate to other marsh accretion models. For example, projections for the year 2100 showed slightly more retention of relict marsh habitat under moderate and high SLR scenarios than WARMER model estimates by

Thorne et al. (2018), but considerably more habitat loss than earlier SLAMM models, which forecasted that almost all the restored and relict marsh would persist through the end of the 21st century (Glick et al. 2007). Discrepancies among models shed light on the need for a comparative analysis that evaluates tradeoffs in simplicity, accuracy, generalizability, cost, and ease of use. With regards to MOSAICS, its application to other estuaries would require basic to intermediate experience with non-linear models and maximum likelihood estimation, and the required data could be a constraint for estuaries that do not already have focused monitoring programs in place. Nevertheless, our study has demonstrated the potential utility of the MOSAICS decision support tool for using site-specific monitoring data to project changes to the estuarine habitat mosaic under varying conditions, especially for river deltas where elevation change is dominated by inputs of inorganic sediment.

Conclusion

Empirically-based decision support tools that allow for multiple climate change and management scenarios are important for restoration planning, especially given the threat of global SLR. To our knowledge, this is the first study to explicitly incorporate multiple management scenarios with projected sea-level rise to forecast changes in the estuarine habitat mosaic. Managers rarely have the opportunity to manipulate suspended sediment inputs on a whole-estuary scale (Thom 2000; Teal and Weishar 2005; Callaway et al. 2007); however, adaptive reservoir management options to increase sediment delivery to sediment-deficient river deltas may help ameliorate the effects of SLR on marsh sustainability (Lee et al. 2016). At Nisqually, this was especially true for the subsided restoration area, which was predicted to be less resilient than the adjacent relict marsh due to its lower starting elevations and lack of vegetative complexity. We expect this will

be true of other systems in which the marsh plain is subsided and/or degraded. As such, managers would benefit from considering long-term mitigation actions before construction even begins (Simenstad et al. 2006). Sediment and stream gauge data are now available for most waterways in online repositories, allowing planners to assess whether current suspended sediment inputs will be sufficient to promote viable accretion rates, and how they might be affected by future drought and flooding events. By incorporating empirical monitoring datasets into ecological models and simplifying decision support tools for ease of use, we can improve our adaptive response to climate change for restored and managed estuaries, especially those have been degraded by human activities.

Acknowledgments

This research was made possible through cooperation between the U.S. Geological Survey Western Ecological Research Center (USGS WERC), Nisqually Indian Tribe, Billy Frank Jr. Nisqually National Wildlife Refuge, and the Nisqually River Foundation. Numerous USGS employees contributed to more than seven years of data collection, including L. Shakeri, S. Blakely, A. Munguia, K. Turner, L. Belleveau, P. Markos, S. Kaviar, M. Holt, H. Minella, H. Allgood, and J.Y. Takekawa. Our sincerest thanks go out to our colleagues at USFWS (G. Nakai, D. Roster, M. Bailey, J. Barham, J.E. Takekawa) and the Nisqually Tribe (C. Ellings, S. Hodgson, W. Duval, E. Perez, A. David). We also appreciate the invaluable input of K. Thorne and K. Buffington. Special thanks to our colleagues at the USGS Biologic Carbon Sequestration Program (Z. Zhu) and the USFWS (J. Schmerfeld, S. Covington, K. Johnson), who supported final data syntheses. Our research benefitted from USGS internship programs, including Students in Support of Native American Relations, National Association of Geoscience Teachers, and

Youth and Education in Science. Any use of trade, firm, or product names is for descriptive purposes only and does not imply endorsement by the U.S. Government.

References

Ballanti, L., Byrd, K.B., Woo, I., & Ellings, C. (2017). Remote sensing for wetland mapping and historical change detection at the Nisqually River Delta. Sustainability, 9, 1919. https://doi.org/10.3390/su9111919.

Barbier, E.B., Hacker, S.D., Kennedy, C., Koch, E.W., Stier, A.C., & Silliman, B.R. (2011). The value of estuarine and coastal ecosystem services. Ecological Monographs, 81, 169–193. https://doi.org/10.1890/10-1510.1.

Barnes, C., Irigoien, X., De Oliveira, J.A.A., Maxwell, D., & Jennings, S. (2011). Predicting marine phytoplankton community size structure from empirical relationships with remotely sensed variables. Journal of Plankton Research, 33, 13–24. https://doi.org/10.1093/plankt/fbq088.

Beaumont, N.J., Austen, M.C., Atkins, J.P., Burdon, D., Degraer, S., Dentinho, T.P., Derous, S., Holm, P., Horton, T., van Ierland, E., Marboe, A.H., Starkey, D.J., Townsend, M., & Zarzycki, T. (2007). Identification, definition, and quantification of goods and services provided by marine biodiversity: Implications for the ecosystem approach. Marine Pollution Bulletin, 54, 253–265. https://doi.org/10.1016/j.marpolbul.2006.12.003.

Belleveau, L.J., Takekawa, J.Y., Woo, I., Turner, K.L., Barham, J.B., Takekawa, J.E., Ellings, C.S., & Chin-Leo, G. (2015). Vegetation community response to tidal marsh restoration of a large river estuary. Northwest Science, 89, 136–147. https://doi.org/10.3955/046.089.0205.

Bockelmann, A.C., Bakker, J.P., Neuhaus, R., & Lage, J. (2002). The relation between vegetation zonation, elevation and inundation frequency in a Wadden Sea salt marsh. Aquatic Botany, 73, 211–221. https://doi.org/10.1016/S0304-3770(02)00022-0.

Bromirski, P.D., Miller, A.J., Flick, R.E., & Auad, G. (2011). Dynamical suppression of sea level rise along the Pacific coast of North America: indications for imminent acceleration. Journal of Geophysical Research, 116, C07005. https://doi.org/10.1029/2010JC006759.

Burdick, D.M., & Roman, C.T. (2012). Salt marsh responses to tidal restriction and restoration. Pp. 373–382 *in* Roman, C.T., Burdick, D.M. (eds.) Tidal Marsh Restoration. Island Press, Washington, DC, USA.

Burnham, K.P., & Anderson, D.R. (2002). Model selection and multi-model inference: a practical information-theoretic approach. Springer-Verlag, New York, New York, USA.

Byrd, K.B., Windham-Myers, L., Leeuw, T., Downing, B., Morris, J.T., & Ferner, M.C. (2016). Forecasting tidal marsh elevation and habitat change through fusion of Earth observations and a process model. Ecosphere, 7, e01582. https://doi.org/10.1002/ecs2.1582.

Cahoon, D.R., Lynch, J.C., Perez, B.C., Segura, B., Holland, R.D., Stelly, C., Stephenson, G., & Hensel, P. (2002). High-precision measurements of wetland sediment elevation: II. The rod surface elevation table. Journal of Sedimentary Research, 72, 734–739. https://doi.org/10.1306/020702720734.

Callaway, J.C., Parker, V.T., Vasey, M.C., & Schile, LM. (2007). Emerging issues for the restoration of tidal marsh ecosystems in the context of predicted climate change. Madroño, 54, 234–248. https://doi.org/10.3120/0024-9637(2007)54[234:EIFTRO]2.0.CO;2.

Christiansen, T., Wiberg, P.L., & Milligan, T.G. (2000). Flow and sediment transport on a tidal salt marsh surface. Estuarine, Coastal and Shelf Science, 50, 315–331. https://doi.org/10.1006/ecss.2000.0548.

Clough, J.S., Polaczyk, A., & Propato, M. (2016). Modeling the potential effects of sea-level rise on the coast of New York: integrating mechanistic accretion and stochastic uncertainty. Environmental Modelling & Software, 84, 349–362. https://doi.org/10.1016/j.envsoft.2016.06.023.

Craft, C., Clough, J., Ehman, J., Joye, S., Park, R., Pennings, S., Guo, H., & Machmuller, M. (2009). Forecasting the effects of accelerated sea-level rise on tidal marsh ecosystem services. Frontiers in Ecology and the Environment, 7, 73–78. https://doi.org/10.1890/070219.

Crosby, S.C., Sax, D.F., Palmer, M.E., Booth, H.S., Deegan, L.A., Bertness, M.D., & Leslie, H.M. (2016). Salt marsh persistence is threatened by predicted sea-level rise. Estuarine, Coastal and Shelf Science, 181, 93–99. https://doi.org/10.1016/j.ecss.2016.08.018.

Curran, C.A., Grossman, E.E., Magirl, C.S., & Foreman, J.R. (2016). Suspended sediment delivery to Puget Sound from the lower Nisqually River, western Washington, July 2010–November 2011. Scientific Investigations Report 2016-5062. U.S. Geological Survey, Reston, Virginia, USA.

Czuba, J.A., Magirl, C.S., Czuba, C.R., Grossman, E.E., Curran, C.A., Gendaszek, A.S., & Dinicola, R.S. (2011). Sediment load from major rivers into Puget Sound and its adjacent waters. U.S. Geological Survey Fact Sheet 2011-3083. U.S. Geological Survey, Reston, Virginia, USA.

Czuba, J.A., Magirl, C.S., Czuba, C.R., Curran, C.A., Johnson, K.H., Olsen, T.D., Kimball, H.K., & Gish, C.C. (2012*a*). Geomorphic analysis of the river response to sedimentation downstream of Mount Rainier, Washington. U.S. Geological Survey Open File Report 2012-1242. U.S. Geological Survey, Reston, Virginia, USA.

Czuba, J.A., Olsen, T.D., Czuba, C.R., Magirl, C.S., & Gish, C.C. (2012*b*). Changes in sediment volume in Alder Lake, Nisqually River Basin, Washington, 1945-2011. U.S. Geological Survey Open File Report 2012-1068. U.S. Geological Survey, Reston, Virginia, USA.

D'Alpaos, A., Lanzoni, S., Marani, M., & Rinaldo, A. (2007). Landscape evolution in tidal embayments: modeling the interplay of erosion, sedimentation, and vegetation dynamics. Journal of Geophysical Research, 112, F01008. https://doi.org/10.1029/2006JF000537.

D'Alpaos, A., Mudd, S.M., & Carniello, L. (2011). Dynamic response of marshes to perturbations in suspended sediment concentrations and rates of relative sea level rise. Journal of Geophysical Research, 116, F04020. https://doi.org/10.1029/2011JF002093.

Davenport, A.E., Davis, J.D., Woo, I., Grossman, E.E., Barham, J., Ellings, C.S., & Takekawa, J.Y. (2017). Comparing automated classification and digitization approaches to detect change in eelgrass bed extent during restoration of a large river delta. Northwest Science, 91, 272–282. https://doi.org/10.3955/046.091.0307.

Davis, M.J., Ellings, C.S., Woo, I., Hodgson, S., Larsen, K, & Nakai, G. (2018). Gauging resource exploitation by juvenile Chinook salmon (*Oncorhynchus tshawytscha*) in restoring estuarine habitat. Restoration Ecology, 26, 976–986. http://doi.org/10.1111/rec.12643.

DeConto, R.M., & Pollard, D. (2016). Contribution of Antarctica to past and future sea-level rise. Nature, 531, 591–597. https://doi.org/10.1038/nature17145.

DeLaune, R.D., Pezeshki, S.R., Pardue, J.H., Whitcomb, J.H., & Patrick, W.H. Jr. (1990). Some influences of sediment addition to a deteriorating salt marsh in the Mississippi River deltaic plain: a pilot study. Journal of Coastal Research, 6, 181–188.

Ellings, C.S., Davis, M.J., Grossman, E.E., Woo, I., Hodgson, S., Turner, K.L., Nakai, G., Takekawa, J.E., & Takekawa, J.Y. (2016). Changes in habitat availability for outmigrating juvenile salmon (*Oncorhynchus* spp.) following estuary restoration. Restoration Ecology, 24, 415–427. https://doi.org/10.1111/rec.12333.

Elliott, M., Mander, L., Mazik, K., Simenstad, C., Valesini, F., Whitfield, A., & Wolanski, E. (2016). Ecoengineering with ecohydrology: successes and failures in estuarine restoration. Estuarine, Coastal and Shelf Science, 176, 12–35. https://doi.org/10.1016/j.ecss.2016.04.003.

Fitzgerald, D.M., Fenster, M.S., Argow, B.A., & Buynevich, I.V. (2008). Coastal impacts due to sea-level rise. Annual Review of Earth and Planetary Sciences, 36, 601–647. https://doi.org/10.1146/annurev.earth.35.031306.140139.

Foley, M.M., Warrick, J.A., Ritchie, A., Stevens, A.W., Shafroth, P.B., Duda, J.J., Beirne, M.M., Paradis, R., Gelfenbaum, G., McCoy, R., & Cubley, E.S. (2017). Coastal habitat and biological community response to dam removal on the Elwha River. Ecological Monographs, 87, 552–577. https://doi.org/10.1002/ecm.1268.

French, J.R. (1993). Numerical simulation of vertical marsh growth and adjustment to accelerated sea-level rise, North Norfolk, U.K. Earth Surface Processes and Landforms, 18, 63–81. https://doi.org/10.1002/esp.3290180105.

French, J.R. (2006). Tidal marsh sedimentation and resilience to environmental change: exploratory modelling of tidal, sea-level and sediment supply forcing in predominantly allochthonous systems. Marine Geology, 235, 119–136. https://doi.org/10.1016/j.margeo.2006.10.009.

Galbraith, H., Jones, R., Park, R., Clough, J., Herrod-Julius, S., Harrington, B., & Page, G. (2002). Global climate change and sea level rise: potential losses of intertidal habitat for shorebirds. Waterbirds, 25, 173–183. https://doi.org/10.1675/1524-4695(2002)025[0173:GCCASL]2.0.CO;2.

Gelfenbaum, G., Stevens, A.W., Miller, I., Warrick, J.A., Ogston, A.S., & Eidam, E. (2015). Large-scale dam removal on the Elwha River, Washington, USA: coastal geomorphic change. Geomorphology, 246, 649–668. https://doi.org/10.1016/j.geomorph.2015.01.002.

Geselbracht, L., Freeman, K., Kelly, E., Gordon, D.R., & Putz, F.E. (2011). Retrospective and prospective model simulations of sea level rise impacts on Gulf of Mexico coastal marshes and forests in Waccasassa Bay, Florida. Climatic Change, 107, 35–57. https://doi.org/10.1007/s10584-011-0084-y.

Glick, P., Clough, J., & Nunley, B. (2007). Sea-level rise and coastal habitats in the Pacific Northwest: an analysis for Puget Sound, Southern Washington, and Northwestern Oregon. National Wildlife Federation, Reston, Virginia, USA.

Greenberg, R., Maldonado, J., Droege, S., McDonald, M.V. (2006). Tidal marshes: a global perspective on the evolution and conservation of their terrestrial vertebrates. BioScience, 56, 675–685. https://doi.org/10.1641/0006-3568(2006)56[675:TMAGPO]2.0.CO;2.

Henley, W.F., Patterson, M.A., Neves, R.J., & Lemly, A.D. (2000). Effects of sedimentation and turbidity on lotic food webs: a concise review for natural resource managers. Reviews in Fisheries Science, 8, 125–139.

Hibma, A., Stive, M.J.F., & Wang, Z.B. (2004). Estuarine morphodynamics. Coastal Engineering, 51, 765–778. https://doi.org/10.1016/j.coastaleng.2004.07.008.

Hinkel, J., & Klein, R.J.T. (2009). Integrating knowledge to assess coastal vulnerability to sea-level rise: the development of the DIVA tool. Global Environmental Change, 19, 384–395. https://doi.org/10.1016/j.gloenvcha.2009.03.002.

International Panel on Climate Change (2014). Climate Change 2014: Synthesis Report. Contribution of Working Groups I, II, and III to the Fifth Assessment Report of the Intergovernmental Panel on Climate Change. Core Writing Team, Pachauri RK and Meyer LA (eds.). International Panel on Climate Change, Geneva, Switzerland.

Jackson, J.B.C. (2010). The future of oceans past. Philosophical Transactions of the Royal Society B Biological Sciences, 365, 3765–3778. https://doi.org/10.1098/rstb.2010.0278.

Joint, I., & Groom, S.B. (2000). Estimation of phytoplankton production from space: current status and future potential of satellite remote sensing. Journal of Experimental Marine Biology and Ecology, 250, 233–255. https://doi.org/10.1016/S0022-0981(00)00199-4.

Kirwan, M.L., & Murray, A.B. (2007). A coupled geomorphic and ecological model of tidal marsh evolution. Proceedings of the National Academy of Sciences, 104, 6118–6122. https://doi.org/10.1073/pnas.0700958104.

Kirwan, M.L., & Murray, A.B. (2008). Ecological and morphological response of brackish tidal marshland to the next century of sea level rise: Westham Island, British Columbia. Global and Planetary Change, 60, 471–486. https://doi.org/10.1016/j.gloplacha.2007.05.005.

Kirwan, M.L., Guntenspergen, G.R., D'Alpaos, A., Morris, J.T., Mudd, S.M., & Temmerman, S. (2010). Limits on the adaptability of coastal marshes to rising sea level. Geophysical Research Letters, 37, L23401. https://doi.org/10.1029/2010GL045489.

Kirwan, M.L., & Megonigal, J.P. (2013). Tidal wetland stability in the face of human impacts and sea-level rise. Nature, 504, 53–60. https://doi.org/10.1038/nature12856.

Lee, S.Y., Hamlet, A.F., & Grossman, E.E. (2016). Impacts of climate change on regulated streamflow, hydrologic extremes, hydropower production, and sediment discharge in the Skagit River basin. Northwest Science, 90, 23–43. https://doi.org/10.3955/046.090.0104.

Li, H., & Yang, S.L. (2009). Trapping effect of tidal marsh vegetation on suspended sediment, Yangtze Delta. Journal of Coastal Research, 25, 915–924. https://doi.org/10.2112/08-1010.1.

Martin, J.F., Reyes, E., Kemp, G.P., Mashriqui, H., & Day, J.W. (2002). Landscape modelling of the Mississippi Delta: using a series of landscape models, we examined the survival and creation of Mississippi Delta marshes and the impact of altered riverine inputs, accelerated sea-level rise, and management proposals on these marshes. BioScience, 52, 357–365. https://doi.org/10.1641/0006-3568(2002)052[0357:LMOTMD]2.0.CO;2.

McAttee, K.J. (2018). Impact of sediment augmentation on plant and invertebrate communities in a Southern California coastal wetland. Master's Thesis, California State University, Long Beach, California, USA.

Mcleod, E., Poulder, B., Hinkel, J., Reyes, E., & Salm, R. (2010*a*). Sea-level rise impact models and environmental conservation: a review of models and their applications. Ocean and Coastal Management, 52, 507–517. https://doi.org/10.1016/j.ocecoaman.2010.06.009.

Mcleod, E., Hinkel, J., Vafeidis, A.T., Nicholls, R.J., Harvey, N., & Salm, R. (2010*b*). Sea-level rise vulnerability in the countries of the Coral Triangle. Sustainability Science, 5, 207–222. https://doi.org/10.1007/s11625-010-0105-1.

McLusky, D.S., & Elliot, M. (2004). The estuarine ecosystem: ecology, threats, and management. Oxford University Press, New York, New York, USA. http://doi.org/10.1093/acprof:oso/9780198525080.001.0001.

Moffett, K.B., Robinson, D.A., & Gorelick, S.M. (2010). Relationship of salt marsh vegetation zonation to spatial patterns in soil moisture, salinity, and topography. Ecosystems, 13, 1287–1302. https://doi.org/10.1007/s10021-010-9385-7.

Moorhead, K.K., & Brinson, M.M. (1995). Response of wetlands to rising sea level in the lower coastal plain of North Carolina. Ecological Applications, 5, 261–271. https://doi.org/10.2307/1942068.

Moreno-Mateos, D., Meli, P., Vara-Rodriguez, M.I., & Aronson, J. (2015). Ecosystem response to interventions: lessons from restored and created wetland ecosystems. Journal of Applied Ecology, 52, 1528–1537. https://doi.org/10.1111/1365-2664.12518.

Morrill, J.C., Bales, R.C., & Conklin, M.H. (2005). Estimating stream temperature from air temperature: implications for future water quality. Journal of Environmental Engineering, 131, 139–146. https://doi.org/10.1061/(ASCE)0733-9372(2005)131:1(139).

Morris, J.T., & Haskin, B. (1990). A 5-yr record of aerial primary production and stand characteristics of *Spartina alterniflora*. Ecology, 71, 2209–2217. https://doi.org/10.2307/1938633.

Morris, J.T., Sundareshwar, P.V., Nietch, C.T., Kjerfve, B., & Cahoon, D.R. (2002). Responses of coastal wetlands to rising sea level. Ecology, 83, 2869–2877. https://doi.org/10.1890/0012-9658(2002)083[2869:ROCWTR]2.0.CO;2.

Morris, J.T., Barber, D.C., Callaway, J.C., Chambers, R., Hagen, S.C., Hopkinson, C.S., Johnson, B.J., Megonigal, P., Neubauer, S.C., Troxler, T., & Wigand, C. (2016). Contributions of organic and inorganic matter to sediment volume and accretion in tidal wetlands at steady state. Earth's Future, 4, 110-121. https://doi.org/10.1002/2015EF000334.

Mudd, S.M., Howell, S.M., & Morris, J.T. (2009). Impact of dynamic feedbacks between sedimentation, sea-level rise, and biomass production on near-surface marsh stratigraphy

and carbon accumulation. Estuarine, Coastal and Shelf Science, 82, 377–389. https://doi.org/10.1016/j.ecss.2009.01.028.

Nelson, L.M. (1974). Sediment transport by streams in the Deschutes and Nisqually River Basins, Washington, November 1971–June 1973. U.S. Geological Survey Open File Report 74-1078. U.S. Geological Survey, Reston, Virginia, USA.

Nicholls, R.J., Hoozemans, F.M.J., & Marchand, M. (1999). Increasing flood risk and wetland losses due to global sea-level rise: regional and global analyses. Global Environmental Change, 9, S69–S87. https://doi.org/10.1016/S0959-3780(99)00019-9.

National Research Council (2011). Missouri River planning: recognizing and incorporating sediment management. National Research Council of the National Academies. National Academies Press, Washington, D.C., USA.

National Research Council (2012). Sea-level rise for the coasts of California, Oregon, and Washington: past, present, and future. National Research Council of the National Academies. National Academies Press, Washington, D.C., USA.

Odum, W.E. (1988). Comparative ecology of tidal freshwater and salt marshes. Annual Review of Ecology and Systematics, 19, 147–176. https://doi.org/10.1146/annurev.es.19.110188.001051.

Pennings, S.C., Grant, M.B., & Bertness, M.D. (2005). Plant zonation in low-latitude salt marshes: disentangling the roles of flooding, salinity, and competition. Journal of Ecology, 93, 159–167. https://doi.org/10.1111/j.1365-2745.2004.00959.x.

Pringle, P., & Scott K. (2001). Postglacial influence of volcanism on the landscape and environmental history of the Puget Lowland, Washington: a review of geologic literature and recent discoveries, with emphasis on the landscape disturbances associated with lahars, lahar runouts, and associated flooding. Proceedings of the Puget Sound Research Conference. Puget Sound Partnership, Olympia, Washington, USA.

R Core Development Team (2017). R: A language environment for Statistical Computing. R Foundation for Statistical Computing, Vienna, Austria.

Reyes, E., White, M.L., Martin, J.F., Kemp, G.P., Day, J.B., & Aravamuthan, V. (2000). Landscape modeling of coastal habitat change in the Mississippi Delta. Ecology, 81, 2331–2349. https://doi.org/10.1890/0012-9658(2000)081[2331:LMOCHC]2.0.CO;2.

Rogers, K., Saintilan, N., & Copeland, C. (2012). Modelling wetland surface elevation dynamics and its application to forecasting the effects of sea-level rise on estuarine wetlands. Ecological Modelling, 244, 148–157. https://doi.org/10.1016/j.ecolmodel.2012.06.014.

Rybczyk, J.M., & Callaway, J.C. (2009). Surface elevation models. *In* Perillo, G.M.E., Wolanski, E., Cahoon, D.R., Brinson, M.M. (eds.) Coastal Wetlands: An Integrated Ecosystem Approach. Elsevier, Amsterdam, The Netherlands.

Sanderson, E.W., Foin, T.C., & Ustin, S.L. (2001). A simple empirical model of salt marsh plant spatial distributions with respect to a tidal channel network. Ecological Modelling, 139, 293–307. https://doi.org/10.1016/S0304-3800(01)00253-8.

Schile, L.M., Callaway, J.C., Morris, J.T., Stralberg, D., Parker, V.T., & Kelly, M. (2014). Modeling tidal marsh distribution with sea-level rise: evaluating the role of vegetation, sediment, and upland habitat in marsh resiliency. PLoS ONE, 9, e88760. https://doi.org/10.1371/journal.pone.0088760.

Sharma, S., Walker, S.C., & Jackson, D.A. (2008). Empirical modelling of lake water-temperature relationships: a comparison of approaches. Freshwater Biology, 53, 897–911. https://doi.org/10.1111/j.1365-2427.2008.01943.x.

Silvestri, S., Defina, A., & Marani, M. (2005). Tidal regime, salinity and salt marsh plant zonation. Estuarine, Coastal and Shelf Science, 62, 119–130. https://doi.org/10.1016/j.ecss.2004.08.010.

Simenstad, C.A., & Cordell, J.R. (2000). Ecological assessment criteria for restoring anadromous salmonid habitat in Pacific Northwest estuaries. Ecological Engineering, 15, 283–302. https//doi.org/10.1016/S0925-8574(00)00082-3.

Simenstad, C.A., Reed, D., & Ford, M. (2006). When is restoration not?: incorporating landscape-scale processes to restore self-sustaining ecosystems in coastal wetland restoration. Ecological Engineering, 26, 27–39. https://doi.org/10.106/j.ecoleng.2005.09.007.

Slocum, M.G., Mendelssohn, I.A., & Kuhn, N.L. (2005). Effects of sediment slurry enrichment on salt marsh rehabilitation: plant and soil responses over seven years. Estuaries, 28, 519–528. https://doi.org/10.1007/BF02696063.

Spencer, T., Schuerch, M., Nicholls, R.J., Hinkel, J., Lincke, D., Vafeidis, A.T., Reef, R., McFadden, L., & Brown, S. (2016). Global coastal wetland change under sea-level rise

and related stresses: the DIVA wetland change model. Global and Planetary Change, 139, 15–30. https://doi.org/10.1016/j.gloplacha.2015.12.018.

Stralberg, D., Brennan, M., Callaway, J.C., Wood, J.K., Schile, L.M., Jongsomjit, D., Kelly, M., Parker, V.T., & Crooks, S. (2011). Evaluating tidal marsh sustainability in the face of sea-level rise: a hybrid modeling approach applied to San Francisco Bay. PLoS ONE, 6, e27388. https://doi.org/10.1371/journal.pone.0027388.

Stumpf, R.P. (1983). The process of sedimentation on the surface of a salt marsh. Estuarine, Coastal and Shelf Science, 17, 495–508. https://doi.org/10.1016/0272-7714(83)90002-1.

Swanson, K.M., Drexler, J.Z., Schoellhamer, D.H., Thorne, K.M., Casazza, M.L., Overton, C.T., Callaway, J.C., & Takekawa, J.Y. (2014). Wetland Accretion Rate Model of Ecosystem Resilience (WARMER) and its application to habitat sustainability for endangered species in the San Francisco Estuary. Estuaries and Coasts, 37, 476–492. https://doi.org/10.1007/s12237-013-9694-0.

Syvitski, J.P.M., Kettner, A.J., Overeem, I., Hutton, E.W.H., Hannon, M.T., Brakenridge, G.R., Day, J., Vörösmarty, C., Saito, Y., Giosan, L., & Nicholls, R.J. (2009). Sinking deltas due to human activities. Nature Geoscience, 2, 681–686. https://doi.org/10.1038/ngeo629.

Teal, J.M., & Weishar, L. (2005). Ecological engineering, adaptive management, and restoration management in Delaware Bay salt marsh restoration. Ecological Engineering, 25, 304–314. https://doi.org/10.1016/j.ecoleng.2005.04.009.

Temmerman, S., Govers, G., Meire, P., & Wartel, S. (2003). Modelling long-term tidal marsh growth under changing tidal conditions and suspended sediment concentrations, Scheldt estuary, Belgium. Marine Geology, 193, 151–169. https://doi.org/10.1016/S0025-3227(02)00642-4.

Thom, R.M. (2000). Adaptive management of coastal ecosystem restoration projects. Ecological Engineering, 15, 365–372. https://doi.org/10.1016/S0925-8574(00)00086-0.

Thorne, K.M., Buffington, K.J., & Takekawa, J.Y. (2015). Tidal marsh susceptibility to sea-level rise: the importance of local-scale models. Journal of Fish and Wildlife Management, 6, 290–304. https://doi.org/10.3996/062014-JFWM-048.

Thorne, K.M., MacDonald, G., Guntenspergen, G., Ambrose, R., Buffington, K., Dugger, B., Freeman, C., Janousek, C., Brown, L., Rosencranz, J., Holmquist, J., Smol, J., Hargan,

K., & Takekawa, J.Y. (2018). U.S. Pacific coastal wetland resilience and vulnerability to sea-level rise. Science Advances, 4, eaao3270. https://doi.org/10.1126/sciadv.aa03270

Thrush, S.F., Hewitt, J.E., Cummings, V.J., Ellis, J.I., Hatton, C., Lohrer, A., & Norkko, A. (2004). Muddy waters: elevating sediment input to coastal and estuarine habitats. Frontiers in Ecology and the Environment, 2, 299–306. https://doi.org/10.1890/1540-9295(2004)002[0299:MWESIT]2.0.CO;2.

Thursby, G.B., Chintala, M.M., Stetson, D., Wigand, C., & Champlin, D.M. (2002). A rapid, non-destructive method for estimating aboveground biomass of salt marsh grasses. Wetlands, 22, 626–630. https://doi.org/10.1672/0277-5212(2002)022[0626:ARNDMF]2.0.CO;2.

Titus, J.G., & Richman, C. (2001). Maps of lands vulnerable to sea level rise: modeled elevations along the US Atlantic and Gulf coasts. Climate Research, 18, 205–228. https://doi.org/10.3354/cr018205.

Torio, D.D., & Chmura, G.L. (2013). Assessing coastal squeeze of tidal wetlands. Journal of Coastal Research, 29, 1049–1061. https://doi.org/JCOASTRES-D-12-00162.1.

Vandenbruwaene, W., Maris, T., Cox, T.J.S., Cahoon, D.R., Meire, P., & Temmerman, S. (2011). Sedimentation and response to sea-level rise of a restored marsh with reduced tidal exchange: comparison with a natural tidal marsh. Geomorphology, 130, 115–126. https://doi.org/10.1016.j.geomorph.2011.03.004.

Verdonck, D. (2006). Contemporary vertical crustal deformation in Cascadia. Tectonophysics, 417, 221–230. https://doi.org/10.1016/j.tecto.2006.01.006.

Warrick, J.A., Bountry, J.A., East, A.E., Magirl, C.S., Randle, T.J., Gelfenbaum, G., Ritchie, A.C., Pess, G.R., Leung, V., & Duda, J.J. (2015). Large-scale dam removal on the Elwha River, Washington, USA: source-to-sink sediment budget and analysis. Geomorphology, 246, 729–750. https://doi.org/10.1016/j.geomorph.2015.01.010.

Woo, I., Davis, M.J., Ellings, C.S., Nakai, G., Takekawa, J.Y., & De La Cruz, S.W. (2018). Enhanced invertebrate prey production following estuarine restoration supports foraging for multiple species of juvenile salmonids (*Oncorhynchus* spp.). Restoration Ecology, 26, 964–975. https://doi.org/10.1111/rec.12658.

Tables

Table 4.1. Some coastal inundation or marsh accretion models that are currently available for use by practitioners and ecologists, along with general information on scale constraints, necessary parameter inputs, software and labor costs, and user interface. Models that have only been designed and calibrated for a single system (e.g., Rogers et al. 2012) were omitted from this synthesis. Models that are available to the public with existing software or a graphical user interface are marked with an asterisk. See Rybczyk and Callaway (2009) and Mcleod et al. (2010*a*) for a more detailed discussion of model tradeoffs.

Model	Spatial extent	Spatial resolution	Parameter inputs	Data outputs	Cost (USD)[a]	Programming language or user interface	References
Numerical	N/A	N/A	Elevation, inundation duration, rate of SLR, suspended sediment concentration, distance from tidal channel, vegetative biomass	Sedimentation or elevation change	<10,000$	Can be run in any statistical language	Morris et al. 2002; Temmerman et al. 2003; D'Alpaos et al. 2007; Kirwan and Murray 2007; Mudd et al. 2009; Kirwan et al. 2010
*Inundation ("bathtub")	Any	Dependent on extent (1 m^2–1 km^2)	Digital elevation model, sediment or elevation change, rate of SLR	Elevation, land cover, map of inundated area	<10,000$	GIS software	Moorhead and Brinson 1995; Titus and Richman 2001; Thorne et al. 2015
*Sea Level Affecting Marshes Model (SLAMM)	Local, regional	Dependent on extent (1 m^2–1 km^2)	Digital elevation model, land cover, salinity, land barriers or roads, rate of SLR	Elevation, depth, land cover, infrastructure effects	<10,000$	User interface	Galbraith et al. 2002; Craft et al. 2009; Geselbracht et al. 2011; Clough et al. 2016
*Marsh Equilibrium Model (MEM[b])	Local	Can be applied to 1 m^2–100 m^2 scale	Elevation, above and belowground vegetative biomass, rate of SLR, suspended sediment concentration, tidal range	Elevation, primary productivity	<10,000$	Web-based, statistical software, GIS	Schile et al. 2014; Byrd et al. 2016; Morris et al. 2016

Wetland Accretion Rate Model of Ecosystem Resilience (WARMER)	Local, regional	Dependent on extent (1 m^2–100 m^2)	Digital elevation model, rate of SLR, inorganic sediment, soil porosity, organic matter	Elevation, land cover	>50,000$	GIS or statistical software	Swanson et al. 2014; Thorne et al. 2018
Barataria-Terrebonne Estuarine Landscape Spatial Simulation (BTELSS)	Local, regional	1 km^2	Digital elevation model, weather (temperature, wind, precipitation), primary productivity, vegetation species' environmental tolerances, suspended sediment, river flow, rate of SLR	Map of inundated area, land cover, primary productivity, salinity, sediment transport	>50,000$	GIS or statistical software	Reyes et al. 2000; Martin et al. 2002
Dynamic Interactive Vulnerability Assessment (DIVA)	Regional, national, global	>10 km^2	Digital elevation model, coastal population centers, land use, economic data, rate of SLR	Map of inundated area, erosion, wetland change, salinity intrusion, economic loss	>50,000$	User interface	Hinkel and Klein 2009; Mcleod et al. 2010*b*; Spencer et al. 2016

[a]Including estimated cost of labor.
[b]MEM was not originally designed as a spatial model.

Table 4.2. Physical, biological, and spatial monitoring data used to calibrate an Empirical, Monitoring-Based Estuarine Resilience Simulation (MOSAICS) for the NRD. Each dataset's contribution to the model's hierarchical parameters, including inundation duration (I), soil pore salinity (S), vegetative biomass (V), elevation change (ΔE), and habitat classification (H) at a cell (x,y) in year t is marked with an X in the appropriate column.

			Model parameters				
Dataset	Equipment	Temporal scale	$I_{t,x,y}$	$S_{t,x,y}$	$V_{t,x,y}$	$\Delta E_{t,x,y}$	$H_{t,x,y}$
Local hydrograph	Solinst® LTC data logger	Continuous, every 6–15 minutes	X	X	X	X	X
Soil pore salinity	Refractometer	Monthly, annually		X	X		X
Vegetative species and biomass	0.25 m^2 PVC quadrat	Monthly, annually			X	X	X
Initial elevation	Lidar-derived DEM	Once, flown in January 2011	X			X	X
Elevation change	Surface elevation table (SET)	Annual				X	
Suspended sediment	Derived from publicly available water gauge data (USGS 2016) and linear model (Curran et al. 2016)	Once (water gauge data varies)				X	
Predicted and present day SLR	Derived from the literature (Bromirski et al. 2011; NRC 2012)	Once	X			X	

Table 4.3. MOSAICS model equations and parameter values as estimated using maximum likelihood estimation in R 3.4.1. Model root-mean-squared error (RMSE) as a percentage of the total observed range of values is shown in parentheses.

Model equation	Parameter	Value	Standard error	Model RMSE
$\Delta E_{t,x,y} = E_{sed} + E_{cap} + E_{org} + E_{er} + E_{geo}$				6.758 (4.56%)
$E_{sed} = L_t \cdot (1 - e^{-i_a \cdot I_{t,x,y}}) \cdot \left(int_1 + r_a \cdot Riv_{x,y} + c_a \cdot e^{-c_b \cdot Chan_{x,y}}\right)$	i_a	51.29	13.19	
	int_1	-0.003	0.001	
	r_a	0.000018	0.000004	
	c_a	0.005	0.001	
	c_b	0.085	0.023	
$E_{cap} = L_t \cdot V_{t,x,y} \cdot (1 - e^{-i_b \cdot I_{t,x,y}}) \cdot \left(int_2 + r_b \cdot Riv_{x,y} + c_d \cdot e^{-c_e \cdot Chan_{x,y}}\right)$	i_b	149.30	16.35	
	int_2	0.0000007	0.0000002	
	r_b	0	N/A	
	c_d	0.00002	0.00001	
	c_e	0.011	0.002	
$E_{org} = v_a \cdot V_{t,x,y}$	v_a	0	N/A	
$E_{er} = i_c \cdot (e^{-i_d \cdot I_{t,x,y}} - 1)$	i_c	-1.39	0.53	
	i_d	-1	N/A	
$I_{t,x,y} = \frac{1}{(1 + a \cdot e^{-b \cdot E_{t,x,y}})^{\frac{1}{c}}}$	a	0.029	0.014	0.015 (1.5%)
	b	-0.904	0.011	
	c	0.050	0.023	
$V_{t,x,y} = N \cdot e^{-\delta \cdot S_{t,x,y}} e^{\frac{-(I_{t,x,y} - \mu)^2}{2 \cdot \sigma^2}}$	N	4031	370	1510 (15.55%)
	δ	0.009	0.004	
	μ	0.099	0.011	
	σ	0.078	0.009	
$S_{t,x,y} = \alpha + \beta \cdot Mar_{x,y} + \left(C + \gamma \cdot I_{t,x,y}\right) \cdot \left(1 - e^{-k \cdot Riv_{x,y}}\right)$	α	15.84	2.61	7.250 (15.10%)
	β	-0.013	0.001	
	γ	-24.74	5.11	
	C	31.99	2.67	
	k	0.003	0.001	

Table 4.4. Predicted delta-wide habitat distributions (%) in 2100 given present day (PD; 2 mm/yr), moderate (MOD; 0.62 m by 2100), and high (HIGH; 1.35 m by 2100) SLR scenarios and different sediment management strategies. Habitat types that experienced > 10% change from initial conditions are marked with a plus (+) or minus (-) sign.

	Subtidal	Eelgrass	Mudflat	Low	Mid	High	Brackish	Freshwater	Upland
Present Day (2011)	43.2	6.4	11.1	16.4	4.9	9.3	4.9	0.3	3.5
No Added Sediment									
PD	44.1	5.5 (-)	8.3 (-)	13.4 (-)	4.4	8.9	3.8 (-)	0.2 (-)	11.4 (+)
MOD	40.4	12.7 (+)	11.0	14.0 (-)	2.3 (-)	12.3 (+)	5.6 (+)	0.3	1.5 (-)
HIGH	50.1 (+)	7.0	21.2 (+)	5.6 (-)	2.6 (-)	6.9 (-)	5.4	0.3	0.8 (-)
Raised 0.5 Meters									
PD	26.9 (-)	16.1 (+)	12.0	4.0 (-)	4.1 (-)	14.1 (+)	2.1 (-)	0.2 (-)	20.6 (+)
MOD	29.5 (-)	17.7 (+)	10.4	7.4 (-)	4.0 (-)	22.3 (+)	4.8	0.3	3.6
HIGH	43.5	10.6 (+)	12.3 (+)	9.1 (-)	4.1 (-)	12.5 (+)	6.3 (+)	0.4 (+)	1.3 (-)
Ten-year Sediment Pulse									
PD	44.2	5.5 (-)	7.9 (-)	11.9 (-)	5.1	8.7	3.5 (-)	0.2 (-)	13.2 (+)
MOD	39.2	13.4 (+)	9.9 (-)	14.6 (-)	2.2 (-)	13.0 (+)	5.6 (+)	0.3	1.9 (-)
HIGH	49.2 (+)	7.6 (+)	20.7 (+)	5.6 (-)	2.3 (-)	8.0 (-)	5.5 (+)	0.3	0.8 (-)
Doubled Sediment									
PD	47.3	2.3 (-)	6.1 (-)	5.7 (-)	4.8 (-)	10.7 (+)	2.9 (-)	0.1 (-)	20.1 (+)
MOD	35.3 (-)	15.0 (+)	7.9 (-)	12.4 (-)	3.0 (-)	14.1 (+)	5.0	0.2 (-)	7.1 (+)
HIGH	38.2 (-)	16.6 (+)	16.0 (+)	8.0 (-)	1.8 (-)	11.4 (+)	5.6 (+)	0.3	2.0 (-)
Dam Removal									
PD	49.2 (+)	0.0 (-)	0.0 (-)	1.3 (-)	0.1 (-)	0.1 (-)	0.9 (-)	0.4 (+)	48.1 (+)
MOD	47.5	2.2 (-)	0.1 (-)	0.3 (-)	0.1 (-)	8.5	3.6 (-)	0.1 (-)	37.6 (+)
HIGH	38.5 (-)	11.8 (+)	0.5 (-)	1.2 (-)	0.4 (-)	14.2 (+)	4.7	0.2 (-)	28.5 (+)

Figures

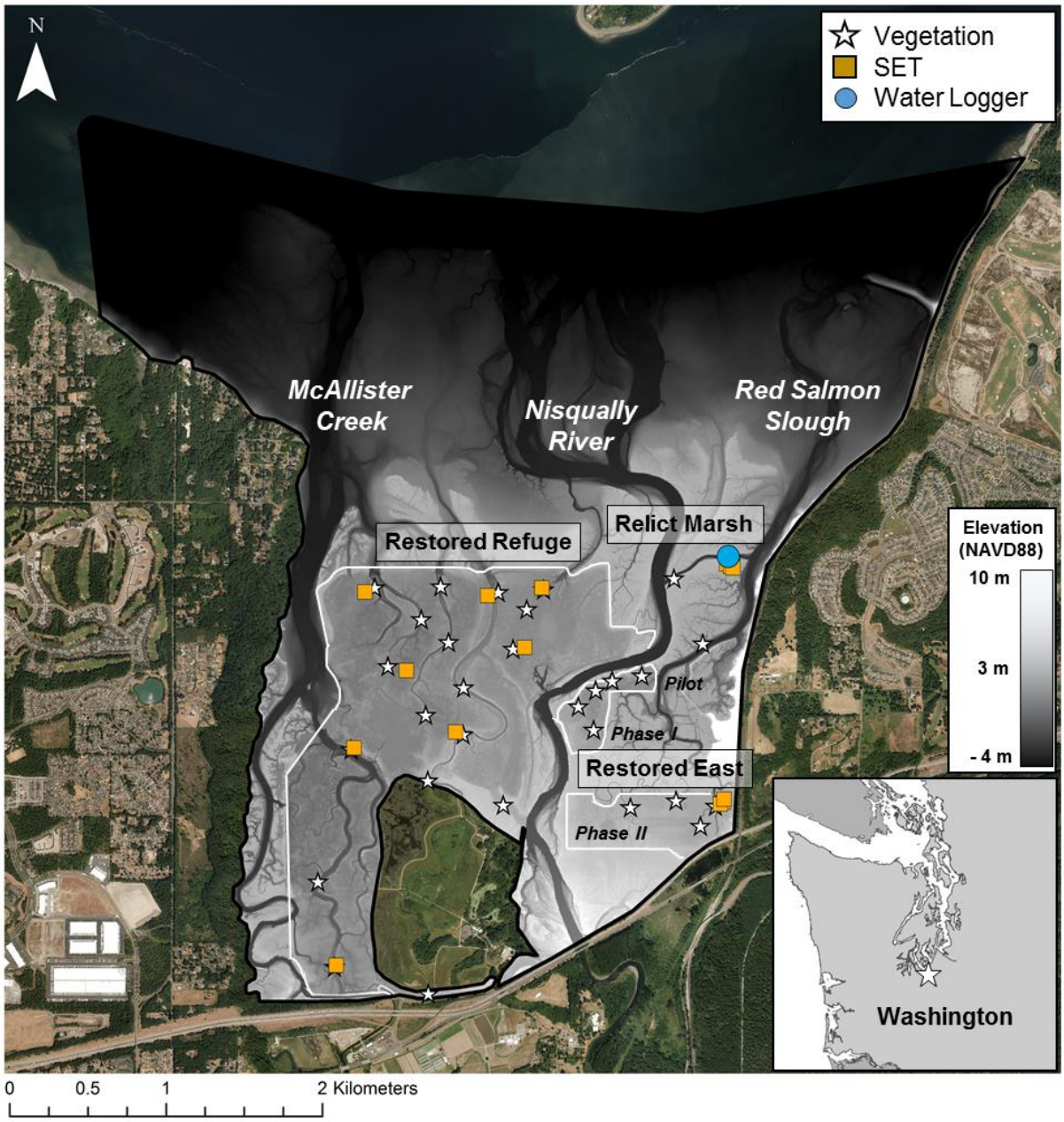

Figure 4.1. Map of post-restoration monitoring sites throughout the Nisqually River Delta (NRD), including vegetation quadrat surveys (white stars), surface elevation tables (SETs; orange squares), and a water level logger (blue circle). The study area is bounded by the 2011 DEM (black and white). Restoration areas are delineated with white lines, with the Restored Refuge located to the west of the Nisqually River, and Restored East (Pilot, Phase I, Phase II) on the east side of the Nisqually River. Relict Marsh includes any low, mid-, or high salt marsh area that is not within restoration boundaries.

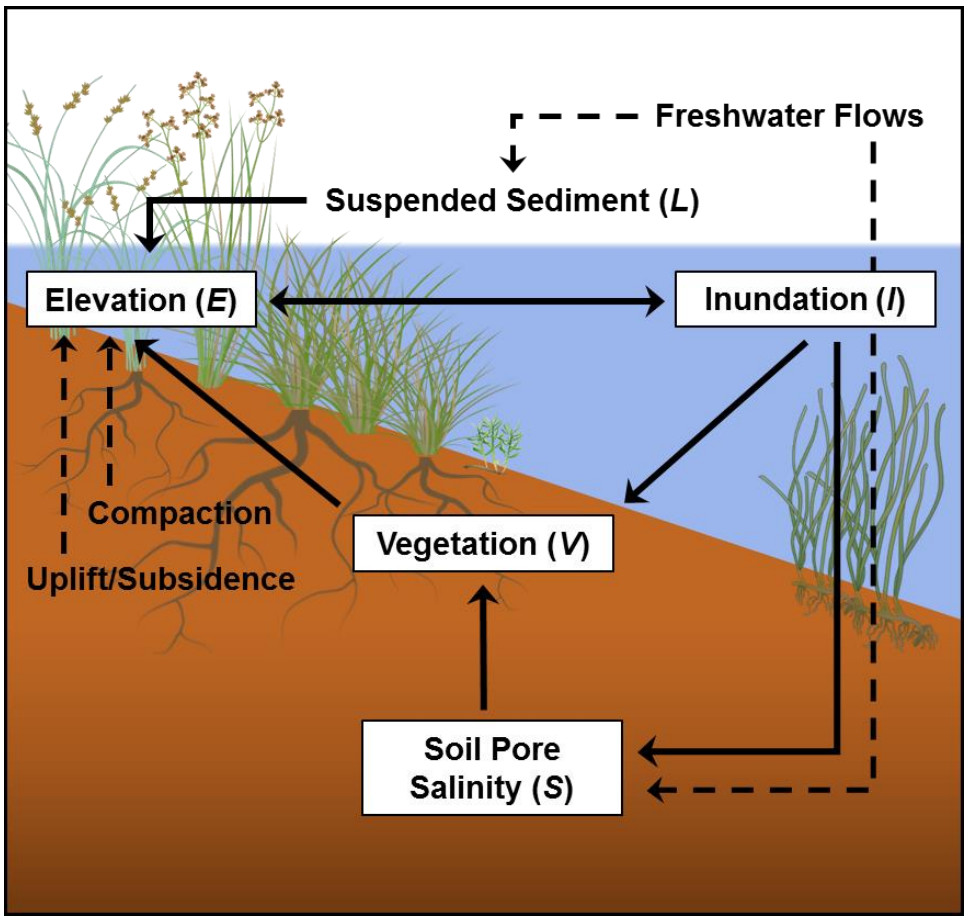

Figure 4.2. Conceptual diagram of the ecomorphodynamic feedbacks between tidal inundation duration (*I*), suspended sediment load (*L*), vegetative growth (*V*), and marsh plain elevation (*E*). Solid lines represent relationships that were explicitly modeled as a hierarchical component of the MOSAICS framework. Dotted lines represent indirect drivers.

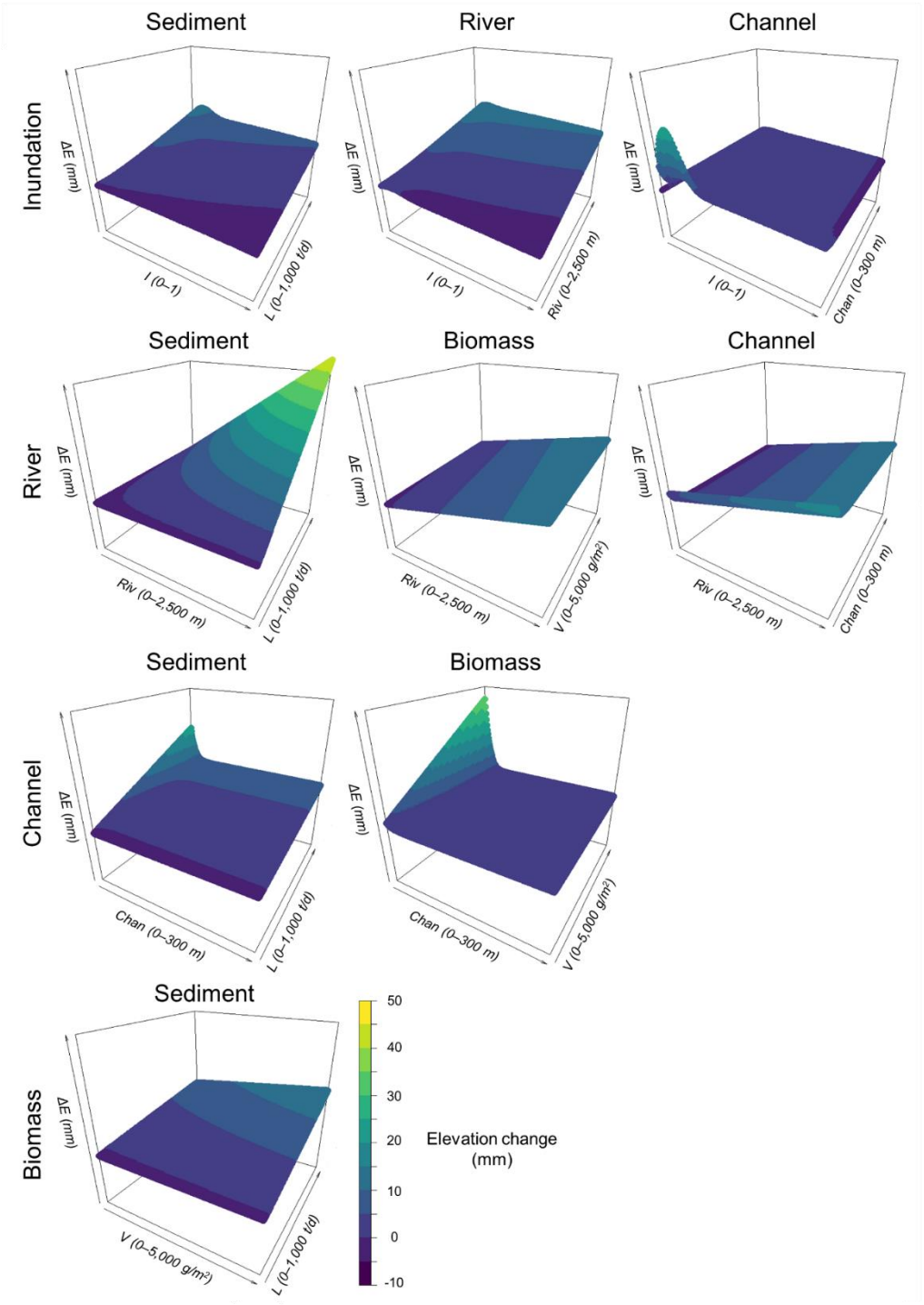

Figure 4.3. Three-dimensional surface plots examining how annual elevation change (*ΔE*; mm) varied in two-parameter space. When not varied, predictor variables were held constant such that *V* (Biomass) was considered a function of *I* (Inundation), *L* (Sediment) was 300 t/d, *Riv* (River) was 550 m, *Chan* (Channel) was 30 m, and *I* was 0.25. These are representative of the mean observed values for the NRD during the monitored time period.

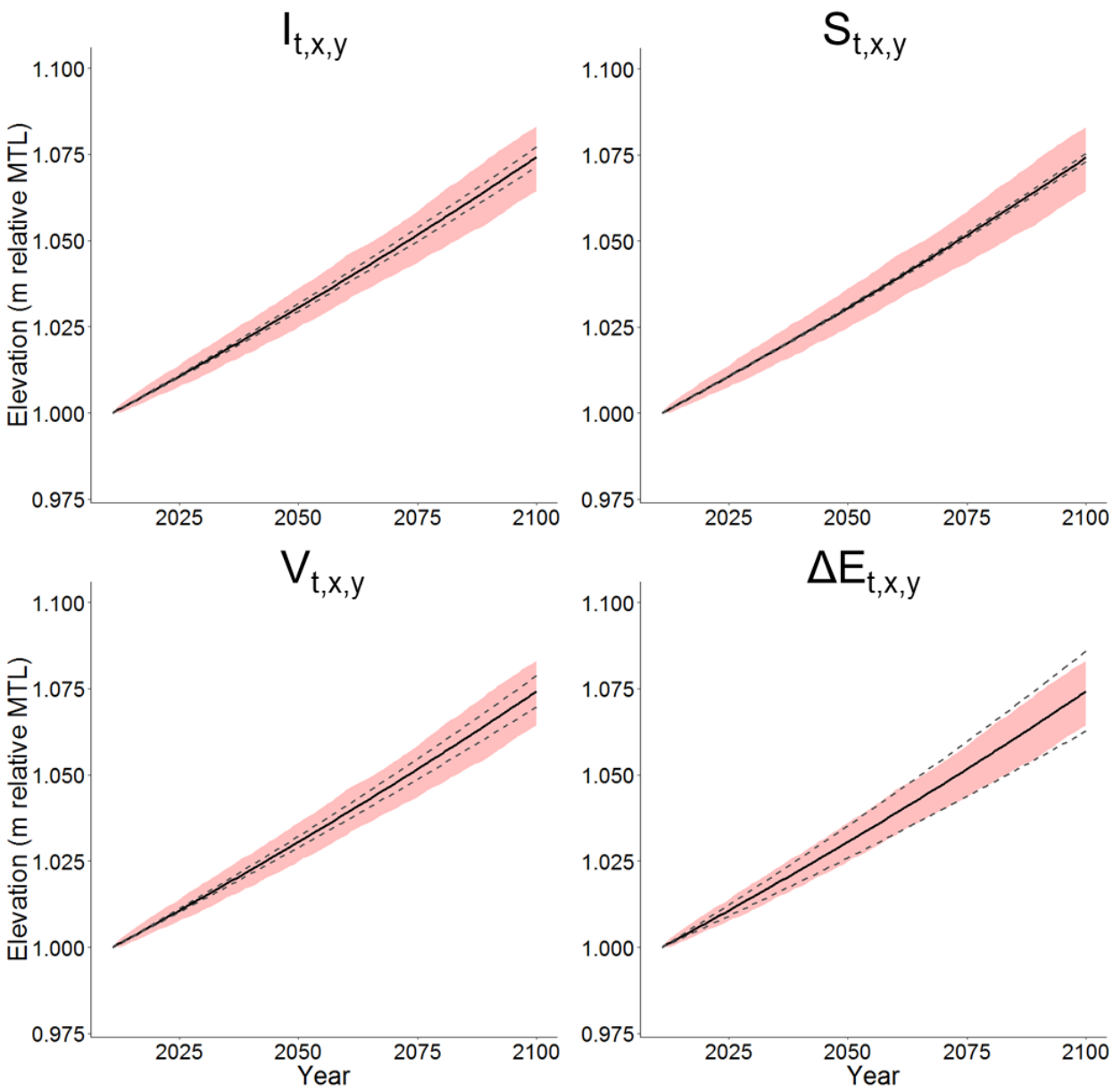

Figure 4.4. Output from a longitudinal sensitivity analysis showing elevation (m relative to MTL) through time for a hypothetical site with an initial starting elevation (E_0) of 1 m. The spatial variables *Riv*, *Mar*, and *Chan* were held constant at 550 m, 550 m, and 30 m respectively. The red shaded area shows uncertainty (± 1 SD) when sediment input was randomly drawn from a normal distribution of 300 ± 100 t/d. The black solid line shows output for model-predicted $I_{t,x,y}$, $S_{t,x,y}$, $V_{t,x,y}$, and $\Delta E_{t,x,y}$ values, while the gray dashed lines represent model predictions when each input was varied by ± 1 RMSE. Sea level was increased by 2 mm per-year according to present-day SLR estimates (Bromirski et al. 2011).

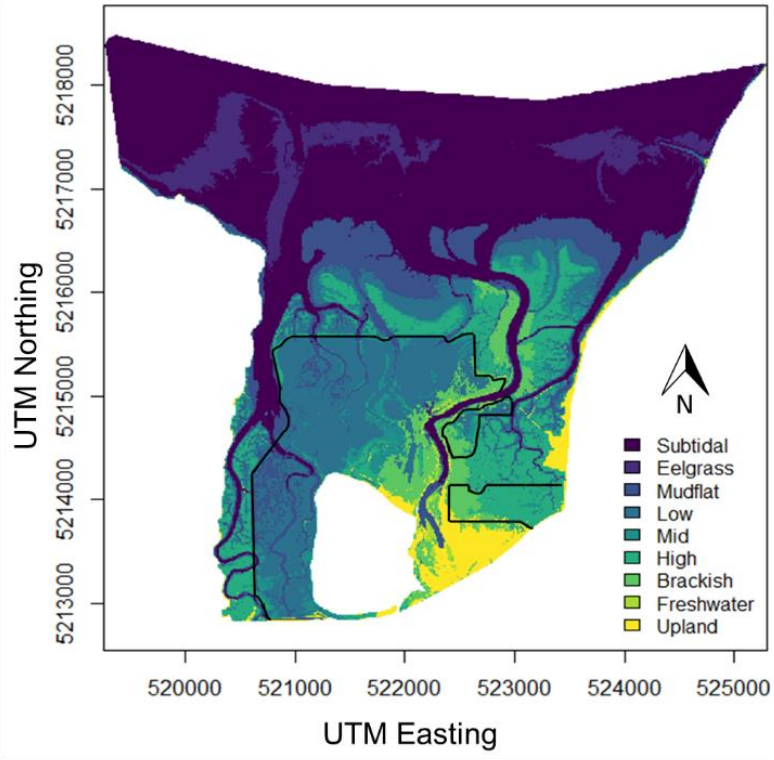

Figure 4.5. Initial (2011) habitat distributions for the NRD, including subtidal, eelgrass, intertidal mudflat, low-elevation salt marsh, mid-elevation salt marsh, high-elevation salt marsh, brackish marsh, freshwater marsh, and upland habitats. Spatial analyses were conducted on a 3 × 3 m raster with a WGS84 reference coordinate system. Restored Refuge and Restored East are bounded by black lines. The depths of the Nisqually River and McAllister Creek were not accounted for when calculating the inundation duration of riverine habitats.

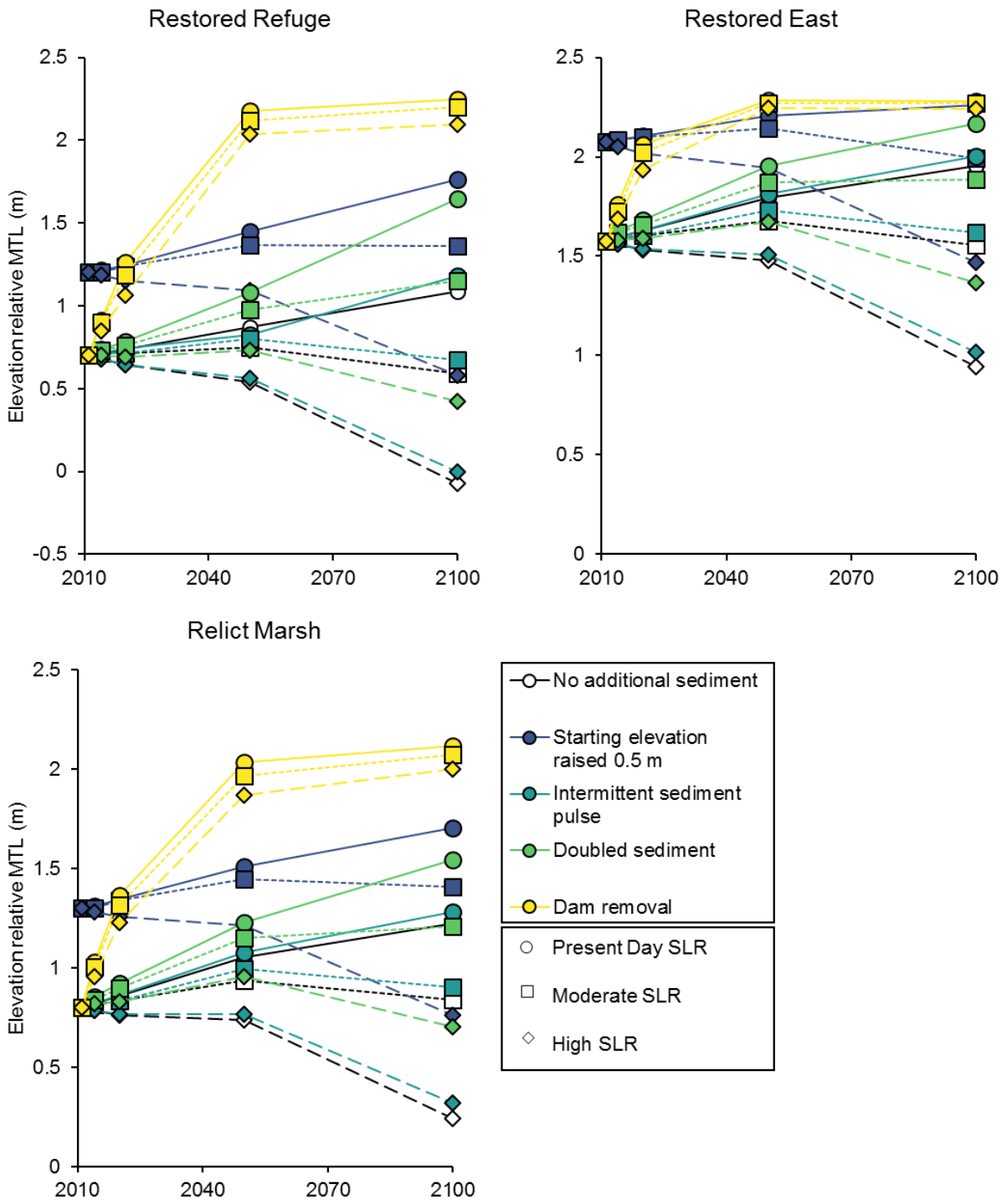

Figure 4.6. Modeled elevation change through time for the Restored Refuge, Restored East, and Relict Marsh sites. Trajectories derived using present day (2 mm/yr), moderate (0.62 m by 2100), and high (1.35 m by 2100) SLR estimates are represented with circles, squares, and diamonds (respectively). Model output for different sediment management scenarios is color coded.

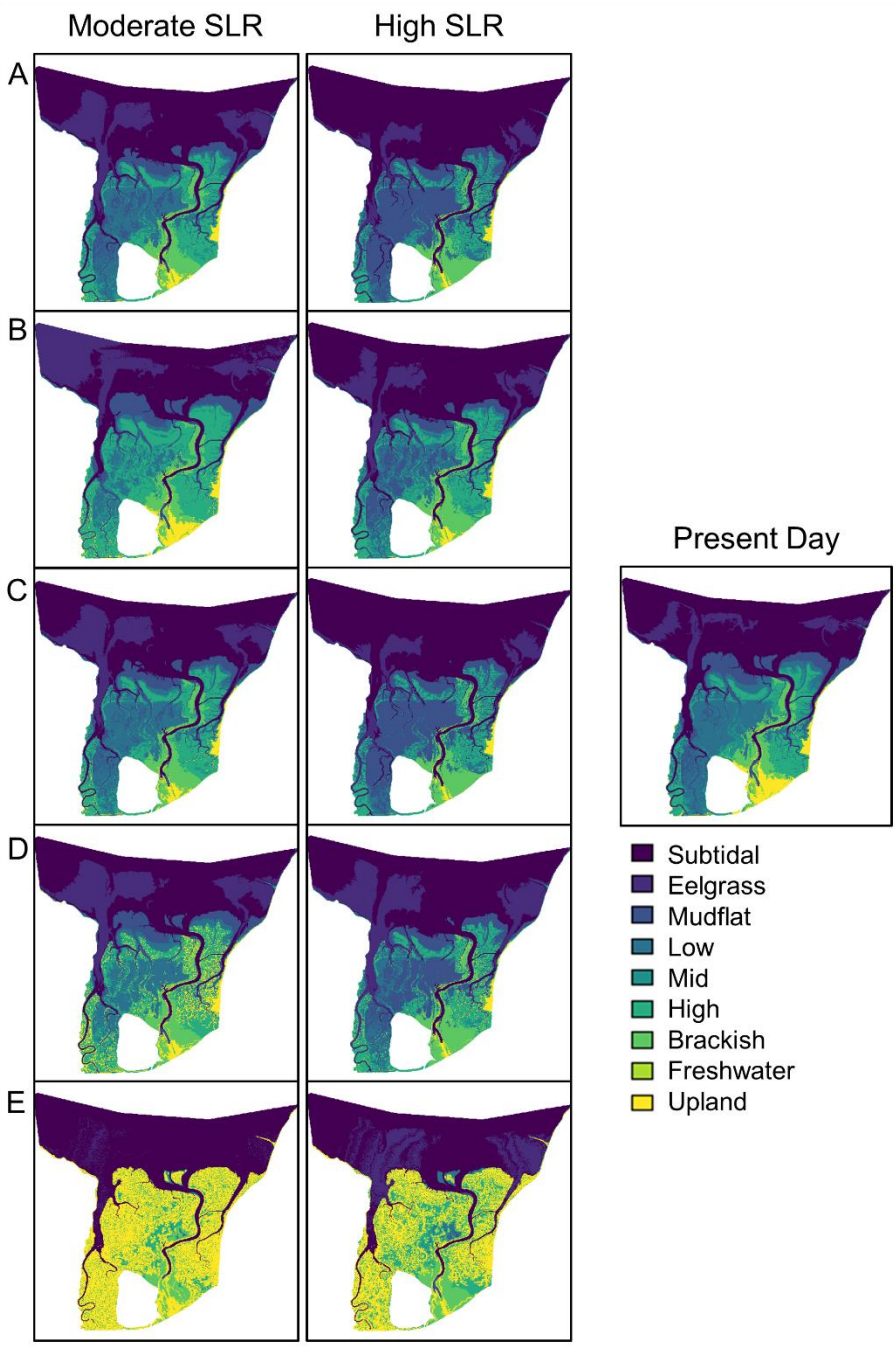

Figure 4.7. Modeled delta-wide habitat distributions for the NRD under moderate (0.62 m by 2100) and high (1.25 m by 2100) SLR scenarios. The MOSAICS model was run with no additional sediment inputs (A), initial elevation values raised by 0.5 m (B), a simulated 10-yr sediment pulse (C), doubled sediment inputs (D), and simulated dam removal (E). Habitat distributions under present day conditions (2011) are shown in the mid-right panel for comparison.

Appendix A: Habitat classification procedure

Methods

We used a hierarchical clustering analysis with the "cluster" package in R 3.4.1 to characterize vegetative community structure and habitat composition across the Nisqually River Delta (NRD). We analyzed data from 2009–2015 vegetation surveys (data collection described in main body of text), and included all plant species with an occurrence > 2.5% in our analysis. We characterized communities by elevation relative to mean tidal level (MTL) and soil pore salinity. All environmental variables were standardized before calculating a Euclidean distance matrix. Because our objective was to group species into distinct habitat types, we chose to test several space-conserving agglomeration methods, including centroid linkage, median linkage, average linkage, and Ward's minimum variance. We used the cophenetic correlation coefficient to evaluate each resultant dendrogram's goodness of fit, and the agglomerative coefficient to measure its degree of clustering. A scree plot of similarity was examined to determine the optimal number of vegetation communities (i.e., habitat types) in the best-fit clustering solution.

To estimate the optimal elevation range for eelgrass growth, we used 2012–2015 presence/absence data from the Puget Sound Submerged Vegetation Monitoring Project (https://www.dnr.wa.gov/programs-and-services/aquatics/aquatic-science/nearshore-habitat-eelgrass-monitoring) to determine the mean and standard deviation range of elevations for which the ratio of shoot presence to shoot absence was greater than 1:1.

Results

A comparison of several clustering methods determined that the average linkage method had the greatest cophenetic correlation coefficient (centroid = 0.68, median = 0.55, average = 0.72, Ward's = 0.70); however, Ward's method produced the highest agglomerative coefficient (centroid = 0.87, median = 0.82, average = 0.80, Ward's = 0.98). A Rand index value of 0.84 supported a high degree of similarity between the average and Ward's clustering methods. Because our objective was to group vegetation species into distinct communities, we chose to use Ward's minimum variance as the best-fit clustering solution. The scree plot showed that partitioning the dendrogram into 6 habitat types offered the most appropriate degree of

separation. The species composition for each habitat type and its associated environmental characteristics are shown in Table A4.1 and Fig. A4.1.

Optimal eelgrass growth on the NRD occurred between -2.97 and -2.31 m elevation relative to MTL, or when habitat was inundated about 94 ± 1.5% of the time. Eelgrass was rarely observed at the mouth of the Nisqually River, even within the modeled elevation range. To account for this in the habitat model, we instituted a buffer whereby no eelgrass habitat was predicted within 500 m path distance of the river.

Table A4.1. Vegetation species included in each habitat type as determined by a hierarchical clustering analysis, with mean ± SD elevation and salinity ranges.

Community	Species	Common name	Elevation relative MTL (m NAVD88)	Salinity (psu)
Upland	*Galium trifidum*	three-petal bedstraw	2.58 ± 0.23	2.79 ± 2.82
	Polystichum munitum	sword fern		
	Pteridium sp.	bracken fern		
	Quercus spp.	oak spp.		
	Ribes divaricatum	black gooseberry		
	Rubus spectabilis	salmonberry		
	Symphoricarpos albus	snowberry		
	Tellima grandiflora	fringecup		
	Urtica dioica	stinging nettle		
Freshwater marsh	*Cirsium* spp.	thistle spp.	1.89 ± 0.60	8.18 ± 7.95
	Lotus corniculatus	birdsfoot trefoil		
	Ranunculus repens	creeping buttercup		
	Rubus armeniacus	Himalayan blackberry		
	Solanum dulcamara	climbing nightshade		
	Typha latifolia	broad-leaf cattail		
Brackish marsh	*Carex lyngbyei*	Lyngbye's sedge	1.46 ± 0.30	14.31 ± 9.47
	Eleocharis acicularis	needle spikerush		
	Juncus acuminatus	tapertip rush		
	Juncus articulatus	jointed rush		
	Juncus balticus	Baltic rush		
	Juncus bufonius	toad rush		
	Juncus effusus	common rush		

	Phalaris arundinacea	reed canary grass						
	Schoenoplectus acutus	common tule						
	Trifolium repens	white clover						
High salt marsh	*Agrostis* spp.	bentgrass spp.	1.61	±	0.23	24.20	±	8.83
	Aster subspicatus	Douglas' aster						
	Atriplex patula	spear saltbush						
	Bolboschoenus robustus	seacoast bullrush						
	Festuca arundinacea	tall fescue						
	Grindelia integrifolia	Puget Sound gumweed						
	Holcus lanatus	velvet grass						
	Hordeum brachyantherum	meadow barley						
	Hordeum jubatum	foxtail barley						
	Leymus triticoides	creeping wildrye						
	Lolium perenne	English ryegrass						
	Puccinella sp.	alkali grass						
Mid-salt marsh	*Cuscuta salina*	salt marsh dodder	1.40	±	0.28	25.48	±	7.92
	Distichlis spicata	saltgrass						
	Jumea carnosa	marsh jaumea						
	Lysimachia maritima	sea milkwart						
	Plantago maritima	salt marsh plantain						
	Potentilla anserina	silverweed						
	Ranunculus cymbalaria	alkali buttercup						
	Salicornia pacifica	pickleweed						
	Stellaria humifusa	salt marsh starwort						
	Triglochin maritima	seaside arrowgrass						
Low salt marsh	*Cotula coronopifolia*	brass buttons	1.02	±	0.40	25.07	±	10.04
	Deschampsia cepitosa	Beringian hairgrass						
	Eleocharis parvula	dwarf club rush						
	Spergularia spp.	sandspurry spp.						

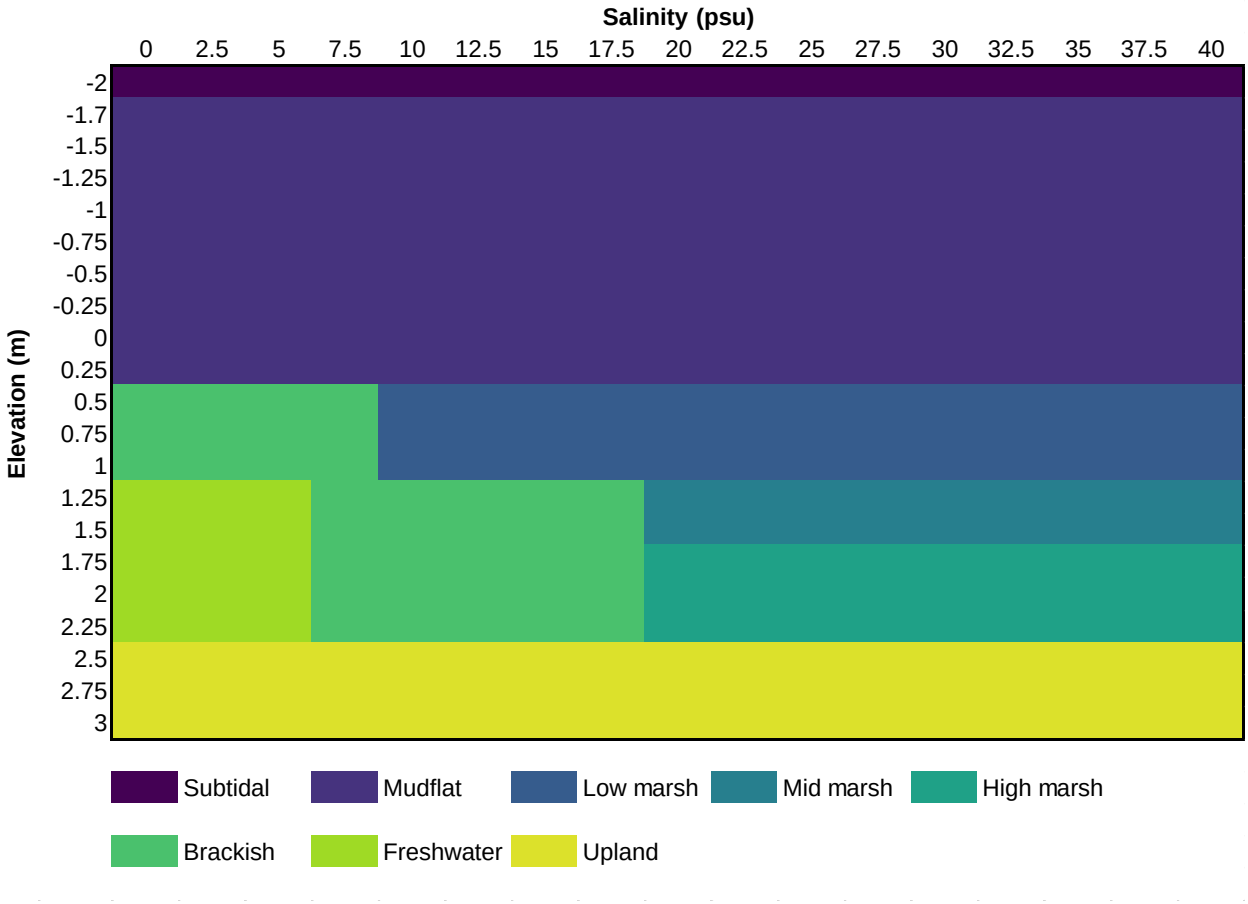

Figure A4.1. Habitat classification based on mean inundation (m NAVD88 relative to MTL) and salinity (psu) ranges for each habitat type.

Appendix B: Soil pore salinity model selection

Table B4.1. Candidate models for soil pore salinity with parameter values estimated using the "bbmle" procedure in R 3.4.1, model degrees of freedom (df), model AIC, ΔAIC, and root-mean-square error (RMSE). The predictor variables were distance from the Nisqually River ($Riv_{x,y}$; m), distance from the marsh edge ($Mar_{x,y}$; m), and inundation duration ($I_{t,x,y}$).

Model equation	Parameter	Value	SE	df	AIC	ΔAIC	RMSE
$S_t = C \cdot (1 - e^{-k \cdot Riv_{x,y}})$	C	27.34	0.633	3	2575.51	79.98	8.12
	k	0.006	0.001				
$S_t = \alpha + \beta \cdot I_{t,x,y} + C \cdot (1 - e^{-k \cdot Riv_{x,y}})$	α	4.94	3.166	5	2573.04	77.51	8.06
	β	5.42	3.152				
	C	2.10	2.987				
	k	0.005	0.010				
$S_t = (C + \alpha \cdot I_{t,x,y}) \cdot (1 - e^{-k \cdot Riv_{x,y}})$	α	4.80	3.321	4	2575.43	79.90	8.11
	C	0.258	1.250				
	k	0.006	0.001				
$S_t = \alpha + \beta \cdot Mar_{x,y} + C \cdot (1 - e^{-k \cdot Riv_{x,y}})$	α	11.93	2.752	5	2521.73	26.20	7.52
	β	-0.008	0.001				
	C	22.65	2.491				
	k	0.004	0.001				
$S_t = (C + \alpha \cdot Mar_{x,y}) \cdot (1 - e^{-k \cdot Riv_{x,y}})$	α	-0.007	0.001	4	2536.60	41.07	7.69
	C	33.47	1.156				
	k	0.006	0.001				
$S_t = \alpha + \beta \cdot I_{t,x,y} + (C + \gamma \cdot Mar_{x,y}) \cdot (1 - e^{-k \cdot Riv_{x,y}})$	α	8.85	2.635	6	2523.30	27.77	7.53
	β	-15.07	4.121				
	γ	-0.012	0.002				
	C	34.07	2.886				
	k	0.004	0.001				
$S_t = (C + \alpha \cdot Mar_{x,y} + \beta \cdot I_{t,x,y} + \gamma \cdot I_{t,x,y} \cdot Mar_{x,y}) \cdot (1 - e^{-k \cdot Riv_{x,y}})$	α	-0.014	0.003	6	2520.34	24.81	7.50
	β	-24.67	9.271				
	γ	0.004	0.010				
	C	45.65	3.992				
	k	0.004	0.000				
$S_t = \alpha + \beta \cdot Mar_{x,y} + (C + \gamma \cdot I_{t,x,y}) \cdot (1 - e^{-k \cdot Riv_{x,y}})$	α	15.84	2.609	6	2495.53	0.00	7.25
	β	-0.013	0.001				
	γ	-24.74	5.109				
	C	31.99	2.672				
	k	0.003	0.001				

Chapter 5

Climate-mediated reduction in the extent of tidal wetland habitat limits prey availability and reduces estuarine nursery quality for juvenile salmon

Abstract

The estuarine habitat mosaic supports the growth and survival of juvenile salmon and other estuary-rearing fishes by providing a gradient (or "portfolio") of unique habitats with varying physical and biological features. With globally increasing water temperatures, rising tidal levels, and changes in riverine hydrology, climate change is likely to have profound effects on the extent and composition of the estuarine habitat mosaic and its associated nursery quality. We used a spatially explicit bioenergetics model to assess how different climate change scenarios might affect juvenile salmon growth rate potential (GRP) relative to present day conditions in the Nisqually River Delta, Washington, USA. Our novel approach is the first to combine a marsh accretion model, a hydrological model, and a bioenergetics model to provide a comprehensive and spatially explicit analysis of habitat quality through time. We found that prey-rich habitats such as low-elevation and high-elevation emergent salt marshes and eelgrass beds were most likely to demonstrate positive GRP. Unmitigated high sea-level rise (1.35 m by 2100) was predicted to diminish the total extent of high and low marsh from 5.42 km^2 to 2.71 km^2, leading to a 2–3 mg h^{-1} reduction in delta GRP by the end of the out-migration season and a 30% reduction in final predicted weights. Increasing water temperatures compounded these effects during the late spring and summer. Although potentially-lethal temperatures (>24°C) were infrequently observed, they were more likely to occur at low tide in July in the mudflat and eelgrass habitats. Our findings indicate that, barring the enactment of targeted management

strategies, rising tidal levels and increasing ocean temperatures will reduce the quality of estuarine habitats for out-migrating juvenile salmon and other anadromous fishes.

Introduction

Coastal ecosystems such as estuaries and their associated tidal wetlands serve as vital nursery grounds for many fish species, providing a diverse mosaic of interconnected habitats that exhibit a variety of geomorphological, hydrological, and biological features (Healey 1982, Simenstad et al. 1982, Ray 2005, Sheaves 2009, Sheaves et al. 2015). This estuarine habitat mosaic (broadly referred to as the "coastal ecosystem mosaic") is positioned at the interface between land and sea, and supports the growth and survival of juvenile fishes via seasonal nutrient pulses, enhanced prey productivity, spatial heterogeneity in biotic and abiotic resources, and protection from predators in complex marsh channels and submerged aquatic vegetation (Beck et al. 2001, Sheaves 2009, Barbier et al. 2011, Vinagre et al. 2011, Meyer & Posey 2014). Unfortunately, coastal ecosystems are highly vulnerable to accelerated climate change and are expected to disappear or degrade at an unprecedented rate over the coming century (Harley et al. 2006, Lotze et al. 2006, Craft et al. 2009, Kirwan & Megonigal 2013). Such climate-mediated habitat loss is likely to have unequivocal consequences for the economically, ecologically, and culturally important fish species that rely on the estuarine habitat mosaic for prey and refugia.

Climate change is expected to diminish estuarine nursery quality in several ways. Sea level rise may change the configuration of the habitat mosaic as productive tidal wetlands without room for inland expansion are converted into unvegetated mudflats (FitzGerald et al. 2008, Kirwan & Megonigal 2013, Thorne et al. 2018). Rising ocean temperatures will likely lead to latitudinal species shifts and could have metabolic consequences for cold-water species (Perry

et al. 2005, Harley et al. 2006, Pörtner & Peck 2010, Neuheimer et al. 2011). Longer tidal inundation durations in tandem with drought events might alter the timing and extent of interconnected habitats in complex ways (Vinagre et al. 2011, Torio & Chmura 2015) with substantial changes to the salinity gradient (Copeland 1966, Mackay & Cyrus 2001, Baptista et al. 2010). When considered in concert, these changes to the estuarine habitat mosaic are likely to reduce its accessibility, complexity, and suitability for juvenile fishes, and could also cause temporal mismatches in rearing and migration events with optimal prey productivity (Logerwell et al. 2003, Harley et al. 2006, Durant et al. 2007). Such a phenological mismatch is particularly concerning for anadromous species like Pacific salmon, which have complex life histories and rear in estuarine habitats at specific times during their life cycle (Healey 1982, Simenstad et al. 1982, Crozier et al. 2008).

Predicting how shifts in the estuarine habitat mosaic — including habitat distribution, water temperature, and prey timing and availability — will affect the growth and survival of juvenile fishes represents a daunting challenge for managers, who must often consider climate change when managing coastal habitats for target species. Pacific salmon present an additional challenge due to the complexity of their life cycle, their diversity of life history strategies, and their propensity to move through multiple habitats over a short time span (Simenstad et al. 1982, Healey 1991, Crozier et al. 2008, Schindler et al. 2010). Habitat-specific measurements of prey availability, diet, and water temperature can shed light on the utility of each habitat type for promoting optimal consumption and growth for juvenile salmon (Sommer et al. 2001, Chittenden et al. 2018, Davis et al. 2018*a*, 2019), but they cannot capture broader, ecosystem-scale patterns that occur when fish use several habitat types that vary in accessibility and connectivity. Thus, an optimal tool would account for the entire estuarine habitat mosaic while also incorporating

fluctuations in habitat accessibility, water temperature, and prey availability that occur at multiple spatiotemporal scales.

A variety of techniques can be used to predict how climate change will affect the nursery quality of estuarine habitats for fish, including bioenergetics models, which are energy balance equations that employ measurements of water temperature, prey quantity, prey quality, and fish size to estimate consumption and growth (Kitchell et al. 1977, Stewart & Ibarra 1991, Beauchamp 2009). Bioenergetics models provide useful measures of habitat quality and can be an important tool for assessing the suitability of various habitat types and configurations (Rosenfeld et al. 2005, Davis et al. 2019). Although these models are typically used to analyze a specific site or habitat type, advances in remote sensing have made it easier to create spatially explicit versions for landscape-scale applications (Brandt et al. 1992, Farley & Trudel 2009, Budy et al. 2011). By using a spatially explicit model, consumption and growth can be discerned for the entire habitat mosaic based on each habitat type's accessibility, temperature, and prey community, making it a valuable tool for evaluating estuarine ecosystems.

Here we demonstrate the utility of a spatially explicit bioenergetics approach for assessing the nursery quality of a mosaic of interconnected estuarine habitats. Specifically, our goal was to determine how different climate change scenarios might affect juvenile salmon growth relative to current conditions via changing habitat configurations and thermal regimes. For our study system, we used the Nisqually River Delta in Puget Sound, Washington, USA — a macrotidal system comprised of a diverse assemblage of mudflat, eelgrass (*Zostera marina*), salt marsh, brackish marsh, and freshwater tidal forested habitats. We ran our bioenergetics model on an hourly time step to account for diurnal shifts in tidal level and water temperature. To simulate the physical conditions of the delta under climate change, we used output (i.e., elevation, habitat

classification) from a marsh accretion model that was run using varying sea-level rise and suspended sediment inputs (Chapter 4). We hypothesized that the loss of productive tidal wetland habitat would detrimentally affect juvenile salmon growth. Furthermore, we predicted that increased water temperatures would result in some habitats becoming inaccessible regardless of depth because they were outside the thermal tolerance of juvenile salmon. Although coastal ecosystems will exhibit unique responses to the effects of climate change, this study sheds light on how managers can apply readily-available modeling tools to identify target nursery habitats for juvenile fishes, and to evaluate alternative approaches to maintain the functionality of the ecosystem mosaic.

Materials and methods

Study area and acquisition of spatial data

Our study system was the Nisqually River Delta in southern Puget Sound, Washington, USA (47°4′48″N, 122°42′20″W; Fig. 5.1), which is comprised of numerous habitat types that vary in salinity, inundation frequency and duration, and vegetative cover (Belleveau et al. 2015, Ballanti et al. 2017, Chapter 4). Tidally-influenced forests and brackish wetlands (0–5 psu) bound the main stem Nisqually River, where seasonal snowmelt and rainfall result in freshwater pulses and flooding events. At the mouth of the delta, roughly 85 km of tidal channels wind through emergent salt marsh (5–30 psu), including 39 km of channels in subsided low-elevation marsh that was restored to tidal influence in 2009 (0–2 m relative to mean tidal level; MTL = 1.34 m NAVD88; Ellings et al. 2016). With an average tidal range of 4 m, most of the marsh plain is inundated at high tide (mean high water [MHW] = 2.82 m NAVD88), especially during the spring tides, which can reach as high as 4 m NAVD88. At low tide (mean low water [MLW] = -

0.11 m NAVD88), the marsh tidal channels dewater completely, and the mudflats and eelgrass beds to the north can become exposed for an hour or more.

Each year, this diverse habitat mosaic supports out-migrating populations of Chinook (*Oncorhynchus tshawytscha*), chum (*O. keta*), coho (*O. kisutch*), and pink (*O. gorbuscha*) salmon, and steelhead trout (*O. mykiss*). Nisqually's ESA-listed fall-run Chinook salmon are especially vulnerable to coastal habitat loss, spending weeks or months rearing in estuarine habitats during smoltification (Thorpe 1994, Bottom et al. 2005, Davis et al. 2018*b*). Thus, the delta is an optimal study system not only for its habitat diversity, but also because it supports economically, ecologically, and culturally important populations of anadromous fishes.

The Nisqually River Delta has been extensively mapped as part of a comprehensive post-restoration monitoring program, and remote sensing data have been used to make climate change projections and to measure habitat change and erosion through time (Ballanti et al. 2017, Thorne et al. 2018, Chapter 4). For our spatially explicit bioenergetics model, we used a 3-m resolution bare earth digital elevation model (DEM) created from airborne lidar flown in January 2011 (Watershed Sciences Inc., Portland, Oregon, USA). The DEM was validated to a vertical accuracy of ± 3 cm using a real-time kinematic global positioning system (RTK GPS) and boat-mounted bathymetry. We used a habitat classification procedure based on inundation duration, soil pore salinity, and vegetative community structure (Chapter 4) to categorize each cell as subtidal, mudflat, eelgrass, low salt marsh, high salt marsh, brackish marsh, or upland tidal forested habitat. We used spatial output from the same study to represent predicted delta conditions given several sea-level rise and suspended sediment scenarios, which we describe in detail below.

Water temperature

Fish are ectotherms, meaning that the temperature of their surrounding environment determines their consumption and respiration rates (Kitchell et al. 1977, Thornton & Lessem 1978). We measured the water temperature of submerged tidal channels throughout the Nisqually River Delta from 2010–2015 using Solinst® LTC data loggers (Georgetown, Ontario, Canada). We deployed loggers at twelve fixed locations representative of multiple habitat types (Fig. 5.1). Each logger was installed in a protective PVC pipe in the middle of an established channel with the sensor positioned about 15 cm from the channel bottom. Loggers measured water temperature continuously at 6, 12, or 15-minute intervals, and were downloaded in the field seasonally to collect uninterrupted data. We extrapolated these measurements across space and time using a non-linear model relating water temperature to air temperature, insolation, water depth, and vegetative cover (Appendix A).

Prey energy density and standing biomass

Fish growth is also determined by the quality and quantity of prey in their surrounding environment. To calculate the energy density (J g^{-1} wet weight) and standing biomass (mg m^{-3} wet weight) of prey in each habitat type, we sampled the water column for zooplankton, nekton, and surface drift. We conducted neuston net tows (width 0.4 m, height 0.2 m, 0.130-mm mesh) in low and high salt marsh from 2010–2012 and in upland tidal forested, brackish marsh, high salt marsh, mudflat, and eelgrass habitats from 2014–2015 (Fig. 5.1). We also concurrently sampled the epibenthos using 10- or 2.5-cm benthic cores (Woo et al. 2018, USGS unpublished data); however, we omitted benthic samples from estimates of prey energy density and standing biomass to avoid grouping taxa that were collected at different spatiotemporal sampling scales.

Prey sampling occurred during the height of the wild Chinook salmon out-migration season from March–July. During the 2010–2012 sampling period, the neuston net was pulled across the surface of the channel along a 120˚ arc measuring 3.85 m for a total estimated sample volume of 0.33 m^3. In 2014–2015, we conducted a three-minute tow at the surface of the water and a six-minute tow at a meter below the surface during each sampling event, and water volume was measured using a flow meter attached to the mouth of the net. For the subtidal zone, we used 2014–2015 bongo net data from nearby Solo Point (47°8′36″N, 122°38′10″W) and Dana Passage (47°10′22″N, 122°50′36″W). Oblique bongo nets (60-cm diameter, 0.335 mm mesh) were towed through the upper 30 m of the water column, while a flow meter attached to the mouth of the net measured water volume (Connelly et al. 2018). Neuston tow samples were preserved in 95% ethanol in the field before being sent to the lab for identification, while bongo tow samples were preserved in 5% $NaHCO_3$-buffered formalin.

We identified and enumerated neuston samples to the lowest possible taxonomic level using a stereo dissection microscope at a magnification range of 7–45×. We obtained per-individual dry weight biomass estimates for important prey taxa by drying a subset of each taxon in a laboratory oven for 24 hours at 80°C and weighing them on a 0.1 mg precision scale. We then extrapolated total sample biomass for each taxon by multiplying sample densities (number of individuals per-m^3) by the estimated per-individual biomass (mg). A dry-to-wet weight biomass conversion factor based on literature values was used to estimate wet weight biomass for the bioenergetics model (Davis et al. 2018*a*). For bongo net tows, preserved samples were split using a Folsom plankton splitter, and large, rare organisms were removed. The split was diluted to a known volume depending on the density of organisms and two aliquots were taken. Each taxon was enumerated, identified, and measured under a dissecting microscope. The

biomass of measured organisms (mg m^{-3}) was then estimated using established length-weight relationships (e.g., Chisholm & Roff 1990).

We used the habitat classification map for each climate change scenario to derive estimates of prey energy density and standing biomass for the Nisqually River Delta habitat mosaic (Chapter 4). We calculated a monthly average for each metric in each habitat type using the neuston or bongo tow data sets. Empirical values were then assigned to cells in the spatial coverage based on the extent and distribution of each habitat type (Fig. 5.2). To account for temporal trends, habitat-specific values were linearly interpolated on an hourly timescale from one month to the next (monthly estimates assigned to day of year [DOY] 74, 105, 135, 166, and 196). Similar to water temperature, the energy density and standing biomass of the available prey field changed on an hourly basis depending on which habitats were tidally inundated (i.e., an uninundated cell was considered unavailable, so its prey field contributed nothing to delta growth potential).

Model framework

We used Farley & Trudel's (2009) bioenergetics model to calculate juvenile salmon growth rate potential (mg h^{-1}; GRP) from spatially explicit estimates of water temperature, prey energy density, and standing biomass (Fig. 5.3). This particular model estimates growth (*G*) as a function of consumption (*C*), standard metabolic rate (*SMR*) and swimming cost (*ACT*) using the equation

$$G = \tau \cdot C - (SMR + ACT)$$

where τ is the proportion of food that can be metabolized (0.7; Ware 1978). It is ideal for spatial applications because *C* is determined directly from prey biomass (*Bio*) and prey energy density

(*ED*), which we assigned to each habitat type based on our sampling of the prey field (Appendix B). Handling time (*h*), swimming speed (*U*), and the cross-sectional area of the reactive field (γ) are body size- (weight; *W*) and temperature- (*T*) associated parameters that also influence the consumption rate of each fish according to a type II functional curve (Koski & Johnson 2002, Farley & Trudel 2009, Haskell et al. 2017):

$$I = ED \cdot \frac{Bio \cdot \gamma \cdot U}{1 + Bio \cdot \gamma \cdot h \cdot U}$$

Standard metabolic rate is calculated as a function of weight and temperature (Trudel & Welch 2005):

$$SMR = \alpha_1 \cdot W^{\beta} \cdot e^{\varphi \cdot T}$$

and *ACT* is a function of swimming speed and temperature (Trudel & Welch 2005):

$$ACT = \alpha_0 \cdot W^{\delta} \cdot U^{\lambda}$$

where α_1, β, φ, α_0, δ, and λ are temperature-dependent intercept and slope parameters. We used parameter values from the literature for Chinook salmon because they have the longest delta residence times spanning March–July, when we collected water temperature and prey availability data.

Model simulations

We ran our spatially explicit bioenergetics model for multiple climate change scenarios in the years 2050 and 2100 (Table 5.1). We used moderate (0.62 m by 2100) and high (1.35 m by 2100) sea-level rise predictions for Washington state to modify tidal inundation regimes (NRC 2012). Chapter 4 showed that doubling suspended sediment inputs might be enough to maintain the estuarine habitat mosaic in the Nisqually River Delta through 2100, so we also included a "sediment management" scenario where the elevation and habitat classification layers accounted

for increases in suspended sediment accordingly. For each sea-level rise/sediment scenario, we calculated the areal extent of each habitat type in the delta (Table 5.2). We also ran each scenario using present day measured air temperatures (https://www.ncdc.noaa.gov) or by increasing the air temperature 2.5°C or 5°C according to NOAA high emissions predictions for Washington State in 2050 and 2100, respectively (Frankson et al. 2017).

We ran the model on an hourly time step from March 1–July 31. The starting weight was set to 0.75 g, which is representative of the size of natural origin fry migrant Chinook salmon upon entering the delta in February or March (Davis et al. 2019). For each time step, size was re-calculated based on the estimated growth of the fish (mg h^{-1}) from the bioenergetics model. We used hourly tidal levels from 2014 to simulate the tidal inundation regime of the delta and to determine which habitats were available for juvenile salmon. We set the following model stipulations: 1) fish can only use inundated habitats (≥0.4 m depth; Hering et al. 2010), 2) fish feed during a 14-hour daylight period between 0600 and 2000 (Schabetsberger et al. 2003, Duffy et al. 2010), 3) fish select for positive-GRP habitats (Railsback & Harvey 2002). This was done to ensure the model was reflective of juvenile salmon behavioral characteristics, since spatially explicit bioenergetics model output can vary widely based on model assumptions (Mason & Brandt 1996). These decision rules assumed that individuals only occupied accessible habitats that offered positive GRP when available. As such, we calculated both a *delta-wide* GRP that integrated good and bad growth regions and an *individual* GRP that accounted for the model stipulations, and thus, was more likely to be a positive value.

Model sensitivity and corroboration

We conducted a longitudinal sensitivity analysis to determine if model error was propagated through time. Individual GRP and weight were simulated on an hourly time step between March 1 and July 31 as described above. The bioenergetics model was run using present day environmental conditions (elevation, water temperature, and water level). We varied the water temperature, prey energy density, and prey biomass inputs by ± 20% and the resultant output was compared to predicted weight and hourly GRP estimates when unmodified inputs were used.

As a measure of corroboration, we used otolith-derived growth rates from 92 juvenile Chinook salmon captured by fyke net in May–July of 2010 and 2011. Fish were sampled from four tidal channels in brackish or saline emergent marsh and had estimated delta residence times ranging from 3 to 33 days at time of capture (Fig. 5.1; Davis et al. 2018*b*). A detailed description of otolith processing procedures and morphometric delta growth rate calculations can be found in Davis et al. 2018*b*. For each fish, we used the bioenergetics model to back-calculate its weight at delta entry. We used hourly measurements of air temperature, insolation, and water level from 2010 and 2011 to ensure model output reflected actual environmental conditions. Average daily growth (g d^{-1}) was calculated using the equation $\frac{W_t - W_0}{d}$ where W_t is each fish's measured wet weight at time of capture, W_0 is its modeled weight at delta entry, and d is its delta residence time. We used a linear regression to compare the average daily growth of each fish as estimated from otoliths and the bioenergetics model, where an intercept that was significantly different from zero was indicative of bias, and a slope of 1 was indicative of a direct relationship between observed and modeled growth estimates.

Results

Water temperature

Under present day conditions, the average temperature of inundated habitat varied from a low of 3.50 ± 0.30°C on March 1 to a high of 19.10 ± 0.65°C on July 14. The non-linear model predicted that water temperatures were cooler in deeper water. This led to a temperature stabilizing effect at high tide, especially during June and July. The presence of vegetative cover also had a stabilizing effect on water temperature, where tidal channels with overhanging vegetation were 1–2°C warmer than exposed bodies of water in the winter and cooler in the summer. Potentially lethal temperatures were rare (>24°C; Plumb & Moffitt 2015) and were most likely to occur in the mudflats and eelgrass beds at low tide in July (Fig. 5.4).

Despite increasing water depths in many parts of the delta, sea-level rise had virtually no effect on modeled water temperatures when air temperature was held constant at present day values. Moderate and high rates of sea-level rise resulted in a 0.6–1.1% decrease in seasonal average water temperatures throughout the delta by 2050, and a 1.8–3.6% decrease by 2100. The magnitude of this temperature change was the same regardless of the effect of suspended sediment on the configuration of the estuarine habitat mosaic. Conversely, increasing air temperature by 5°C affected water temperatures considerably. Seasonal average water temperatures increased from 10.73 ± 3.78°C under present day conditions to 14.22 ± 3.18°C in 2100. The maximum observed hourly average in 2100 was 20.89 ± 0.72°C on July 14, and water temperatures at low tide were far more likely to reach sub-lethal or lethal levels throughout the summer than under present day conditions. Sea-level rise slightly mitigated temperature increases by 0.6–1.2% in 2050 and 1.9–3.7% in 2100, but again, this effect was marginal.

Prey energy density and standing biomass

Aquatic prey energy density under present day conditions averaged 3899 ± 158 J g^{-1} and varied slightly from month-to-month (Table 5.3). The upland tidal forested (6161 ± 481 J g^{-1}) and brackish marsh (5279 ± 905 J g^{-1}) habitats along the main stem Nisqually River provided high-energy insect drift (Fig. 5.2; Davis et al. 2018*a*). Meanwhile, prey in the low-elevation salt marsh (4214 ± 1083 J g^{-1}), high-elevation salt marsh (4166 ± 572 J g^{-1}), delta mudflats (4144 ± 652 J g^{-1}), eelgrass beds (3716 ± 591 J g^{-1}), and subtidal zone (3188 ±497 J g^{-1}) were characterized by energy-poor crustaceans such as mysids, amphipods, and crab larvae. Moderate and high sea-level rise resulted in minor reductions in delta-wide prey energy density (-33 J g^{-1} and -129 J g^{-1} by 2100, respectively), which was likely the result of a 40–70% reduction in upland tidal forested habitat (Table 5.2). The addition of suspended sediment successfully maintained, or even expanded, the amount of tidal forested and brackish marsh habitat, thereby mitigating the predicted decline in prey quality. This was especially true for the moderate sea-level rise scenario, where prey energy density increased by 85 J g^{-1} through 2100.

Prey standing biomass averaged 43.93 ± 8.58 mg m^{-3} under present day conditions, and was greatest in May, June, and July for all scenarios (Table 5.3). Unlike prey energy density, the upland tidal forested habitat had the lowest prey biomass (3.68 ± 2.88 mg m^{-3}), followed by the subtidal zone (12.36 ± 11.14 mg m^{-3}), delta mudflats (17.75 ± 18.44 mg m^{-3}), and brackish marsh (24.36 ± 36.73 mg m^{-3}). Saline habitats with dense vegetation such as the low- (159.00 ± 209.33 mg m^{-3}) and high-elevation salt marshes (47.34 ± 98.96 mg m^{-3}) and eelgrass beds (93.22 ± 132.37 mg m^{-3}) provided the most prey (Fig. 5.2). Moderate sea-level rise was predicted to have no effect on delta-wide standing biomass despite a 0.48 km^2 (16%) reduction in the extent of prey-rich low salt marsh habitat (Table 5.2). Conversely, high sea-level rise reduced the delta-wide average by 14.56 mg m^{-3} through 2100, which was accompanied by a 1.86 km^2 (64%)

reduction in low-elevation salt marsh and a 0.85 km^2 (34%) reduction in high-elevation salt marsh. The addition of suspended sediment mitigated habitat loss, thereby increasing standing prey biomass from a delta-wide average of 29.37 ± 7.02 mg m^{-3} to 40.77 ± 12.40 mg m^{-3} according to model predictions for the year 2100.

Bioenergetics model performance

Using the water temperature, prey energy density, and prey standing biomass inputs, the bioenergetics model predicted juvenile salmon GRP through space and time, indicating specific habitats where fish were more likely to experience growth during each hourly time step (Fig. 5.5). The subtidal habitat consistently had negative GRP values, despite being available for juvenile salmon at all tides. Conversely, low- and high-elevation emergent salt marsh had the highest GRP values but were only available during high tide. Eelgrass was the only habitat type that had consistently positive estimated GRP values and was available to fish throughout the tidal cycle. In terms of *delta-wide* GRP, the model predicted that it was slightly negative on average throughout the out-migration season, with the exception of May (Mean ± SD: March = -0.16 ± 0.21 mg h^{-1}, April = -0.13 ± 0.32 mg h^{-1}, May = 0.23 ± 0.52 mg h^{-1}, June = -0.14 ± 1.55 mg h^{-1}, July = -0.52 ± 5.48 mg h^{-1}) and did not increase though time concurrent with fish size. To simulate juvenile salmon growth, we applied the assumption that fish selected for positive-GRP habitats. Consequently, *individual* GRP estimates increased throughout the growing season and were much more likely to be positive, averaging 0.47 ± 0.69 mg h^{-1} in March, 0.51 ± 0.94 mg h^{-1} in April, 2.09 ± 2.55 mg h^{-1} in May, 6.84 ± 7.45 mg h^{-1} in June, and 8.48 ± 14.77 mg h^{-1} in July.

The longitudinal sensitivity analysis indicated that perturbation of each of the model inputs by 20% had a noticeable effect on predicted growth through time, especially later in the

out-migration season (Fig. 5.6). The model was more sensitive to the prey inputs (energy density, standing biomass) than to water temperature, although decreasing water temperatures did result in a 2.74 g (19%) reduction in predicted final weight. When prey energy density was decreased by 20%, the frequency of occurrence of highly positive GRP values (> 3 mg h^{-1}) throughout the growing season decreased by 22.6% and predicted final weight decreased from 14.25 g to 9.31 g. Conversely, when prey energy density was increased by 20%, final weight tripled to 31.14 g and the frequency of highly positive GRP values increased by 19.1%. Shifts in prey standing biomass had a similar effect, whereby decreasing biomass by 20% reduced final predicted weight from 14.25 g to 11.81 g and increasing biomass by 20% doubled it to 23.88 g.

Despite the potential for model output to be influenced by miscalculations of prey quality and quantity, the corroboration procedure indicated that model performance was robust over shorter (3–33 day) periods. Average daily growth for 2010 and 2011 was 0.126 ± 0.048 g d^{-1} as estimated by otoliths and 0.147 ± 0.064 g d^{-1} as estimated by the bioenergetics model. A linear regression of otolith- and model-derived growth estimates for individual fish found a significant linear relationship (df = 91, R^2 = 0.44; Fig. 5.7) with an intercept of 0.038 g d^{-1} and a slope of 0.863 (parameters were corrected for heteroskedasticity). The intercept was significantly different from 0 (p = 0.010) and the slope term was slightly less than 1.0, indicating that the model was more likely to overestimate growth in high GRP habitats. Nevertheless, the linear relationship between observed and modeled values indicated that our model parameters and assumptions were reasonable, and that the bioenergetics model is likely a comprehensive measure of relative habitat quality.

Climate scenarios

Moderate rates of sea-level rise resulted in positive delta-wide GRP estimates in 2050 and 2100, both with and without the addition of suspended sediment (Fig. 5.8, Fig. 5.9). This was particularly noticeable for the month of June. High rates of sea-level rise, on the other hand, led to a substantial reduction in delta GRP by 2100 (as low as -3 mg h^{-1}) unless suspended sediment inputs were doubled to maintain the extent of low- and high-elevation salt marsh (Table 5.2). Concurrent temperature changes also affected delta-wide growth estimates. Specifically, increasing air temperatures by 2.5°C in 2050 or 5°C in 2100 resulted in a modest (< 1 mg h^{-1}) reduction in delta GRP, regardless of the sea-level rise scenario. Scenario 9 (high sea-level rise, +5°C) resulted in the lowest predicted delta GRP values, which led to a 4.3 g decrease in predicted final weight (Table 5.4).

We applied several decision tools to our model, including the assumption that juvenile salmon selected for positive-GRP habitats. As such, the individual GRP of a modeled fish and its body weight through time was greater than delta-wide GRP estimates. While predicted delta GRP increased under several of the sea-level rise scenarios, individual GRP almost always decreased, especially in late June and July (Fig. 5.8). We observed a modest reduction under moderate rates sea-level rise that was only apparent later in the out-migration season, while under high rates of sea-level rise juvenile salmon were predicted to see larger-magnitude reductions in individual GRP as early as April. Although the addition of suspended sediment had a beneficial effect on delta GRP, it did not bolster individual GRP estimates. This is likely because the conversion of prey-rich low marsh habitat to mudflats resulted in a substantial (up to 10 mg h^{-1}) reduction in their predicted GRP (Fig. 5.9).

Discussion

We successfully applied a spatially explicit bioenergetics framework to characterize the quality of nursery habitat in the Nisqually River Delta. Our findings suggest that the maintenance of the estuarine habitat mosaic, especially prey-rich salt marsh and eelgrass habitats, is pivotal for promoting the growth and survival of estuary-rearing juvenile Pacific salmon. Output from the bioenergetics model indicated that high rates of sea-level rise, which were associated with the greatest amount of emergent marsh habitat loss, would substantially decrease the GRP of delta habitats and the juvenile salmon that rely on them. This supports our first hypothesis: that the loss of productive tidal marsh would detrimentally affect juvenile salmon growth. We also predicted that increasing air temperatures (5°C by 2100) would result in some parts of the delta becoming inaccessible to juvenile salmon. This was true for the mudflat and eelgrass habitats during July low tides, but lethal temperatures (>24°C; Plumb & Moffitt 2015) were still infrequently observed. Overall, our model output suggests that rising tidal levels in tandem with increasing ocean temperatures will reduce the quality of estuarine habitats for juvenile salmon and other anadromous fishes by decreasing the accessibility and extent of prey-rich habitats, even if targeted management strategies (such as the addition of suspended sediment to the marsh plain) are enacted.

Model predictions for present day conditions found the most favorable growth in low-elevation salt marsh, high-elevation salt marsh, and eelgrass habitats, each of which exhibited variable accessibility depending on the tide. Because Nisqually's tidal sloughs dewater at low tide (Ellings et al. 2016), both delta-wide and individual GRP were greatest at high tide when salt marsh channels were accessible, with a clear inflection point around 1.75–2.25 m NAVD88. Higher water temperatures in June and July may have also contributed to the reduction in delta GRP associated with low tide, because bioenergetically detrimental temperatures of 20–23°C

were observed in otherwise high-GRP eelgrass beds (Plumb & Moffitt 2015). Average delta GRP under present day conditions trended negative, reaching a peak daily average of 0.23 ± 0.52 mg h^{-1} in May. Negative delta GRP estimates are consistent with Farley & Trudel's (2009) findings from their spatially explicit model of sockeye salmon GRP in the Bering Sea. This is most likely because the type II functional response curve is sensitive to lower prey densities (Koski & Johnson 2002, Haskell et al. 2017), as indicated by the longitudinal sensitivity analysis. Thus, although delta GRP was frequently negative, it is still a reliable measure of relative habitat quality throughout the estuarine habitat mosaic if it accounts for the habitat available to and occupied by fish.

When we applied specific decision rules to the bioenergetics model (i.e., juvenile salmon select for positive-GRP habitats and only feed during daylight hours), individual GRP reflected the short-term growth of natural and hatchery origin juvenile Chinook salmon, which was corroborated by the otolith microstructure analyses. Although delta GRP peaked in May, individual GRP peaked in June (6.84 ± 7.45 mg h^{-1}) and July (8.48 ± 14.77 mg h^{-1}) due to the allometric relationship between body size and growth. Throughout most of the year, the low-elevation emergent marsh, high-elevation emergent marsh, and eelgrass beds were the only habitats to have positive GRP values, with eelgrass being the only positive-GRP habitat accessible at low tide. The GRP of the eelgrass beds was most positive in June, meaning that during this month the model was more likely to predict positive delta and individual GRP values throughout the entire tidal cycle, not just at high tide. Studies in Puget Sound have found that juvenile salmon and other resident fishes are more likely to use native eelgrass beds than unvegetated habitats in the nearshore zone (Rubin et al. 2018), thereby highlighting the importance of eelgrass as a low tide alternative to tidal marsh channels.

When compared to present day conditions, rising tidal levels and ocean temperatures were predicted to have a detrimental effect on the nursery quality of the estuarine habitat mosaic. Even though moderate SLR resulted in a slight increase in delta GRP in 2050 and 2100 (especially in June), individual GRP declined concurrent with the predicted loss of low salt marsh. Conversely, the high SLR scenario — which is becoming more likely as ice sheets in Greenland and Antarctica continue to melt (DeConto & Pollard 2016) — led to a substantial decline in both delta and individual GRP estimates, with delta GRP decreasing to -3 mg h^{-1} by July. Increasing water temperatures almost always reduced delta GRP, and this effect was not offset by SLR. These results highlight how SLR and increasing ocean temperatures may act in tandem to reduce the growth of estuary-rearing juvenile salmon, both directly through the disruption of consumption and respiration rates (Beauchamp 2009, Plumb & Moffitt 2015), and indirectly by affecting the energy density and availability of prey throughout the estuarine environment. They highlight the need for adaptive management solutions to conserve and restore coastal ecosystems as environmental conditions change.

The addition of sediment to encourage marsh accretion represents one potential solution for preserving the current extent and configuration of estuarine habitats (Thrush et al. 2004, Kirwan et al. 2010, Chapter 4). The maintenance of tidally-influenced freshwater, brackish, and salt marsh is important not only because tidal marshes supply high densities of energy-rich prey, but also because the overhanging vegetation and deep tidal channels can provide thermal refuge for fish (Martin et al. 1986, Balling & Resh 1991, Romanuk & Levings 2003, Broadmeadow et al. 2011). Our model predicted mixed results with respect to the effect of sediment addition on nursery habitat quality and juvenile salmon growth. Delta GRP greatly improved through 2100 when sediment inputs were doubled to maintain the estuarine habitat mosaic, with delta GRP

becoming greater than present day estimates regardless of SLR and temperature, especially during June. Conversely, the addition of sediment slightly decreased individual GRP values and predicted final weights, again indicating that the extent, distribution, and accessibility of high-quality habitat may be the best indicator of salmon growth.

Our corroboration procedure using juvenile Chinook salmon otoliths indicated that model performance was acceptable, but there are several caveats and assumptions that are worth mentioning. For instance, the longitudinal sensitivity analysis showed that model output was most sensitive to prey inputs, yet these inputs were the most difficult to model through space and time. Prey abundance can vary widely from week-to-week and among sampling sites within a given habitat type. For simplicity's sake, we chose a coarse-scale technique where monthly empirical measurements of aquatic prey energy density and standing biomass were applied directly to a habitat classification map, but this technique did not account for the effect of rising ocean temperatures on prey abundance and community structure. Non-linear models (NLMs), generalized additive models (GAMs), canonical correspondence analysis (CCA), and multivariate regression trees (MRT) are other methods for predicting prey distributions based on environmental characteristics such as temperature, salinity, vegetative cover, and inundation duration (Guisan et al. 1999, De'ath 2002, Olden & Jackson 2002, Ferrier & Guisan 2006). Although they vary widely in terms of their ability to extrapolate marcoecological properties (such as energy density and standing biomass), these methods may be worth exploring for spatially explicit bioenergetics models in complex habitats.

Other caveats to our modeling approach were that it assumed that fish were equally likely to use any available positive-GRP habitat, that they remained in the delta for the entire five-month period, that they did not experience density-dependent effects on consumption, and that

there was no mortality due to predation. Some of these caveats could be addressed through an individual-based (or "agent-based") modeling approach (DeAngelis & Gross 1992, Railsback & Harvey 2002, Railsback et al. 2003, Harvey & Railsback 2009), which models the behavior of each individual fish in a simulated population. To apply an individual-based model to a dynamic coastal ecosystem such as the Nisqually River Delta, one would require detailed data relating tidal currents and river flows to prey productivity on an hourly timescale. These data were unavailable to us, which is why we chose a more "habitat-centric" approach.

Finally, our model was reliant on spatial output from a site-specific marsh accretion model. Although we used an empirical model that was designed and calibrated specifically for the Nisqually River Delta (Chapter 4), managers have access to a variety of prediction tools, including simple inundation (or "bathtub") models, the Sea Level Affecting Marshes Model (SLAMM), the Marsh Equilibrium Model (MEM), or the Wetland Accretion Rate Model of Ecosystem Resilience (WARMER), all of which vary in accuracy, cost, and usability (Mcleod et al. 2010). With the increasing availability of climate change prediction tools and spatial techniques, we see the opportunity for managers to combine methodologies as a component of adaptive management for estuary-dependent fish species. Such an approach has broader applications beyond the realm of anadromous Pacific salmon, and could be used to assess habitat quality for resident pelagic and demersal species.

In terms of its ecological implications, our study found that the quantity of prey-rich salt marsh and eelgrass habitats (and, presumably, the duration of their availability) drove individual GRP values. Although we lack data from other study systems, this trend could be indicative of broader ecological processes. Certainly, a more diverse estuarine habitat mosaic would be expected to provide a portfolio of prey communities and thermal regimes, thereby supporting

multiple fish species with varying diet and habitat use strategies (Sheaves 2009, Yates et al. 2012, Armstrong and Schindler 2013, Schindler et al. 2015). We used Pacific (Chinook) salmon as our model species due to its role as an economically, ecologically, and culturally important resource in Puget Sound, but managers may have to consider other coastal fishes when assessing nursery habitat quality. For instance, anadromous species like longfin smelt (*Spirinchus thaleichthys*) and eulachon (*Thaleichthys pacificus*) may use the same habitats as salmon, but with different residence times, sizes, feeding strategies, and energetic needs (Bottom & Jones 1990, Simenstad et al. 2002). There is room for advancement with regards to developing more sophisticated techniques to model prey quality, quantity, and fish behavior, and accounting for multiple species and study sites. Nevertheless, our work provides a foundation for incorporating climate change models into spatially explicit measurements of nursery habitat quality in dynamic coastal ecosystems such as estuaries and their associated tidal wetlands. It demonstrates how directed sampling can be closely linked to inform model development, parameterization, and input variables to assess major source of variability in important ecological phenomena.

Acknowledgments

This research was carried out as part of a collaborative effort between the U.S. Geological Survey, the Nisqually Indian Tribe, and Billy Frank Jr. Nisqually National Wildlife Refuge. USGS employees L. Shakeri, S. Blakely, A. Munguia, A. Hissem, L. Lamere, C. Freeman, S. Kaviar, L. Belleveau, J. Donald, Y. Chan, C. Norton, H. Mittelstaedt, and J.Y. Takekawa; Tribal employees W. Duval, E. Perez, J. Moore, and A. David; Refuge staff D. Roster, M. Bailey, J. Barham; and University of Washington biologists K. Connelly, J. Gardner, and M. Gamble were a vital part of this project's success. Thanks to J. Keister and her lab for sharing bongo tow data

from the Salish Sea Marine Survival Project. We'd also like to acknowledge Z. Zhu, J. Schmerfeld, and S. Covington for their financial and logistical support. This research was funded by the Washington State Estuary and Salmon Restoration Program (ESRP Project #13-1583P) with a grant awarded to the USGS Western Ecological Research Center. Additional science support came from the Salish Sea Marine Survival Program, WERC program funds, the USGS Ecosystem Mission Area, the USGS Biologic Carbon Sequestration Program, the USFWS Coastal Program, and several USGS internship programs (Students in Support of Native American Relations, National Association of Geoscience Teachers, and Youth and Education in Science). Graduate student author M. Davis was supported by an American Dissertation Fellowship through the American Association of University Women. Government disclaimer: any use of trade, firm, or product names is for descriptive purposes only and does not imply endorsement by the U.S. Government.

References

Armstrong JB, Schindler DE (2013) Going with the flow: spatial distributions of juvenile coho salmon track an annually shifting mosaic of water temperature. Ecosystems 16:1429–1441

Ballanti L, Byrd KB, Woo I, Ellings CS (2017) Remote sensing for wetland mapping and historical change detection at the Nisqually River Delta. Sustainability 9:1919

Balling S, Resh V (1991) Seasonal patterns in a San Francisco Bay, California salt-marsh arthropod community. Pan-Pacific Entomologist 67:138–144

Baptista J, Martinho F, Dolbeth M, Viegas I, Cabral H, Pardal M (2010) Effects of freshwater flow on the fish assemblage of the Mondego estuary (Portugal): comparison between drought and non-drought years. Marine and Freshwater Research 61:490–501

Barbier EB, Hacker SD, Kennedy C, Koch EW, Stier AC, Silliman BR (2011) The value of estuarine and coastal ecosystem services. Ecological Monographs 81:169–193

Beauchamp DA (2009) Bioenergetic ontogeny: linking climate and mass-specific feeding to life-cycle growth and survival of salmon. Pages 53–72 *in* Krueger CC, Zimmerman CE (eds.) American Fisheries Society Symposium 70, Bethesda, Maryland, USA

Beck MW, Heck KL Jr., Able KW, Childers DL, Eggleston DB, Gillanders BM, Halpern B, Hays CG, Hoshino K, Minello TJ, Orth RJ, Sheridan PF, Weinstein MP (2001) The identification, conservation, and management of estuarine and marine nurseries for fish and invertebrates. Bioscience 51:633–641

Belleveau LJ, Takekawa JY, Woo I, Turner KL, Barham JB, Takekawa JE, Ellings CS, Chin-Leo G (2015) Vegetation community response to tidal marsh restoration of a large river estuary. Northwest Science 89:136–147

Bottom DL, Jones KK (1990) Species composition, distribution, and invertebrate prey of fish assemblages in the Columbia River Estuary. Progress in Oceanography 25:243–270

Bottom DL, Jones KK, Cornwell TJ, Gray A, Simenstad CA (2005) Patterns of Chinook salmon migration and residency in the Salmon River estuary (Oregon). Estuarine, Coastal and Shelf Science 64:79–93

Brandt SB, Mason DM, Patrick EV (1992) Spatially-explicit models of fish growth rate. Fisheries 17:23–35

Broadmeadow SB, Jones JG, Langford TEL, Shaw PJ, Nisbet TR (2011) The influence of riparian shade on lowland stream water temperatures in southern England and their viability for brown trout. River Research and Applications 27:226–237

Budy P, Baker M, Dahle SK (2011) Predicting fish growth potential and identifying water quality constraints: a spatially-explicit bioenergetics approach. Environmental Management 48:691–709

Chisholm LA, Roff JC (1990) Size-weight relationships and biomass of tropical neritic copepods off Kingston, Jamaica. Marine Biology 106:71–77

Chittenden CM, Sweeting R, Neville CM, Young K, Galbraith M, Carmack E, Vagle S, Dempsey M, Eert J, Beamish RJ (2018) Estuarine and marine diets of out-migrating Chinook salmon smolts in relation to local zooplankton populations, including harmful blooms. Estuarine, Coastal and Shelf Science 200:335–348

Connelly KA, Gardner JR, Gamble MM, Chamberlin JW, Winans A, Keister J, Beauchamp DA (2018) Marine survival of Puget Sound Chinook: size-selective mortality growth

limitation and bioenergetics of sub-yearling Chinook salmon in Puget Sound, Washington. Final Technical Report for Long Live the Kings, LLTK-SSMSP-9.

Copeland BJ (1966) Effects of decreased river flow on estuarine ecology. Journal of the Water Pollution Control Federation 38:1831–1939

Craft C, Clough J, Ehman J, Joye S, Park R, Pennings S, Guo H, Machmuller M (2009) Forecasting the effects of accelerated sea-level rise on tidal marsh ecosystem services. Frontiers in Ecology and the Environment 7:73–78

Crozier LG, Hendry AP, Lawson PW, Quinn TP, Mantua NJ, Battin J, Shaw RG, Huey RB (2008) Potential responses to climate change in organisms with complex life histories: evolution and plasticity in Pacific salmon. Evolutionary Applications 1:252–270

Davis MJ, Ellings CS, Woo I, Hodgson S, Larsen K, Nakai G (2018*b*) Gauging resource exploitation by juvenile Chinook salmon (*Oncorhynchus tshawytscha*) in restoring estuarine habitat. Restoration Ecology 26:976-986

Davis MJ, Woo I, Ellings CS, Beauchamp DA, Nakai G, De La Cruz SEW (2018*a*) Integrated diet analyses reveal contrasting trophic niches for wild and hatchery juvenile salmon in a large river delta. Transactions of the American Fisheries Society 147:818–841

Davis MJ, Woo I, Ellings CS, Hodgson S, Beauchamp DA, Nakai G, De La Cruz SEW (2019) Freshwater tidal forests and estuarine wetlands may confer early-life growth advantages for delta-rearing Chinook salmon. Transactions of the American Fisheries Society DOI:101002/tafs.10134

DeAngelis DL, Gross LJ (1992) Individual-based models and approaches in ecology: concepts and models. Chapman & Hall, London, United Kingdom

De'ath G (2002) Multivariate regression trees: a new technique for modeling species-environment relationships. Ecology 83:1105–1117

DeConto RM, Pollard D (2016) Contribution of Antarctica to past and future sea-level rise. Nature 531:591–597

Durant JM, Hjermann DO, Ottersen G, Stenseth NC (2007) Climate and the match or mismatch between predator requirements and resource availability. Climate Research 33:271–283

Ellings CS, Davis MJ, Grossman EE, Woo I, Hodgson S, Turner KL, Nakai G, Takekawa JE, Takekawa JY. Changes in habitat availability for outmigrating juvenile salmon (*Oncorhynchus* spp.) following estuary restoration. Restoration Ecology 24:415–427

Farley EV Jr., Trudel M (2009) Growth rate potential of juvenile sockeye salmon in warmer and cooler years on the Eastern Bering Sea Shelf. Journal of Marine Biology 2009:640215

Ferrier S, Guisan A (2006) Spatial modelling of biodiversity at the community level. Journal of Applied Ecology 43:393–404

FitzGerald DM, Fenster MS, Argow BA, Buynevich IV (2008) Coastal impacts due to sea-level rise. Annual Review of Earth and Planetary Sciences 36:601–647

Frankson R, Kunkel K, Champion S, Easterling D, Stevens L, Bumbaco K, Bond N, Casola J, Sweet W (2017) Washington State Climate Summary. NOAA Technical Report NESDIS 141-WA

Guisan A, Weiss SB, Weiss AD (1999) GLM versus CCA spatial modeling of plant species distribution. Plant Ecology 143:107–122

Harley CDG, Hughes AR, Hultgren KM, Miner BG, Sorte CJB, Thornber CS, Rodriguez LF, Tomanek L, Williams SL (2006) The impacts of climate change in coastal marine systems. Ecology Letters 9:228–241

Harvey BC, Railsback SF (2009) Exploring the persistence of stream-dwelling trout populations under alternative real-world turbidity regimes with an individual-based model. Transactions of the American Fisheries Society 138:348–360

Haskell CA, Beauchamp DA, Bollens SM (2017) Linking functional response and bioenergetics to estimate juvenile salmon growth in a reservoir food web. PLoS One 12:e0185933

Healey MC (1982) Juvenile Pacific salmon in estuaries: the life support system. Estuarine Comparisons. Proceedings of the Sixth Biennial International Estuarine Research Conference, Gleneden Beach, Oregon, USA, pp. 315–341

Healey MC (1991) Life history of Chinook salmon (*Oncorhynchus tshawytscha*). Pages 311–394 *in* Groot C, Margolis L (eds.) Pacific salmon life histories. University of British Columbia Press, Vancouver, Canada.

Hering DK, Bottom DL, Prentice EF, Jones KK, Fleming IA (2010) Tidal movements and residency of subyearling Chinook salmon (*Oncorhynchus tshawytscha*) in an Oregon salt marsh channel. Canadian Journal of Fisheries and Aquatic Sciences 67:524–533

Kirwan ML, Megonigal JP (2013) Tidal wetland stability in the face of human impacts and sea-level rise. Nature 504:53–60

Kirwan ML, Guntenspergen GR, D'Alpaos A, Morris JT, Mudd SM, Temmerman S (2010) Limits on the adaptability of coastal marshes to rising sea level. Geophysical Research Letters 37:L23401

Kitchell JF, Stewart DJ, Weininger D (1977) Applications of a bioenergetics model to yellow perch (*Perca flavescens*) and walleye (*Stizostedion vitreum vitreum*). Journal of the Fisheries Research Board of Canada 34:1910–1921

Koski ML, Johnson BM (2002) Functional response of kokanee salmon (*Oncorhynchus nerka*) to *Daphnia* at different light levels. Canadian Journal of Fisheries and Aquatic Sciences 59:707–716

Logerwell EA, Mantua N, Lawson PW, Francis RC, Agostini VN (2003) Tracking environmental processes in the coastal zone for understanding and predicting Oregon coho (*Oncorhynchus kisutch*) marine survival. Fisheries Oceanography 12:554–568

Lotze HK, Lenihan HS, Bourque BJ, Bradbury RH, Cooke RG, Kay MC, Kidwell SM, Kirby MX, Peterson CH, Jackson JBC (2006) Depletion, degradation, and recovery potential of estuaries and coastal seas. Science 312:1806–1809

Mackay CF, Cyrus DP (2001) Is freshwater quality adequately defined by physico-chemical components? Results from two drought-affected estuaries on the east coast of South Africa. Marine and Freshwater Research 52:267–282

Martin DJ, Wasserman LJ, Dale VH (1986) Influence of riparian vegetation on posteruption survival of coho salmon fingerlings on the west-side streams of Mount St. Helens, Washington. North American Journal of Fisheries Management 6:1–8

Mason DM, Brandt SB (1996) Effects of spatial scale and foraging efficiency on the predictions made by spatially-explicit models of fish growth rate potential. Environmental Biology of Fishes 45:283–298

Mcleod E, Poulder B, Hinkel J, Reyes E, Salm R (2010) Sea-level rise impact models and environmental conservation: a review of models and their applications. Ocean and Coastal Management 52:507–517

Meyer DL, Posey MH (2014) Influence of salt marsh size and landscape setting on salt marsh nekton populations. Estuaries and Coasts 37:548–560

National Research Council (2012) Sea-level rise for the coasts of California, Oregon, and Washington: past, present, and future. National Research Council of the National Academies. National Academies Press, Washington, D.C., USA

Neuheimer AB, thresher RE, Lyle JM, Semmens JM (2011) Tolerance limit for fish growth exceeded by warming waters. Nature Climate Change 1:110–113

Olden JD, Jackson DA (2002) A comparison of statistical approaches for modelling fish species distributions. Freshwater Biology 47:1–20

Perry AL, Low PJ, Ellis JR, Reynods JD (2005) Climate change and distribution shifts in marine fishes. Science 307:1912–1915

Plumb J, Moffitt CM (2015) Re-estimating temperature-dependent consumption parameters in bioenergetics models for juvenile Chinook salmon. Transactions of the American Fisheries Society 144:323–330

Pörtner HO, Peck MA (2010) Climate change effects on fishes and fisheries: towards a cause-and-effect understanding. Journal of Fish Biology 77:1745–1779

Railsback SF, Harvey BC (2002) Analysis of habitat-selection rules using an individual-based model. Ecology 83:1817–1830

Railsback SF, Stauffer HB, Harvey BC (2003) What can habitat preference tell us? tests using a virtual trout population. Ecological Applications 13:1580–1594

Ray GC (2005) Connectivities of estuarine fishes to the coastal realm. Estuarine, Coastal and Shelf Science 64:18–32

Romanuk TN, Levings CD (2003) Associations between arthropods and the supralittoral ecotone: dependence of aquatic and terrestrial taxa on riparian vegetation. Environmental Entomology 32:1343–1353

Rosenfeld JS, Leiter T, Lindner G, Rothman L (2005) Food abundance and fish density alters habitat selection, growth, and habitat suitability curves for juvenile coho salmon (*Oncorhynchus kisutch*). Canadian Journal of Fisheries and Aquatic Sciences 62:1691–1701

Rubin SP, Hayes MC, Grossman EE (2018) Juvenile Chinook salmon and forage fish use of eelgrass habitats in a diked and channelized Puget Sound river delta. Marine and Coastal Fisheries 10:435–451

Schabetsberger R, Morgan CA, Brodeur RD, Potts CL, Peterson WT, Emmett RL (2003) Prey selectivity and diel feeding chronology of juvenile Chinook (*Oncorhynchus tshawytscha*) and coho (*O. kisutch*) salmon in the Columbia River plume. Fisheries Oceanography 12:523–540

Schindler DE, Hilborn R, Chasco B, Boatright CP, Quinn TP, Rogers LA, Webster MS (2010) Population diversity and the portfolio effect in an exploited species. Nature 465:609–612

Schindler DE, Armstrong JB, Reed TE (2015) The portfolio concept in ecology and evolution. Frontiers in Ecology and the Environment 13:257–263

Sheaves M (2009) Consequences of ecological connectivity: the coastal ecosystem mosaic. Marine Ecology Progress Series 391:107–115

Sheaves M, Baker R, Nagelkerken I, Connolly RM (2015) True value of estuarine and coastal nurseries for fish: incorporating complexity and dynamics. Estuaries and Coasts 38:401–414

Simenstad CA, Fresh KL, Salo EO (1982). The role of Puget Sound and Washington coastal estuaries in the life history of Pacific salmon: and unappreciated function. Estuarine Comparisons. Proceedings of the Sixth Biennial International Estuarine Research Conference, Gleneden Beach, Oregon, USA, pp. 343–364

Simenstad CA, Hood WG, Thom RM, Levy DA, Bottom DL (2002) Landscape structure and scale constraints on restoring estuarine wetlands for pacific coast juvenile fishes. pp. 597–630 in Weinstein MP, Kreeger DA (eds.) Concepts and Controversies in Tidal Marsh Ecology. Springer, Dordrecht, Netherlands

Sommer TR, Nobriga ML, Harrell WC, Batham W, Kimmerer WJ (2001) Floodplain rearing of juvenile Chinook salmon: evidence of enhanced growth and survival. Canadian Journal of Fisheries and Aquatic Sciences 58:325–333

Stewart DJ, Ibarra M (1991) Predation and production by salmonine fishes in Lake Michigan, 1978–88. Canadian Journal of Fisheries and Aquatic Sciences 48:909–922

Thorne K, MacDonald G, Guntenspergen G, Ambrose R, Buffington K, Dugger B, Freeman C, Janousek C, Brown L, Rosencranz J, Holmquist J, Smol J, Hargan K, Takekawa J (2018) U.S. Pacific coastal wetland resilience and vulnerability to sea-level rise. Science Advances 4:eaao3270

Thornton KW, Lessem AS (1978) A temperature algorithm for modifying biological rates. Transactions of the American Fisheries Society 107:284–287

Thorpe JE (1994) Salmonid fishes and the estuarine environment. Estuaries 17:76–93

Thrush SF, Hewitt JE, Cummings VJ, Ellis JI, Hatton C, Lohrer A, Norkko A (2004) Muddy waters: elevating sediment input to coastal and estuarine habitats. Frontiers in Ecology and the Environment 2:299–306

Torio DD, Chmura GL (2015) Impacts of sea level rise on marsh as fish habitat. Estuaries and Coasts 38:1288–1303

Trudel M, Welch DW (2005) Modeling the oxygen consumption rates in Pacific salmon and steelhead: model development. Transactions of the American Fisheries Society 134:1542–1561

Vinagre C, Salgado J, Cabral HN, Costa MJ (2011) Food web structure and habitat connectivity in fish estuarine nurseries—impact of river flow. Estuaries and Coasts 34:663–674

Ware DM (1978) Bioenergetics of pelagic fish: theoretical change in swimming speed and ration with body size. Journal of the Fisheries Research Board Canada 35:220–228

Woo I, Davis MJ, Ellings CS, Nakai G, Takekawa JY, De La Cruz SEW (2018) Enhanced invertebrate prey production following estuarine restoration supports foraging for multiple species of juvenile salmonids (*Oncorhynchus* spp.). Restoration Ecology 26:964–975

Yates PM, Heupel MR, Tobin AJ, Simpfendorfer CA (2012) Diversity in young shark habitats provides the potential for portfolio effects. Marine Ecology Progress Series 458:269–281

Tables

Table 5.1. We tested the effect of ten climate change scenarios on the growth rate potential (GRP) of available delta habitat, individual GRP, and juvenile salmon weight through time. The first two scenarios used a bare earth DEM flown in 2011 to classify the habitat mosaic, while sea-level rise (SLR) scenarios 3-10 used marsh accretion model output from Chapter 4. For scenarios 2, 5, 6, 9, and 10, air temperature was increased by 5°C to account for high emissions climate change scenarios for Washington state in the year 2100 (Frankson et al. 2017).

Scenario	Present Day	Moderate SLR	High SLR	Doubled Sediment	+5°C (high emissions)
1	X				
2	X				X
3		X			
4		X		X	
5		X			X
6		X		X	X
7			X		
8			X	X	
9			X		X
10			X	X	X

Table 5.2. Composition of the Nisqually River Delta habitat mosaic for each sea-level rise (SLR) scenario, including present day conditions, moderate SLR (0.62 m by 2100), high SLR (1.35 m by 2100), moderate SLR with the addition of twice the current amount of suspended sediment inputs from the Nisqually River, and high SLR with twice the current amount of suspended sediment (Chapter 4). The areal extent of each habitat type was calculated for each scenario in 2050 and 2100.

Scenario		Subtidal (km^2)	Eelgrass (km^2)	Mudflat (km^2)	Low Marsh (km^2)	High Marsh (km^2)	Brackish Marsh (km^2)	Upland Tidal Forest (km^2)
Present Day		7.69	1.13	2.02	2.92	2.50	0.87	0.71
Moderate SLR								
	2050	7.32	1.60	1.81	2.93	2.73	0.87	0.59
	2100	7.27	2.19	2.01	2.44	2.52	1.00	0.43
High SLR								
	2050	7.44	1.87	2.04	2.77	2.35	0.96	0.42
	2100	8.97	1.21	3.80	1.06	1.65	0.96	0.21
Moderate SLR + Sediment								
	2050	7.45	1.40	1.52	2.65	2.59	0.77	1.47
	2100	6.27	2.66	1.41	2.21	3.19	0.91	1.20
High SLR + Sediment								
	2050	6.89	2.13	1.66	2.95	2.67	0.91	0.65
	2100	6.81	2.93	2.79	1.41	2.61	1.04	0.25

Table 5.3. Mean ± SD delta-wide prey energy density (top, J g^{-1}) and standing biomass (mg m^{-3}) for each scenario in each month.

Scanario	March	April	May	June	July	Total
Energy Density (J g^{-1})						
Present Day	4158 ± 52	3914 ± 60	3784 ± 32	3715 ± 29	3871 ± 36	3889 ± 158
Moderate SLR						
2050	4150 ± 52	3905 ± 60	3778 ± 31	3711 ± 29	3864 ± 35	3883 ± 156
2100	4136 ± 56	3879 ± 60	3762 ± 31	3683 ± 26	3820 ± 33	3856 ± 161
High SLR						
2050	4138 ± 55	3881 ± 62	3752 ± 32	3677 ± 28	3827 ± 35	3856 ± 164
2100	4082 ± 63	3794 ± 67	3668 ± 37	3558 ± 27	3693 ± 33	3760 ± 185
Moderate SLR + Sediment						
2050	4219 ± 48	3995 ± 53	3887 ± 29	3814 ± 24	3941 ± 30	3972 ± 143
2100	4207 ± 48	3989 ± 49	3905 ± 26	3828 ± 22	3940 ± 27	3974 ± 133
High SLR + Sediment						
2050	4164 ± 52	3922 ± 59	3799 ± 30	3731 ± 28	3878 ± 34	3900 ± 154
2100	4118 ± 57	3858 ± 59	3758 ± 31	3662 ± 25	3786 ± 30	3837 ± 160
Biomass (mg m^{-3})						
Present Day	31.05 ± 0.98	37.63 ± 3.65	51.26 ± 2.44	47.22 ± 1.32	52.39 ± 1.36	43.93 ± 8.58
Moderate SLR						
2050	32.14 ± 0.94	38.75 ± 3.90	54.17 ± 2.83	52.49 ± 0.78	54.10 ± 0.50	46.34 ± 9.44
2100	30.14 ± 0.75	36.09 ± 4.02	53.40 ± 3.60	55.42 ± 1.08	50.32 ± 1.09	45.07 ± 10.40
High SLR						
2050	31.60 ± 0.78	37.64 ± 3.98	54.10 ± 3.14	53.60 ± 0.67	53.09 ± 0.01	46.01 ± 9.79
2100	19.28 ± 0.71	24.16 ± 3.01	36.54 ± 2.40	36.08 ± 1.29	30.86 ± 1.06	29.37 ± 7.02
Moderate SLR + Sediment						
2050	29.35 ± 1.00	36.03 ± 3.66	50.06 ± 2.53	47.89 ± 0.83	49.47 ± 0.50	42.57 ± 8.64
2100	29.48 ± 0.81	35.79 ± 4.11	54.19 ± 4.36	59.86 ± 2.08	48.82 ± 2.52	45.60 ± 11.74
High SLR + Sediment						
2050	33.33 ± 0.80	39.62 ± 4.17	57.12 ± 3.45	57.81 ± 0.64	56.02 ± 0.32	48.78 ± 10.56
2100	25.45 ± 0.53	30.43 ± 3.99	49.58 ± 5.04	57.69 ± 3.15	40.92 ± 3.86	40.77 ± 12.40

Table 5.4. Final juvenile salmon weight (g) for the Nisqually River Delta under each climate change scenario. Bioenergetics model simulations were run on an hourly time step from March 1 through July 31. Output marked with an asterisk (*) is representative of present day (2011–2015) conditions.

	Final Weight (g)	
Scenario	2050	2100
1: Present Day	*14.25	
2: Present Day +5°C	*14.96	
3: Moderate SLR	13.31	11.88
4: Moderate SLR + Sediment	13.16	10.47
5: Moderate SLR +5°C	13.95	12.32
6: Moderate SLR + Sediment +5°C	13.79	10.66
7: High SLR	12.91	9.87
8: High SLR + Sediment	12.71	9.33
9: High SLR +5°C	13.53	9.95
10: High SLR + Sediment +5°C	13.24	9.35

Figures

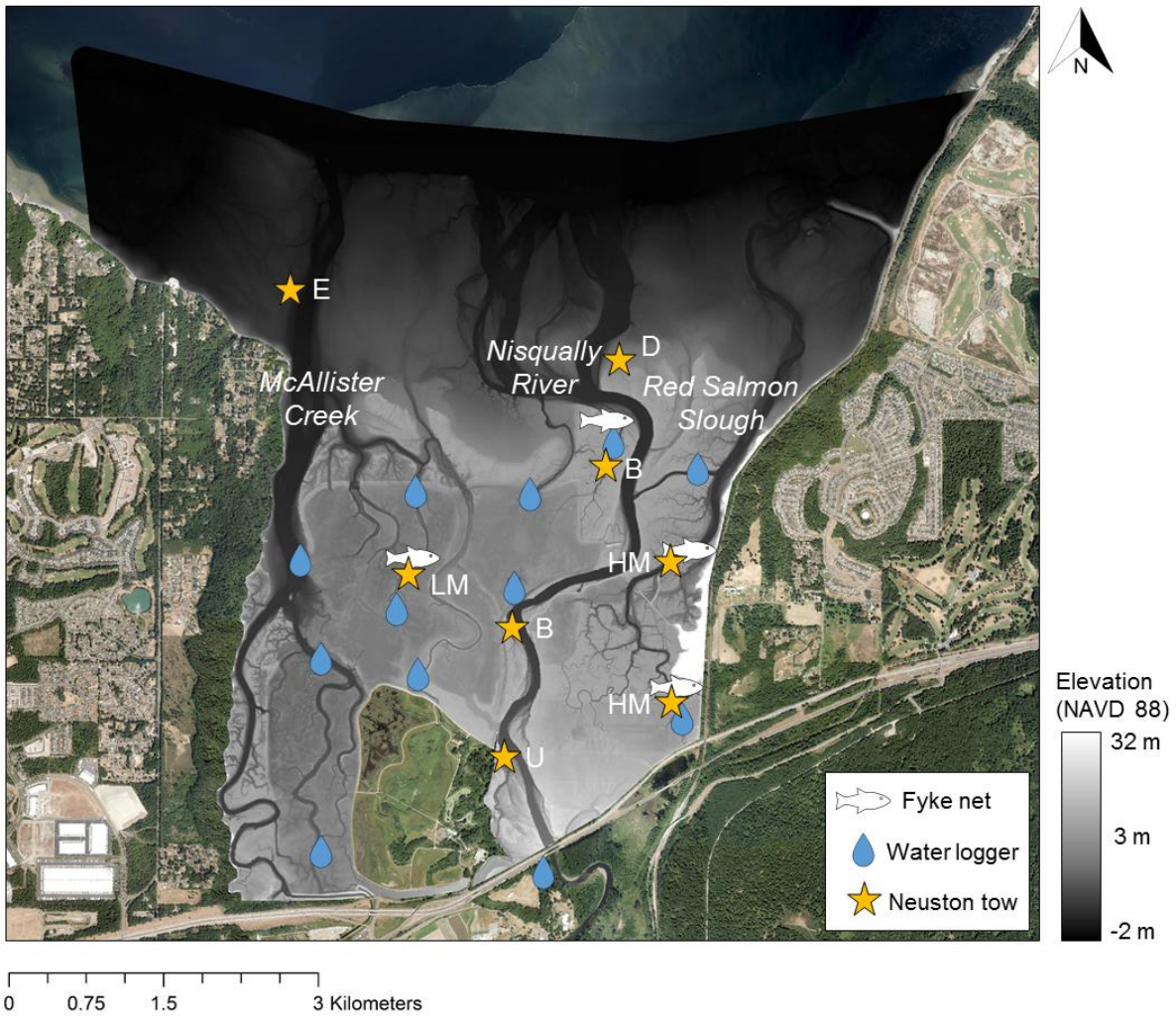

Figure 5.1. Map of sampling locations in the Nisqually River Delta, Washington, USA. The grayscale DEM shows the spatial extent of the study area, for which growth was modeled for juvenile salmon from March 1 through July 31. Fish symbols represent fyke netting locations, where subyearling Chinook salmon were sampled in 2010 and 2011 for otolith analysis. Blue droplets represent Solinst® data loggers that collected continuous water temperature measurements between 2010 and 2015. Orange stars mark the location of neuston tows in upland tidal forested (U), brackish marsh (B), high salt marsh (HM), low salt marsh (LM), delta mudflat (D), and eelgrass (E) habitats. Not pictured are the locations of bongo net tows to sample aquatic prey in subtidal areas at Solo Point (7 km to the northeast) and at Dana Passage (12 km to the northwest).

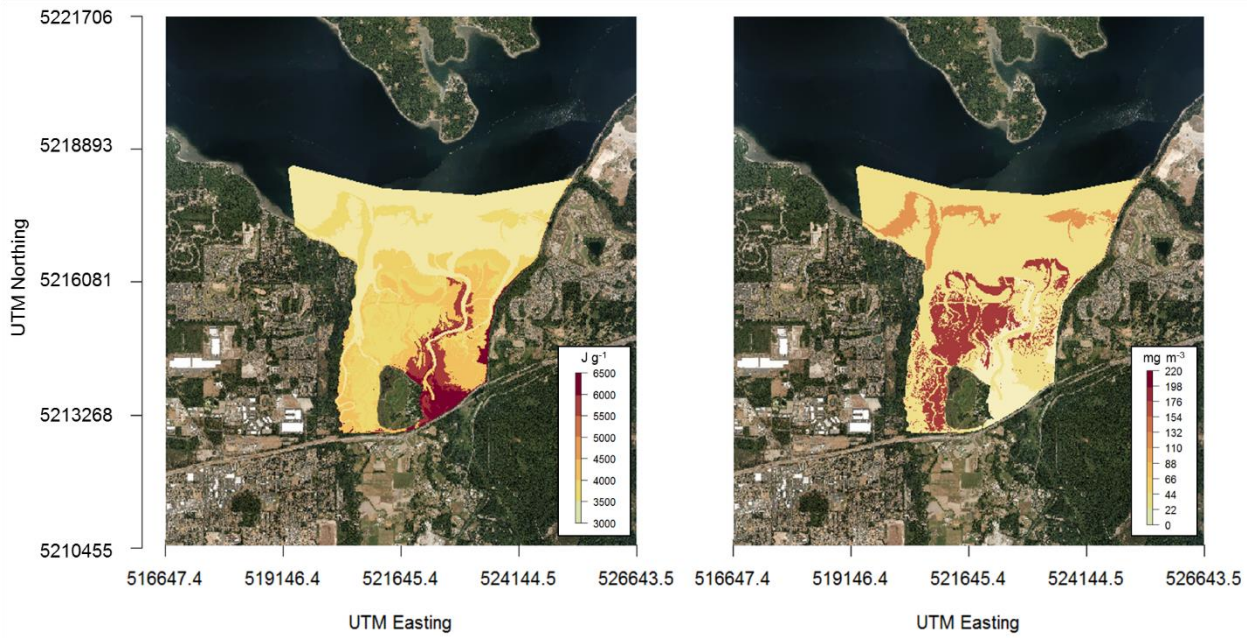

Figure 5.2. Example of spatially explicit prey inputs from the month of May (DOY=135) under present day conditions. Prey energy density (J g^{-1}) is shown on the left and standing biomass (mg m^{-3}) is shown on the right.

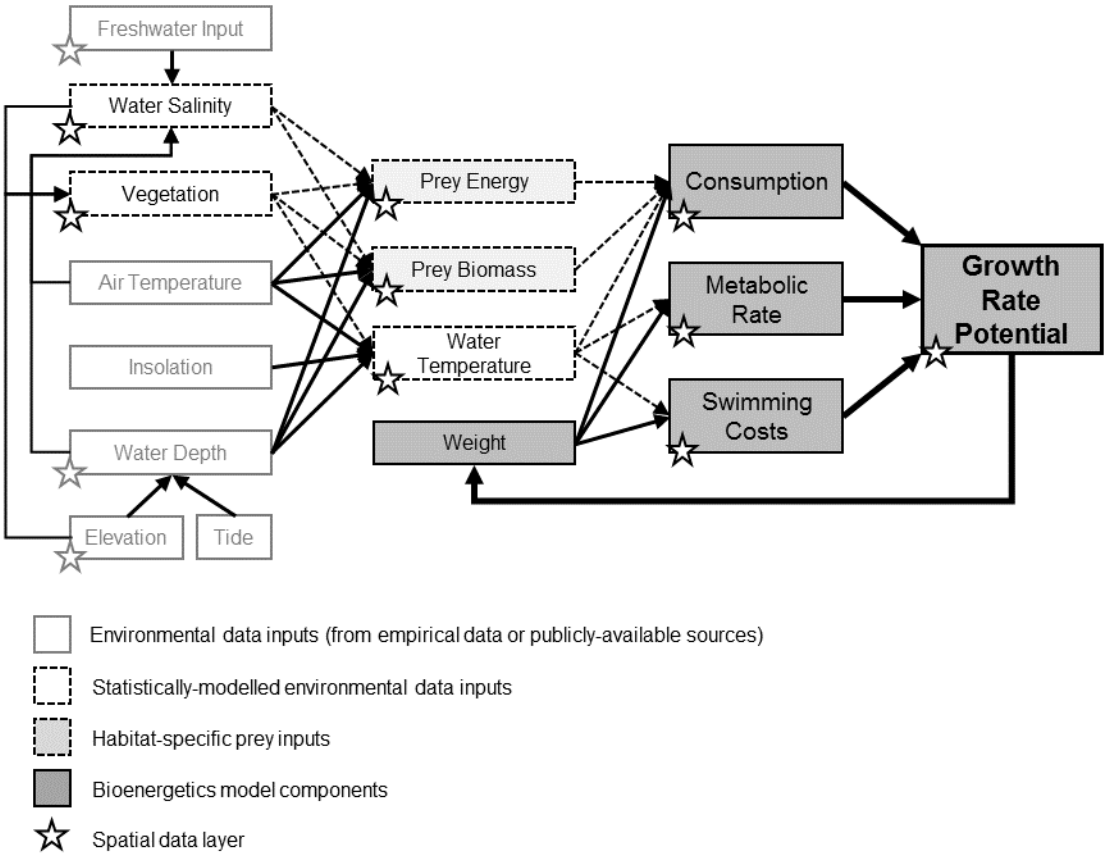

Figure 5.3. Conceptual diagram showing the hierarchical structure of a spatially explicit bioenergetics model of juvenile salmon growth rate potential.

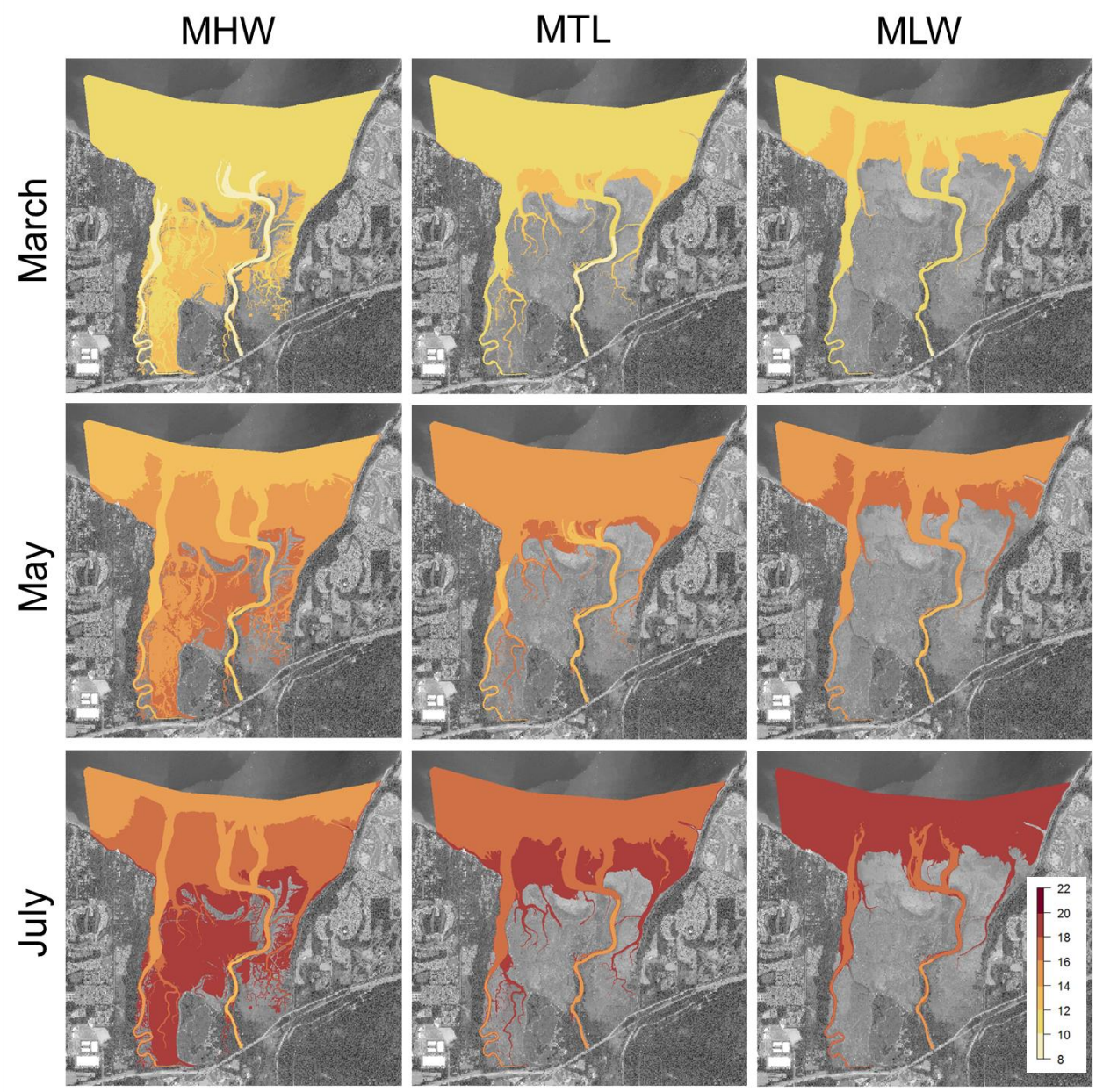

Figure 5.4. Predicted mid-day (1300) water temperatures (°C) for the Nisqually River Delta in March (DOY = 74), May (DOY = 135), and July (DOY = 196). Columns display temperature outputs for the delta at mean high water (MHW = 2.82 m NAVD88), mean tidal level (MTL = 1.34 m NAVD88), and mean low water (MLW = -0.11 m NAVD88).

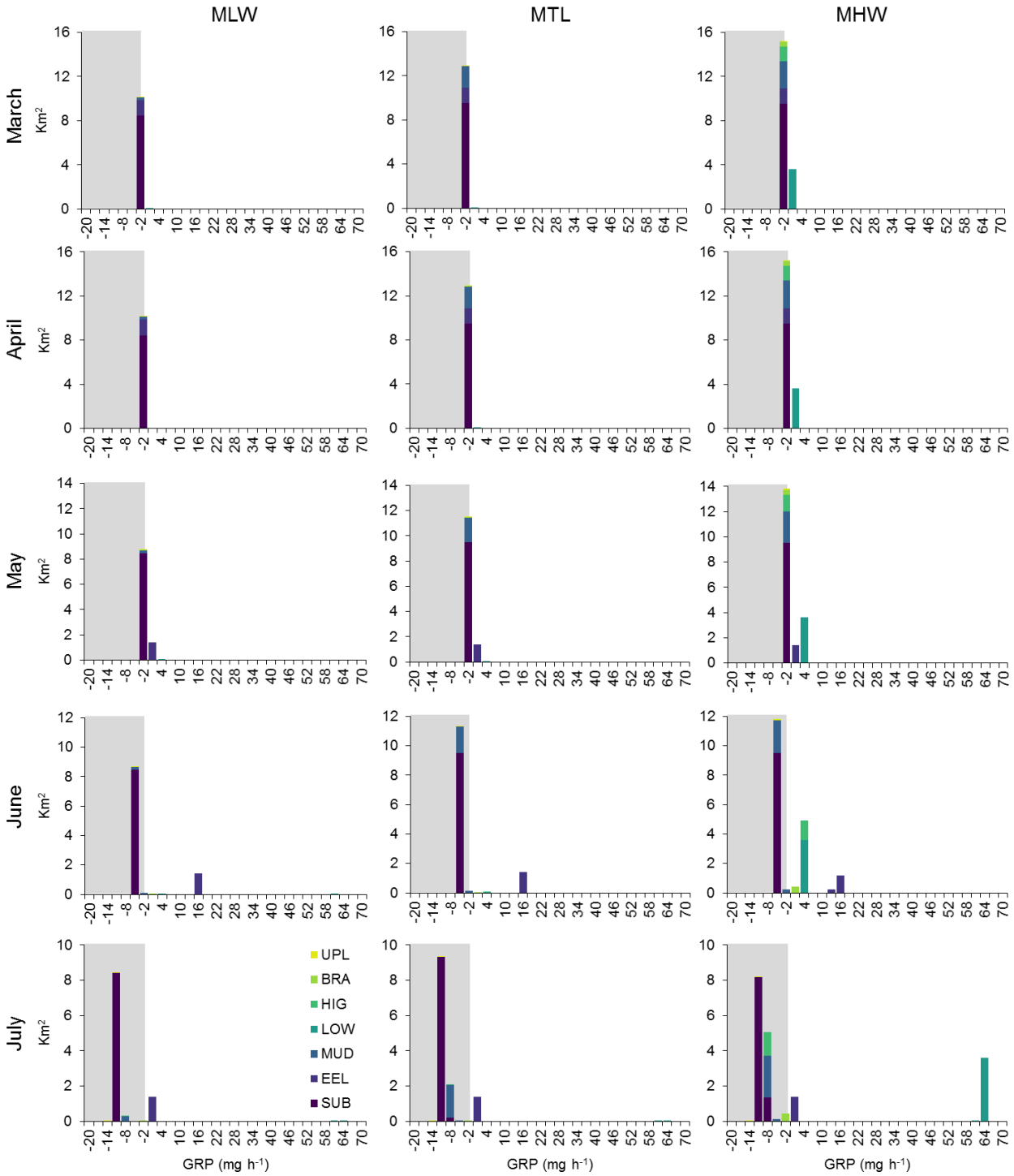

Figure 5.5. Areal distribution (km^2) of predicted delta growth rate potential (GRP; mg h^{-1}) by month, tide, and accessible habitat (UPL = upland tidal forested, BRA = brackish marsh, HIG = high-elevation salt marsh, LOW = low-elevation salt marsh, MUD = delta mudflat, EEL = eelgrass, SUB = subtidal). The gray box indicates negative delta GRP values.

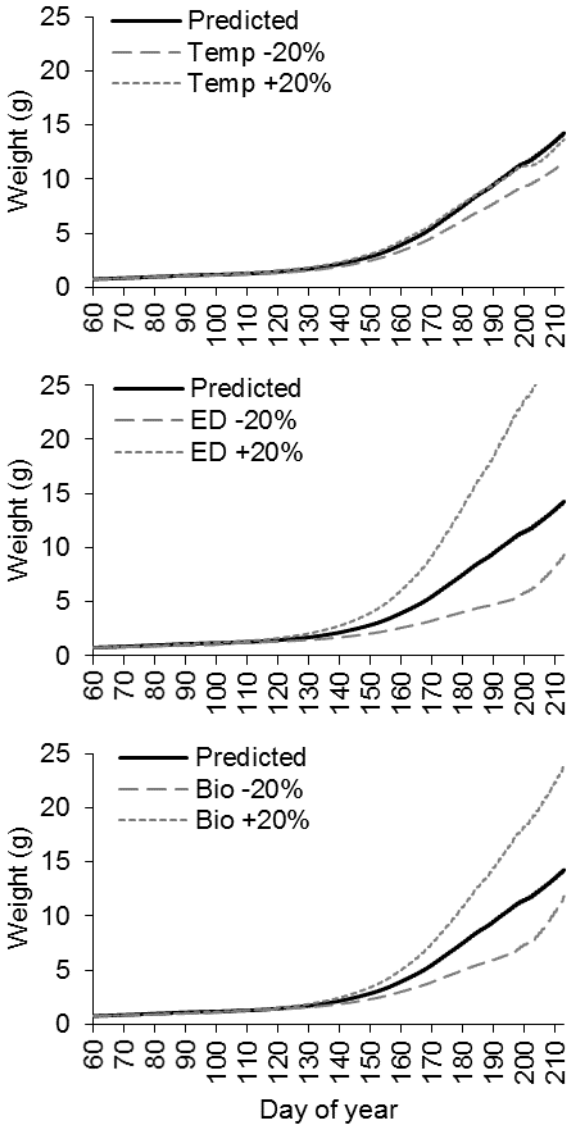

Figure 5.6. Spatially explicit bioenergetics model output from a longitudinal sensitivity analysis where water temperature (Temp), prey energy density (ED), and standing biomass (Bio) were varied by ± 20%. Modeled juvenile salmon weight through time is shown for March 1 (DOY 60)–July 31 (DOY 212).

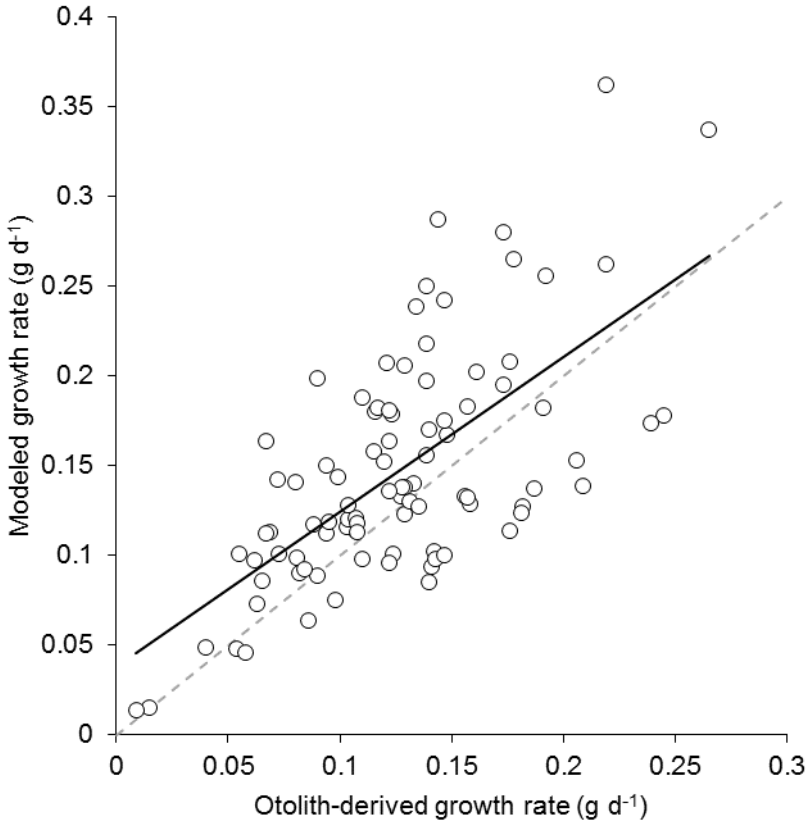

Figure 5.7. Output from a model corroboration procedure comparing otolith-derived daily growth rates to model output from the same period of growth for individual juvenile Chinook salmon captured in 2010 and 2011. The black line represents the modeled fit between observed and predicted growth rates (R^2 = 0.44). The dashed gray line represents an ideal 1:1 relationship between observed and predicted values for comparison.

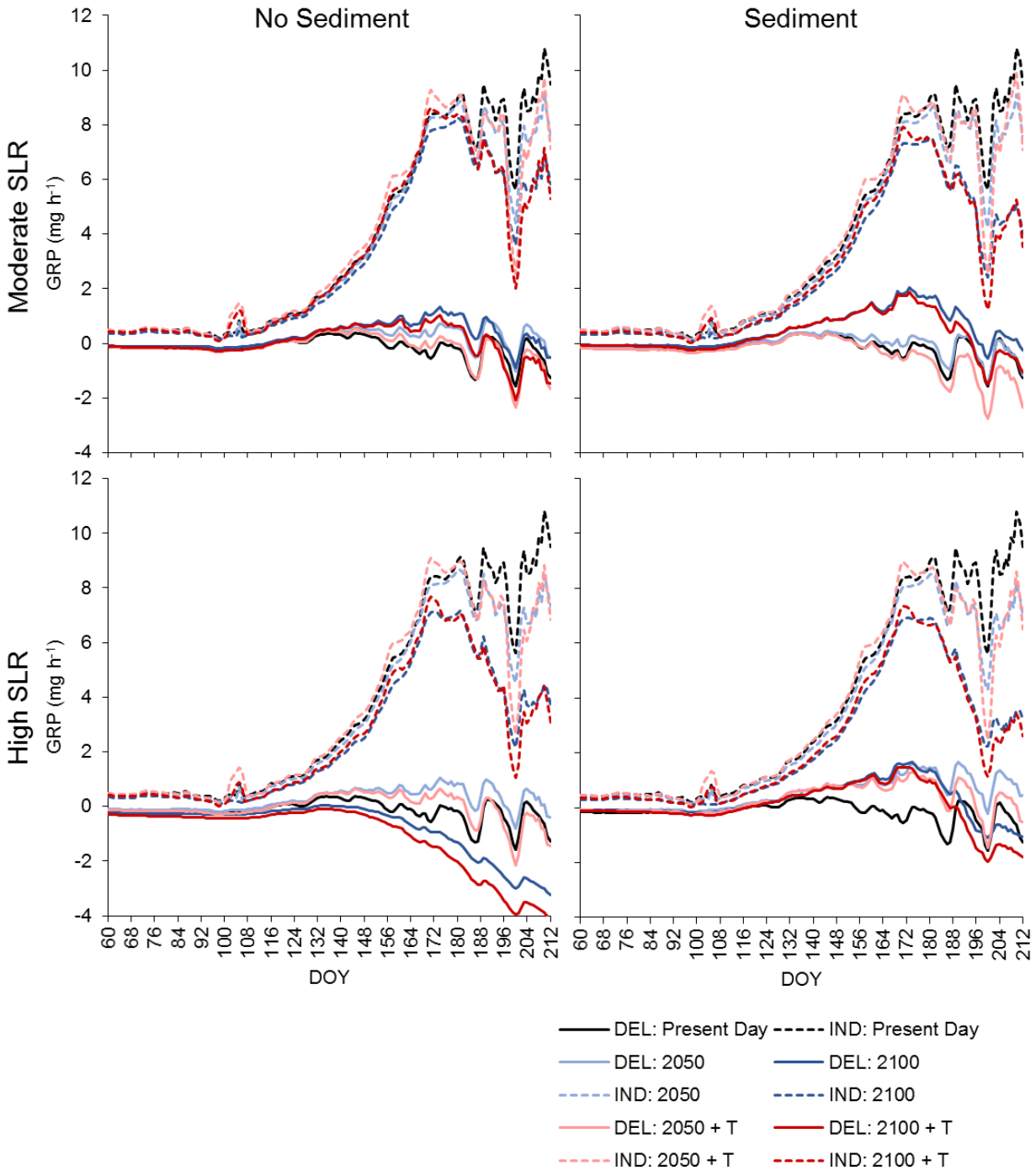

Figure 5.8. Modeled average daily delta (DEL; all available habitat) and individual (IND) GRP values for the Nisqually River Delta under each climate change scenario. Bioenergetics simulations were run on an hourly time step from March 1 (DOY = 60) through July 31 (DOY = 212).

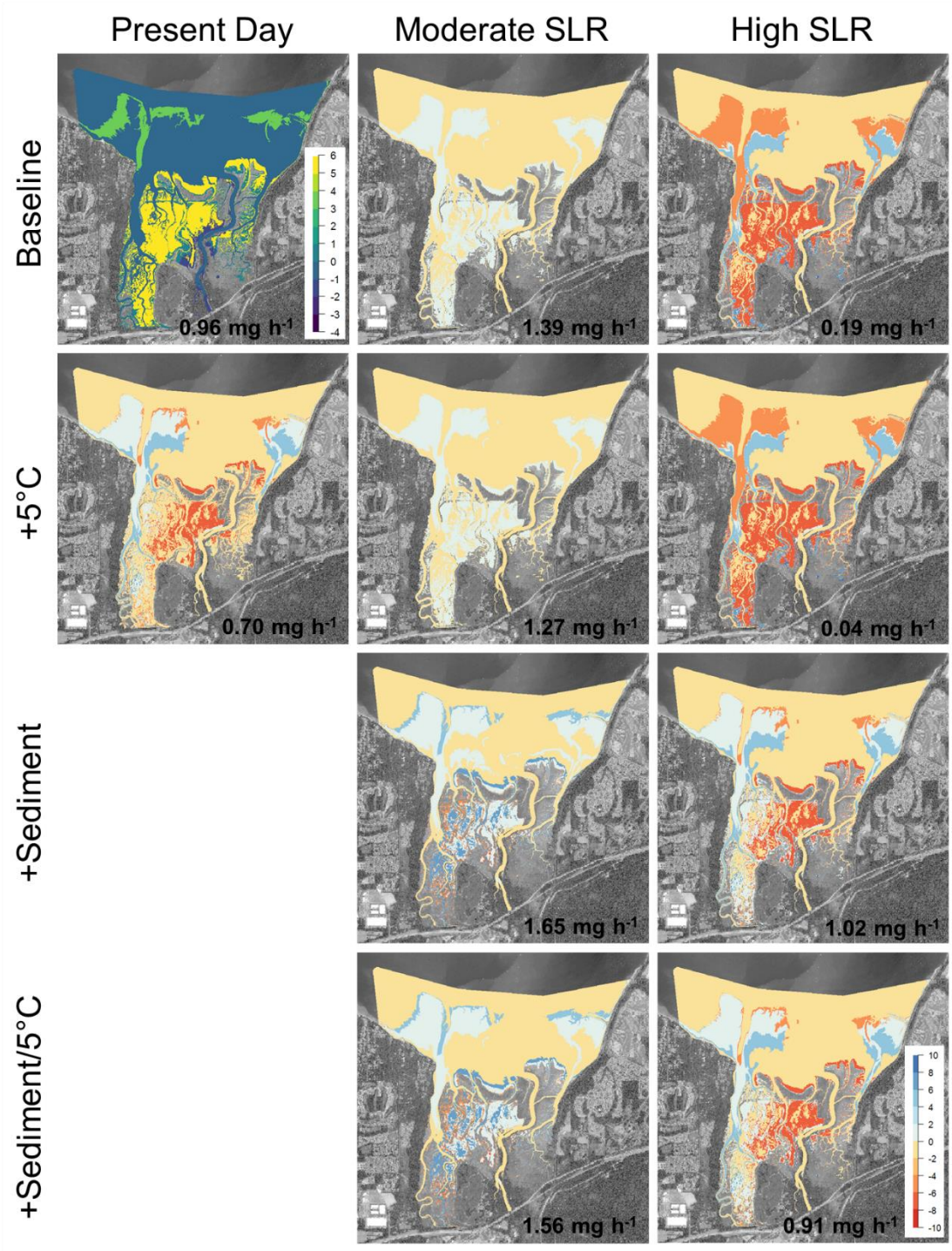

Figure 5.9. An example of predicted baseline delta GRP values for inundated areas of the Nisqually River Delta in May at MHW (top left corner) and the magnitude of change for each climate change scenario (mg h^{-1}). Bolded values in the bottom right corner indicate average delta GRP values for all accessible habitats.

Appendix A: Detailed description of hydrological model

Data collection

We used a combination of publicly-available datasets and monitoring data to build and calibrate a hydrological model of water depth and temperature (Table A5.1), which were determinants of habitat accessibility and growth rate potential in the spatially explicit bioenergetics model. We downloaded hourly, land-based weather data for 2010–2015 from the National Climactic Data Center (NCDC; https://www.ncdc.noaa.gov) for the Olympia, Washington (#WBAN:24227) weather station. We obtained hourly and daily insolation data for 2010–2015 from the Washington State University database (http://www.weather.wsu.edu). We also used Maptech® Tides & Currents software (Maptech, New Bedford, Massachusetts, USA) to download predicted hourly tidal levels (m NAVD88) for the Nisqually Reach (ID: 9446828) tide gauge.

To calibrate the temperature model, we used water level (m) and temperature (˚C) data from twelve Solinst® LTC data loggers (Georgetown, Ontario, Canada) positioned throughout a range of habitat types in the Nisqually River Delta (Fig. A5.1; Table A5.2). Loggers were deployed at fixed locations from 2010–2015. We installed each logger in a protective PVC casing in the middle of an established channel with the sensor positioned about 15 cm from the channel bottom. Data loggers measured hydrological variables continuously at 6, 12, or 15-minute intervals, and were downloaded in the field seasonally to collect uninterrupted data.

After collection, we quality checked the data to ensure that values were within a biologically valid range ($-15^{\circ}C < T < 50^{\circ}C$). Any temperature outliers were excluded from analysis. Water level data were checked for outliers and barometrically compensated using atmospheric pressure (kPA) from a terrestrial Solinst® Barologger Edge device that was installed nearby. For model calibration purposes, we only included data that were collected from the top of the hour. This allowed us to easily pair each water temperature data point with the corresponding, hourly air temperature and insolation data.

We also included path distance from the Nisqually River main stem and adjacent vegetative biomass as predictor variables in the modeling exercise. Path distance was calculated using the “path distance” function in ArcGIS 10.3 software (ESRI Inc., Redlands, California, USA) with a 3 × 3 m bare earth digital elevation model (DEM) produced using LIDAR in 2011 (Watershed Sciences Inc., Portland, Oregon, USA). Adjacent vegetative biomass was estimated

for each logger using annual quadrat surveys, during which the number and type of plant species, percent cover, maximum stem height, and stem density were recorded within a 0.5 × 0.5 m quadrat positioned 0, 20, or 40 m from the edge of the channel. We calculated per-area biomass for each species *j* observed in a sampling quadrat using the equation $V_j = 0.04 n_j h_j$, where n_j is the species' extrapolated stem density per m^2 and h_j is its average stem height. This equation was based off literature values and observed height-biomass relationships for regionally prevalent marsh vegetation species such as *Carex lyngbyei*, *Distichlis spicata*, and *Salicornia pacifica* (USGS unpublished data).

Statistical model

We used a regression-based modeling framework similar to Wagner et al. (2011) to model the relationship between water temperature and air temperature. Because we were working with a tidally-influenced system in which channels dewatered frequently, we did not include an autoregressive parameter in our model (i.e., water temperature at *t-1*). We assumed that most of our predictor variables, including air temperature, would interact non-linearly with water temperature. To elucidate these non-linear relationships, we conducted a preliminary analysis using a generalized additive model (GAM; Reckhow & Quian 1994, Borsuk et al. 2001). Generalized additive models use a non-parametric smoothing function to characterize persistent patterns in the relationship between the response variable and each predictor variable. We used the "mgcv" package in R version 3.4.1 (R Core Development Team 2018) to run the GAM analyses, where the smoothing functions and partial residuals were visually assessed to determine each predictor variable's importance in determining hourly water temperature.

After using the GAM to identify the appropriate relationships between water temperature and the predictor variables, we used maximum likelihood estimation in R to conduct a model parameterization and selection procedure on a set of candidate non-linear models. These models included some combination of predictor variables, including air temperature (˚C), daily mean insolation (MJ m^{-2}), water depth (m), distance from the river main stem (m), and vegetative biomass (standardized from 0–1). We used a model selection procedure, whereby Akaike's Information Criterion (AIC), root-mean-square error (RMSE), and the Nash-Sutcliffe efficiency coefficient (NSE) were used to select the best-fit model and assess goodness of fit (Burnham &

Anderson 2002). For simplicity, we included a maximum of three interacting terms when parameterizing and testing candidate models.

To check that model output represented realistic values, we conducted a sensitivity analysis using latin hypercube sampling (LHS function in R package "pse"). We varied predictor variables over a range of uniformly distributed realistic values; -5–35˚C for air temperature, 0–8 m for water depth, 0–30 MJ m^{-2} for insolation, 0–1 for standardized vegetative biomass, and 0–2500 m for path distance to the Nisqually River. We produced three-dimensional surface plots for the estimated model output where parameter space was manipulated for two variables at a time. We also used a bootstrapping procedure to estimate prediction error and confidence intervals for the parameter values.

Model simulation inputs

Our aim in constructing and parameterizing the hydrological model was to simulate water depth and temperature throughout a typical out-migration season (March 1 – July 31) to use as inputs for the spatially explicit bioenergetics model. To do this, we needed standard, hourly inputs for air temperature, insolation, and tidal level. Air temperature was derived from the NCDC weather data. We averaged hourly temperature measurements across years (2010–2015) and converted them into a time series dataset in R with a frequency of 24 hours across 365 days. We then decomposed the air temperature time series into a daily trend, an hourly trend, and an associated error value. We smoothed the daily trend using a moving average window (order = 1,200). This smoothed dataset was added to the hourly trend to derive the baseline air temperature input for the model simulation (Fig. A5.2).

We calculated model inputs for insolation using time series decomposition as described above; however, because hourly data were recorded in W m^{-2} and daily data were recorded in MJ m^{-2}, we first had to convert hourly values to a standardized daily mean. We did this using the equation:

$$S_d = \frac{3600 * S_h}{1000000} \times d$$

where S_d is a standardized daily insolation estimate in MJ m^{-2}, 3600 is the number of seconds in an hour, S_h is the measured average insolation value in W m^{-2}, and d is the number of daylight hours for a given date. The resultant dataset was treated as described for air temperature, except

instead of adding daily and hourly trends, we multiplied them. The hourly trend was converted to a multiplier by adding the minimum value and dividing by 8. This resulted in total insolation values ranging between 0 and 30 MJ m^{-2} (Fig. A5.2).

For water level input, we used hourly predicted tidal level data from 2014. To ensure these data were representative of true conditions, we compared the predicted dataset to measured values from a data logger in an unaltered, historic marsh channel (Reference; Table A5.2). A visual comparison using linear regression showed that the predicted and measured values overlapped completely ($R^2 = 0.98$), thus confirming that the tidal predictions were appropriate for use in our model simulation.

Spatial application

We used the best-fit candidate model for water temperature to predict environmental conditions throughout the delta based on the air temperature, insolation, and tidal level inputs. For spatial coverages, we used bare earth DEMs for calculating water depth and a raster of vegetation biomass values estimated based on elevation and soil pore salinity (Chapter 4). The model was run iteratively for each hourly time step by applying the parameterized statistical model to the raster layers along with the air temperature, insolation, and tidal level inputs. In each hourly time step, water temperature was only calculated for cells that were inundated (depth > 0). To account for freshwater inputs, the Nisqually River and McAllister Creek were adjusted for river depth along land-to-sea gradient. This prevented model output from showing that they dewatered at low tide and, consequently, predicting incorrect water temperatures.

Model parameterization and performance

The results of the GAM indicated that all six variables contributed significantly ($p < 0.05$) to trends in water temperature. The relationship between air temperature and water temperature appeared to follow a logistic growth curve, while the contributions of water depth, insolation, and vegetative biomass were more linear in nature. There was no clear trend between distance from the river and water temperature.

The candidate models that we parameterized and tested using maximum likelihood estimation were based off the GAM output. We analyzed water temperature as a non-linear function of air temperature, insolation, water depth, and vegetative biomass. The best-fit model

included an interaction effect between air temperature, water depth, and vegetative biomass, and an interaction effect between insolation and vegetative biomass (Table A5.3). The relationship between air temperature and water temperature was best-characterized by a logistic growth curve, as predicted by the GAM. Conversely, water temperature had a non-linear relationship with insolation and water depth that was best modeled as an increasing exponential decay function. The final model equation was:

$$T_{t,x,y} = \left(\frac{e^{-d_1 \cdot D_{t,x,y}}}{1 + t_1 \cdot e^{-t_2 \cdot Air_t}}\right) \cdot \left(dv_1 + dv_2 \cdot V_{x,y}\right) + \left(1 - e^{-s_1 \cdot Sol_t}\right) \cdot \left(sv_1 + sv_2 \cdot V_{x,y}\right)$$

where $T_{t,x,y}$ is water temperature at time t in cell x,y, Air_t is air temperature, $D_{t,x,y}$ is water depth, $V_{x,y}$ is vegetation, and Sol_t is insolation. Estimated values for the shape parameters d_1, t_1, t_2, dv_1, dv_2, s_1, sv_1, and sv_2 are shown in Table B5.1.

Readily-observed trends in the three-dimensional surface plots showed that air temperature was the strongest force in determining water temperature. Furthermore, the cumulative distribution function of model output across a range of realistic parameter inputs showed that the majority of predicted water temperature values fell between 2°C and 20°C. Nash-Sutcliffe efficiency values were 0.76 out of a maximum of 1 and a minimum of -∞, demonstrating that model performance was satisfactory, even in the absence of the autoregressive or time lag terms (Fig. A5.3).

Spatially explicit model output verified trends predicted by the sensitivity analysis and three-dimensional surface plots. Namely, water temperature fluctuated hourly and seasonally with air temperature and insolation, and overhanging vegetation had a stabilizing effect on water temperature. Water temperature was generally more variable with increasing surface elevation relative to mean tidal level, but decreased with increasing vegetative cover, regardless of elevation or season (Fig. 5.4).

Borsuk ME, Stow CA, Luettich RA, Paerl HW, Pinckney JL (2001) Modelling oxygen dynamics in an intermittently stratified estuary: estimation of process rates using field data. Estuarine, Coastal and Shelf Science 52:33–49

Burnham KP, Anderson DR (2002) Model selection and inference: a practical information-theoretical approach. Springer-Verlag, New York, New York, USA

R Core Development Team (2018) R: a language and environment for statistical computing. R Foundation for Statistical Computing, Vienna, Austria

Reckhow KH, Quian SS (1994) Modeling phosphorus trapping in wetlands using generalized additive models. Water Resources Research 30:3105–3114

Wagner RW, Stacey M, Brown LR, Dettinger M (2011) Statistical models of temperature in the Sacramento-San Joaquin Delta under climate-change scenarios. Estuaries and Coasts 34:544–556

Table A5.1. Datasets used to construct and calibrate a spatially explicit hydrological model of estuarine water temperature, tidal inundation, and water depth.

Dataset	Collection frequency	Use	Source
Water temperature (°C)	Hourly	Model calibration	Continuous data loggers
Water level (m NAVD88)	Hourly	Model calibration	Continuous data loggers
Air temperature (°C)	Hourly	Model calibration, prediction inputs	NOAA NCDC (https://www.ncdc.noaa.gov)
Insolation (MJ/m^2)	Hourly	Model calibration, prediction inputs	WSU Weather (http://www.weather.wsu.edu); National Solar Radiation Database (http://rredc.nrel.gov/solar/old_data/nsrdb)
Tidal level (m NAVD88)	Hourly	Model calibration, prediction inputs	Maptech® Tides & Currents software; NOAA Tides & Currents database (http://tidesandcurrents.noaa.gov)
Vegetation biomass ($g\ m^{-2}$)	Annual	Model calibration, prediction inputs, spatial coverage	Annual surveys
Digital elevation model	Once	Spatial coverage	LIDAR imagery (Watershed Sciences Inc.)
Distance from nearest freshwater source	Once	Model calibration, prediction inputs, spatial coverage	Calculated using "path distance" tool in ArcGIS

Table A5.2. Coordinates and characteristics of data loggers installed in the Nisqually River Delta (NRD).

Logger number	Logger name	Latitude	Longitude	Dates active	Average salinity (psu)	Habitat type
NRD-1	I-5	47°04′13″	-122°42′13″	July 2009 – June 2015	0.01 ± 0.00	Upland
NRD-2	Phase II	47°04′46″	-122°41′33″	June 2009 – Present	5.59 ± 5.14	High salt marsh
NRD-3	Reference (Red Salmon)	47°05′39″	-122°41′27″	February 2010 – November 2015	12.94 ± 10.56	High salt marsh
NRD-4	Animal Slough	47°05′48″	-122°41′52″	June 2010 – November 2015	6.26 ± 6.43	Brackish marsh
NRD-5	Unit 2 South	47°04′54″	-122°42′59″	September 2009 – July 2015	8.24 ± 4.48	High salt marsh
NRD-6	Unit 3 North	47°05′34″	-122°42′23″	April 2010 – Present	7.71 ± 6.74	Low salt marsh
NRD-7	Unit 3 South	47°05′18″	-122°42′32″	March 2010 – January 2012	6.51 ± 5.93	Low salt marsh
NRD-8	Unit 4 North	47°04′59″	-122°43′24″	March 2010 – September 2013	14.01 ± 8.33	Low salt marsh
NRD-9	Unit 4 South	47°04′17″	-122°43′29″	January 2010 – July 2015	9.20 ± 6.52	Low salt marsh
NRD-10	Madrone North	47°05′32″	-122°42′57″	February 2010 – June 2015	10.42 ± 8.08	Low salt marsh
NRD-11	Madrone South	47°05′16″	-122°43′03″	February 2010 – September 2013	7.54 ± 8.44	Low salt marsh
NRD-12	McAllister Creek	47°05′28″	-122°43′38″	July 2010 – September 2013	9.78 ± 7.29	High salt marsh

Table A5.3. Candidate models of water temperature with degrees of freedom (df), Akaike's Information Criteria (AIC), ΔAIC, AIC weights, and root-mean-square error (RMSE) for each parameterized model. We used maximum likelihood estimation to test linear (*lin*), exponential decay (*exp*), and logistic (*log*) relationships for air temperature (*Air*), insolation (*Sol*), water depth (*D*), and vegetative biomass (*V*).

Model	df	AIC	ΔAIC	AIC Wt	RMSE
Air (*lin*)	3	86098.55	4053.79	0.00	2.62
Air (*log*)	4	85136.24	3091.48	0.00	2.55
D (*lin*)	3	107453.00	25408.24	0.00	4.72
D (*exp*)	4	107452.60	25407.84	0.00	4.72
Sol (*lin*)	3	100116.95	18072.19	0.00	3.85
Sol (*exp*)	4	99804.43	17759.67	0.00	3.82
Air (*log*) + *Sol* (*lin*)	5	83287.29	1242.53	0.00	2.42
Air (*log*) + *Sol* (*exp*)	6	83089.04	1044.28	0.00	2.41
Air (*log*) × *Sol* (*lin*)	5	83685.42	1640.66	0.00	2.45
Air (*log*) × *Sol* (*exp*)	5	84777.94	2733.18	0.00	2.52
Air (*log*) + *D* (*lin*)	5	85065.35	3020.59	0.00	2.54
Air (*log*) + *D* (*exp*)	6	84999.50	2954.74	0.00	2.54
Air (*log*) × *D* (*lin*)	5	84398.51	2353.75	0.00	2.50
Air (*log*) × *D* (*exp*)	5	84387.55	2342.79	0.00	2.50
Air (*log*) × *D* (*exp*) + *Sol* (*exp*)	7	82202.58	157.82	0.00	2.35
Air (*log*) × *D* (*exp*) × *Sol* (*exp*)	6	84041.87	1997.11	0.00	2.47
Air (*log*) × *D* (*exp*) + *Air* (*log*) × *Sol* (*exp*)	7	82566.34	521.58	0.00	2.37
Air (*log*) × *D* (*exp*) + *Sol* (*exp*) × *D* (*exp*)	7	82257.01	212.25	0.00	2.35
Air (*log*) × *D* (*exp*) + *V* (*lin*)	6	84382.73	2337.97	0.00	2.49
Air (*log*) × *D* (*exp*) × *V* (*lin*)	6	84349.20	2304.44	0.00	2.49
Air (*log*) × *D* (*exp*) × *V* (*lin*) + *Sol* (*exp*)	8	82199.48	154.72	0.00	2.35
Air (*log*) × *D* (*exp*) × *V* (*lin*) + *Sol* (*exp*) × *V* (*lin*)	9	82044.76	0.00	1.00	2.34
Air (*lin*) × *D* (*exp*) × *V* (*lin*) + *Sol* (*exp*) × *V* (*lin*)	9	82434.97	390.21	0.00	2.36
Air (*log*) × *D* (*exp*) × *V* (*lin*) + *Air* (*log*) × *Sol* (*exp*) × *V* (*lin*)	9	82445.05	400.29	0.00	2.36

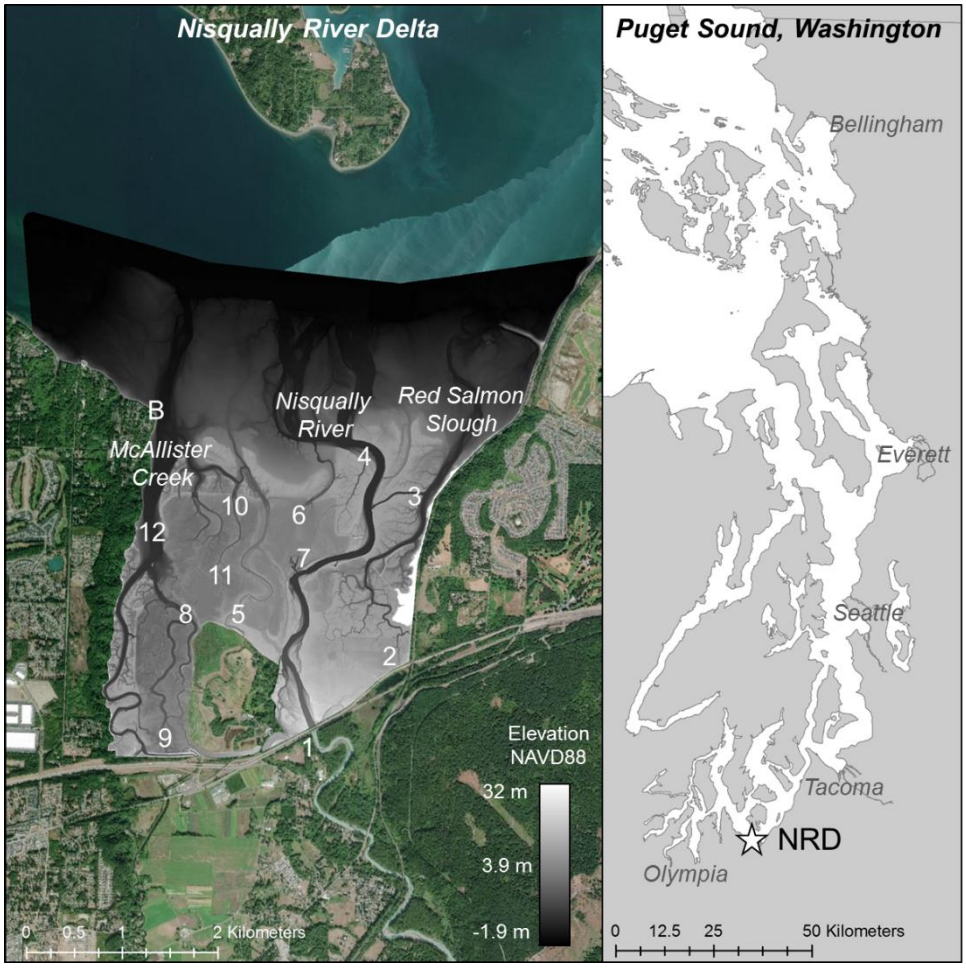

Figure A5.1. Sampling locations in the Nisqually River Delta (NRD). Numbers correspond with data outlined in Table A5.2 and denote the locations of Solinst® LTC data loggers used to collect continuous water level (m) and temperature (°C) datasets from 2010–2015. The location marked with the letter "B" indicates the barometric pressure logger. The digital elevation model (DEM) was flown by Watershed Sciences Inc. (Portland, Oregon, USA). Base layer imagery source: Google Earth Pro version 7.3.

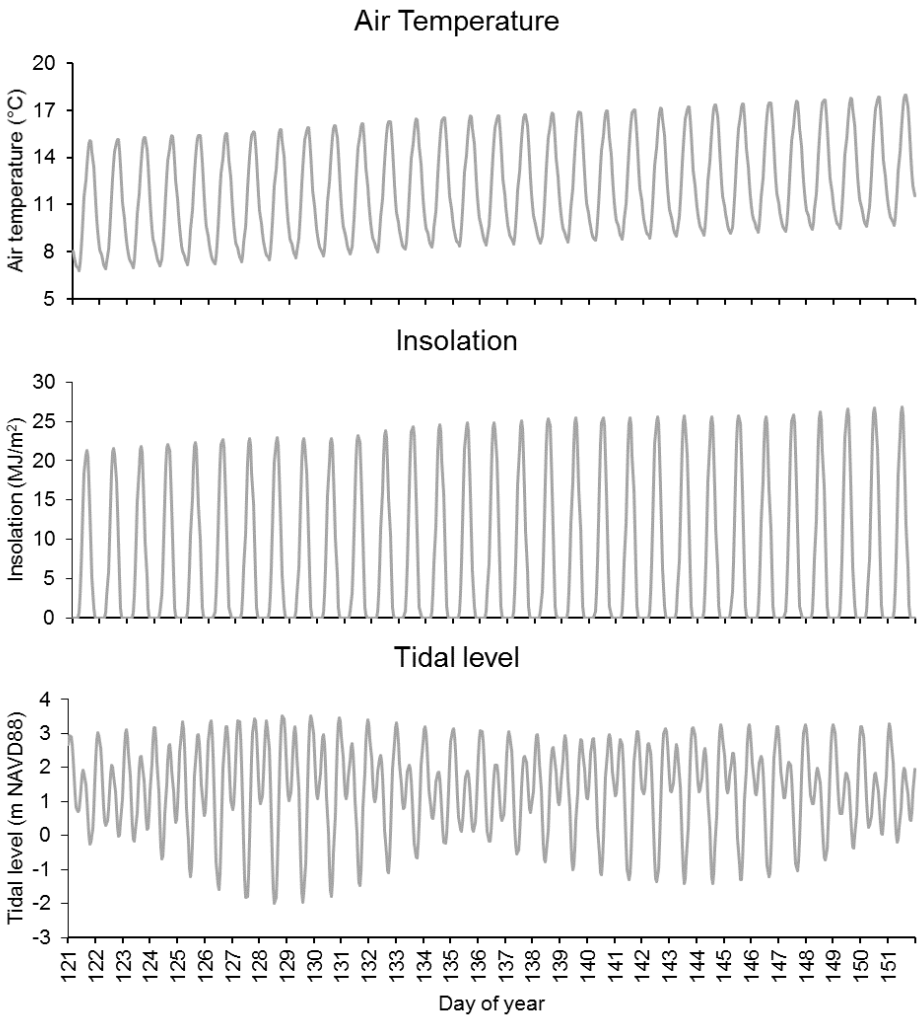

Figure A5.2. Example hourly air temperature (°C), insolation (MJ m^{-2}), and tidal level inputs (m NAVD88). Data are only shown for the month of May to display hourly patterns more clearly.

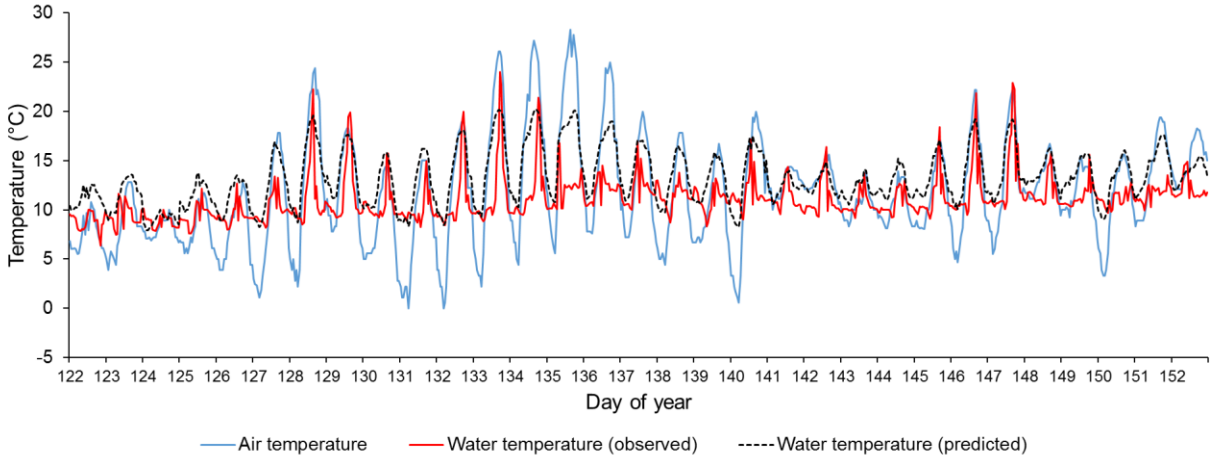

Figure A5.3. Observed and predicted hourly water temperatures during May 2014. Data were collected in a historic marsh channel using a continuous data logger (NRD-3 in Table A5.2). The channel depth was such that this particular channel did not dewater completely.

Appendix B: Model equations and parameters

Table B5.1. Model inputs, equations, and parameters for environmental conditions in the Nisqually River Delta.

Input	Equation	Parameter	Value	Source
Elevation		$E_{x,y}$		3 m Digital Elevation Model (DEM; Watershed Sciences Inc., Portland, Oregon, USA)
Path distance to river main stem (m)		$Riv_{x,y}$		Calculated from DEM
Path distance to marsh edge (m)		$Mar_{x,y}$		Calculated from DEM
Inundation duration	$I_{x,y} = \frac{1}{(1 + a \cdot e^{-b \cdot E_{x,y}})^{\frac{1}{c}}}$	$I_{x,y}$		Chapter 4 Note: $E_{x,y}$ converted to elevation relative to mean tidal level (MTL = 1.34 m NAVD88)
		a	0.029	
		b	-0.904	
		c	0.050	
Soil pore salinity (psu)	$S_{x,y} = m_1 + m_2 \cdot Mar_{x,y} + (C + i_1 \cdot I_{x,y}) \cdot (1 - e^{-k \cdot Riv_{x,y}})$	$S_{x,y}$		Chapter 4
		m_1	15.84	
		m_2	-0.013	
		i_1	-24.74	
		C	31.99	
		k	0.003	
Vegetative biomass (g m^{-2})	$V_{x,y} = N \cdot e^{-p_1 \cdot S_{x,y}} e^{\frac{-(I_{x,y} - \mu)^2}{2 \cdot \sigma^2}}$	$V_{x,y}$		Chapter 4
		N	4031	
		p_1	0.009	
		μ	0.099	
		σ	0.078	
Tidal level (m NAVD 88)		L_t		Predicted water level for Nisqually Reach tide gauge (ID: 9446828)
Air temperature (°C)		Air_t		NCDC (https://www.ncdc.noaa.gov)
Insolation (MJ m^{-2})		Sol_t		Washington State University database (http://www.weather.wsu.edu)
Water depth (m)	$D_{t,x,y} = \begin{cases} L_t - E_{x,y} & if\ L_t > E_{x,y} \\ 0 & if\ L_t < E_{x,y} \end{cases}$	$D_{t,x,y}$		

Water temperature (°C)	$T_{t,x,y} = \left(\frac{e^{-d_1 \cdot D_{t,x,y}}}{1 + t_1 \cdot e^{-t_2 \cdot Air_t}}\right) \cdot \left(dv_1 + dv_2 \cdot V_{x,y}\right) + \left(1 - e^{-s_1 \cdot Sol_t}\right) \cdot \left(sv_1 + sv_2 \cdot V_{x,y}\right)$	$T_{t,x,y}$		Appendix A
		s_1	0.140	
		sv_1	3.307	
		sv_2	2.597	
		d_1	0.059	
		t_1	4.701	
		t_2	0.149	
		dv_1	19.334	
		dv_2	-3.610	
Prey energy density (J g^{-1})		$ED_{t,x,y}$		Neuston tow data Note: model input as cal g^{-1}
Standing prey biomass (mg m^{-3})		$Bio_{t,x,y}$		Neuston tow data Note: model input as g cm^{-2}

Table B5.2. Model equations and parameters for a spatially explicit bioenergetics model of juvenile Chinook salmon growth rate potential.

Input	Equation	Parameter	Value	Source
Weight (g)		W_t		
Swimming speed (cm s^{-1})	$U_{t,x,y} = \omega \cdot {W_t}^{\nu} \cdot e^{\kappa \cdot T_{t,x,y}}$	$U_{t,x,y}$		Trudel & Welch 2005
		ω	9.70	
		ν	0.130	
		κ	0.040	
Swimming cost (cal s^{-1})	$ACT_{t,x,y} = \alpha_0 \cdot {W_t}^{\delta} \cdot {U_{t,x,y}}^{\lambda}$	$ACT_{t,x,y}$		Trudel & Welch 2005 Note: multiplied by 15,062 to convert to J h^{-1}
		α_0	0.00000174	
		δ	0.720	
		λ	1.60	
Standard metabolic rate (cal s^{-1})	$SMR_{t,x,y} = \alpha_1 \cdot {W_t}^{\beta} \cdot e^{\varphi \cdot T_{t,x,y}}$	$SMR_{t,x,y}$		Trudel & Welch 2005 Note: multiplied by 15,062 to convert to J h^{-1}
		α_1	0.0000476	
		β	0.870	
		φ	0.064	
Temperature adjustment function	$f(T_{t,x,y}) = K_a \cdot K_b$	$f(T_{t,x,y})$		Stewart & Ibarra 1991 Plumb & Moffitt 2015
	$K_a = \frac{0.36 \cdot L_1}{1 + 0.36 \cdot (L_1 - 1)}$	K_a		

	$L_1 = e^{G_1 \cdot (T_{t,x,y} - 5)}$	L_1		
		G_1	0.447	
	$K_b = \frac{0.01 \cdot L_2}{1 + 0.01 \cdot (L_2 - 1)}$	K_b		
	$L_2 = e^{G_2 \cdot (24 - T_{t,x,y})}$	L_2		
		G_2	1.414	
Handling time (s g^{-1})	$h_{t,x,y} = \frac{W_t^{CB-1}}{CA \cdot f(T_{t,x,y})}$	$h_{t,x,y}$		Beauchamp et al. 1989 Note: divided by 3,600,000 to convert to h mg^{-1}
		CA	0.00000351	
		CB	-0.275	
Cross sectional area of the reactive field (cm^2)	$\gamma_t = \alpha_3 \cdot W_t^{\beta_3}$	γ_t		Ware 1978
		α_3	1	
		β_3	0.69	
Consumption (cal s^{-1})	$C_{t,x,y} = ED_{t,x,y} \cdot \frac{Bio_{t,x,y} \cdot \gamma_t \cdot U_{t,x,y}}{1 + Bio_{t,x,y} \cdot \gamma_t \cdot h_{t,x,y} \cdot U_{t,x,y}}$	$C_{t,x,y}$		Farley & Trudel 2009 Note: multiplied by 15,062 to convert to J h^{-1}
Growth (cal s^{-1})	$G_{t,x,y} = \tau \cdot C_{t,x,y} - (SMR_{t,x,y} + ACT_{t,x,y})$	$G_{t,x,y}$		Farley & Trudel 2009 Note: expressed as J h^{-1} after conversion of *C*, *SMR*, and *ACT*
		τ	0.7	

Beauchamp DA, Stewart DJ, Thomas GL (1989) Corroboration of a bioenergetics model for sockeye salmon. Transactions of the American Fisheries Society 118:597–607

Farley EV, Trudel M (2009) Growth rate potential of juvenile sockey salmon in warmer and cooler years on the eastern Bering Sea shelf. Journal of Marine Biology 2009:10

Plumb J, Moffitt CM (2015) Re-estimating temperature-dependent consumption parameters in bioenergetics models for juvenile Chinook salmon. Transactions of the American Fisheries Society 144:323–330

Stewart DJ, Ibarra M (1991) Predation and production by salmonine fishes in Lake Michigan, 1978–88. Canadian Journal of Fisheries and Aquatic Sciences 48:909–922

Trudel M, Welch DW (2005) Modeling the oxygen consumption rates in Pacific salmon and steelhead: model development. Transactions of the American Fisheries Society 134:1542–1561

Ware DM (1978) Bioenergetics of pelagic fish: theoretical change in swimming speed and ration with body size. Journal of the Fisheries Research Board Canada 35:220–228.

Conclusion and Synthesis

These studies highlight how a diverse mosaic of estuarine habitats provides optimal foraging and growth opportunities for out-migrating juvenile salmon. Habitat diversity has long been recognized to support population and community resilience through a portfolio effect, whereby multiple interconnected habitats with varying physical and biological characteristics provide opportunities for growth and survival by stabilizing environmental conditions at the landscape scale (Sheaves 2009; Beechie et al. 2013; Schindler et al. 2015). In the Nisqually River Delta, this portfolio effect was illustrated by clear quantity-for-quality tradeoffs in the energy density and availability of prey. Freshwater and brackish tidal habitats along the main stem river had lower prey abundances because the prey field was comprised primarily of energy-dense insects that entered the water column from the terrestrial realm or that transitioned from aquatic life stages. Nevertheless, the juvenile Chinook salmon that were captured in these habitats did not appear to have been affected by the measured scarcity of prey in terms of their consumption and growth, most likely because fish densities were also lower within the main stem river. In the emergent salt marsh and mudflat habitats, juveniles consumed primarily mysids, which were large-bodied and abundant, but also relatively energy-poor. Emergent salt marsh was predicted to result in above average growth in both the habitat-specific (Chapter 3) and spatially explicit (Chapter 5) bioenergetics models. Meanwhile, the nearshore intertidal (unvegetated mudflats) and offshore subtidal zones were predicted to produce the lowest growth rates, with the exception of the prey-rich eelgrass beds. However, these habitats were more likely to be inundated at low tide and may have provided alternative foraging areas when the tidal channels and mudflats dewatered. These quantity-for-quality tradeoffs highlight the need to maintain the Nisqually River Delta habitat mosaic to support local fall run populations of Pacific salmon.

Each spring, almost 4 million hatchery-reared Chinook salmon are released into the Nisqually River Delta alongside 50,000–400,000 wild juveniles. Hatchery fish are released at a larger size and at elevated densities over a shorter timeframe, leading to concern about potential density-dependent effects in certain parts of the delta (Weber and Fausch 2003; Weber and Fausch 2005; Tatara and Berejikian 2012). In Chapter 2, I found evidence for distinct habitat and dietary partitioning among wild and hatchery Chinook salmon. Stable isotope analyses indicated that wild fish were more likely to rear for longer periods in freshwater tidal forested areas along the main stem river, consuming energy-dense adult and larval insects. In contrast, hatchery fish were rarely captured in freshwater habitats. Instead, they tended to move directly to the nearshore zone, where they ate aquatic crustaceans such as mysids, amphipods, and crab larvae. These findings support previous evidence for truncated delta residence times in Nisqually hatchery fish (Davis et al. 2018). While trophic overlap between wild and hatchery juvenile salmon appears to be minimal within the delta, my results indicate that wild juveniles may be more sensitive to diet-mediated effects on growth and survival because they are dependent on the availability of insect drift in emergent marsh habitats.

My results from Chapter 3 also pointed to distinct growth benefits from insect prey. I used a bioenergetics model concurrently with morphometric scale measurements to determine whether among-habitat dietary differences affected juvenile salmon consumption and growth. Estimated consumption rates were lower in the freshwater tidal forested habitat than in the nearshore and offshore zones, yet this habitat type still had the highest modeled growth rate potential. Similarly, realized growth (as estimated from scales) was up to 0.5% higher per-day in the freshwater tidal area than in the offshore zone, and wild fish (which, as shown in Chapter 2, were more likely to be found in freshwater habitat) grew up to 11% faster on average than

hatchery fish. Distinct growth benefits were also observed in the emergent salt marsh, further demonstrating how tidal forests and emergent marshes may positively contribute to the functional capacity of the entire delta by offering early-life growth advantages for juvenile Chinook salmon.

The Nisqually Delta restoration was completed in 2009 and added over 360 ha of brackish and emergent salt marsh habitat, thus expanding the estuarine habitat mosaic and bolstering overall delta habitat quality for juvenile salmon (Ellings et al. 2016, Woo et al. 2018, Davis et al. 2018). Unfortunately, the configuration and extent of coastal habitat is expected to change as sea levels rise, which is likely to impact Nisqually's restored and relict habitats (Harley et al. 2006; Lotze et al. 2006; Craft et al. 2009). In Chapter 4, I used an empirically-based marsh accretion model to project how the estuarine habitat mosaic will change under different sea-level rise and sediment management scenarios. The model predicted that without the addition of suspended sediment, the extent of low- and high-elevation emergent salt marsh in the Nisqually River Delta will decrease through the year 2100. When considered jointly with my findings from Chapters 2 and 3, these projections suggest that the loss of tidal marsh will negatively impact estuary-dependent species of salmon by lowering the abundance of available aquatic and terrestrial prey and reducing growth potential. Indeed, my findings in Chapter 5 robustly supported this assertion. The spatially explicit version of the bioenergetics model highlighted how the loss of emergent salt marsh decreased available prey resources. Modeled juvenile salmon growth was thus negatively impacted by sea level rise as the extent of prey-rich habitats decreased.

These complementary chapters provide the most comprehensive analysis of a single delta ecosystem to-date, demonstrating how prey-rich tidal marsh habitats enhance the nursery quality

of the estuarine habitat mosaic by providing abundant prey resources and thermal refugia. They highlight the need for strategic management actions, including an adaptive management framework that incorporates long-term monitoring and modeling procedures. Most importantly, my research supports a contextualist approach when examining a target study system. Before conducting restoration and enhancement actions, managers should ask themselves: How does this system fit into the broader estuarine habitat mosaic or coastal ecosystem mosaic? What is the structure and function of the system in its present state, and how would its function improve given alternative states? How is this system likely to respond to restoration actions, nearby anthropogenic development, and climate change through time? Do we have the economic, ecological, and social capital to return this system to an optimal functional state? By viewing a target site in a broader spatiotemporal context, managers can promote lasting, positive outcomes with benefits for multiple dependent species and interconnected ecosystems.

References

Beechie, T., H. Imaki, J. Greene, A. Wade, H. Wu, G. Pess, P. Roni, J. Kimball, J. Stanford, P. Kiffney, and N. Mantua. 2013. Restoring salmon habitat for a changing climate. River Research and Applications 29:939–960.

Craft C, Clough J, Ehman J, Joye S, Park R, Pennings S, Guo H, Machmuller M (2009) Forecasting the effects of accelerated sea-level rise on tidal marsh ecosystem services. Frontiers in Ecology and the Environment 7:73–78

Davis, M. J., C. S. Ellings, I. Woo, S. Hodgson, K. Larsen, G. Nakai, and S. De La Cruz. 2018. Gauging resource exploitation by juvenile Chinook salmon (*Oncorhynchus tshawytcha*) in restoring estuarine habitat. Restoration Ecology 26:976–986.

Ellings, C.S., M.J. Davis, E.E. Grossman, I. Woo, S. Hodgson, K. Turner, G. Nakai, J.E. Takekawa, and J.Y. Takekawa. 2016. Changes in habitat availability for outmigrating

juvenile salmon (Oncorhynchus spp.) following estuary restoration. Restoration Ecology 24:415–427.

Harley CDG, Hughes AR, Hultgren KM, Miner BG, Sorte CJB, Thornber CS, Rodriguez LF, Tomanek L, Williams SL (2006) The impacts of climate change in coastal marine systems. Ecology Letters 9:228–241

Lotze HK, Lenihan HS, Bourque BJ, Bradbury RH, Cooke RG, Kay MC, Kidwell SM, Kirby MX, Peterson CH, Jackson JBC (2006) Depletion, degradation, and recovery potential of estuaries and coastal seas. Science 312:1806–1809

Schindler, D.E., J.B. Armstrong, and T.E. Reed. 2015. The portfolio concept in ecology and evolution. Frontiers in Ecology and the Environment 13:257–263.

Sheaves, M. 2009. Consequences of ecological connectivity: the coastal ecosystem mosaic. Marine Ecology Progress Series 391:107–115.

Tatara, C. P., and B. A. Berejikian. 2012. Mechanisms influencing competition between hatchery and wild juvenile anadromous Pacific salmonids in fresh water and their relative competitive abilities. Environmental Biology of Fishes 94:7–19.

Weber, E. D., and K. D. Fausch. 2005. Interactions between hatchery and wild salmonids in streams: differences in biology and evidence for competition. Canadian Journal of Fisheries and Aquatic Sciences 60:1018–1036.

Weber, E. D., and K. D. Fausch. 2003. Competition between hatchery-reared and wild juvenile Chinook salmon in enclosures in the Sacramento River, California. Transactions of the American Fisheries Society 134:44–58.

Woo, I., M. J. Davis, C. S. Ellings, G. Nakai, J. Y. Takekawa, and S. De La Cruz. 2018. Enhanced invertebrate prey production following estuarine restoration supports foraging for multiple species of juvenile salmonids (*Oncorhynchus* spp.). Restoration Ecology 26:964–975.